BANGLADESH NETWORK
OFFICE FOR URBAN SAFETY

BNUS ANNUAL REPORT-2021

BANGLADESH
NETWORK OFFICE FOR
URBAN SAFETY

BUET, DHAKA, BANGLADESH

Edited By:

Mehedi Ahmed Ansary

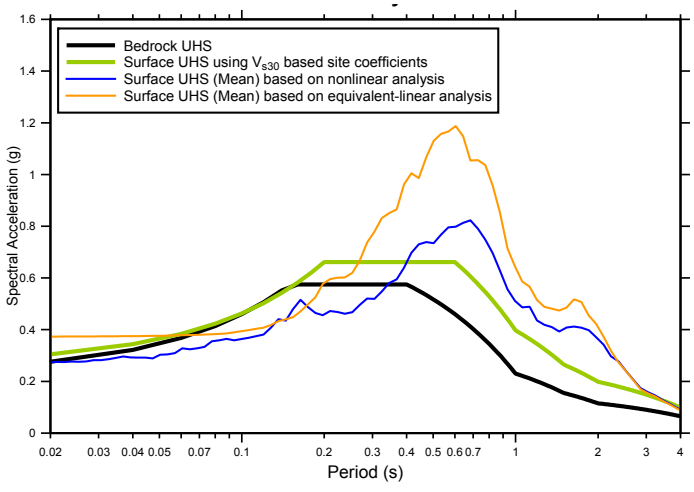

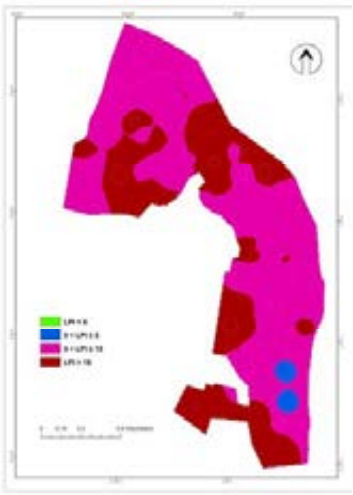

April 2022

BANGLADESH NETWORK
OFFICE FOR URBAN SAFETY

CONTENTS

BANGLADESH NETWORK
OFFICE FOR URBAN SAFETY

PART-I

SLOPE STABILITY ANALYSIS OF REFUGEE CAMP STABILITY STRUCTURE USING BAMBOO AND SYNTHETIC GEO-TEXTILE IN UKHIYA, COX'S BAZAR

BANGLADESH NETWORK OFFICE FOR URBAN SAFETY (BNUS), BUET, DHAKA

Prepared By: **Maiesha Tabassum**

Mehedi Ahmed Ansary

1.1 General

The south-eastern region of Bangladesh consists of many hilly tracks and coastal ridges laying by the Bay of Bengal. The Cox's Bazar district of that zone has both the features currently providing shelter for more than 1.1 million Rohingyas. Especially in the Ukhiya Upazila of the district is confirmed to have at least 0.9 million Rohingyas. After that, the land use of the zone has increased tremendously. For that, many retaining structures near the Rohingya camps are built like dams, backfill protection, bamboo ring protection, etc. as the lives of the people matter there as well as to facilitate their livelihood.

In the Palongkhali union, Ukhiya the earth retaining structures built were needed to be analyzed for slope stability as different measures protect the structures and people to a different extent. Therefore, five samples were taken from the Balukhali Bazar area from which one was from the block dam, two from the bridge dam, and the last two from the culvert dam with road protection.

So, Slope stability analysis of these measures taking samples from some of the locations by doing both laboratory testing and software analysis for all the samples collected. With and without additional stability measures, the analysis is done checking the factor of safety against stability. Thus, this chapter covers the geological site description, objective, and outline of the research regarding the slope stability of protection measures of Ukhiya Upazila.

1.2 Geology of Study Area

Ukhiya Upazila of Cox's Bazar district with an area of 261.8 sq km is located between 21°08' and 21°21' north latitudes and in between 92°03' and 92°12' east longitudes. Ramu Upazila bounds it on the north, Teknaf Upazila on the south, the Arakan state of Myanmar, and Naikhongchhari Upazila on the east, the Bay of Bengal on the west.

The location of the collected samples was from Balukhali Bazar and Gundum in the Kutupalong union of this Upazila. The region is hot and humid with some seasons of temperate weather. The average rainfall of Ukhiya is 4285 mm with a maximum and minimum temperature of 32.8° C. and 16.1° C respectively on an annual basis. The only river flowing through the Upazila is the Rejur canal flowing to the Bay of Bengal.

Most of the bedrocks of Cox's Bazar were formed in the Pleistocene and Pliocene age with Dihing and Dupi Tila formation. Balukhali Bazar area is formed explicitly by Boka Bil formation and Bhubon formation of the Neocene and Miocene age, respectively.

Dakhin Nhila structure lies under Teknaf Upazila near Ukhiya of Cox's Bazar district and bounded by latitude 20°52' to 21°07'N and longitude 92°08' to 92°18'E and is situated at the extreme southeast of Bangladesh territory. Hills and valleys striking N I7'W and S 17'E represent it. The maximum elevation is about 266m above mean sea level. The northern pitch is defined by low relief due to the saddle separating from the Inani anticline, whereas the southern slope abruptly merges with the bare land.

Dakhin Nhila anticline is an elongated, asymmetric, and box-like structure. It is a complicated structure due to the presence of longitudinal and transverse faults. The oldest exposed rock is Upper Bhuban that is about 545m thick. The exposed rock formations from older to younger are Upper Bhuban, Boka Bil, Topham, and Dupi Tila. Mostly argillaceous sediments with little coverage of arenaceous deposits characterize the structure. The axis of the frame runs along the NNW-SSE direction. Some portion of the western flank and younger formation of the southern pitch has been eroded due to the Bay of Bengal.

This location stands nearly 3 to 4 meters above sea level. The dams from which the samples were collected were more likely to have sandy clay to clay in most of the cases with one sandy soil deposit for sample number four.

1.3 The objective of the research

The main objective of the research is as follows:

a) To determine the sub-soil profile of all five samples by determining the types and parameters of the representatives of the location by laboratory procedures.

b) To discuss and select appropriate slope protection measures for the established structures of the location.

c) To analyze earth structures without any protection measures and decide if any protection measure is needed

d) To utilize bamboo anti-slide pile for protective measure and check for the stability of slopese) To study synthetic Geotextile as an alternate protective technique and compare the two approaches against slope protection.

Figure 1.1: Geological Map of Ukhiya Upazilla

1.4 Scope of the Research

In this research, soil samples from five different locations of Ukhiya Upazila are collected and analyzed for checking slope stability against the failure of any kind. The software, GEO5, is used to measure the factor of safety against failure in only Bishop's simplified method of analysis. A specific slip circle is provided for all the models with different soil parameters as well as earth structure dimensions in the optimization model.

As there were no in-situ soil tests or boring done to get some parameters to the exact, the parameters found using laboratory procedures, might be distorted to some extent. Moreover, as only five samples were collected, also having limitations with slope protection techniques, the actual proper treatment measure may not have been found out. Following other methods

for slope stability analysis also might have changed some outcomes for having different principles.

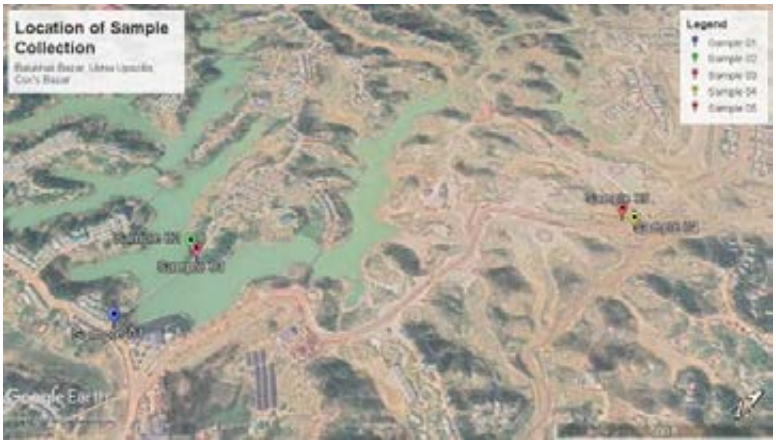

Figure 1.2: Location of Sample Collection Map

Figure 1.3: Slope protection measure in the locations of Ukhiya (a)close-up view (b)full view

2.1 Methodology

The slope stability analysis of the five soil samples collected from Ukhia Upazila is to be first tested on the laboratory for gaining the parameters needed for the software analysis were implying these data slope stability analysis is done. Keeping that in mind, as the soils were disturbed and no bore-logs were collected, tests such as grain size analysis, specific gravity test, standard proctor test and finally consolidated direct shear test are done for getting the value of dry density, saturated dry density, confined shear stress and the angle of internal friction. After getting all these values and inputting them on slope stability software, GEO5 for further investigation slope stability analysis is done using Bishop's simplified method of slices. The research was done considering different slopes, tread height and width and extra pile height. The slip surface in the GEO5 software was taken to be circular not the polygonal one following the Bishop's method of analysis. No groundwater table criteria or change in water level height was considered for the examination. Taking the allowable Factor of Factor of safety 2.5 to 3 for both cases of bamboo and Geotextile, slope stability analysis is completed. However, in this chapter, only the laboratory testings are defined and discussed, and the GEO5 analysis is described in the following chapter.

2.2 Laboratory Tests

For the collection of undisturbed samples from the site, the complete set of laboratory investigation consisted of the following test procedures on all the samples:

- Grain size analysis
    - Sieve analysis
    - Hydrometer analysis
- Specific Gravity Test
- Standard Proctor Test
- Direct Shear Test

These tests are discussed below after which the data collected from these tests are provided in the upcoming sub-sections.

3.3.1 Grain Size Analysis

Grain size analysis provides the grain size distribution as the distribution of different grain sizes affects the engineering properties of the soil. Sieve analysis provides the distribution of coarser particles, and hydrometer analysis significantly shows the distribution of finer particles of the earth.

Figure 3.1: Opening of different sieves to be used

les was conducted to determine the distribution of larger-sized particles (usually retained on #200 sieve). The equipment required for the tests are #4, #8, #16, #30, #50, #100, #200 sieve; Pan; Lead; Brush; Container; Spoon; Bowel; Balance and Sieve shaker.

3.3.1.2 Hydrometer Analysis

Hydrometer analysis is required for the determination of the grain size distribution of the more delicate portion of the soil that passes #200 sieve. ASTM 152H hydrometers are calibrated such that when inserted in a soil-water suspension the reading on the hydrometer stem indicates grams of soil that are in 1000cc suspension

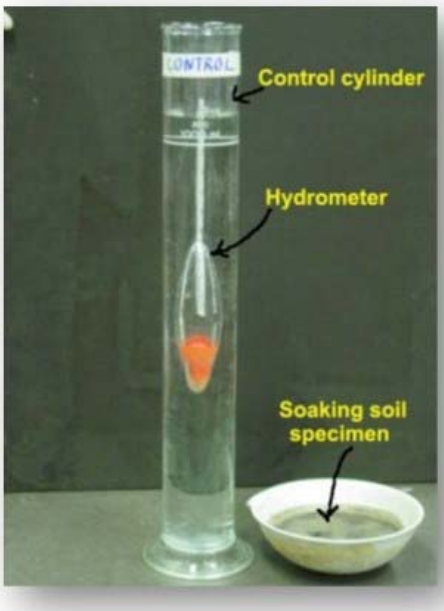

Figure 3.2: Hydrometer dipped in control cylinder with soaked specimen beside it

centre of the bulb following the Stokes law. The scale of the 152H reads -5 to +60 g/L graduated/marked. The equipment needed is 152H Hydrometer; Hydrometer jar; Measuring cylinder / graduated jar; Car; Wash bottle; Stopwatch; Mechanical mixture & mixing pot; Balance; Thermometer and Water bath.

3.3.2. Specific Gravity

As neither of the five soil samples was highly organic, this test was performed to determine the Specific Gravity of the soil passing 4.75 mm sieve by using a water pycnometer. It is used in the phase relationship and for determining soil density. The code followed to conduct the test was ASTM D 854-02: Standard Test Methods for Specific Gravity of Soil Solids by Water Pycnometer. The equipment needed is Volumetric flask; Wash bottle; Funnel; Pipette; Can; Balance Burner/gas stove; Vacuum pump; Oven and Thermometer.

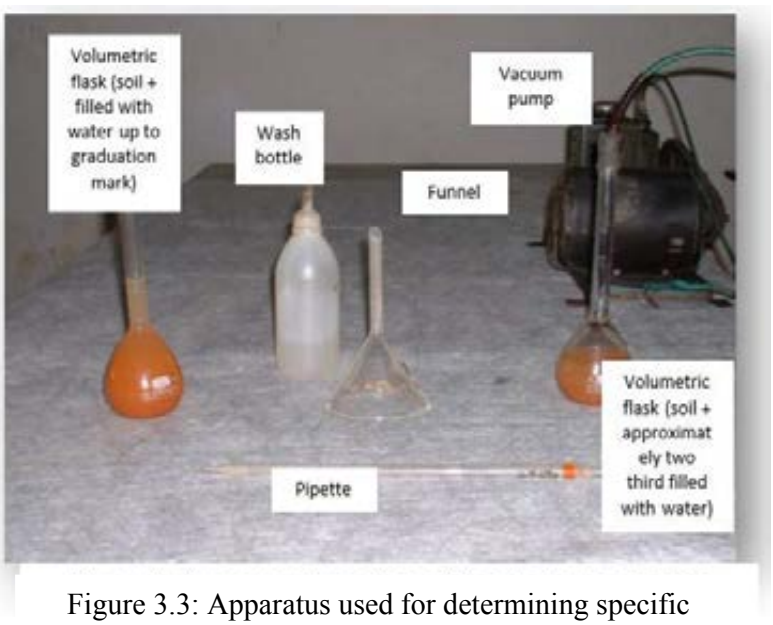

Figure 3.3: Apparatus used for determining specific

3.3.3 Standard Proctor Test

Mechanical compaction is one of the most common and cost-effective means of stabilizing soils. So, to determine the proper amount of mixing water to use when compacting the earth in the field and the resulting degree of denseness which can be expected from compaction at this optimum water content. Design specifications usually state the required density and

Figure 3.4: Apparatus used for Standard Proctor

optimum water content which can improve strength, stiffness, resistance to shrinkage and imperviousness of the soil. Following the standard proctor test of compaction, with the specification of ASTM D698, this test is only applicable for soils that have 30% or less by mass of particles retained on the 19.0 mm sieve. To complete the test, following instruments are needed are Moisture sprayer; No 4 sieve; Rubber tripped pestle; Scoop; Straight edge and knife; Drying oven; Standard Proctor test mould and Standard Proctor Test hammer (5.5 lbs.)

3.3.4 Direct Shear Test

Following the standard, ASTM D-3080-03-Direct Shear Test of Soils Under Consolidated Drained Conditions, a direct shear test of all the five samples is conducted. This test is performed to determine the consolidated-drained shear strength of silty and sandy soil. The shear strength of the ground is one of the most significant engineering properties of the earth as it is necessary whenever a structure is dependent on the soil's shearing resistance. The shear strength is required for engineering practical problems like determining the stability of slopes or cuts, calculating the pressure exerted by the ground on a retaining wall and finding the bearing capacity for foundations.

The direct shear test is one of the oldest strength tests for soils. In this laboratory, a direct shear device will be used to determine the shear strength of a cohesionless soil (i.e., angle of internal friction (Φ)). From the plot of the shear stress versus the horizontal displacement, the maximum shear stress is obtained for a specific vertical confining stress. After the experiment is run several times for various vertical-confining stresses, a plot of the maximum shear stresses versus the vertical (normal) confining stresses for each of the tests is produced. From the plot, a straight-line approximation of the Mohr-Coulomb failure envelope curve can be drawn, f may be determined, and, for cohesionless soils (c = 0), the shear strength can be computed from the following equation:

$$\mathbf{S = \sigma \tan \Phi}$$ Where, S = Shear strength

σ = Shear stress Φ = Angle of internal friction

The necessary equipment for the test is Direct Shear Device; Load and deformation dial gauges; Shear box; Balance; Vertical load; Pressure plate; Porous plate; Screw; Filter paper; Scale Dish Stopwatch and Probe ring.

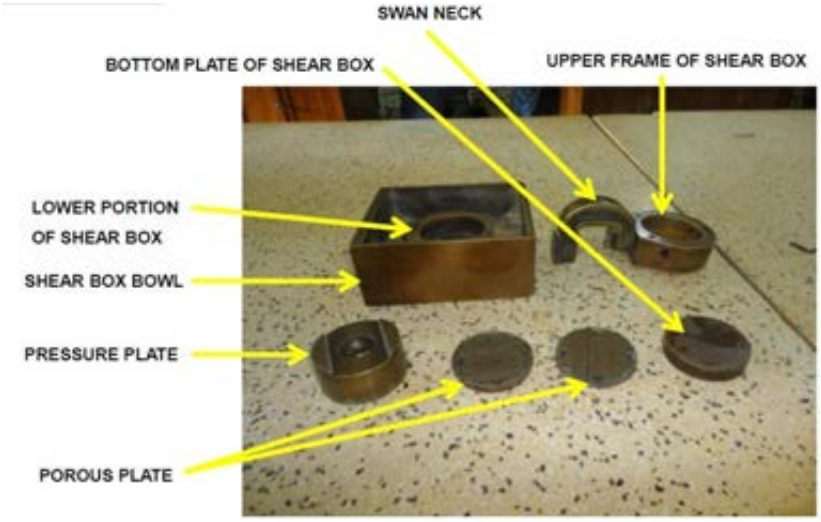

Figure 3.5: Different parts of a shear box

3.3.4.1 Sample preparation:

- For cohesive soil: Sample 1,2,3 and 5 were tested out to be cohesive soil with relative higher amount of clay than that of sand. For preparing the sample, the new example is to be ready using optimum water content calculated from the standard proctor test graphs. At first, nearly 10 lbs. of the model is to be taken on a tray, and optimum water is added and mixed with the soil. Then the soil is to be set into three layers in a standard proctor mould to the top, and 25 blows in each layer are given. The soil is then extruded out and cut into three equal cylinders to fill in the probe rings. Then using three individual probing ring soil samples are moulded, and thus soil samples for the shear test are prepared. In addition to that, the weight of the individual probe rings and ring with soil are also calculated.
- For cohesionless soil: Sample 4 was found out to be cohesionless as a higher number of sandy particles was found during the grain size analysis. For preparing the sample, a certain amount of soil sample is to be taken for filling three probing rings. Then mixing with ample amount of water with hand and filling the ring with 5-7 blows of wooden tamper in three layers to the top of the probing ring, cohesionless soil samples are made.

3.3.4.2 Apparatus setup:

At first, the soil sample for testing was transferred into the shear box. For this, the bottom plate and one porous plate was inserted into the shear box after which the upper frame was inserted with the alignment pins. The placing one filter paper, the soil sample was extruded from the ring to the box with the help of a wooden tamper. Then another filter paper was placed with the remaining porous plate on top, and the pressure plate was placed on top of everything. In the next step, after placing the shear box in the shear device, all the gages were adjusted and set to zero except the normal displacement dial gauge. Also, the hollow space in the box was filled with water. The initial dial reading of normal displacement dial gauge was recorded. Then a normal vertical load of 10 kg was applied, and the alignment pins were removed.

3.4 Data Collection

After the setup of all the tests, appropriate data need is needed to be collected for further analysis in GEO5 software. The procedure and collected data re provided in the following subsections

3.4.1 Sieve Analysis Data

After writing down the weight of each sieve along with the bottom pan, the weight of the given oven-dried soil sample is recorded. Cleaning all sieves and assembling them in the ascending order of sieve numbers the soil sample is placed on the top sieve, and the cap is placed on top. This sieve stack is placed in the mechanical sieve shaker then the sieve stack is shaken for 10-15 minutes. Then removing the stack, each sieve with its retained soil is weighed. The same is also done for the bottom pan with its refined soil. Placing the values in the sieve analysis chart following gradation chart informed for all five samples.

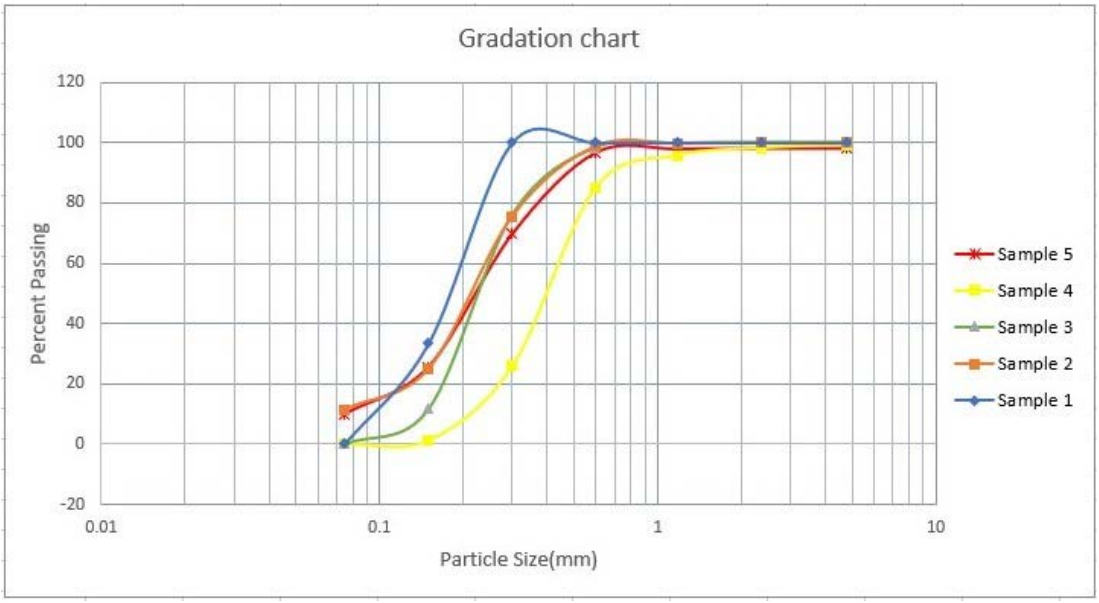

Figure 3.6: Gradation chart of the samples obtained from Sieve Analysis

.4.2 Hydrometer Analysis Data

For conducting the test, precisely 50 g of oven-dry, well-pulverized soil was measured. The weight was recorded in the datasheet. The ground was placed in the mixing pot. 125 ml of 4% NaPO3 (sodium hexa meta phosphate) was mixed in the solution. Then the mixture was transferred to a mixing pot, and tap water was added until the cup was two-thirds full. It was mixed for 3 to 5 minutes in the mixing device. All the contents of the mixer pot were transferred to the hydrometer jar being very careful not to lose any material. Tap water was added to fill the cylinder to the 1000-ml mark. Also, the graduated cylinder was filled (later referred to as water jar) to about 1000 ml mark with tap water. The palm of the left hand was put on the open end of the hydrometer jar, and the soil water suspension was mixed by quickly overturning the pot up and down several times. Then the hydrometer jar was placed on the table. Care was taken so that the jar was not disturbed by any vibration. Immediately after placing the hydrometer jar on the table, the Hydrometer was inserted in the soil water suspension, the timer was started, and the readings were taken at elapsed times of 0.25, 0.5, 1, and 2 minutes. After 2 minutes, the Hydrometer was removed from the soil water suspension, and it was placed in the water jar.

The suspension was remixed in the hydrometer jar. If the last set of four readings (at an elapsed time of 0.25, 0.5, 1 and 2 minutes) were almost the same as the previous set, then these readings were recorded in continue with next step otherwise previous steps were repeated. Taking hydrometer readings were continued at elapsed times of 4, 8, 15, 30, 60 min., and 2, 4, 8, 16, and 24 hours. Between hydrometer readings, the Hydrometer was stored in the water jar. The internal diameter of the hydrometer jar was measured after which the volume of the hydrometer bulb was measured. Similar graph of per cent finer vs pa Figure

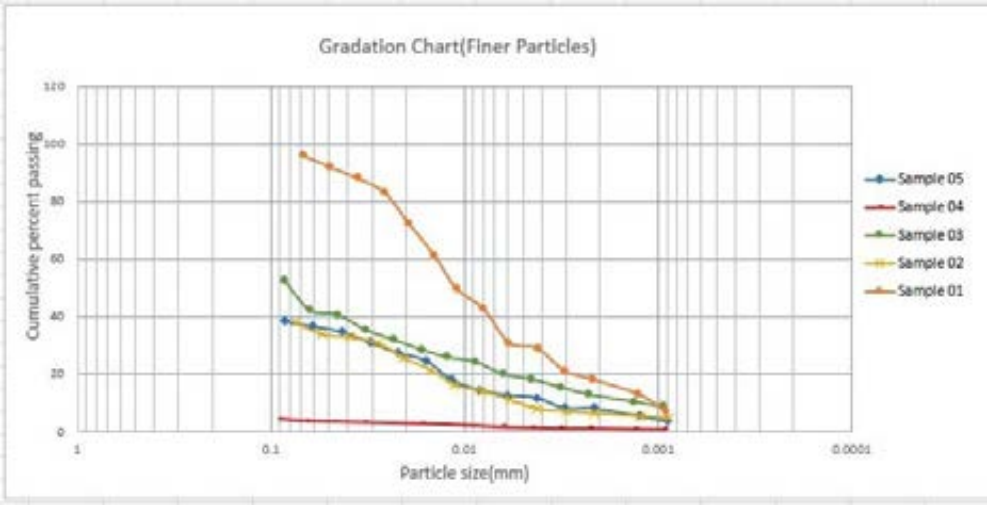

3.7: Gradation chart of the samples obtained from Hydrometer rticle size was plotted for all the samples.

So, a final percentage of sand, silt and clay can be derived and attached below:

Sample Number	Amount of Sand (%)	Amount of Silt (%)	Amount of Clay (%)
01	1	81	18
02	41	53	6
03	41	46	13
04	89	10	1
05	45	47	8

3.4.3 Specific Gravity Test Data

Table 3.1: Percentage of sand, silt and clay for all samples from grain size analysis

For commencing the test, the volumetric flask was weighed in a dry state. The weight of the empty and clean pycnometer was determined and recorded. By measuring 50 gm of the oven-dry soil sample, it was placed in the pycnometer, and about 2/3 of pycnometer was filled with tap water. Then the model was kept soaking for 10 minutes. After heating the sample until the water in the soil-water mixture starting to boil, the vacuum was applied to the contents for 10 minutes during boiling of water in the mix to remove the entrapped air. Then stopping the vacuum and carefully drawing the line from pycnometer, the pycnometer was filled with water to the mark and kept for a day to bring it to the room temperature. On the following day, the weight of the pycnometer filled with water and soil sample was recorded. The emptying the pycnometer and filling with water to the mark, the weight of pycnometer with water was determined. With a thermometer, the room temperature was recorded as well. The using appropriate equation specific Gravity for each sample was determined.

The value of the Specific Gravity of the five samples are as below:

Sample No.	Specific Gravity (at room temperature)	Specific Gravity (at 20° C)
01	2.646	2.640
02	2.762	2.756
03	2.551	2.545
04	2.716	2.710
05	2.762	2.756

3.4.4 Standard Proctor Test Data

For starting the test, approximately 10lbs of the soil sample is taken, which is then pulverized and ran through #4 sieve. After that, the weight of both the soil sample and compaction mould with base (without the collar) are taken separately. Then computing the initial amount of water to be added, the water is measured out, added to the soil and mixed thoroughly with the earth.

Therefore, assembling the compaction mould to the base, some soil is placed into the mould and the ground is compacted in three layers with 25 blows in each layer with every fall height of 12 inches. It was ensured that the drops were to be applied at a uniform rate not exceeding 1.5 seconds per drop. For filling the cylinder, the last compacted layer was made to extend slightly above the collar joint. Then the collar was carefully removed, and the compacted soil was trimmed to the top of the mould. After that, the mould with base and dirt was weighed and extruding the sample, and soil moisture content samples were taken from top and bottom of the extruded compacted sample from which wet density and dry density of the soil is to be found. Then by plotting the graph of dry density vs moisture content, optimum moisture content can be figured out.

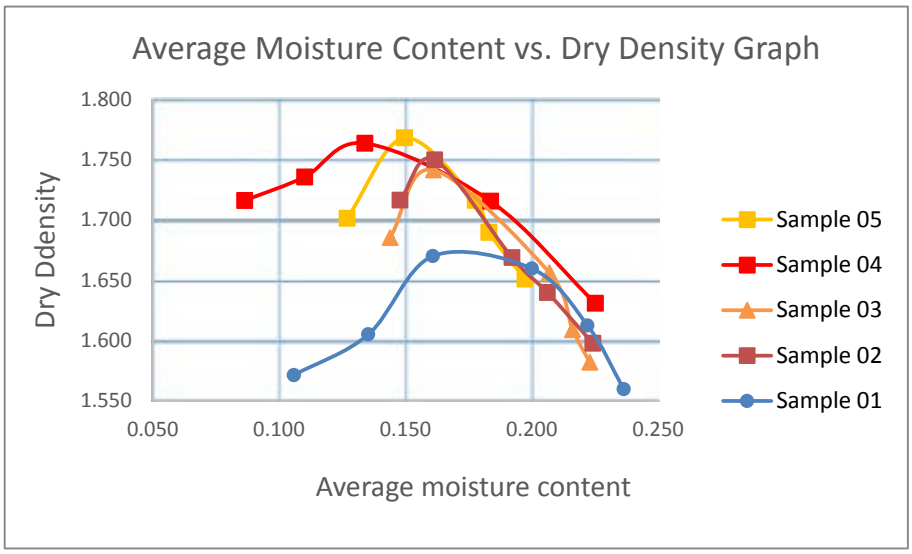

The graphs from the standard proctor test of dry density vs water content of the five samples are given below:According to these graphs, the optimum water content for each sample is calculated as below:

Sample No.	Optimum moisture content (%)
01	19.38
02	19.56
03	20.16
04	19.41
05	18.4

3.4.5 Direct Shear Test

An average vertical load of 10 kg was applied, and the alignment pins were removed. After that, the soil was kept being fully consolidated, and we had to wait until the change in standard displacement dial was unnoticeable. The time can take 30 mins to 2 hours depending on soil and load. When the typical displacement gauge dial was constant, motor speed was set for the required strain rate, and the machine was started. Instantly starting the stopwatch, the shear load reading, regular displacement dial reading and horizontal displacement dial reading were recorded at 0, 0.25, 0.5, 0.75, 1, 1.25, 1.5, 1.75, 2 etc. minutes. A similar procedure was done for a vertical load of 20 kgs and 40 kgs. For obtaining the result shear stress vs, shear displacement

graph is to be plotted from which peak shear stress for each case is to be taken, after which shear stress vs typical stress graph is plotted from which values of cohesion, c and

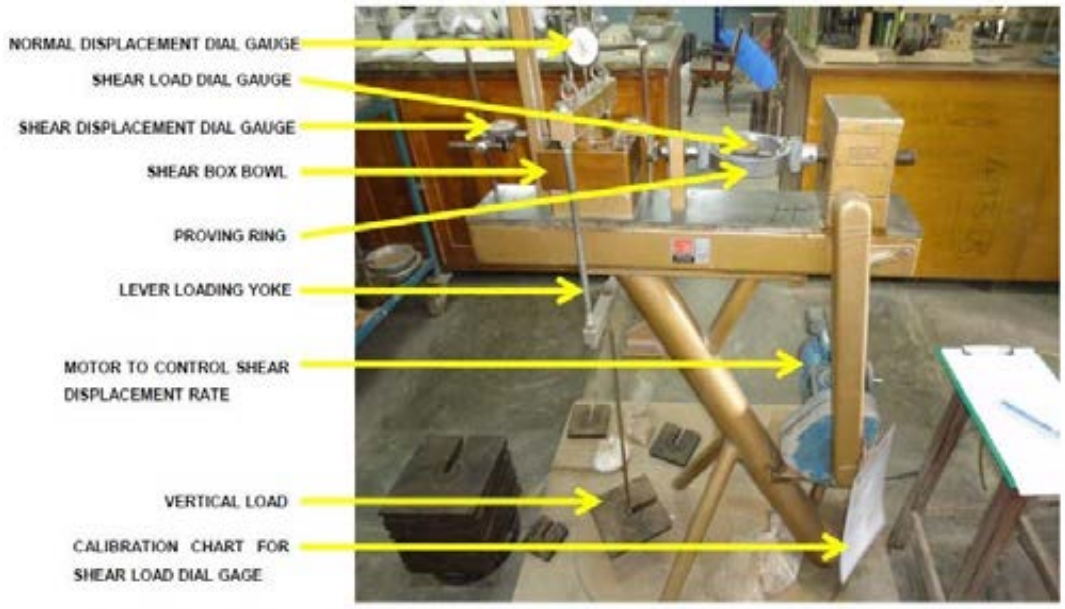

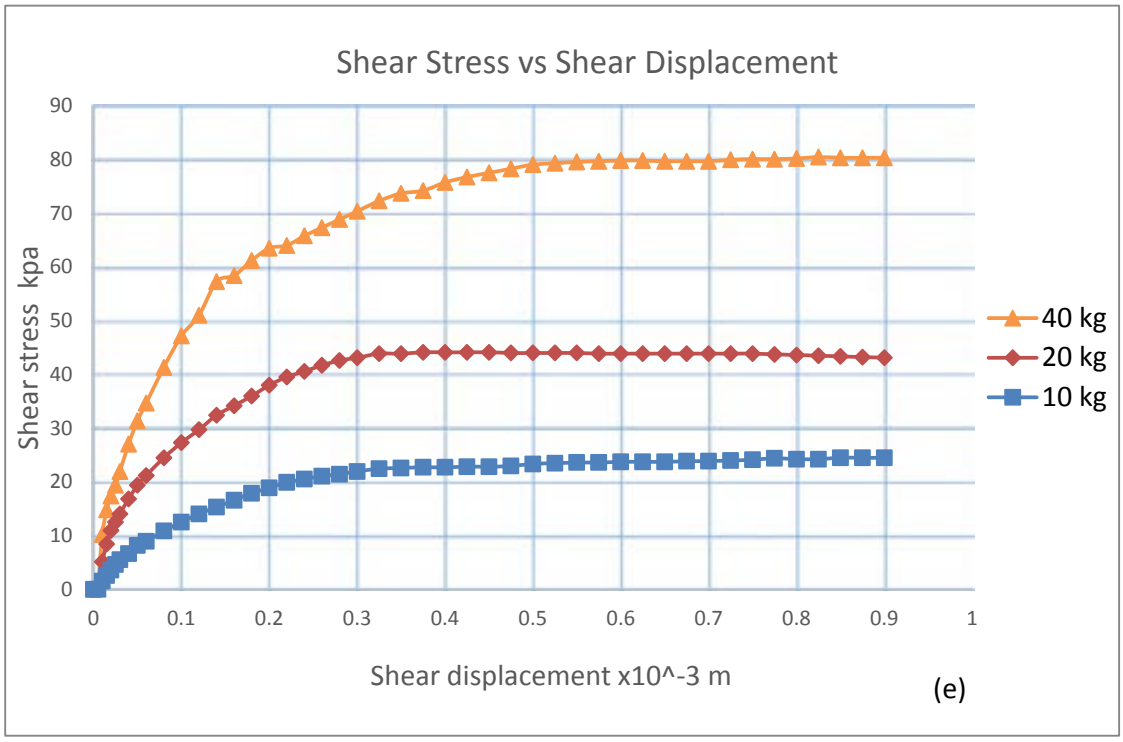

Figure 3.10: Shear Stress vs. Shear Displacement curve for (a)Sample 01 (b)Sample 02 (c)Sample 03 (d)Sample 04 (e)Sample 05

The shear stress vs normal stress values for finding c and Φ values are as follows:

The final data obtained from this laboratory analysis for further software analysis is provided below:

Sample No.	C (kPa)	Φ (degree)	Density (KN/m3)	Saturated Density (KN/m3)
01	15	20.2	19.17	19.42
02	10.5	21.1	19.24	19.67
03	2.73	26.9	18.93	19.95
04	0	31	19.82	20.31
05	4.44	28.9	18.39	18.66

Table 3.4: Parameters obtained from the direct shear test graphs

These data are directly put into the parameter values of the five soil samples for slope stability analysis on GEO5 software using Bishop's simplified method.

The stability of any slope with or without stabilizing techniques is needed to be analyzed using manual calculation or specific software. In this chapter, for our analysis of slopes with synthetic geotextile and bamboo anti-slide pile, a software named GEO5 is going to be used. It is a versatile yet straightforward software for geotechnical issues among which one of the prominent ones is slope stability analysis. In this software, slope with or without retaining structures can be analyzed with various loads and groundwater table location after inputting the soil data. So, in this chapter, the factor of safety of the slope is calculated using Bishop's method and further discussed to check the stability.

4.2 Sub-soil Profile

For our research, five samples were collected from Ukhia Upazila in Cox's Bazar district from different types of dams already constructed. As no field data were collected, in the previous chapter, all the data needed for further analysis were measured in a different laboratory procedure. From those, the following information of the soil is gathered:

Sample No.	Soil Sample Type	Soil Particle Percentage	C (kPa)	Φ (degree)	Density (KN/m3)	Saturated Density (KN/m3)
01	Clay Soil Top	Sand= 1% Silt=81% Clay=18%	15	20.2	19.17	19.42
02	Soft Clay	Sand= 41% Silt=53% Clay=6%	10.5	21.1	19.24	19.67
03	Sandy Clay	Sand= 41% Silt=46% Clay=13%	2.73	26.9	18.93	19.95
04	Sandy Soil	Sand= 89% Silt=10% Clay=1%	0	31	19.82	20.31
05	Sandy Clay	Sand= 45% Silt=47% Clay=8%	4.44	28.9	18.39	18.66

4.3 Factor of Safety Calculation

The factor of safety of the slopes are to be measured with Geotextile is the first phase as an alternative of bamboo and further with bamboo anti-slide piles which were used in the location of dams from which the samples were collected. Changing the parameters for both techniques, analysis of the slopes was done assuming circular slip for both measures of Bishop's method in GEO5.

The factor of safety of the dams, assuming different height with three different slopes for each height with no protective measure is given below:

Sample No	Slope Ht. (m)	FS without any protection		
		1V:1H	1.5V:1H	2V:1H

Table 4.1: Sub-soil parameters of the Soil Samples

1	10	1.18	1.07	1.13
	12	1.08	0.96	1.03
	14	1.45	1.01	0.9
2	10	1.03	0.87	0.89
	12	0.95	0.8	0.81
	14	1.34	0.89	0.73
3	10	0.77	0.56	0.48
	12	0.74	0.54	0.46
	14	0.92	0.71	0.45
4	10	0.12	0.12	0.12
	12	0.12	0.12	0.12
	14	0.13	0.12	0.12
5	10	0.92	0.7	1.33
	12	0.88	0.84	0.58
	14	1.35	1.18	0.84

Table 4.2: Factor of safety chart using all five samples with different slope and slope height

4.3.1 Factor of Safety check using Geo-textile

The kind of Geotextile used for the analysis was Monofilament polypropylene geotextile, which is a prominent kind of synthetic Geotextile available in Bangladesh. As its ultimate tensile strength varies from 16 to 70 kN/m2, taking 16, 24 and 32 kN/m2 as the tensile strength of that with a change in the slope of 1:1, 1:1.5 and 1:2 for heights of 10, 12 and 14 meters, slope stability analysis was done with no presence of excess load or groundwater level.

Dam height 10 m

Tensile strength (KN/m)	1H:1V	1H:1.5V	1H:2V
16	2.08	2.24	2.54
24	2.44	2.73	3.09
32	2.78	3.19	3.92

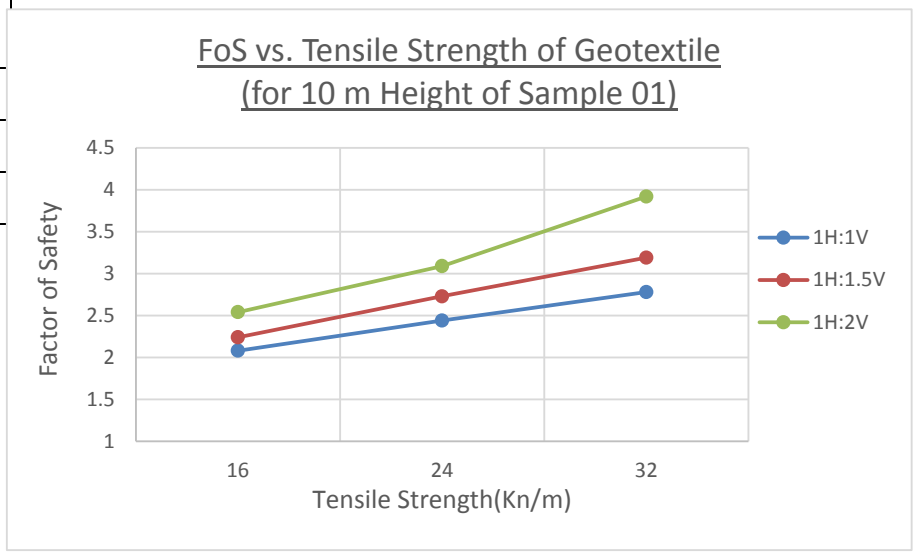

Tensile strength (KN/m)	1H:1V	1H:1.5V	1H:2V
16	1.93	2.07	2.32
24	2.29	2.56	2.87
32	2.64	3.01	3.38

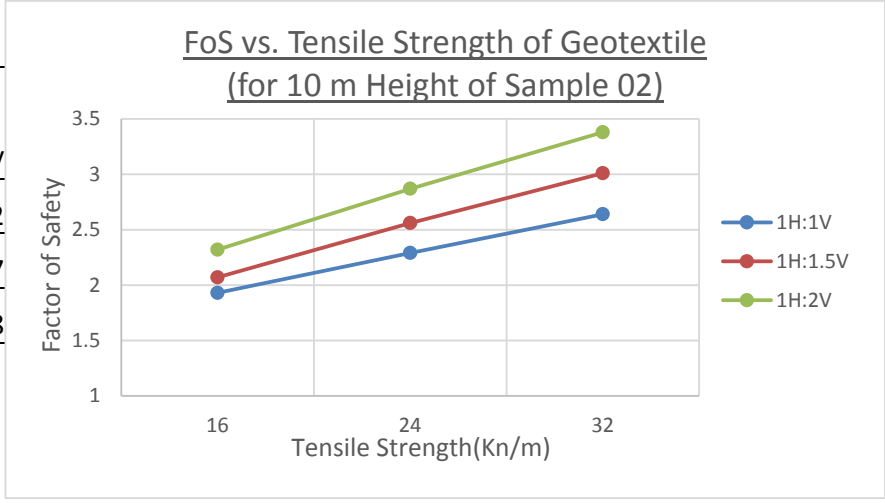

Tensile Strength (KN/m)	1H:1V	1H:1.5V	1H:2V
16	1.17	1.85	1.64
24	1.17	2.41	1.55
32	1.17	2.29	1.39

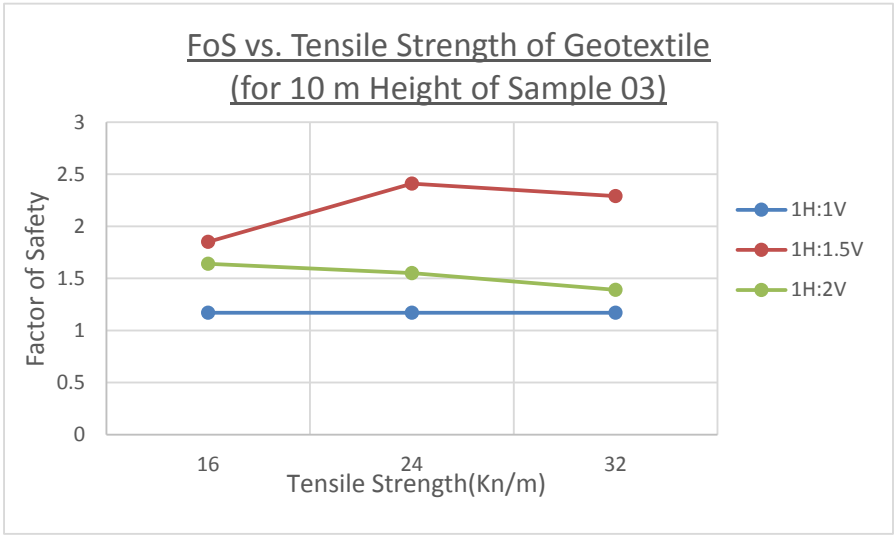

Tensile Strength (KN/m)	1H:1V	1H:1.5V	1H:2V
16	0.17	0.13	1.04
24	0.17	0.13	0.72
32	0.17	0.13	0.98

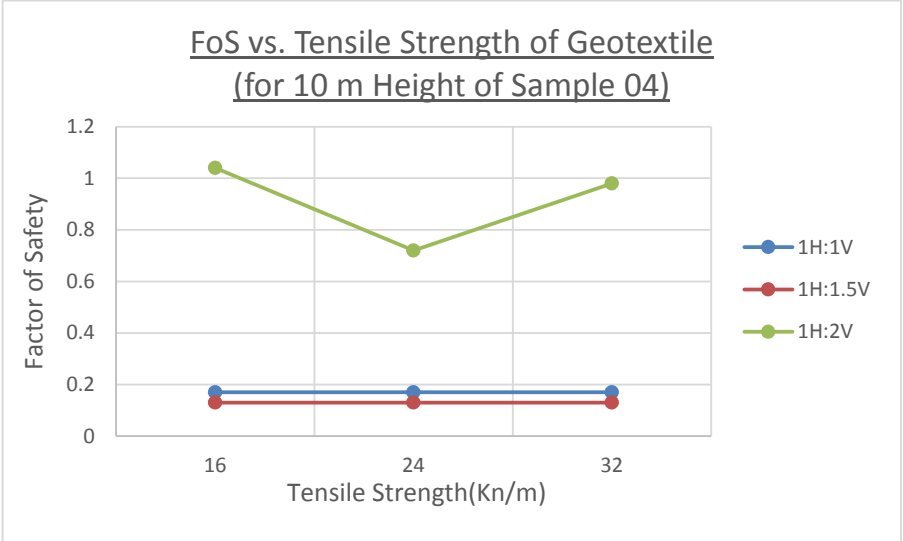

Tensile strength (KN/m)	1H:1V	1H:1.5V	1H:2V
16	1.82	2.07	2.23
24	1.82	2.6	2.23
32	2.15	2.97	2.23

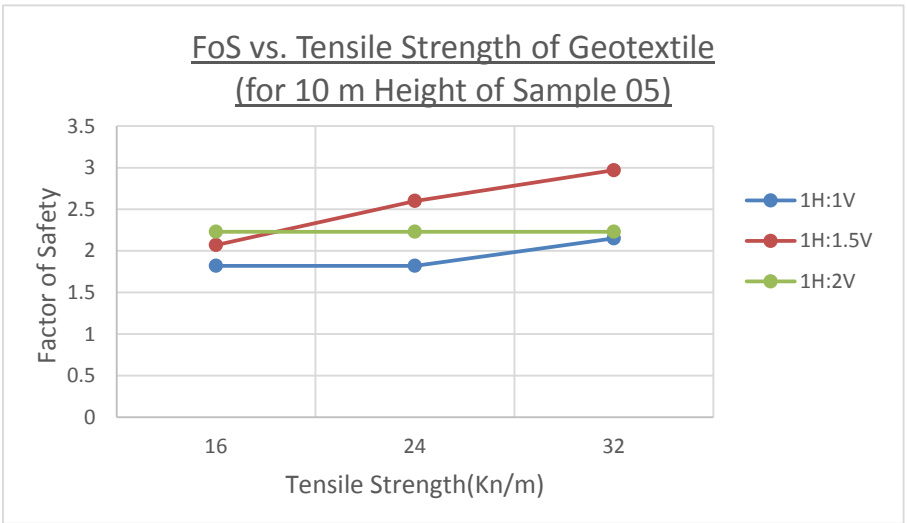

Dam Height 12 m

Tensile Strength (KN/m)	1H:1V	1H:1.5V	1H:2V
16	1.65	1.04	0.91
24	1.97	1.04	0.91
32	2.27	1.04	0.91

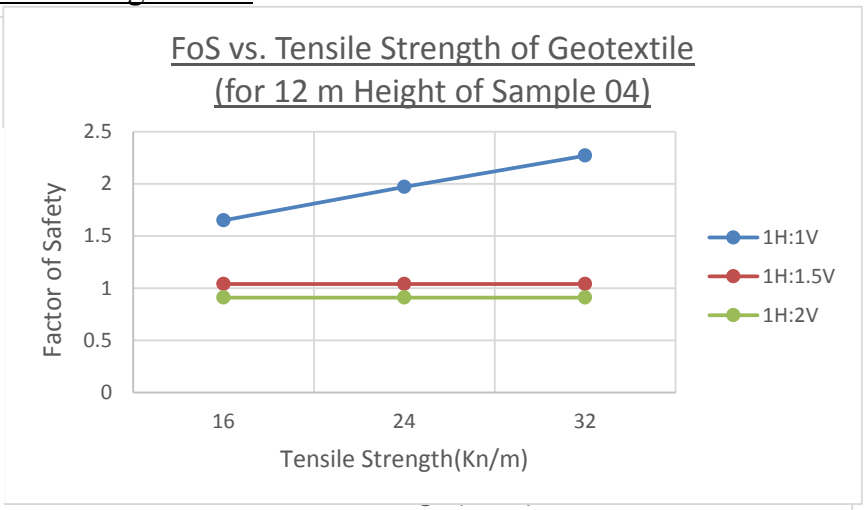

Tensile Strength (KN/m)	1H:1V	1H:1.5V	1H:2V
16	1.77	1.79	1.83
24	2.1	2.36	2.54
32	2.41	2.28	2.1

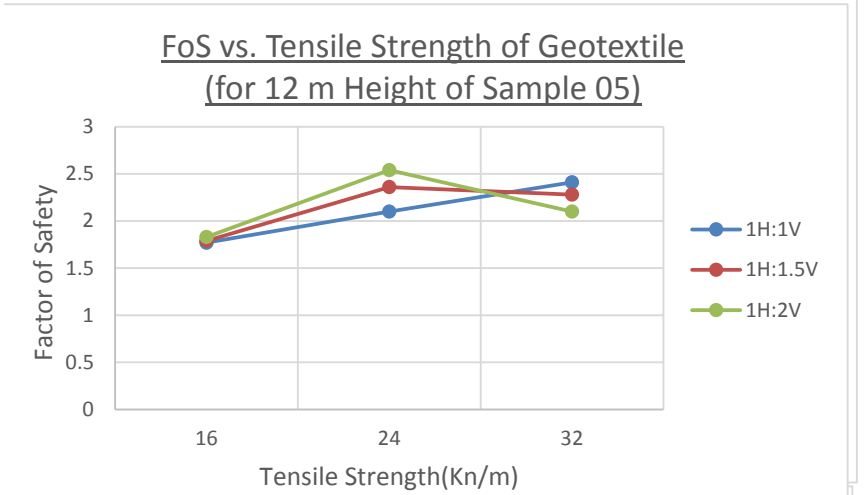

Tensile Strength (KN/m)	1H:1V	1H:1.5V	1H:2V
16	1.66	1.86	2.02
24	1.96	2.3	2.5
32	2.24	2.69	2.95

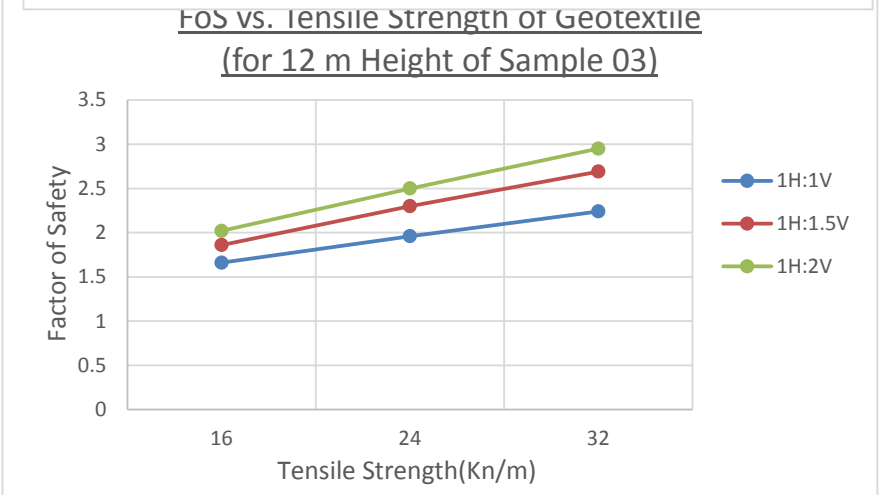

Dam Height 14

Tensile strength (KN/m)	1H:1V	1H:1.5V	1H:2V
16	1.52	1.83	1.92
24	1.79	2.17	2.38
32	2.05	2.43	2.81

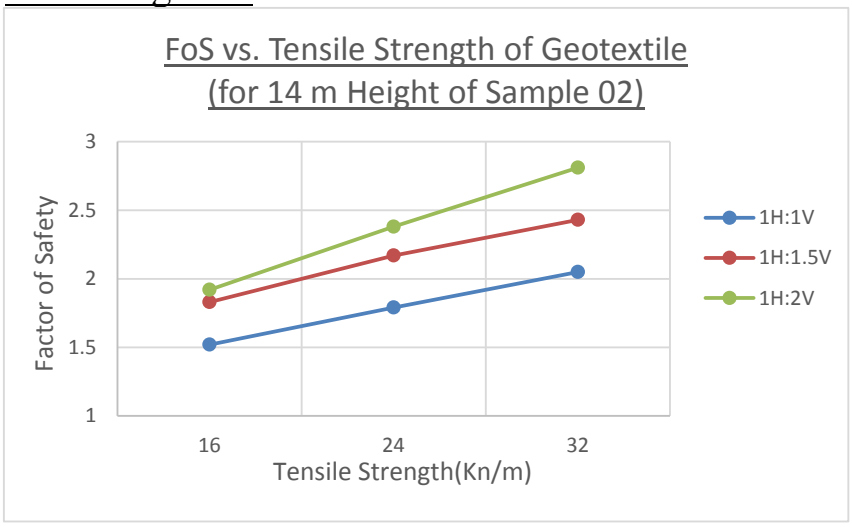

Tensile Strength (KN/m)	1H:1V	1H:1.5V	1H:2V
16	1.51	1.71	1.77
24	1.8	2	2.25
32	2.07	2.38	2.44

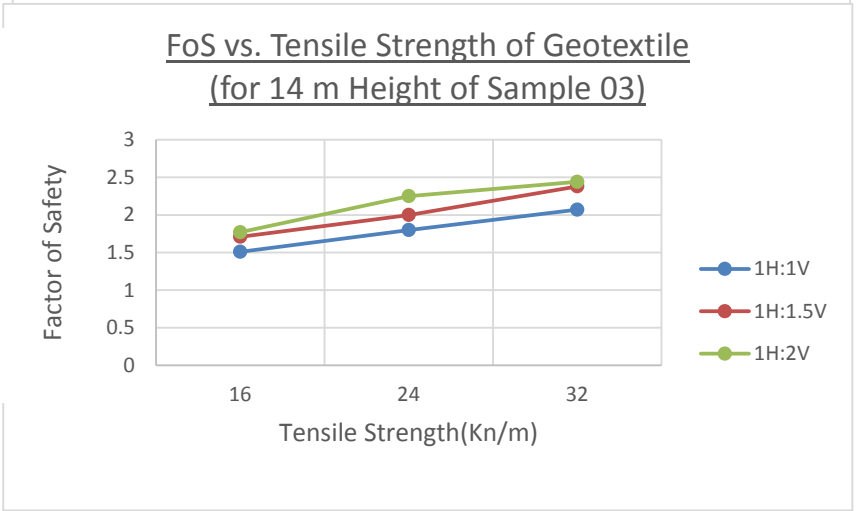

Tensile Strength (KN/m)	1H:1V	1H:1.5V	1H:2V
16	1.57	1.69	1.73
24	1.85	1.99	2.22
32	2.11	2.37	2.32

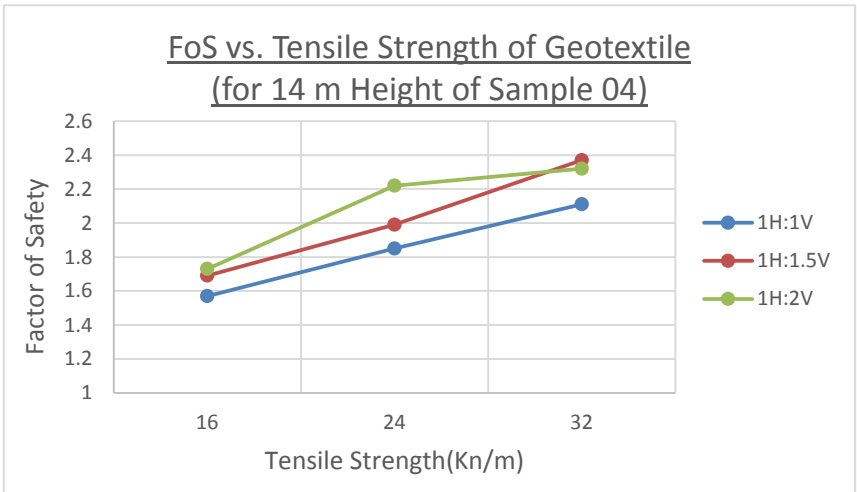

Tensile strength (KN/m)	1H:1V	1H:1.5V	1H:2V
16	1.66	1.86	1.92
24	1.95	2.15	2.43
32	2.23	2.55	2.9

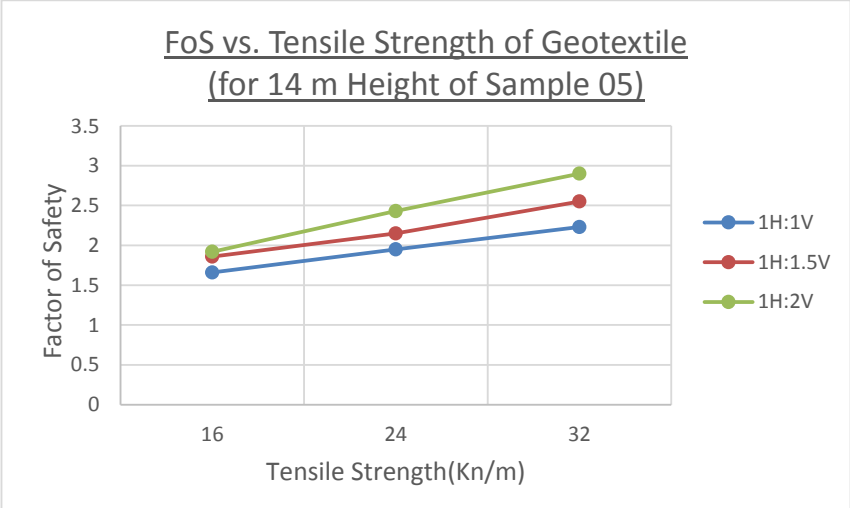

Figure 4.1: F.S vs Tensile strength graph using geotextile for different dam height and slope

4.3.2 Factor of Safety check using Bamboo as Anti-slide pile

As for the focus of our research, bamboo used as an anti-slide pile for slope stabilization is done in this sub-section. Using *Arundinaria gigantia* bamboo with variations of length of 1 m to 4 m with 1 m increment and spacing of 10 cm to 30 cm with 10 cm increment, with the height variation of 10m, 12m and 14 m, each with the change in the slope of 1:1, 1:1.5 and 1:2, slope stability analysis is done using Bishop's simplified method of accounting. No surcharge load or groundwater table criteria were taken into consideration.

Damn Height 10 m

- For slope 1V:1H

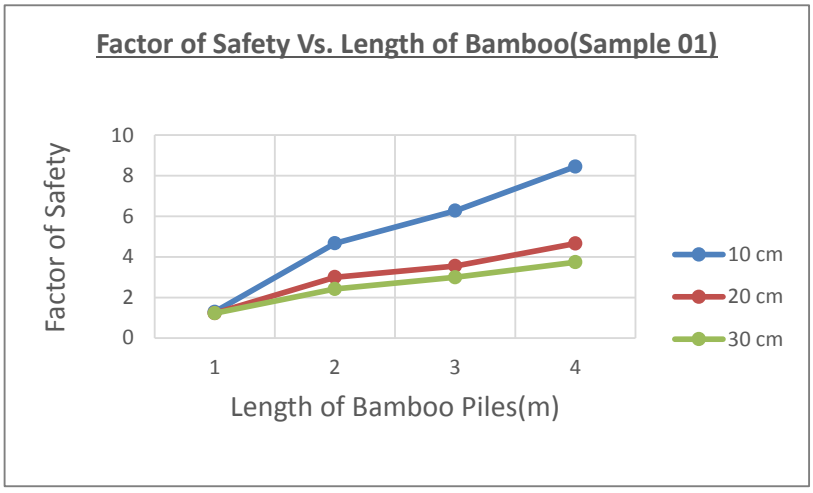

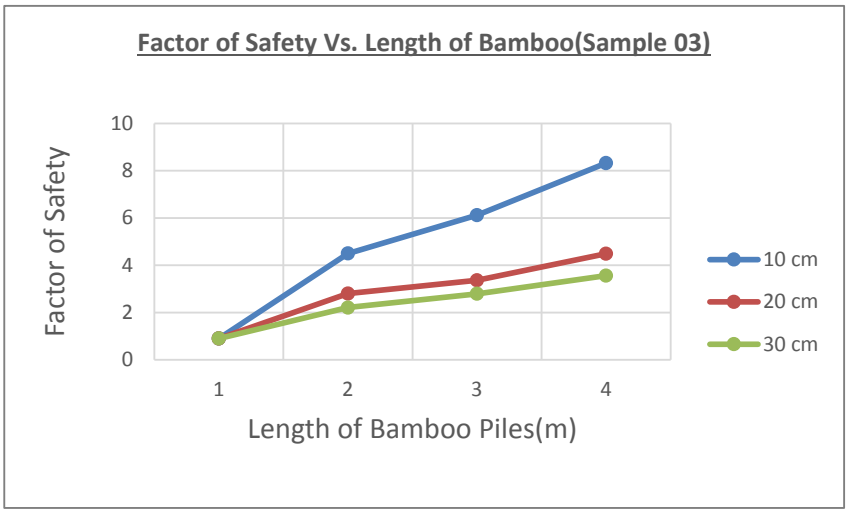
Factor of Safety Vs. Length of Bamboo(Sample 03)
Factor of Safety
10
8
6
4
2
0
1
2
3
4
Length of Bamboo Piles(m)
10 cm
20 cm
30 cm

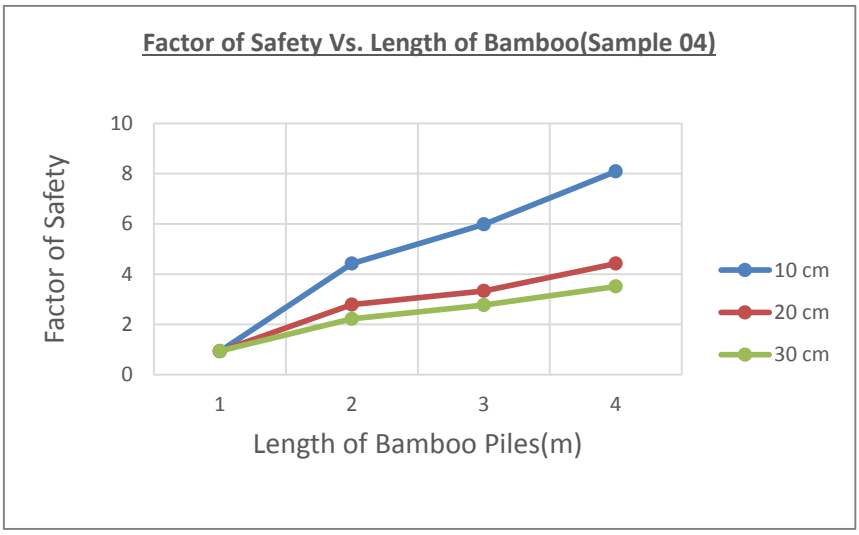
Factor of Safety Vs. Length of Bamboo(Sample 04)
Factor of Safety
10
8
6
4
2
0
1
2
3
4
Length of Bamboo Piles(m)
10 cm
20 cm
30 cm

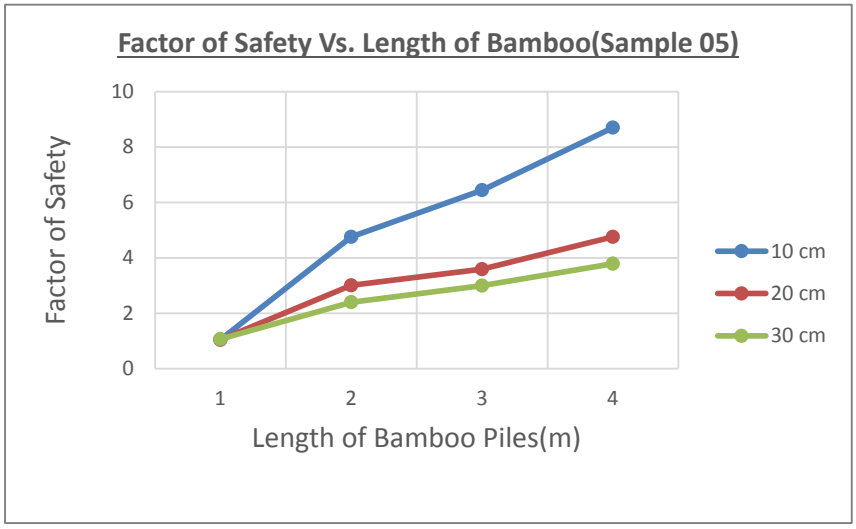

- For slope 1.5V:1H

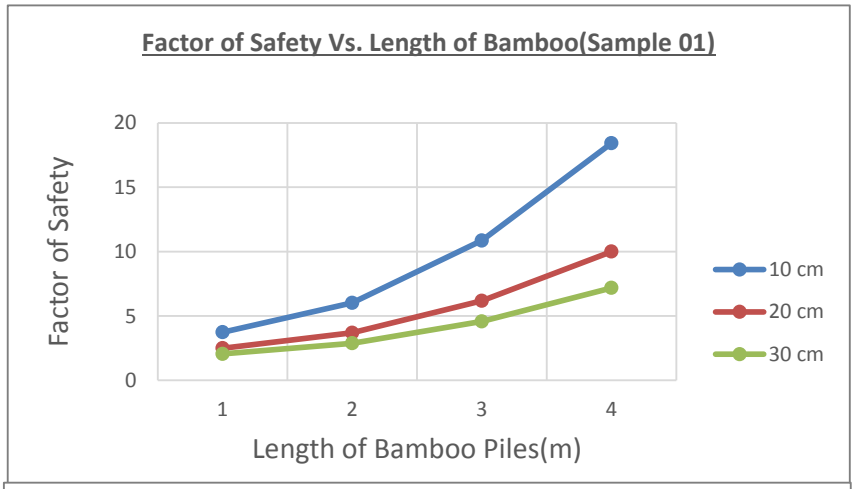

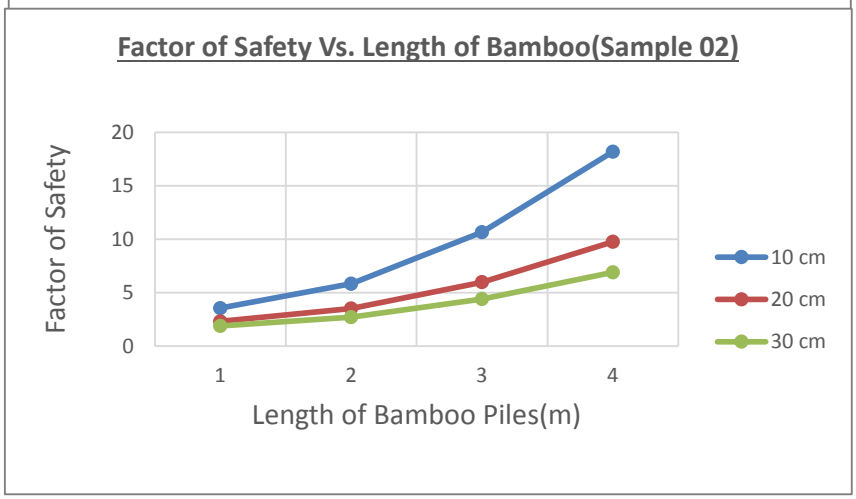

4.4 Concluding Remarks

From the graphs of the factor of safety for both geotextile and bamboo anti-slide pile, a change of pattern of the trendline is seen for the provided parameters. From the laboratory tests and slope stability analysis having software effectiveness of the two slope stability measures were compared. The main concluding remarks of the study are:

a) Five soil samples were collected from the Ukhiya Upazila, Cox's Bazar with no field test conducted and provide for laboratory analysis from which it results that four of them are silty clay with one having high sand properties.
b) The leading cause of slope failure of the constructed structure is found to be landslide as the location is in a hilly area with an adjacent coastal zone with a high amount of salinity.
c) The residing location was provided with bamboo anti-slide piles in the form of symmetric stairs for local availability of bamboo.
d) Synthetic Geotextile with comparison to bamboo anti-slide piles as is regarded as an alternative to bamboo for using as a slope stability technique.
e) Analyzing the chart trends of both bamboo and synthetic Geotextile, it is visible that the charts show an upward trend for varying parameters for both the cases. However, some variations are seen for two samples for having different soil properties than that of others in all cases.
f) Bamboo anti-slide piles show a higher factor of safety comparing with synthetic Geotextile for all the five samples.
g) According to the cost and availability of material, the bamboo used initially as the anti-slide pile will always have a higher chance compared to the alternative of synthetic Geotextile.

BANGLADESH NETWORK
OFFICE FOR URBAN SAFETY

PART-II

COMPARISON OF AXIAL LOAD CAPACITY OF PILES FROM THEORETICAL METHODS AND STATIC LOAD TESTS

BANGLADESH NETWORK OFFICE FOR URBAN SAFETY (BNUS), BUET, DHAKA

Prepared By: Sandip Dey

Mehedi Ahmed Ansary

1.1 Background

Piles are structural members that transmit the superstructure loads to deep soil layers. They are preferred to be used as a foundation material when the shallow foundation is not practical to use it. Piles and pile foundations have been in use since prehistoric times. The Roman wooden piles are a classic example of this. Today piles can be made of wood, concrete, or steel.

Soft soil is very common in many parts of Bangladesh which is not suitable for the construction of a shallow foundation. Pile foundation provides the best possible solution to transfer the load to the deeper harder layers of soil. In Bangladesh, driven piles are used in large numbers because of their various advantages over bored piles; like the high quality of construction, idea of capacity during driving, etc. Recently large diameter cast in situ piles is also used in large numbers for bridge structures and high-rise buildings.

Estimating pile capacity accurately is a difficult job even for the experienced geotechnical engineer. There are many conventional methods for calculating pile capacity, but the selection of each method requires knowledge of soil properties as well as the limitation or applicability of any method in a regional boundary. Traditionally, pile capacity can be evaluated by using a bore log of the subsoil investigation report (Bowles 1997), and then, later it needs to be confirmed by the static load test. As per, static load testing of the driven pile and bored cast in situ pile is very time-consuming and expensive as well as needs constant supervision on operation processes. It is often very difficult to ensure the chances of accuracy and precision. Moreover, the test has several problems like transferring the load to the pile due to frictional errors. Besides, a manual data collection system introduces human error possibilities. In these circumstances, a suitable alternative to static load test or cross-checking options were necessary for foundation engineers. Pile capacity determination is a difficult thing. Several different designs practices here in Bangladesh and internationally exist, but seldom have they given the same computed capacity. Especially, determining the skin friction component is not an easy thing since the soil is not intact after the pile is driven or drilled and loses its intact engineering property (strength). So far, the precise determination of this value has not been possible. Thus, today design offices only believe a load test can only give a reliable capacity of the pile at the time of the test. After installation, the design values, i.e. the load-carrying capacities of piles are usually verified using different methods such as pile loading test and dynamic analysis.

Scientific approaches to pile design have advanced enormously in recent decades and yet, still the most fundamental aspect of pile design - that of estimating capacity –relies heavily upon empirical correlations.

Western researchers provided empirical methods based on extensive explorations and investigations for different types and conditions of soil. Meyerhof (1959) has arranged a speculative relationship between the corrected standard penetration test data and the ultimate axial capacity of driven pile. Also in 1976, he administered another formula for estimating the capacity of bored cast in situ piles based on the behavior of pile in granular soil. Whereas Vesic (1977) modified the bearing capacity factor that (Meyerhof 1976)provided for end bearing of driven pile and bored pile in granular soil founded by the relationship between rigidity modulus and angle of internal friction of soil. The American Petroleum Institute (API) provides a static analysis procedure design developed for offshore construction. These projects almost exclusively use large diameter, open-end, steel pipe piles which are driven by impact hammer to final penetration (American Petroleum Institute 2003). Recently, large-diameter open-end pipe pile usage has increased significantly on transportation projects. This has heightened the need for more accurate nominal resistance estimates on these larger piles. So the design method proposed by API has more significance on large diameter steel piles rather than concrete piles. Tomlinson (1994) studied the behavior of driven piles in cohesive soil specially and established fascinating improvements of the adhesion or sometimes called the reduction factor previously provided by (Peck et al. 1974). As with any design method, the one should also confirm the appropriateness of selected coefficients in a given soil condition with local correlations between static resistance calculations and load test results. American navy in 1982 provided a guideline for offshore and onshore piles design named NAVFAC DM 7.2 and modified in 1984.Also, AASHTO time to time updated their code about pile capacity determination. O'Neill and Reese (1988) studied the behavior of piles in cohesive and cohesion less soil and established an acceptable theory for pile capacity determination later in 2005 AASHTO adopted this theory to their code for bored cast in situ piles.

The study focuses on some of the selected empirical (semi-empirical) and theoretical mathematical models used here in Bangladesh and internationally. To compare the various models, some of the thirty piles have been chosen from different projects all over Bangladesh

including MRT (Mass Rapid Transit) project and Rajuk high rise building project. During the investigation, static load tests are performed to determine the pile capacity. The load tests are performed on single piles.

The study focuses only on the capacity of a single pile under compressive loading. Of course, seldom single piles are used; however, the capacity of group piles entirely depends on the capacity of a single pile within a group. It should be noted that the pile group capacity is not the intension of this study. A pile foundation is much more expensive than spread footings and is likely to be more expensive than mat foundation. Therefore, great care should be exercised in determining the soil properties at the site for the entire depth of possible pile penetration so that it can be accurately detern1ined whether a pile foundation is needed at all and, if so, the design can be optimized so that neither an excessive number nor excessive lengths are specified. This purpose can be achieved in two ways:

1. By taking adequate field and laboratory test programs which will help the designer to estimate the soil properties more accurately to design the foundation more economically.
2. By determining the ultimate carrying capacity of a pile by load test.

1.2 Scope and Objective of the Study

The scope of the project work includes

1) Literature survey the focus is to do an intensive literature survey about empirical and theoretical based practices.

2) Analysis and evaluation

The focus is to compare the empirical and theoretical based mathematical models with pile load test and of the selected piles. The Major objectives of the study are as follows:

i. To compare the ultimate capacity of piles determined by theoretical methods and from a static load, test results in selected areas.

ii. To compare among ultimate pile capacity using different semi-empirical methods for Cast-in-situ and Driven Piles.

iii. To establish a correlation between ultimate theoretical capacity [(Q_{theory})] and capacity determined from static load test [(Q_{test})].

METHODOLOGY

The exact analysis of a pile theoretically is impossible because of the higher degree of indeterminacy and unpredictable behaviors. The pile may be analyzed theoretically in many ways considering the empirical relations and suggestions offered by numerous authors. This chapter deals mainly with the collection of pile data, development of soil model for the estimation of ultimate pile capacity, and discuss the methodology to establish correlations between ultimate pile capacity from static analysis and pile load tests, Figure 3.1 gives a flowchart, which explains different components of this study.

3.2 Collection of Data

Sub-soil investigation reports and corresponding pile load test results have been collected from twenty-two projects all over the country. Among these projects, from twelve projects fifteen precast piles have been tested and from ten projects fifteen cast-in-situ piles have been tested. The tests are performed between 1997 to 2018 and funded by the Public Works Department (PWD), Bangladesh, RAJUK, R&H Department, Bangladesh, and Dhaka Mass Transit Company (MRT). Almost 70% pile load tests are carried out under the direct supervision of the Department of Civil Engineering, BUET, and the rest of the pile load test carried out by Icon Engineering Services, Dhaka. The approximate geographical locations of the projects are shown in Fig. 3.2. Although most of the data are obtained from BUET, PWD, and Icon Engineering Services, Dhaka. The author felt the necessity of proper data archiving under a central national Organization such as BUET for future research purposes.

.3 Idealization of Soil Data

Identical borehole locations and test piles have been identified. For the estimation of ultimate pile capacity in the static method, the total soil strata have been divided into some reasonable

layers with specified soil properties. For the convenience of soil modeling, non-plastic silt is assumed as cohesion less soil and plastic silt assumed as cohesive soil. Field SPT value determined every one-meter interval. But for simplicity here average SPT value of every layer has to be used. The precast piles are indexed as PTP-1, 2, 3 etc. and the cast-in-situ piles are indexed as CTP-1, 2, 3 etc. The soil models together with other relevant information of the piles are presented in table 3.2 and 3.3 and Appendix A.

3.4 Analysis of Data

The principle approach used to calculate the pile's capacities to resist the compressive loads is the static or soil mechanics approach. During the past years, more research work is done to express a method based on the practical soil mechanics theory. For example, the calculation of skin friction on a pile shaft was based on a simple relationship between the effective overburden pressure, the drained angle of shearing resistance of the soil, and the coefficient of earth pressure at rest, but they realized through the results of the practical tests and researches that the coefficient of earth pressure must be modified by a factor takes into consideration the installation method of the pile.

In the same way, the calculation of the pile end bearing resistance was based on the undisturbed shearing resistance of the soil at the pile toe level, but they recognized the importance of the pile settlement at the working load and methods have been evolved to calculate this settlement, based on elastic theory and considering the transfer of load in shaft friction from the pile to the soil. A pile is subjected to a progressively increasing compressive load at a steady rate of application, the resulting load - settlement relationship plotted in Fig. 3.4. There is a straight-line relationship up to point A on the curve, this is means if the load released at any stage up to point ‘A’ the deformation or settlement of the pile head will return to its original condition. when the loading increased beyond point ‘A’ the relationship will have changed from linear to a nonlinear relationship, and there will be yielding at the pile-soil interface till reaching the maximum shaft friction 'point ‘B’. In case of load releasing at this stage, the pile head will have reached to point ‘C’. and the distance ‘OC’ will be the movement required to mobilize the maximum pile shaft resistance, usually, this distance is equal to 0.3% to 1% of the pile diameter. The pile base resistance requires more downward movement to full mobilization, point 'D', that movement is based on the pile diameter, and it is ranged between 10% to 20% of the pile diameter after point 'D' the pile will move downward without any increase in the load "failure point" in figure 3.4.

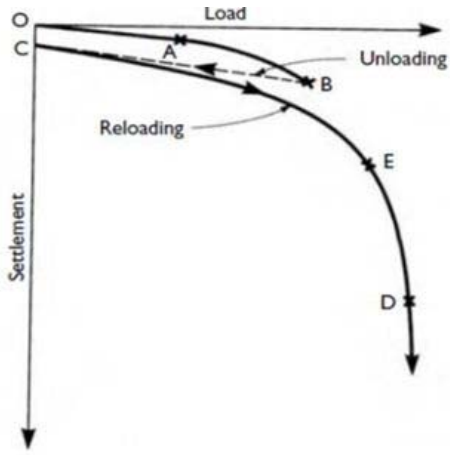

Figure 3.4: Load /settlement curve for the compressive load to failure on a pile

The exact calculation of the load-carrying capacity of a pile is a complex matter, which is based partly on theoretical concepts but mostly on empirical methods based on experience. The practice of calculating the ultimate load-carrying capacity of a pile based on the principles of soil mechanics differs greatly from the application of these principles to shallow spread foundations.

The conditions, which govern the supporting capacity of the pile foundation, are quite different. No matter whether the pile is installed by driving with a hammer, by jetting, by vibration, by jacking, screwing or drilling, the soil in contact with the pile face from which the pile derives its support by skin friction and its resistance to lateral loads, is completely disturbed by the method of installation. Similarly, the soil beneath the toe of a pile is compressed or loosened to some extent which may affect significantly its end bearing resistance. Changes take place in the conditions at the pile-soil interface over periods of days, months, or years which materially affect the skin friction resistance of a pile.

3.4.1 Pile Load Capacity from Static Analysis

Static analysis methods estimate shaft and base resistances separately and differently. For shaft resistance, in cohesive as well as non-cohesive soils, considerable uncertainty and debate exist over the appropriate choice of the horizontal stress coefficient, Ks. Normally, bearing capacity theory is applied to estimate base resistance in non-cohesive soils. However, the theory involves a rather approximate Φ-Nq relationship coupled with the difficulty of determining a reliable and representative in-situ value of the Φ angle and the assumption of a

proper shear failure surface around the pile tip. This creates doubts about relying on the bearing capacity theory in pile foundation design. Design guidelines based on static analysis often recommend using the critical depth concept. However, the critical depth is an idealization that has neither theoretical nor reliable experimental support and contradicts physical laws. For static analysis, few selected methods have been used to predict the ultimate capacity of driven and cast-in-situ bored piles. These methods are described elaborately in chapter two. For analysis purposes, the saturated and dry unit weight of soil obtained from the chart referred by Bowles (1977) is based on the SPT value of soil. For calculating the effective stress and total stress using the unit weight of every layer of soil individually and this value obtained from table 3.1 and figure 3.4. Different formulas have been used to compute the skin friction and end bearing of piles as per the early described methods. The Sum of the end bearing and skin friction of a single pile is the ultimate capacity of that pile. For a given soil condition different methods predict the different ultimate capacity of the same piles due to the postulation criteria of the methods. This has been discussed in chapter two and some of the points will be discussed in chapter four. Some of the calculation sheet attached in Appendix-C.

3.4.2 Pile Load Capacity from Pile Load Tests

Different criteria for obtaining ultimate pile load capacity from pile load test results are mentioned in chapter two. In this study, load settlement curves (sample curve is shown in Appendix-B) from pile load test results are used to find out the ultimate capacity of the pile by Davisson offset method, Indian Standard and BNBC Code. Davisson offset method is probably the best known and widely used in North America and other regions worldwide because it provides the lowest estimate of axial compression capacity from the actual load-settlement curve and for this versatile use of the Davisson offset method influenced the author to take as the ultimate capacity of piles for analysis. The other two methods have to use to show their validation. Generally, all three methods give almost nearly ultimate capacity, but the settlement of piles differs from one method to another. In Appendix-A load test results and corresponding settlement are presented. In chapter two we already discuss the load test methods and their theory. In some projects extrapolated load settlement curves for Test and Services piles are used for this purpose to determine the failure load. The validity of the extrapolated load settlement curve has been justified with some of the known load settlement curves. And it found the very little amount of error (+/-10%).

3.4.3 Data for Further Analysis

After obtaining ultimate capacities from both static and load test results, Table 4.2 is compiled for precast piles and Table 4.1 is compiled for cast-in-situ piles. From the twenty-two projects, fifteen results for precast pile and fifteen results for cast-in-situ piles are obtained. For all the pile load tests, settlement corresponding to the ultimate capacity of the piles obtained from load settlement curves by the early mentioned methods and are shown in Table 4.1 and 4.2.

3.5 Statistical Analysis

For comparison of the prediction of the pile's bearing capacity estimation approaches and evaluation of their accuracy and efficiency, the Rank Index, RI was utilized. This index is calculated as follows:

RI=R1+R2+R3+R4+R5

Where

R1 is the rank of the method based on the highest value of the coefficient of determination of Qp/Qm, R2 and R3 are the methods rank based on statistical analysis using the arithmetic mean and standard deviation, R4, and R5 is methods rank based on cumulative probability analysis. The lower the RI, the more precise would be the method. Analyses of residual error, the difference between observed and predicted values, can be used to evaluate method performance by characterizing, i.e., systematic under or over-prediction. In this approach, the Coefficient of Determination (COD) or modeling efficiency is employed to check the compatibility of predictions and measured values. COD is measured by equation 3.1.

$$COD=1-\frac{\sum_{i=1}^{n}(Qpi-Qmi)2}{\sum_{i=1}^{n}(Qmi-Qma)2} \quad (3.1)$$

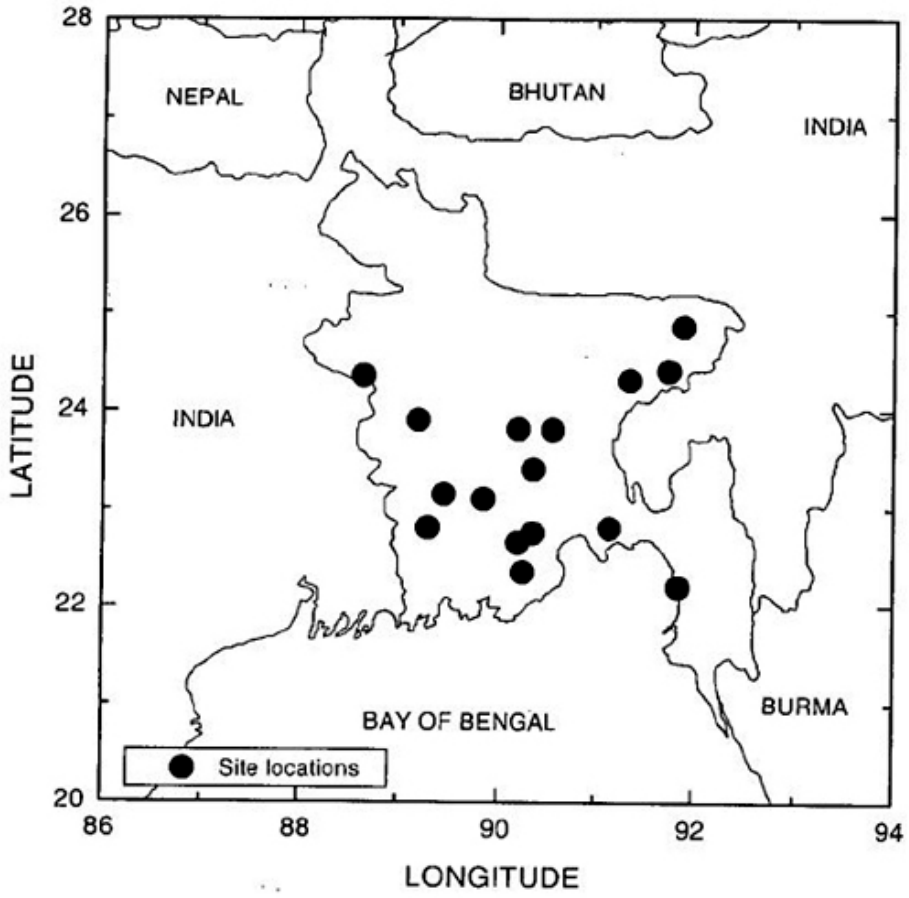

Figure 2 Geographical locations of pile load tests and soil borehole

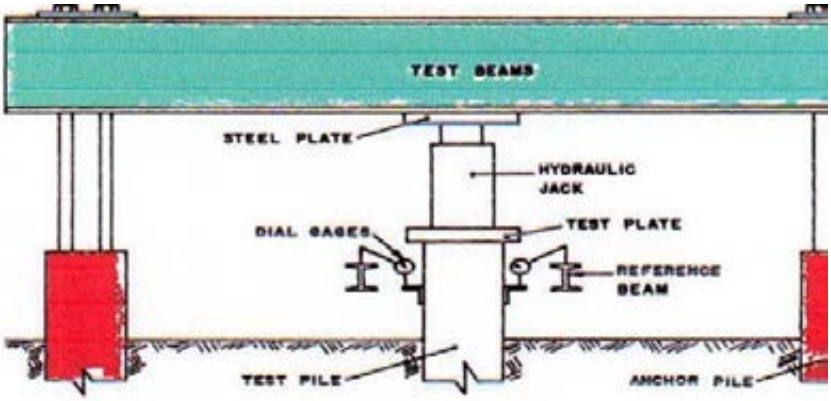

Figure 3.6: Schematic arrangement of the static load test.

RESULTS AND DISCUSSIONS

In this study, the main focus is to determine the compressive load capacity of piles using different existing methods of pile capacity estimation and compare with static load test. In this chapter, pile capacity calculation was done based on the Meyerhof (1976), NAVFAC DM 7.2 (1984), AASHTO (1986), O'Neil & Reese (1988), and Decourt (1995) methods for cast-in-situ bored piles and Drilled Shafts. And for calculation of capacity of driven piles based on Meyerhof (1976), API RP 2A (1993), Tomlinson (1994), Norwegian Pile Guideline (2005) and Indian Standard (2010) methods. For the selected fifteen precast driven pile eight cast in situ bored pile and seven Drilled shaft capacities was predicted and later compared with static load test. The later part of the study uses compared data for capacity and correlate with prediction and measured capacity for precast and cast in situ piles and Drilled shafts. Based on these compared (prediction and measured capacity) data selection of best theoretical methods for predicting the capacity of precast driven piles and cast in situ bored piles and Drilled shafts.

4.2 Determination of Pile Capacity by Theoretical Methods

4.2.1 Precast driven pile

In this study, fifteen numbers of precast driven piles have been selected from different projects all over Bangladesh in the time 1998 to 2018.By using the following methods their ultimate capacity has been measured. It has been discussed elaborately on the following methods in chapter two for both cohesive and cohesion less soil. The methods are:

- Meyerhof (1976)
- API RP 2A (1993)
- Tomlinson (1994)
- Norwegian Pile Guideline (2005)
- Indian Standard (2010)

Summary of the predicted ultimate capacity of fifteen Precast drivren piles shown in table 4.2 The detailed calculation of these fifteen driven piles is included in the Appendix.

4.2.2 Cast in Situ Bored Pile and Drilled Shaft

In this study, eight numbers of the cast in situ bored piles and seven numbers of drilled shaft have been selected from different projects all over Bangladesh in the time 1998 to 2018.By using the following methods their ultimate capacity has been measured. It has been discussed elaborately about the following methods in chapter two for both cohesive and cohesionless soil. The methods are:

- Meyerhof (1976)
- NAVFAC DM 7.2 (1984)
- AASHTO (1986)
- O'neil & Reese (1988)
- Decourt (1995)

Summary of the predicted ultimate capacity of eight casts in situ bored pilesand seven drilled shafts shown in table 4.1. The detailed calculation of these fifteen bored piles is included in the Appendix.

4.3 Determination of Pile Capacity from Load Test by Different Standards and Methods

The load was applied to piles in stages up to 200% to 300% of the design load. Pile settlement in mm against applied load in tons has been plotted for piles (Appendix-3). To measure the ultimate vertical load-carrying capacity of the test piles the following methods are followed. These are

(i) Davisson's offset limit method- In Davisson's (1973) method, the failure load is defined as the load corresponding to the movement which exceeds the elastic compression of the pile, when considered as a free column, by a value of O.I 5in. plus a factor depending upon the diameter of the pile. This critical movement can be expressed as follows:

$$S_r = S + (0.15x25.4 + 0.008D) \quad (4.1)$$

Where, S_r is the movement of the pile head (in mm), D is the pile diameter or width (inmm), and S is the elastic deformation of the total pile length (in mm). In this study to calculate the elastic compression of the pile the Modulus of Elasticity of the concrete (Ec) has been taken as

$$E_c = 57000\sqrt{f'c} \quad (4.2)$$

Where, Ultimate compressive strength of the concrete, fc' = 4000 psi

(ii) Indian Standards (IS) code (1979) recommends that the ultimate capacity of pi Ie is smaller of the following two-

a) Load corresponding to a settlement equal to 10% of the pile diameter
b) Load corresponding to a settlement of 12 mm

The same code states that the allowable pile capacity is smaller of the following:

a) Two-thirds of the final load at which total settlement is 12 mm.
b) Half of the final load at which total settlement is equal to 10% of the pile diameter.

(iv) The Bangladesh National Building Code (1993) recommends that the allowable load capacity of the pile shall not be more than one half of that test load which produces a permanent not settlement (i.e. gross settlement less rebound) of not more than 0.00028 mm/kg of test load nor 20mm. The result of load tests on piles under this study is presented in table 4.1 andtable4.2. And compare of each pile with predicted theoretical capacities presented in table 4.1 and table 4.2 Appendix.

4.3.1 Analysis of Load–Settlement Curves

As the load tests used in this study out of thirty piles (fifteen of the precast and fifteen of the cast in situ) ten numbers of piles (seven of bored piles) were not carried to failure which would have facilitated determination of the precise value of the ultimate load capacity of the piles, a method of extrapolation of load settlement curves has been used to estimate as nearly as possible; the failure load from load settlement curves. The assumptions used in the extrapolation are;

Load settlement curves follow the trend of a parabola after an initial straight portion. The piles under this study predominantly end bearing with a low to moderate contribution of frictional resistance. Before applying the extrapolation method, a clear idea of the nature of the load settlement curves of different types of piles is needed. The following discussions are provided to fulfill the above objective. As cited by Peck et al. (1980) the results of typical load tests are shown in fig. 4.1 in which the total load is plotted as a function of the settlement of the pile head. Curve 'a' represents a pile that slipped or plunged suddenly when

the load reached a definite value termed as the ultimate pile load or pile capacity. The nature of the curve indicates that the pile under test is a friction pile with negligible end bearing. Curve ‘b’ does not show a well-defined break as in curve "a" and continues to penetrate the ground showing a predominant contribution of the end bearing. Curve 'c' on the other hand takes a parabolic shape after an initial straight portion showing both the contribution of friction and end bearing.

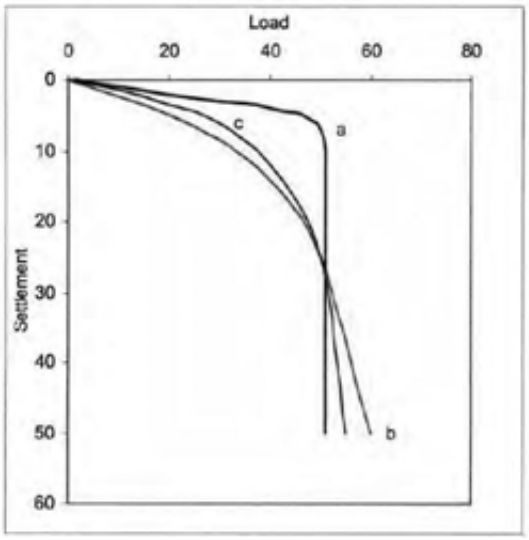

Figure 4.1: Typical results of load test on (a) friction pile, (b) end bearing pile and (c) pile deriving support from both end bearing and friction

Analysis of the bearing capacity of piles by static methods under this study in Chapter two shows that the piles are predominantly base resistance but has a good contribution from the friction since the embedded depth of the piles in layered soil. Thus, the piles of which the load test results are being discussed fall in the group 'c' as discussed in this section earlier.

4.3.2 Procedure of Extrapolation

- Step-1: With a careful examination of the load settlement curve, the parabolic portion of the curve is selected.

- Step-2: The general equation of the curve is taken as y =ax^2-+bx+e, where a, b, c are constants. Taking any three points on this curve the constants can be detel1nined. Therefore, the equation of the parabola is established.
- Step-3: With this equation the curve can be extrapolated up to the next load increment in the load settlement plot.
- Step-4: Using any three points on the extrapolated curve, another equation of parabola can be established. With this equation, the curve can be extrapolated up to the next load increment in the load settlement curve. Following the above procedure, the load settlement curves can be plotted up to a distinct break and using this curve estimates can be made of ultimate pile capacity using recommendations and standards as for full-scale load tests carried to failure. some of the extrapolated load settlement curve shown in figure 4.2.

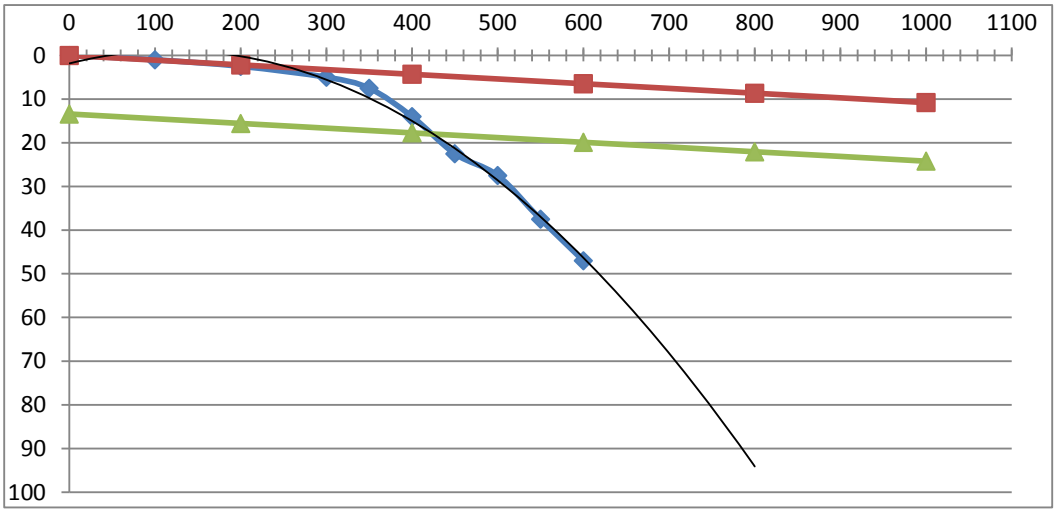

Figure 4.2 (a): Load settlement curve of CTP-12 (Postogola under Pass)

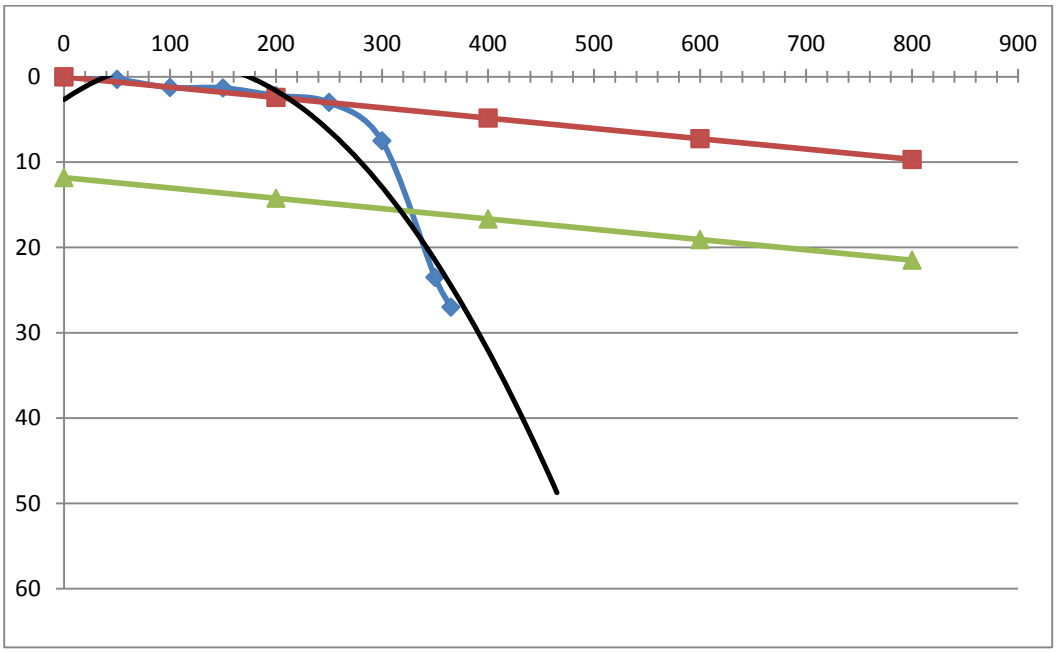

Figure 4.2(b): Settlement curve of CTP-15 (Shibpur Bridge, Tangail)

Figure 4.2(a) and 4.2(b) shown that the extrapolated value is almost like the actual failure load. This gives a validation of extrapolation methods for the other eight pile's load settlement curves.

4.4 Statistical Analysis

For comparison of the prediction of the pile's bearing capacity estimation approaches and evaluation of their accuracy and efficiency, the Rank Index, RI was utilized. This index is calculated as follows:

$$RI=R1+R2+R3+R4+R5 \quad (4.3)$$

Where R1 is the rank of the method based on the highest value of the coefficient of determination of Qp/Qm, R2 and R3 are the methods rank based on statistical analysis using the arithmetic mean and standard deviation, R4, and R5 is methods rank based on cumulative probability analysis. The lower the RI, the more precise would be the method. Fig. 4.3(a) and 4.3(b), illustrates the variation of the predicted capacities with measured capacities for different methods. According to this figure, the solid line in each diagram reveals perfect

agreement between predicted and measured pile capacity passing the origin with a slope equal to unity. Analyses of residual error, the difference between observed and predicted values, can be used to evaluate method performance by characterizing, i.e., systematic under or over-prediction. In this approach, the Coefficient of Determination (COD) or modeling efficiency is employed to check the compatibility of predictions and measured values. CODismeasured by equation 4.4.

$$\text{COD}=1-\frac{\sum_{i=1}^{n}(Qpi-Qmi)2}{\sum_{i=1}^{n}(Qmi-Qma)2} \quad (4.4)$$

Where,

*Qpi*and*Qmi*are the predicted and measured values, and Qmais the mean of the measured values, respectively, and n is the number of samples. The COD provides a dimensionless statistic summary very similar to the coefficient of determination, R^2 from linear regression. It has been similarly interpreted as the proportional reduction in variation of observed values around the model expectation to variation around the observed mean value. Note Qmrepresents the "worst-case" regression line (slope = 0) indicating a lower bound of 0 for R^2, but Loehle pointed out that no such lower bound exists for COD. In the case of 100% accuracy in method predictions, the COD will be equal to one. The arithmetic average (μ) and standard deviation (σ) of the Qp/Qm values were calculated and utilized as a second-ranking criterion. The closer the arithmetic averages to one, the lower the methods prediction's error. Also, the closer the standard deviation to zero, the lower the scatter of the predictions.

The third approach employed to evaluate the accuracy of methods is the cumulative probability measure. According to the cumulative probability approach, the ratio of the predicted value (Qp) to the measured value (Qm) has been drawn versus cumulative probability. For a series of numerals, Qp/Qm has been set ascending and indexed with 1 to n. Then for each of the relative amounts, the cumulative probability factor has been calculated as follows:

$$P(\%)=\frac{i}{n+1}X100 \quad (4.5)$$

Where P is the cumulative probability factor, iis the index of the considered case, and n is the number of total cases. To determine the convergence or deviation tendency of the output of prediction, the following criteria have been referred: The value of Qp/Qm at the cumulative

probability of 50% is a measurement of the tendency to overestimate or underestimate the pile capacity. The closer to a ratio of unity, the better the agreement. To estimate the average error the following equation can be used:

$$E_{ave} = (\frac{\text{Qp}}{\text{Qm}})_{\%50} - 1$$

The slope of the line through the data points is a measurement of the dispersion or standard deviation. The flatter the line, the better the general agreement. Fig. 4.3 illustrates the cumulative probability analysis in this research.

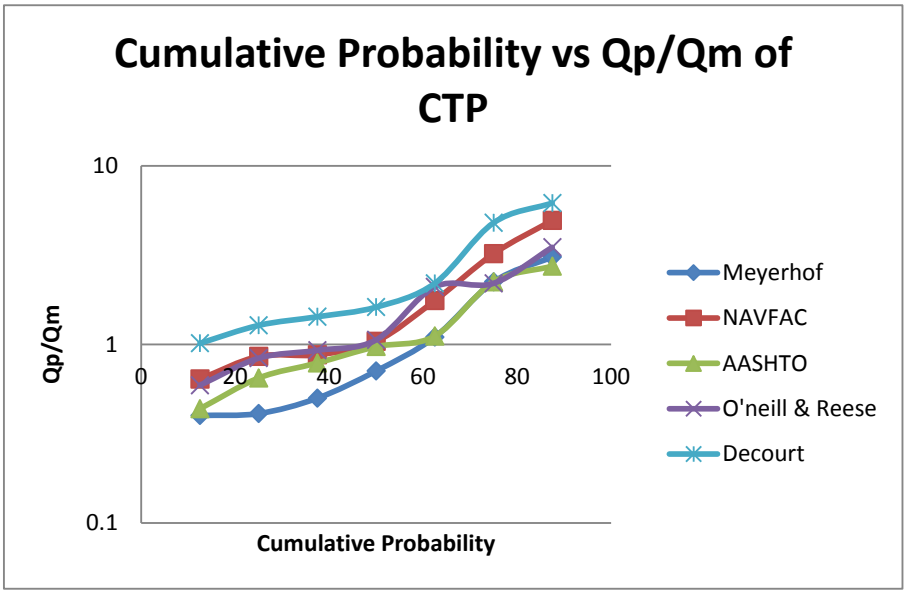

Figure 4.3(a): Cumulative probability for Drilled Shaft in different methods.

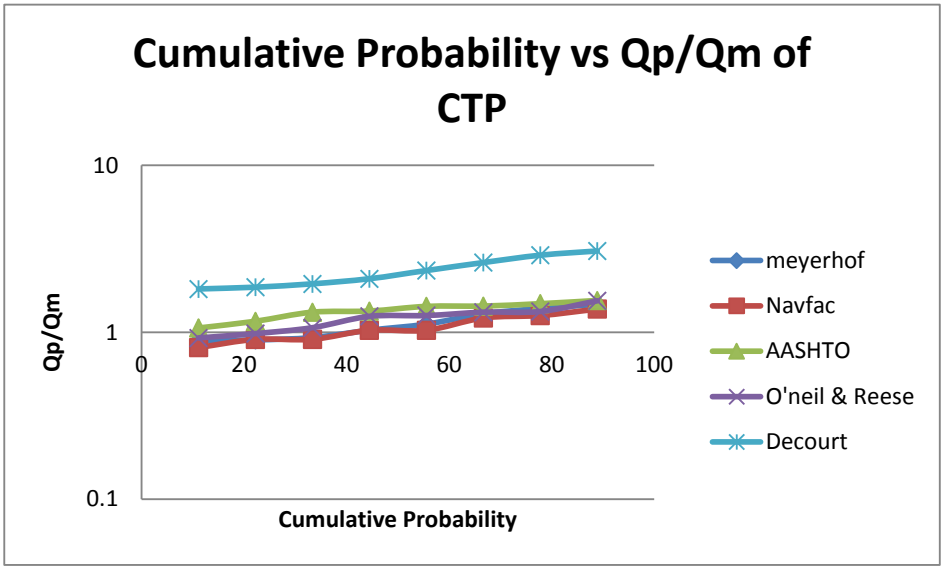

Figure 4.3(b): Cumulative Probability graph for bored pile in different methods.

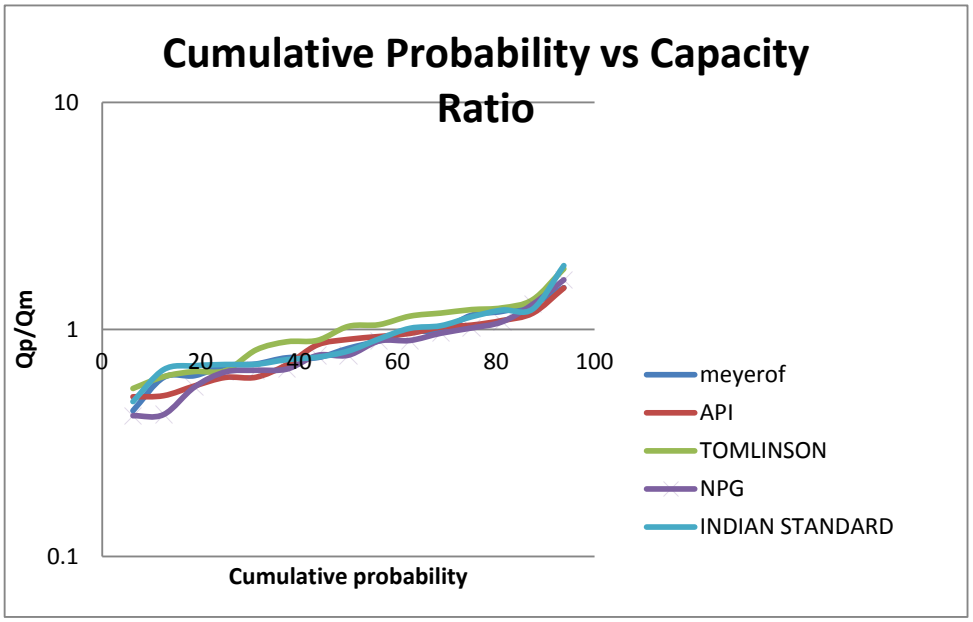

Figure 4.3(c): Cumulative Probability graph for driven pile in different methods.

4.5 Establishment of Correlation

The establishment of a correlation between predicted capacity and measured capacity of PTP and CTP for different theoretical and semi-empirical methods is the goal of this study. For this purpose, Microsoft excel has been used here. A regression equation has been used to compare capacities. The R2 values give this study the compatibility of these regression equations. The value of R2 near to unity gives the most compatible equation. But it does not represent the accuracy of the statics equation to predict the capacity for different methods. This accuracy of the statics equation has been determined by a statistical analysis which has been discussed earlier.

4.5.1 Precast Driven Pile

Meyerhof (1976) Method

Compare the predicted capacity from Meyerhof (1976) method with measured capacity from load test for fifteen numbers of precast driven piles gives a regression equation, Q_p $=0.685Q_m+24.98$ with $R^2=0.935$. High value of R_2 indicates a better correlation between

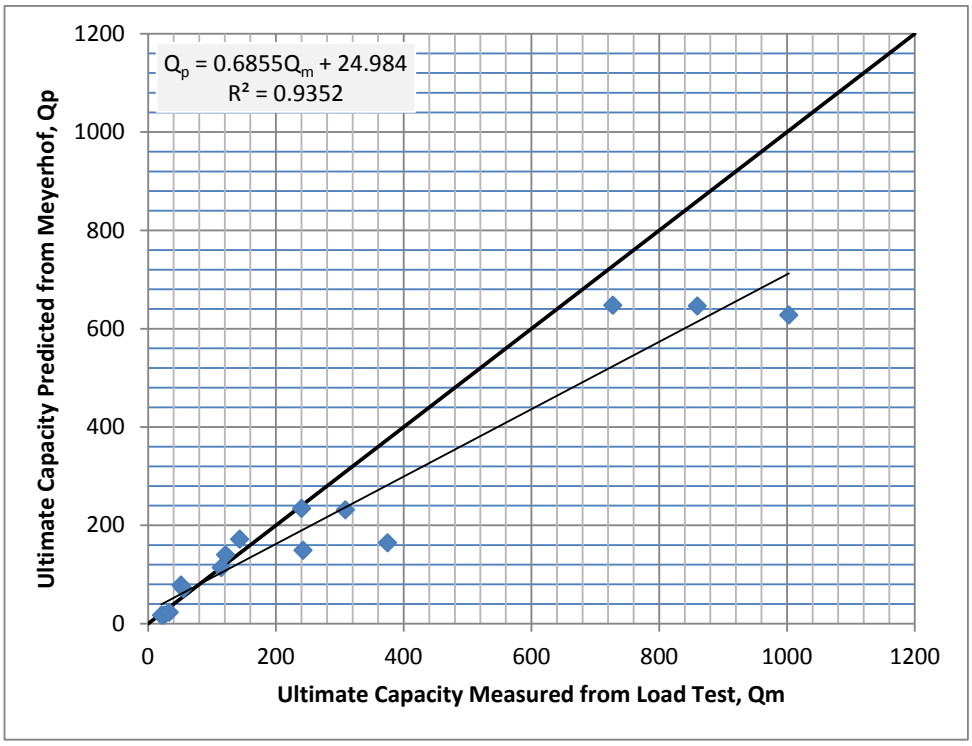

Figure 4.4(a): Correlation between Q_p and Q_m for Meyerhof methods

Predicted and measured capacity. From statistical analysis and cumulative probability (shown in table 4.3), it has been observed that a moderate RI(RI=15) ranked this method third amongst all other methods in precast driven piles. Also, this method predicts to underestimate the ultimate capacity by 17.40%. Figure 4.3(c) justify this error. COD value of 0.824 indicates the good compatibility of the predicted theory. Limiting value of effective stress after 10D for loose sand, 15D for mid dense sand, and 20D for dense to very dense sand recommended by Das control the skin resistance as well as end-bearing capacity. It is one of the major causes of underpredict the capacity.

API RP 2A (1993) Method

Compare the predicted capacity from API (1993) method with measured capacity from load test for fifteen numbers of precast driven piles gives a regression equation, $Q_p = 1.01Q_m - 31.95$ with $R^2 = 0.949$. High value of R^2 indicates a better correlation between

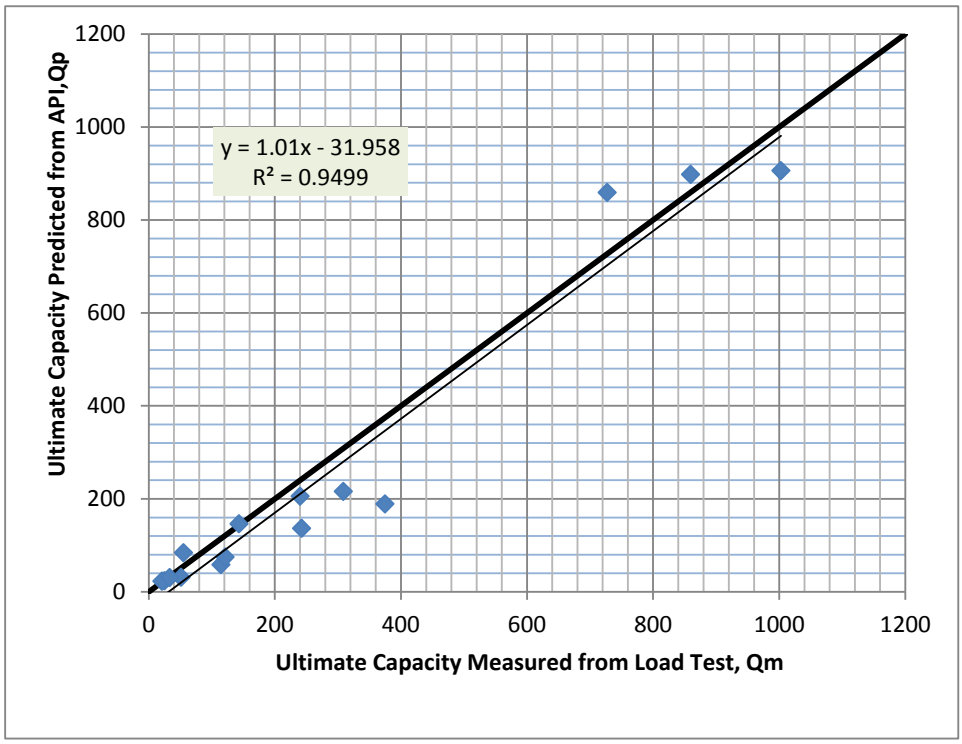

Figure 4.4(b): Correlation between Q_p and Q_m for API methods

Predicted and measured capacity. From statistical analysis and cumulative probability (shown in table 4.3), it has been observed that the lowest RI(RI=10) ranked this method second amongst all other methods in precast driven piles. Also, this method predicts to underestimate the ultimate capacity by 9.60%. Figure 4.3(c) justify this error. COD value of 0.937 indicates very good compatibility of the predicted theory. No such limit for the determination of effective stress. For this large value of end bearing obtained for large displacement piles. But API recommended limiting unit skin friction and limiting unit end bearing keep the ultimate capacity justified with measured capacity.

Tomlinson (1994) Method

Compare the predicted capacity from Tomlinson (1994) method with measured capacity from load test for fifteen numbers of precast driven piles gives a regression equation, $Q_p = 0.752Q_m + 26.67$ with $R^2 = 0.919$. High value of R^2 indicates a better correlation between

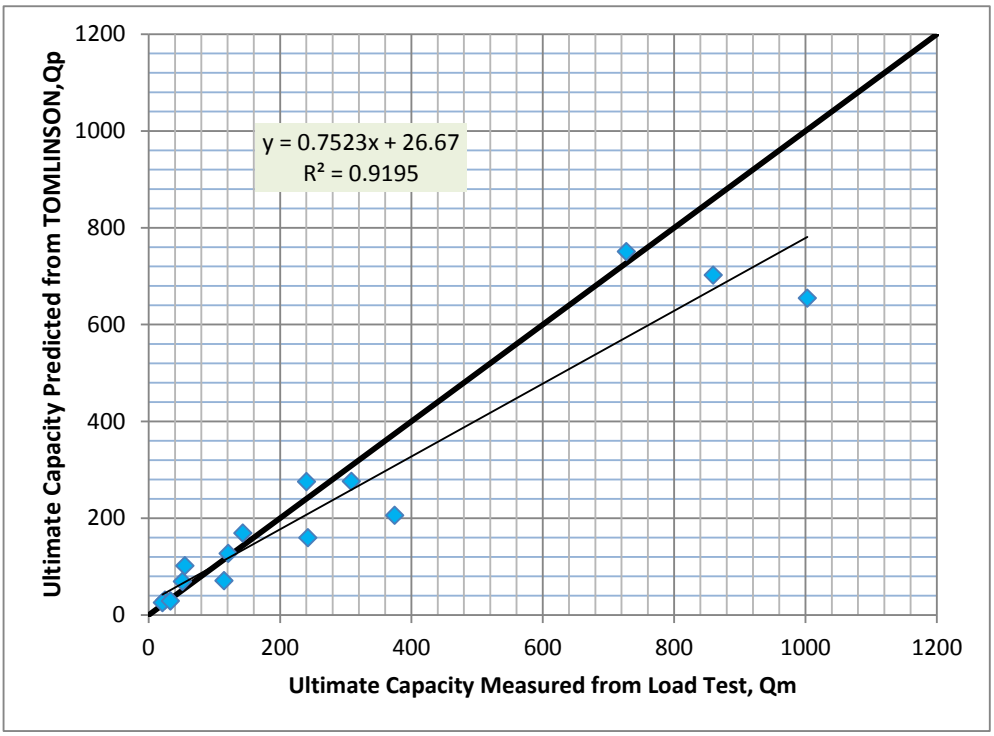

Figure 4.4(c): Correlation between Q_p and Q_m for Tomlinson methods

Predicted and measured capacity. From statistical analysis and cumulative probability (shown in table 4.3), it has been observed that the lowest RI(RI=10) ranked this method first amongst all other methods in precast driven piles. This is the best method to predict the ultimate capacity of precast driven piles with 3.20% overestimation. Figure 4.3(c) justify this error. The COD value of 0.868 indicates very good compatibility of the predicted theory. No such limit for the determination of effective stress. For this large value of end bearing obtained for large displacement piles. But Peck recommended limiting unit end bearing (11mn/m2) adopted by Tomlinson to keep the ultimate capacity justified with measured capacity.

Norwegian Pile Guideline (2005) Method

Compare the predicted capacity from Norwegian Pile Guideline (2005) method with measured capacity from load test for fifteen numbers of precast driven piles gives a regression equation, $Q_p = 0.725Q_m - 0.273$ with $R^2 = 0.944$. High value of R^2 indicates a better correlation between

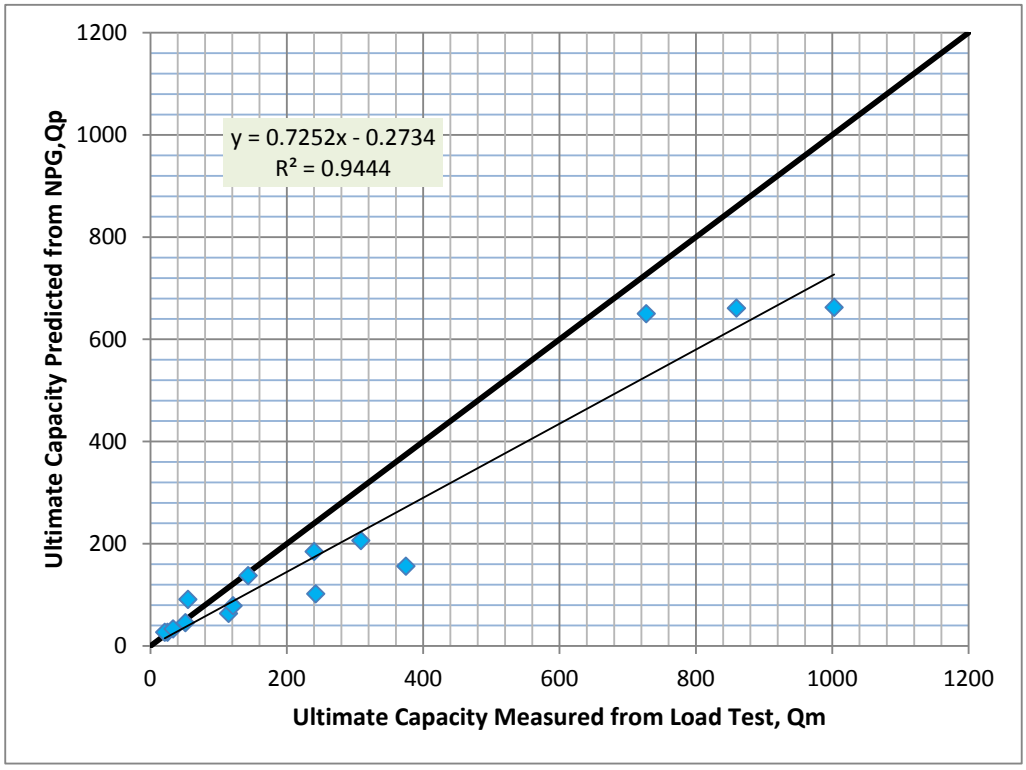

Figure 4.4(d): Correlation between Q_p and Q_m for NPG methods

Predicted and measured capacity. From statistical analysis and cumulative probability (shown in table 4.3), it has been observed that the highest RI(RI=21) ranked this method fifth amongst all other methods in precast driven piles. This is the worst conservative method to predict the ultimate capacity of precast driven piles with 23.10% underestimation. Figure 4.3(c) justify this error. COD value of 0.827 indicates the good compatibility of the predicted theory. No such limit for the determination of effective stress. An effective stress method is used to calculate skin friction for cohesion less soil. The co-efficient of skin friction β is a function of OCR. Largely driven piles give very high side resistance for higher β value and highly effective stress value. But bearing capacity factor Nq is very conservative.

Indian Standard (2010) Method

Compare the predicted capacity from Indian Standard (2010) method with measured capacity from load test for fifteen numbers of precast driven piles gives a regression equation, Q_p =0.659Q_m+23.98 with R^2=0. 972. Highest value of R^2 indicates a better correlation between

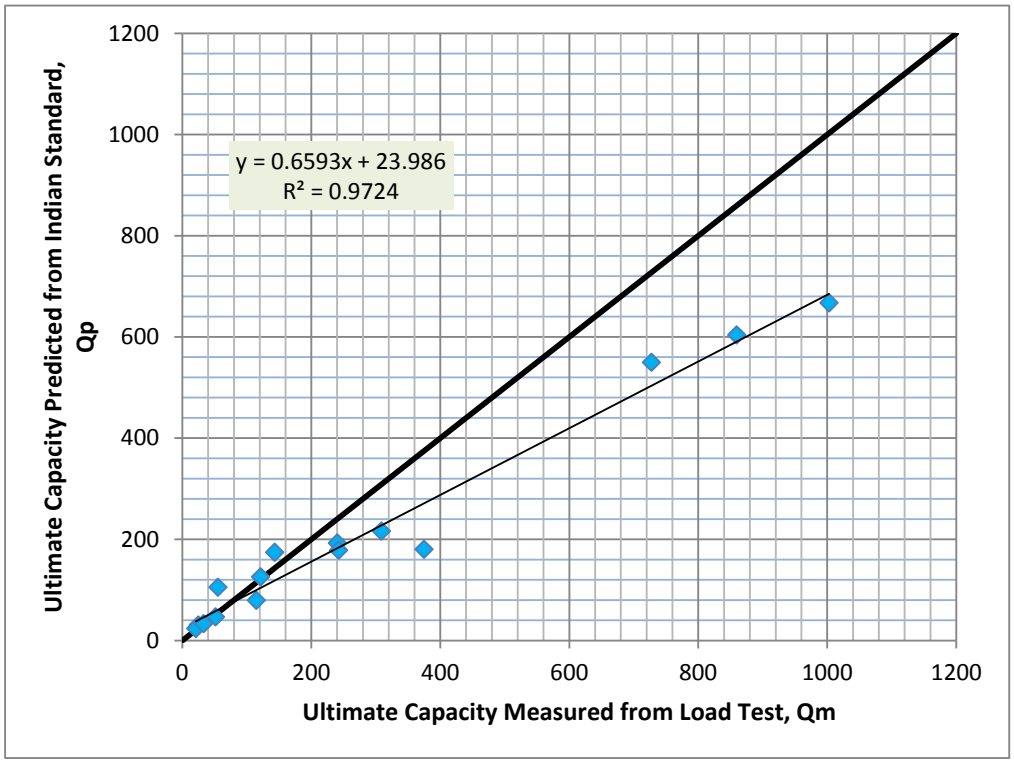

Figure 4.4(e): Correlation between Q_p and Q_m for Indian Standard methods

Predicted and measured capacity. From statistical analysis and cumulative probability (shown in table 4.3), it has been observed that a high RI(RI=19) ranked this method fourth amongst all other methods in precast driven piles. This is a very conservative method to predict the ultimate capacity of precast driven piles with 20% underestimation. Figure 4.3(c) justify this error. COD value of 0.814 indicates the good compatibility of the predicted theory. Indian Standard(2010) adopted Terzaghi Bearing Capacity equation to calculate the end bearing capacity of piles. Hence the length and shape of piles play an important role in the computation of capacity.

4.5.2 Cast in situ Bored Pile

Meyerhof (1976) Method

Compare the predicted capacity from Meyerhof (1976) method with measured capacity from load test for eight numbers of the cast in situ bored piles gives a regression equation, Q_p=0.957Qm+50.32 with R^2=0.555.Moderate value of R^2 indicates a pretty good correlation between

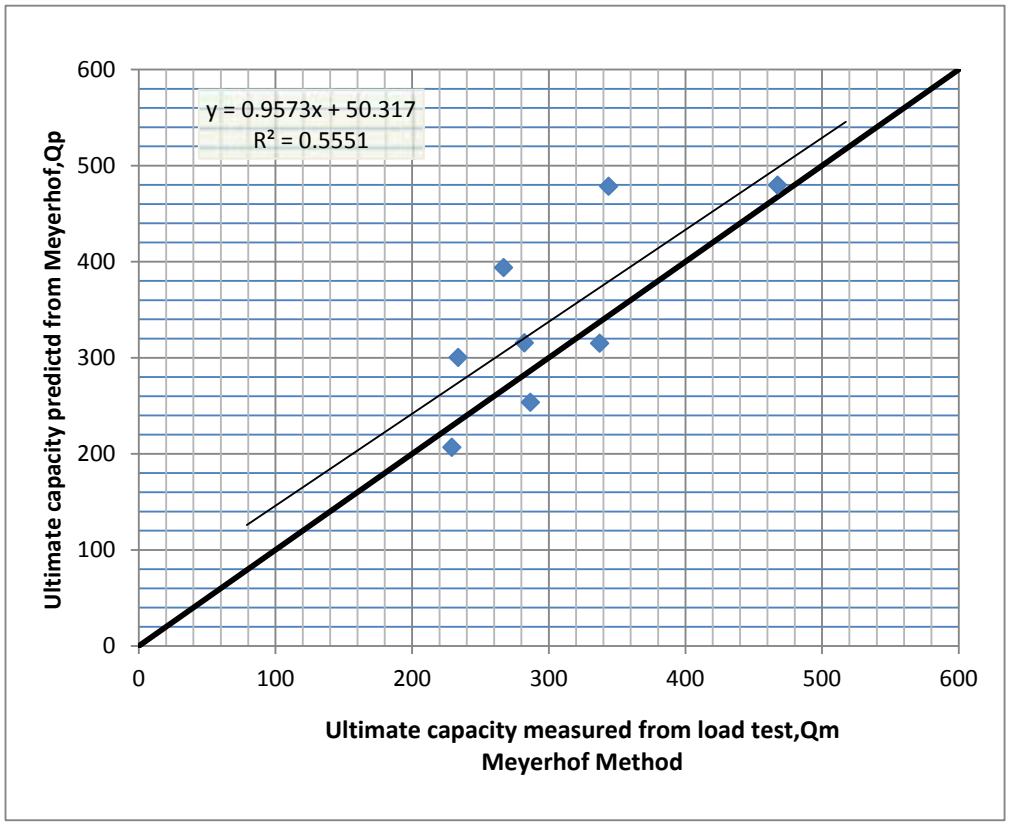

Figure 4.5(a): Correlation between Q_p and Q_m for Meyerhof methods

Predicted and measured capacity. From statistical analysis and cumulative probability (shown in table 4.4(A)), it has been observed that the lowest RI(RI=10) ranked this method second amongst all other methods in bored piles. Also, this method predicts to overestimate the ultimate capacity of9%. Figure 4.3(b) justify this error. This method to predict the capacity of bored piles is based on SPT. In this method field, SPT has been used. But for calculating the side friction field SPT has been used other hand for computing end bearing overburden pressure correction for SPT has been taken places. Also, Meyerhof limiting unit friction and limiting end bearing has been considered. This is kept the predicted capacity in minor error.

NAVFAC (1984) Method

Compare the predicted capacity from NAVFAC (1984) method with measured capacity from load test for fifteen numbers of the cast in situ bored piles gives a regression equation, $Q_p=0.995Q_m+21.62$ with $R^2=0.64$.Moderate value of R^2 indicates a pretty good correlation between

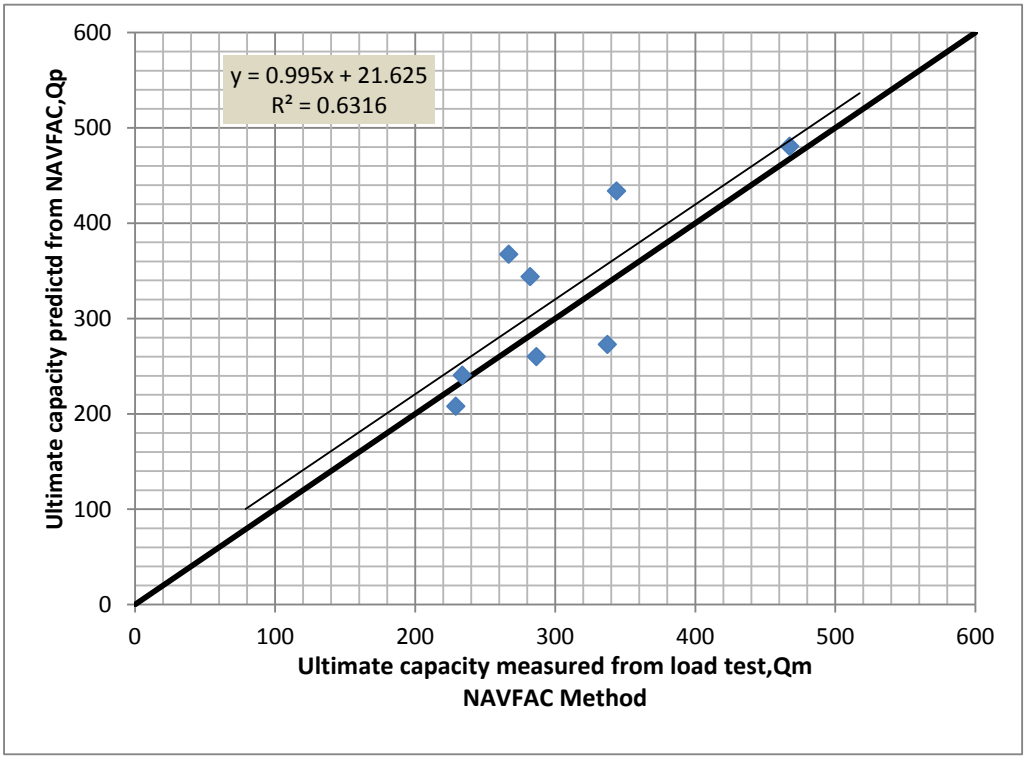

Figure 4.5(b): Correlation between Q_p and Q_m for NAVFAC methods

Predicted and measured capacity. From statistical analysis and cumulative probability (shown in table 4.4(A)), it has been observed that a lower RI(RI=6) ranked this method first amongst all other methods in bored piles. Also, this method predicts to overestimate the ultimate capacity of 1%. Figure 4.3(b) justify this error. COD value of 0.35 indicates the fair reliability of the predicted theory. This method predicts the capacity of bored piles in clay-based on total stress and in sand based on effective stress. In sand high bearing capacity factor for high SPT values gives the high capacity for long piles. But, limiting value of unit toe resistance and unit side resistance keep the predicted capacity relevant with measured capacity.

AASHTO (1986) Method

Compare the predicted capacity from AASHTO (1986) method with measured capacity from load test for eight numbers of the cast in situ bored piles gives a regression equation, $Q_p=1.22Q_m+37.75$ with $R^2=0.794$.Higher value of R^2 indicates a good correlation between

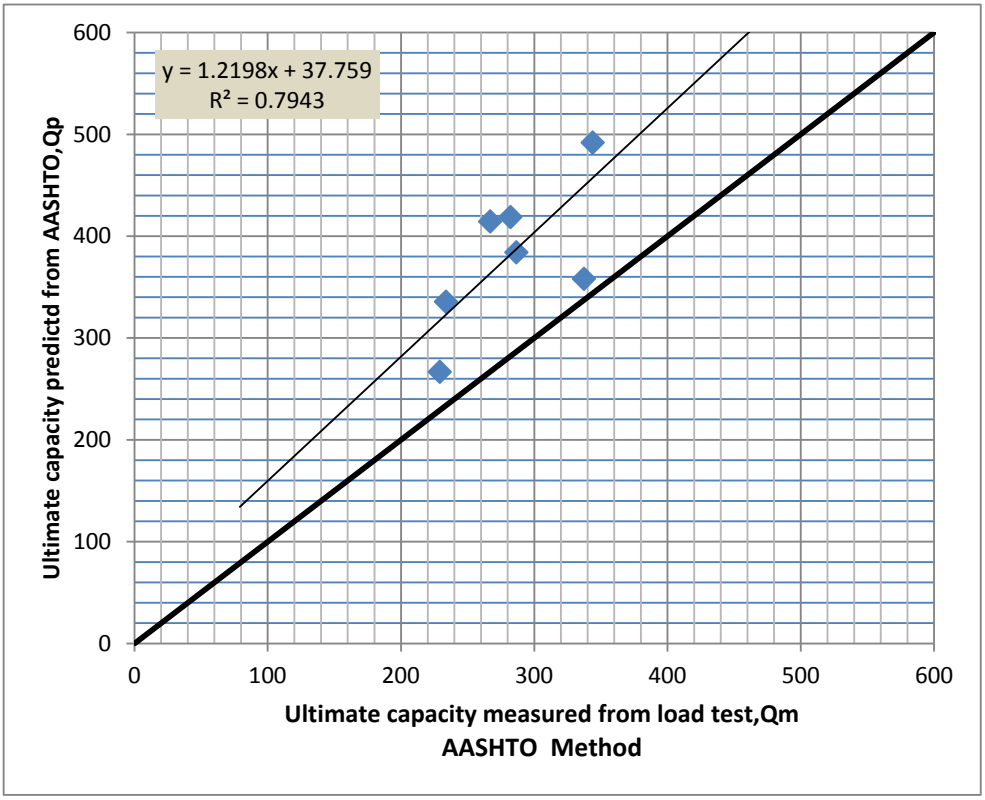

Figure 4.5(c): Correlation between Q_p and Q_m for AASHTO methods

Predicted and measured capacity. From statistical analysis and cumulative probability (shown in table 4.4(A)), it has been observed that a moderate RI(RI=17) ranked this method fourth amongst all other methods in bored piles. Also, this method predicts to overestimate the ultimate capacity by 40%.Figure 4.3(b) justify this error. This method predicts the capacity of bored piles in clay-based on total stress and in the sand based on effective stress. In sand side friction factor β is the function of the depth of the pile. It has an upper value of 1.2 for short length pile and a lower value of 0.25 after 87.5 feet depth of piles. Piles of low depth predict high value compare with long length piles. In sand end bearing capacity depends on SPT value. For high depth piles, it gives higher values.

O'neill & Reese (1988) Method

Compare the predicted capacity from O'Neill& Reese (1988) method with measured capacity from load test for eight numbers of the cast in situ bored piles gives a regression equation, $Q_p=1.40Q_m-56$ with $R^2=0.763$.Higher value of R^2 indicates a good correlation between

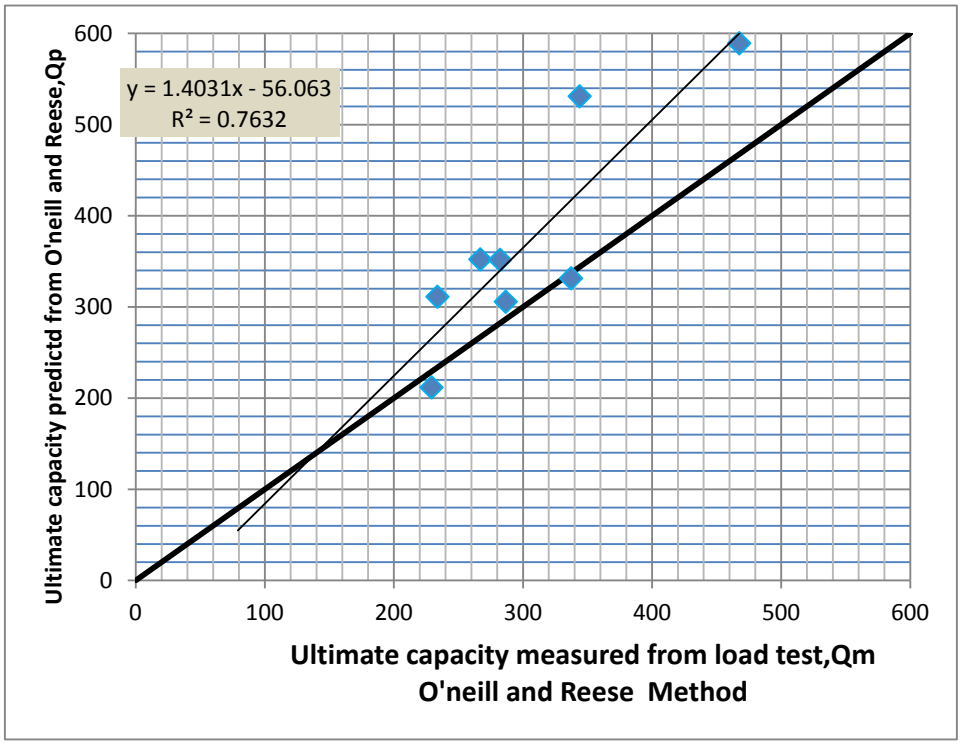

Figure 4.5(e): Correlation between Q_p and Q_m for O'Neill and Reese methods

Predicted and measured capacity. From statistical analysis and cumulative probability (shown in table 4.4(A)), it has been observed that a lower RI(RI=13) ranked this method third amongst all other methods in bored piles. Also, this method predicts to overestimate the ultimate capacity by 24.60%.Figure 4.3(b) justifies this error. This method predicts the capacity of bored piles in clay-based on total stress and in the sand based on effective stress. In sand side friction factor β is the function of the coefficient of lateral earth pressurev(k). This k is the function of pre consolidated stress and over consolidation ratio. With the increase of depth of pile effective stress increase abruptly. This causes higher depth piles to give more side friction due to excess vertical stress. Piles of high depth predict high value compare with short length piles. In sand end bearing capacity depends on SPT value. For high depth piles, it gives higher values.

Decourt (1995) Method

Compare the predicted capacity from Decourt's (1995) method with measured capacity from load test for eight numbers of the cast in situ bored piles gives a regression equation, $Q_p=1.89Q_m+130.54$ with $R^2=0.518$.Moderate value of R^2 indicates a pretty good correlation between

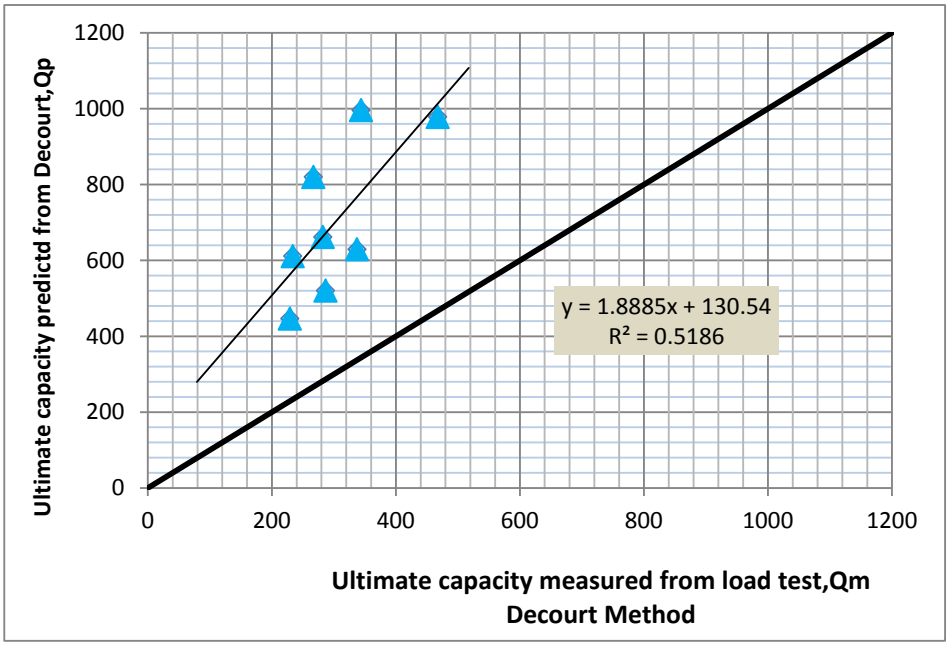

Figure 4.5(e): Correlation between Q_p and Q_m for Decourt methods

Predicted and measured capacity. From statistical analysis and cumulative probability (shown in table 4.4(A), it has been observed that the highest RI(RI=23) ranked this method fifth amongst all other methods in bored piles. Also, this method predicts to overestimate the ultimate capacity of134%.Figure 4.3(b) justify this error. COD value of -33.84 indicates very poor reliability of the predicted theory. It is a SPT based empirical formula invents by Decourt with numbers of the load test. This empirical formula gives justified values for skin friction both clay and sand. But computation of end bearing capacity in the sand gives very high values due to the overestimate of end bearing co-efficient.

4.5.3 Cast in Situ Drilled Shaft

Meyerhof (1976) Method

Compare the predicted capacity from Meyerhof (1976) method with measured capacity from load test for seven numbers of the cast in situ drilled shafts gives a regression equation, $Q_p=0.04Q_m+1937$ with $R^2=0$.Value of R^2 and other statistical data indicates the inability of this method to predict the capacity of drilled shaft.

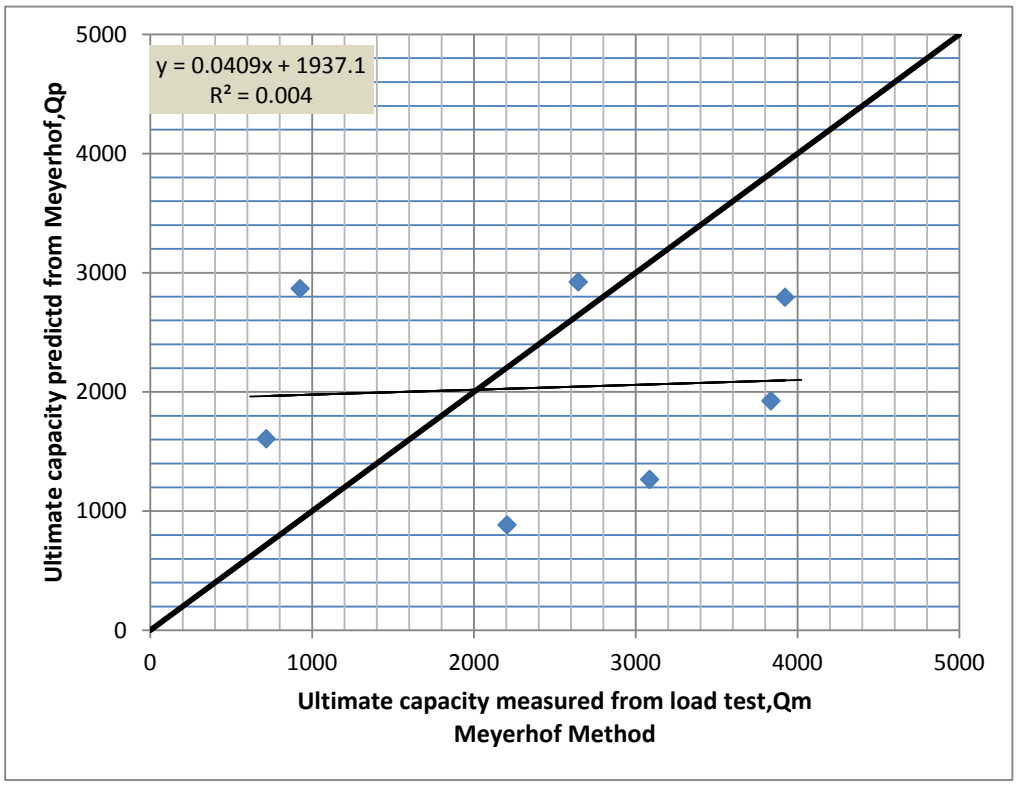

Figure 4.6 (a): Correlation between Q_p and Q_m for Meyerhof methods

NAVFAC (1984) Method

Compare the predicted capacity from NAVFAC (1984) method with measured capacity from load test for seven numbers of the cast in situ drilled shafts gives a regression equation, $Q_p=0.006Q_m+3231$ with $R^2=0$.Value of R^2 and other statistical data indicates the inability of this method to predict the capacity of drilled shaft.

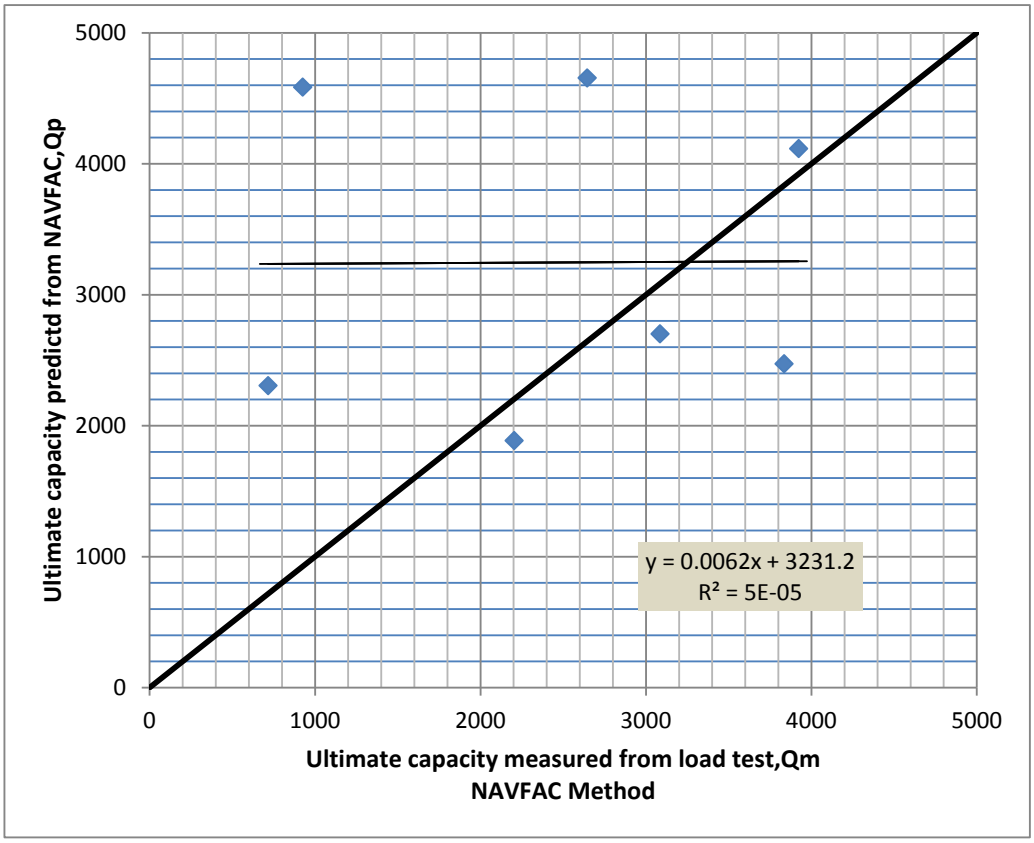

Figure 4.6(b): Correlation between Q_p and Q_m for NAVFAC methods

This method predicts the capacity of bored piles in clay based on total stress and in sand based on effective stress. In sand high bearing capacity factor for high SPT values gives the irrelevant capacity for long piles.

AASHTO (1986) Method

Compare the predicted capacity from AASHTO (1986) method with measured capacity from load test for seven numbers of the cast in situ drilled shafts gives a regression equation, $Q_p=0.228Q_m+1764.6$ with $R^2=0.13$.Low value of R^2 indicates a some correlation between

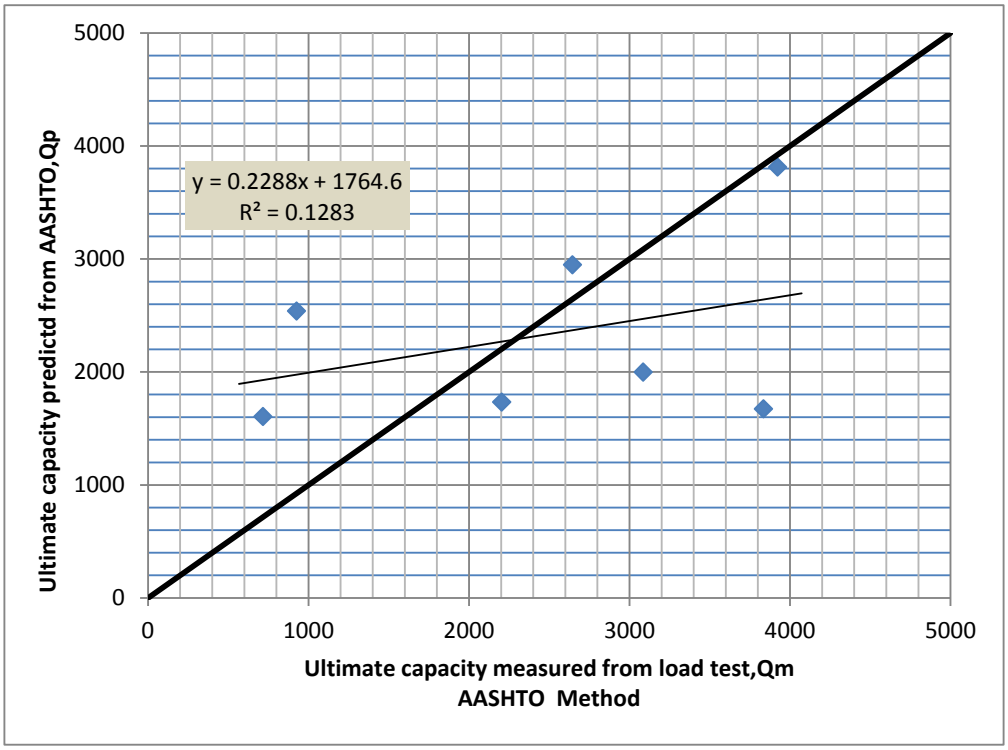

Figure 4.6(c): Correlation between Q_p and Q_m for AASHTO methods

Predicted and measured capacity. From statistical analysis and cumulative probability (shown in table 4.4(B)), it has been observed that a lower RI(RI=7) ranked this method first amongst all other methods in drilled shaft. Also, this method predicts to underestimate the ultimate capacity by 3%. Figure 4.3(a) justify this error. COD value of 0.5 indicates a good reliability of the predicted theory.

O'neill & Reese (1988) Method

Compare the predicted capacity from O'Neill & Reese (1988) method with measured capacity from load test for seven numbers of the cast in situ drilled shafts gives a regression equation, $Q_p=0.347Q_m+2234$ with $R^2=0.1$.Lower value of R^2 indicates some correlation between

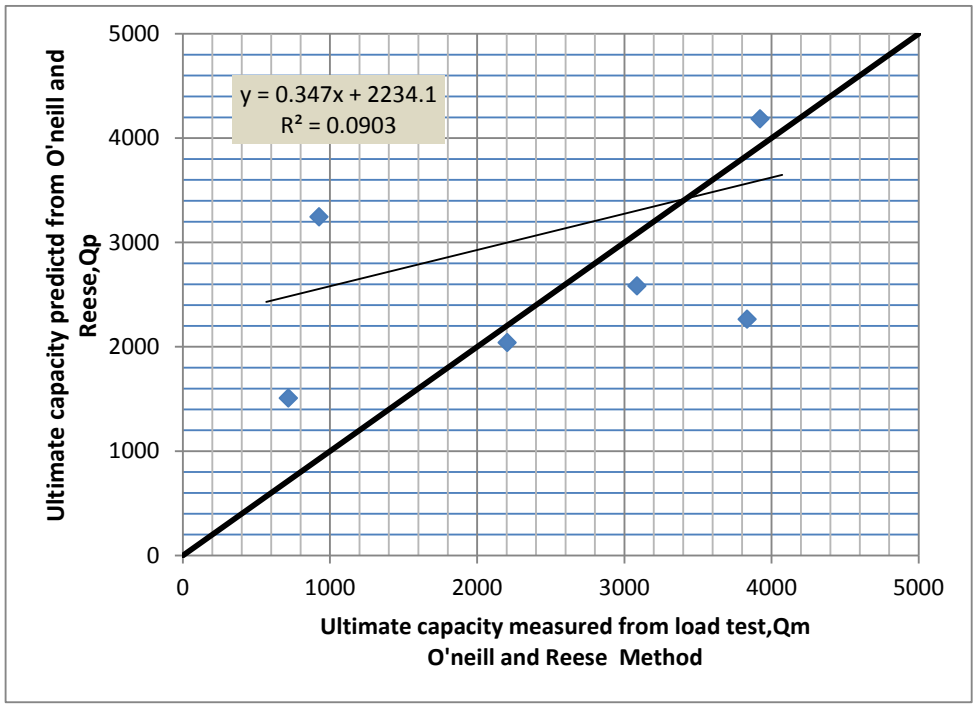

Figure 4.6(d): Correlation between Q_p and Q_m for O'Neill and Reese methods

Predicted and measured capacity. From statistical analysis and cumulative probability (shown in table 4.4(B)), it has been observed that a lower RI(RI=15) ranked this method third amongst all other methods in drilled shafts. Also, this method predicts to overestimate the ultimate capacity by 6%. Figure 4.3(a) justifies this error.

Decourt (1995) Method

Compare the predicted capacity from Decourt's (1995) method with measured capacity from load test for seven numbers of the cast in situ drilled shafts gives a regression equation, $Q_p=0.087Q_m+4356$ with $R^2=0.01$.Very low value of R^2 indicates a poor correlation between

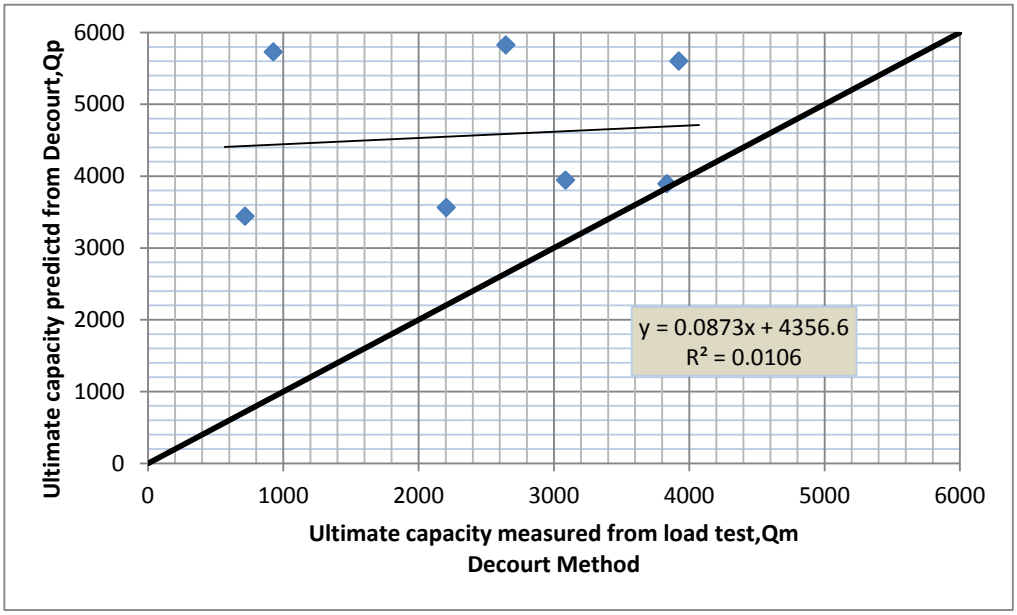

Figure 4.6(e): Correlation between Q_p and Q_m for Decourt methods

Predicted and measured capacity. From statistical analysis and cumulative probability (shown in table 4.4(B)), it has been observed that the highest RI(RI=24) ranked this method fifth amongst all other methods in drilled shafts. Also, this method predicts to overestimate the ultimate capacity of62%.Figure 4.3(a) justify this error. It is a SPT based empirical formula invents by Decourt with numbers of the load test. This empirical formula gives justified values for skin friction both clay and sand. But computation of end bearing capacity in the sand gives very high values due to the overestimate of end bearing co-efficient. Also, the uncorrected SPT value gives higher results for long piles.

CONCLUDING REMARKS

In this study sub-soil investigation report and corresponding pile load test results have been collected from twenty-two projects all over the country. Among these projects, twelve projects have been selected where fifteen precast piles have been tested and ten projects have been selected where fifteen cast-in-situ piles have been tested. The tests are performed between 1997 to 2018 and funded by the Public Works Department (PWD), Bangladesh, RAJUK, R&H Department, Bangladesh, and Dhaka Mass Transit Company (MRT). Almost 70% pile load tests are carried out under the direct supervision of the Department of Civil Engineering, BUET, and the rest of the pile load test carried out by Icon Engineering Services, Dhaka. The findings of this study are as follows:

The length of fifteen cast in situ piles vary from 12 meters to 52 metershavingdiameters of 400 mm to 1200 mm. For convenience of analysis it has been divide in to two categories named Bored pile and Drilled shaft. Ithasbeen observed that the long piles with large diameter generally conservatively predict the capacity of piles than the short piles (shorter than 18 m) for different statics methods except the Decourt(1995) method. It can be concluded for bored piles that the long and larger diameter pile capacity are governed by settlement rather than capacity.

Cast in situ piles larger than 600 m diameter considered as drilled shafts. No such good regression equation found by analyzing the selected theoretical methods in this thesis. Only AASHTO (1986) and O'neill and Reese (1988) gives some reliability to predict the ultimate capacity. On the other hand, the length of fifteen precast piles vary from 7 meters to 30.5 meters having sizes of 175 mmX175mm to 400 mm X 400 mm. It has been found in this study that the predicted pile capacity using all the methods are relatively conservative. Pile driving energy plays an important role to increase the capacity of piles.

In this study, it has been observed that the Tomlinson (1994), API (1993) and Meyerhof (1976) methods provide the most reliable and justified correlation with predicted and measured capacity for the precast piles.

For the cast in situ bored piles, the AASHTO (1986), O;neill and Reese (1988) and NAVFAC (1984) methods provide the most reliable and justified correlation with predicted and measured capacity. For the cast in situ drilled shafts, the AASHTO (1986) and Onell and Reese (1988) methods provide little reliable and justified correlation with predicted and

measured capacity. Other theoretical methods describe here are not suitable to predict the capacity of drilled shafts. Drilled Shaft installation is a highly technological task. During boring of drilled shaft mud slurry has been used. This slurry creates a thin layer around the borehole of the drilled shaft. If this thin layer does not disappear during concreting it causes to reduce the skin friction between soil and D.S. It lowers the measured capacity of the D.S.

In D.S construction first 5 feet of the soil formed cracks. This layer of cracked soil doesn't exhibit any skin friction. This consideration ignored by most of the theory used in this thesis except AASHTO and Reese et. al. Hence reduce the measured capacity compared with theoretical capacity. Caving, necking, and construction faults in enormous scale reduce the measured capacity of D.S. The above things didn't consider in the theoretical prediction. This is why an insignificant correlation found.

It has also been observed that the methods for predicting the ultimate capacity of precast/ driven piles give relatively more reliable and justified result with minimum error compared with the cast in situ/ bored piles. In all the cases a considerable correlation between the static analysis of pile capacity and capacity of the pile from the static load test are found. This study has supported the idea to put a higher degree of confidence to use the statics formulae to find out the ultimate capacity of the piles. The following correlations are proposed to obtain the predicted capacity of different methods:

For Precast Piles

- Meyerhof(1976) $Q_p=0.685Q_m+24.98$ with $R^2=0.935$
- API RP 2A(1993) $Q_p=1.01Q_m-31.95$ with $R^2=0.949$
- Tomlinson(1994) $Q_p=0.752Q_m+26.67$ with $R^2=0.919$
- Norwegian Pile Guideline (2005)$Q_p=0.725Q_m-0.273$ with $R^2=0.944$
- Indian Standard (2010) $Q_p=0.659Qm+23.98$ with $R^2=0.972$

For Cast-in-situ Piles (Bored Piles)

- Meyerhof(1976) $Q_p=0.957Q_m+50.317$ with $R^2=0.555$
- NAVFAC DM 7.2(1984)$Q_p=0.995Q_m+21.62$ with $R^2=0.631$
- AASHTO(1986) $Q_p=1.219Q_m+37.759$ with $R^2=0.0.794$
- O'Neil&Reese(1988) $Q_p=1.403Q_m^{-}56.06$ with $R^2=0.763$

BANGLADESH NETWORK
OFFICE FOR URBAN SAFETY

PART-III

CAN RANA PLAZA HAPPEN AGAIN IN BANGLADESH

BANGLADESH NETWORK OFFICE FOR URBAN SAFETY (BNUS), BUET, DHAKA

Prepared By: Uttama Barua

Mehedi Ahmed Ansary

1. Introduction

In the world's apparel sector, the Ready-Made Garment (RMG) industry in Bangladesh is the world's second-largest exporter which has also provided a primary source of livelihood for over four million workers (mostly women) and their family resulting in a significant contribution to the country's social and economic development (ILO 2017b). Despite such remarkable achievement, the sector has been facing challenges to ensure workplace safety and better working conditions for the millions of garment workers. Among others, building collapse has been common in this sector. In 2005, the building of the Spectrum factory collapsed causing the death of 64 garment workers and the injury of 84 (Miller 2012). In 2006, 22 workers died due to the collapse of the six-storied Phoenix Garments building (Ansary and Barua 2015). In 2012 due to the partial collapse of the Siams Superior Ltd. factory building in Chittagong Export Processing Zone (CEPZ), five workers received minor injuries (Solidarity Center 2019). In November 2012 at Ashulia's Tazreen garments factory in Dhaka, 112 people died due to a severe fire break out. In February 2013, at the factory building of Envoy Garments Ltd. in Ashulia, Dhaka at least 100 garment workers were injured in a stampede triggered by a false fire alarm and the consequent collapse of stairs railing (Solidarity Center 2019). Just months after this accident, the nine-storied Rana Plaza housing five RMG factories located in Savar, Dhaka collapsed on 24 April 2013. In 2005, the Local Municipality (Savar) permitted the owner of Rana Plaza to construct a five-story commercial building with one basement. Though the foundation of the building was for five-story, later the owner was allowed to extend the building up to nine-story without considering the structural design. Moreover, the building was converted from commercial to industrial use, and power generators were placed on higher floors. As a result of such violations in building construction, on 23 April 2013, a day before the fateful day, cracks developed on some columns and the building jolted. After inspection, the industrial police requested the building authorities to close the building and to suspend operations of the factories on that day. However, the building owner and top-management of the garment factories ignored the warning and forced the workers to work in the next morning on 24th April 2013 (Ansary and Barua 2015). As a consequence, the collapse of the building resulted in a high death toll of 1,134, and more than 2500 people were badly injured at the end of the rescue operation on 14 May 2013 (Solidarity Center 2019). It was the most fatal industrial accident in the RMG sector in Bangladesh, and one of the deadliest industrial disasters in the world, which was the result of the reluctant attitude of the stakeholders towards the compliance issues. This tragic

accident received global attention and brought forward diverse issues concerning millions of stakeholders in the RMG sector of Bangladesh (Ansary and Barua 2015).

All these accidents represent poor workplace safety conditions in Bangladesh RMG factories. After the Rana Plaza accident different diversified national and international initiatives have been taken to improve workplace safety conditions in this sector. Seven years after the accident the question is now whether these initiatives could truly succeed to ensure workplace safety or can accidents like the Rana Plaza collapse happen again. This paper aims to explore the answer to this question by reviewing the initiatives and their progress to achieve workplace safety in the Bangladesh RMG industry with special attention to structural safety. The objectives of this research are threefold. Firstly, to review the process of ensuring the structural safety; secondly, to review and understand the progress and the way forward in the process; thirdly, to discuss the possibility of any such accidents in Bangladesh RMG sector in light of the findings from first two objectives. This research has been carried out through review of relevant literatures from different sources.

2. Initiatives after Rana Plaza collapse

Considering the potential of the RMG industry in Bangladesh and to ensure its safety and sustainability, several and diverse national and international commitments and initiatives resulted as part of the reform and restructuring of the RMG sector after the Rana Plaza accident (Khan and Wichterich 2015, Barua and Ansary 2017, Moazzem and Islam 2015, RCC 2018b). As the National Initiative, a Joint Statement was signed by tripartite partners (GoB, RMG workers, and RMG employers) in May 2013. Afterward, as part of the National Initiative, the National Tripartite Plan of Action (NTPA) on Fire Safety and Structural Integrity in the RMG Sector of Bangladesh was formed in July 2013 merging the Joint Statement with the NTPA on Fire Safety (outlined on March 2013 after Tazreen Fashion fire accident) without altering the content (RCC 2018b). It included 25 commitments divided into three categories: legislation and policy, administration, and practical activities. To ensure and monitor its implementation the National Tripartite Committee (NTC) was established at the same time under NTPA commitment. The committee is chaired by Labour Secretary and includes Government agencies (Ministry of Labour and Employment, Department of Inspections for Factories and Establishments (DIFE)), Employers' Organizations (Bangladesh Employer's Federation (BEF), Bangladesh Garment Manufacturers & Exporters Association (BGMEA) and Bangladesh Knitwear Manufacturers & Exporters Association (BKMEA)), and Workers' Organizations (National Coordination Committee for Worker's

Education (NCCWE), and IndustriALL Bangladesh Council (IBC)) (Barua and Ansary 2017, Moazzem and Islam 2015).

Based on NTPA, the European Union (EU), the Government of the People's Republic of Bangladesh (GoB), and the International Labour Organization (ILO) issued an agreement of time-bound actions, "The Sustainability Compact: Compact for Continuous Improvements in Labour Rights and Factory Safety in the Ready-Made Garment and Knitwear Industry in Bangladesh" in July 2013 to promote improved labour standards and responsible business conduct in the RMG and knitwear industry in Bangladesh. A total of twenty-nine activities were listed in the EU Sustainability Compact (Khan and Wichterich 2015, Barua and Ansary 2017). Besides, the United States Trade Representative (USTR) requested GoB to implement a sixteen-point action plan within one year to reinstate Bangladesh's GSP status in the US market. The USTR Action Plan endorsed the EU Sustainability Compact particularly for trade union-related activities (Moazzem and Islam 2015, Barua and Ansary 2017, RCC 2018b). To support the National Initiative, ILO Bangladesh launched the "Improving Working Conditions in the Ready-Made Garment (RMG) Sector" programme in September 2013 with funding from Canada, the Netherlands, and the United Kingdom (RCC 2018g, 2020, ILO 2017a, b). The duration of this program is 22 October 2013 to 30 June 2023 (ILO 2017a).

In addition to these initiatives, two different factory inspection programmes were established to make the workplace safer in Bangladesh where ILO fulfils the role of neutral chair. They are The Bangladesh Accord on Fire and Building Safety in Bangladesh (the Accord), and the Alliance for Bangladesh Worker Safety (the Alliance). The Accord was initiated by over 190 apparel companies from over 20 countries in Europe, North America, Asia, and Australia; two global trade unions, IndustriALL and UNI Global; and eight Bangladeshi trade unions on May 15, 2013. It is a five-year independent and legally binding agreement designed to build a safe and healthy Bangladeshi RMG Industry (Accord on Fire and Building Safety In Bangladesh 2015). The Alliance officially launched its local operation in Dhaka on December 9, 2013, which is also a five-year independent and legally binding agreement initiated by a group of North American apparel companies and retailers and brands (26 North American retailers and brands) to develop and launch the Bangladesh Worker Safety Initiative (Alliance for Bangladesh, 2013). The targets and objectives of these initiatives are the same, which is to improve the safety of workers in Bangladesh's RMG sector (Alliance for Bangladesh Worker Safety 2014a, Accord on Fire and Building Safety In Bangladesh 2014). They share some common courses of action aiming at the improvement of workplace

safety to safeguard the lives of over four million RMG workers and to retain the confidence of global buyers following the Rana Plaza accident (Barua and Ansary 2017, Moazzem and Islam 2015, Alliance for Bangladesh Worker Safety 2018f).

Among the common actions considered in these initiatives, improving the structural safety of RMG factory buildings to ensure a safe working environment is the focus of this research.

4. Actions regarding the structural safety of RMG factory buildings

All garment factories in Bangladesh need to meet accepted standards regarding their structural safety, for which they need to pass through a process to ensure and maintain safety (RCC 2018h). It is important because failure by any factory to comply may perpetuate unsafe working conditions and put workers at risk (Alliance for Bangladesh Worker Safety 2018a). The initiatives related to the structural safety in the RMG sector of Bangladesh comprised of two phases, the first phase emphasizing on building safety assessments; and the second phase focusing on ensuring factory safety through remediation (ILO 2017a, b). The Accord and the Alliance covered factories from which their members source garments and the remaining factories were covered by the Bangladesh University of Engineering and Technology (BUET) and two private engineering firms TUV SUD Bangladesh (Pvt.) Ltd and Veritas Engineering & Consultant on behalf of the National Initiative (RCC 2018g, 2020). In January 2014, the Chief Inspector of Factories and Establishment office was upgraded to the Department of Inspection for Factories and Establishments (DIFE) under the Ministry of Labour and Employment (MoLE) to support the structural safety actions (ILO 2017a, Barua and Ansary 2017). The process to ensure structural safety in the Bangladesh RMG sector is discussed below:

4.1 Building safety assessments

4.1.1 Inspection of factory buildings

(a) Preliminary Inspection

All the factories are required to undergo preliminary inspections by qualified assessment teams (RCC 2018h, ILO 2018). To undertake the initial structural assessment of factory buildings with a common approach, “Guidelines for Assessment of Structural Integrity and Fire and Safety” was developed by the technical experts from the BUET on behalf of the NTC, the Accord, and the Alliance in 2013 (NTPA 2013). In 2014, Accord and Alliance in collaboration with local and international experts consolidated national rules and regulations related to building integrity and prepared a comprehensive document consisting of a strict set of guidelines (Accord on Fire and Building Safety In Bangladesh 2014, Alliance for Bangladesh Worker Safety 2014a). But, in case of insufficiency in local rules, the standards

have been strengthened by taking support from international rules and guideline where deemed necessary and practical (Alliance for Bangladesh Worker Safety 2018f, d, i, Accord on Fire and Building Safety In Bangladesh 2014, Alliance for Bangladesh Worker Safety 2014a). In the process of standards development, the ILO played a vital role (Accord on Fire and Building Safety In Bangladesh 2014, Alliance for Bangladesh Worker Safety 2014a). Alliance also developed an assessment protocol to conduct the initial assessment (Alliance for Bangladesh Worker Safety 2014b).

The initial assessments for structures include basic capacity evaluation of critical members or columns or foundations through visual inspection (RCC 2018h, ILO 2018). Based on the findings from the initial building assessments, the immediate threat of collapse of the building from current building use is assumed considering that the condition of the column ultimately represents the vulnerability of the buildings to collapse. Therefore, the working stresses of key columns represented by the Factor of Safety (FOS) are calculated, which is the Column Ultimate Strength, divided by the Column Working Stress. Based on the calculated FOS, the factory buildings are classified into four color-coded classes indicating the level of vulnerability (green, yellow, amber, and red where green is the safest and red is the most vulnerable). The details of these colour coding procedures have been discussed in the research of Ansary and Barua (2015). Such classification helps to prioritize further work plans and provide factory owners with a technical understanding of the safety concerns (Alliance for Bangladesh Worker Safety 2018c, RCC 2018h).

(b) Detailed Engineering Assessment (DEA)

After the initial assessment, a Detailed Engineering Assessment (DEA) is carried out for all the factory buildings. Considering the number of factory buildings and the detailing required for DEA, it is not possible to carry out the DEA of all factory buildings at the same time. Here the findings from the initial assessment help to set priority for conducting DEA. The priority is given to the factory buildings which are found to have a potential structural weakness after initial assessment (red and amber) or if there is insufficient information and documentation on the building structure to determine the safety of the structure (Accord on Fire and Building Safety In Bangladesh 2018f, DIFE 2015a, Accord on Fire and Building Safety In Bangladesh 2020b, RCC 2018h, Ansary and Barua 2015, ILO 2018). Later on, DEA of factory buildings found to be safe during the initial assessment (yellow and green) are also carried out because in some cases initial assessment may not depict true scenario which can be verified or found out through DEA.

To carry out the DEA, "DEA Guidelines" has been developed by DIFE (DIFE 2015a). According to the guideline, the DEA should only be carried out by the qualified engineering firms by the RCC Structural Task Force. For approval, an engineering firm must have at least three years of relevant experience, should be enlisted with the RAJUK, and must have two Engineers (can include two structural engineers or one structural and one geotechnical engineer). The Engineers should be suitably qualified to check, approve, and certify a DEA Report. Therefore, according to the guideline, the Engineers must have Bachelor's degree in Civil Engineering from a recognized university, should have a minimum of five years' experience with both engineers having a combined 15 years of professional experience with proven skills and expertise in the relevant field; should have experience of at least three DEAs or similar in a comparable area in the last two years, and having knowledge of the institutional context and RMG sector in Bangladesh should be considered as an advantage.

According to the DEA Guideline (DIFE 2015a), the DEA involves acquiring accurate as-built information of the structure to use as input data for analysis and structural analysis of the performance of the existing structure under the specified loading conditions (Accord on Fire and Building Safety In Bangladesh 2018f, 2020b, ILO 2018). The as-built drawing records verified architectural drawings of each floor with use, newly developed structural as-built drawings (plans and sections) accurately reflecting the structural system and all structural elements, reinforcement details, overall and floor wise load plan, foundation details, etc. For structural analysis, the existing loading on the structure is prepared including actual dead loads and live loads, as well as details and magnitude of the wind and seismic loading to be adopted for the analysis. The assessment involves intrusive or destructive assessment, which means partial removal or destruction of some structural elements for assessment, e.g. taking a core out of a concrete column, removing soil for lab testing, or removing finishes to see hidden or covered details (DIFE 2015a, ILO 2018). For geotechnical investigation (if required), sufficient on-site opening up is carried out to test or investigate the foundation system, bearing levels, bearing capacities, and condition of a representative sample of elements below ground for size, corrosion, and condition. Subsoil Investigation is carried out to verify the existing foundation and check the adequacy

Irrespective of the state of the existing records, testing of the in-situ concrete is mandatory for all DEAs to verify the concrete strength in the building. In this regard, several sample cores (minimum four) that are representative of the concrete under investigation are collected ensuring proper witness and documentation. The number and locations of sample cores are determined by the Engineer considering that concretes in different structures or constructed at

different times are likely to be of differing strength. If the cores are not ideal (i.e. low-quality concrete, cores include aggregates larger than one-third the core diameter, or if there is the potential that at least one of the cores may produce an erroneous result through a flaw in the core or accidental damage) the Engineer considers the benefit of taking additional samples. According to the guideline, the requirement is minimum four cores with minimum size 100 mm in diameter each. These test values are then used to calculate the equivalent compressive strength for evaluating the strength capacity of the existing structure using in situ strengths following ACI 562-13 (ACI 2013).

Some key signs during the preliminary inspection may indicate the deterioration of the apparent condition of the concrete structure, like cracking, spalling, discoloration, leaks, damp patches, signs of reinforcement corrosion such as staining, delamination of the surface or even exposed corroded reinforcement, and signs of previous repairs. Figure 1(a) shows flat plate system structure and diagonal cracks on the ceiling in the cantilever portion and Figure 1(b) shows the condition of a column of an RMG factory building observed during a preliminary inspection under the National Initiative representing the apparent condition of the concrete structure. Even though the visible signs of the deterioration are not yet apparent, the Engineer may suspect it, particularly the corrosion of reinforcement. In these cases, the Engineer uses further lab tests to diagnose the cause of deterioration. Guidance on the selection of appropriate tests has not been prescribed in the Guideline, as the selection depends largely on the nature of the concrete, the nature of the deterioration, and its suspected cause. Moreover, multiple tests may have to be considered combining Engineering judgment and visual inspection to gain a full understanding. The Engineer takes the decision accordingly. Some of the suggested tests are visual inspection with localized exposure of reinforcement where required; carbonation depth measurement test to determine whether the alkalinity of the concrete has been neutralized to the depth of the reinforcing bars and hence corrosion may be occurring; chloride profile testing to determine the presence of chlorides which can accelerate the corrosion process; ultrasonic methods to measure the sound velocity and reflections in concrete to give an indication of potential voids and unseen surfaces, etc.

Figure 1(a): Flat plate system structure and diagonal cracks on the ceiling in the cantilever portion

Figure 1(b): Condition of a column

Figure 1: Apparent condition of the concrete structure of an RMG factory building observed during a preliminary inspection under the National Initiative (Source: (National Initiative 2020))

A structural model of the building is developed using an internationally recognized computer analysis package, e.g. ETABS, STAAD pro, etc. The analysis based on the as-built drawing considers the vertical and lateral stability of the structure. Based on the analysis results, the overall performance of the structure is described indicating the elements which fail to satisfy the requirements (if any). Then corrective measures are considered and the analysis is re-run. This process is repeated until the satisfactory performance of all structural elements has been demonstrated. The final analysis must show the structural adequacy of all the members.

Based on the findings from the DEA, the color-coded classification of the factory buildings are again revised based on recalculated FOS (Ansary and Barua 2015). Some factory buildings found to be green through initial assessment have been assessed as red after DEA, which further justifies the conduction of DEA of all the RMG factory buildings.

(c) Review panel

Factory buildings found to be vulnerable (red) from initial inspection and/or the DEA are instructed to be deactivated, evacuated, and stop production until the determination of its safety for re-occupancy through corrective actions (Accord on Fire and Building Safety In Bangladesh 2020b). Even after deactivation, the factory owners are supported as long as they show commitment to safety (Alliance for Bangladesh Worker Safety 2018c). When deemed necessary, the inspection results are submitted to the Review Panel (Accord on Fire and Building Safety In Bangladesh 2020b).

The review panel assesses the recommendation of the closure of a factory building (Accord on Fire and Building Safety In Bangladesh 2020b). In May 2014, a Review Panel along with a review mechanism was established in Bangladesh through the Ministry of Labour and Employment (MoLE) led NTPA under DIFE to handle urgent safety issues in these garment factories which are considered to pose an imminent danger to workers' safety and make the decision regarding the closure or non-closure of such factories (RCC 2018c, Accord on Fire and Building Safety In Bangladesh 2020a, b, Alliance for Bangladesh Worker Safety 2018e). This panel is comprised of the DIFE, the Accord, the Alliance, BGMEA, and BKMEA with technical support from BUET, and consists of four Review Panel engineers: one representing the Accord, one representing the Alliance, and two representing the BUET on behalf of GoB (RCC 2018c, Accord on Fire and Building Safety In Bangladesh 2020a, b, Alliance for Bangladesh Worker Safety 2018e). When the Review Panel receives a report from one of the three initiatives, it immediately convenes a visit to the concerned factory, and then a unanimous decision is taken by the Review Panel engineers ordering full or partial closure of factory operations as necessary. Once closed due to recommendation by the Review Panel,

the factory may be re-opened only after due remediation is completed and the Review Panel has given its unanimous recommendation confirming improved structural integrity (Alliance for Bangladesh Worker Safety 2018e).

4.1.2 Corrective Action Plan (CAP) development and approval

After the inspections, the reports are shared with the factory owners along with a list of observations and recommendations to improve the safety of the factory addressing the non-compliances (DIFE 2015b, Alliance for Bangladesh Worker Safety 2018d, f, Accord on Fire and Building Safety In Bangladesh 2020b). Based on the report, the factory owners or managers have to develop a time-bound Corrective Action Plan (CAP) in conjunction with the expert for technical guidance and support (DIFE 2015b, Accord on Fire and Building Safety In Bangladesh 2020d). It contains detailed remedial actions corresponding to the non-compliances identified in the inspection with a clear timeline and a financial plan giving priority to the most urgent non-compliant issues (Accord on Fire and Building Safety In Bangladesh 2020b, ILO 2018). To guide the process, a CAP development guide has been prepared by the DIFE (DIFE 2015b). The prepared CAP is submitted to the respective responsible authority (the Accord, the Alliance, or the NTC respectively) for review and approval (Alliance for Bangladesh Worker Safety 2018f, Accord on Fire and Building Safety In Bangladesh 2020b, RCC 2018h).

4.2 Remediation

After CAP approval, the remediation phase begins which refers to the implementation of the approved CAP (ILO 2018). This will create a greater workplace harmony, help to gain the trust of buyers, and thereby ensure business continuity which may also lead to more work orders (ILO 2018). This will in turn enhance the image of the Bangladesh RMG industry as a safe source attracting more foreign direct investment (ILO 2018).

4.2.1 Remediation Coordination Cell (RCC)

In May 2017, the Remediation Coordination Cell (RCC) was officially launched for the Bangladesh RMG sector for managing the remediation process (of factories initially under National Initiative and later other factories under Accord and Alliance), marking a major step towards improving workplace safety in the Bangladesh RMG sector (RCC 2020, 2018b, a, g, ILO 2018). It has been established through the collaboration of the GoB, BGMEA, and BKMEA, in consultation with trade unions and international buyers, with technical support from ILO, and with funding from Canada, the Netherlands, and the United Kingdom (RCC 2018g, 2020, ILO 2018). RCC is led by the DIFE comprising of four teams: the core body (to ensure smooth operations and coordination among and between regulatory departments,)

field monitoring committee (to monitor remediation activities at field level), the task force (to monitor the progress of remediation activities), and case handler and co-case handler (RCC 2018c).

4.2.2 Remediation process

Implementation of the remediation is the responsibility of the factory owners considering it as an investment to ensure compliance (RCC 2018a, h). Such responsibilities may include prioritization of remediation work; undertaking the steps as per CAP which may involve careful planning, temporary relocation or closure of factory production to enable remedial actions to be carried out; engaging an enlisted private consultancy firm and in-house building engineers to monitor progress; liaising with relevant engineers through a case handler under the initiatives accordingly, and recording and reporting the progress made regularly (ILO 2018).

The remediation process in factories under National Initiatives is carried out based on the Remediation Strategy for the RMG sector developed by the Ministry of Labour and Employment (MOLE) and DIFE with the support of ILO and with inputs from international engineering specialists (RCC 2020). The Accord and the Alliance follow their strategy for remediation work (Accord on Fire and Building Safety In Bangladesh 2020b, Alliance for Bangladesh Worker Safety 2018a). Factories begin remediation through the implementation of the approved CAP working with technical experts (Alliance for Bangladesh Worker Safety 2018f, Accord on Fire and Building Safety In Bangladesh 2020b). Among the developed corrective actions, some can or need to be addressed immediately, but some can take a longer time to complete (Alliance for Bangladesh Worker Safety 2018d). Thus the remediation work continues until the factory addresses all non-compliances as per its CAP (Alliance for Bangladesh Worker Safety 2018d). The progress of the remediation work is monitored and verified with the assessment report and the CAP through follow-up visits (Alliance for Bangladesh Worker Safety 2018d, Accord on Fire and Building Safety In Bangladesh 2020b, ILO 2018). After each follow-up visit, the CAPs are updated accordingly (Alliance for Bangladesh Worker Safety 2018g, Accord on Fire and Building Safety In Bangladesh 2020d). When the remediation is marked to be completed, a third party final inspection is conducted to ensure the final closure of CAPs (Alliance for Bangladesh Worker Safety 2018f). After the successful implementation of the CAP, the factories receive remediation completion approval (ILO 2018). On the contrary, if there is any disagreement with the results of the final remediation assessment, then the case is referred to as the Remediation

Coordination Cell (RCC) Review Panel to respect the technical view and ensuring transparency in decision-making (RCC 2018c).

The GoB is responsible for coordinating between the regulatory bodies as well as the remediation initiatives, and execute its legal mandate to ensure enforcement of national laws (RCC 2018a). Thus, the Government is accountable for furthermore confirming transparency and ensuring the availability of the remediation data (RCC 2018a). The BGMEA and BKMEA are responsible for supporting the remediation process by encouraging factory owners to carry out required remediation work while also taking steps against any factory that does not carry out remediation as required (RCC 2018a). Workers' organizations can help monitor the process of remediation in factories and act as a channel through which workers can convey any concerns in this regard (RCC 2018a).

4.3 Escalation process

In the whole process of assessment and remediation, the RMG factory owners have to participate fully maintaining compliance over time (Accord on Fire and Building Safety In Bangladesh 2018d, Alliance for Bangladesh Worker Safety 2018a). They may fail to do so by refusing to temporarily evacuate the factory as instructed; showing a lack of progress in finalizing or executing the CAPs within a reasonable timeframe; refusing to resolve worker complaints on safety issues; showing a lack of cooperation; or conducting fraudulent acts (Accord on Fire and Building Safety In Bangladesh 2018d, Alliance for Bangladesh Worker Safety 2018a, RCC 2018b). In such cases, the factories are considered to be in severe and imminent danger. To take measures for such non-compliance within the legal framework, an Escalation Protocol has been developed by RCC which contains the steps to be taken about those factories (RCC 2018b). Similar methods are also followed by the Accord and the Alliance.

In such cases of non-compliance, the factory owners are given notice and warning leading to termination of the business relationship and other supports due to the continuation of inadequate participation (Accord on Fire and Building Safety In Bangladesh 2018d, 2020d, Alliance for Bangladesh Worker Safety 2018f, RCC 2018b). When a factory is made ineligible, an ineligibility statement and a letter of notification to workers informing them about the status are generally issued (Accord on Fire and Building Safety In Bangladesh 2018e, RCC 2018b). Factories made ineligible or suspended are handed over to the DIFE, along with the inspection reports and CAPs to address the ongoing safety concerns at these factories (Accord on Fire and Building Safety In Bangladesh 2018d, 2020d, RCC 2018b).

Except for the cases of fraud or violence, the ineligible factories under the Accord and the Alliance may requalify for business after no less than 18 months from the date of ineligibility (Accord on Fire and Building Safety In Bangladesh 2018d, Alliance for Bangladesh Worker Safety 2018f). For this purpose, the factories have to inform the relevant initiatives notifying the completion of CAP and corresponding remediation and requesting for verification inspection at their own cost (Accord on Fire and Building Safety In Bangladesh 2018d, Alliance for Bangladesh Worker Safety 2018a). If these factories can demonstrate satisfactory preparation of an acceptable time-bound CAP and completion of all remediation during the verification inspection, then they can requalify for business (Accord on Fire and Building Safety In Bangladesh 2018d, Alliance for Bangladesh Worker Safety 2018a).

Figure 2 illustrates the overall process flow to ensure structural safety in the Bangladesh RMG sector.

4.4 Overall status determination at different steps of the process

Observing the factories in the whole process of assessment and remediation, the overall status is determined to increase transparency and support progress (Alliance for Bangladesh Worker Safety 2018a, RCC 2018g, Accord on Fire and Building Safety In Bangladesh 2020d). Such status includes: completed (completed initial requirements of assessment and remediation); participating or on track (progressing adequately with requirements); behind schedule or needs intervention (falling behind on or refusing to follow requirements); critical (at risk of being removed from compliant factory list based on lack of progress with requirements); suspended or made ineligible (officially removed from compliant factory list based on lack of progress in one or more requirements) (Alliance for Bangladesh Worker Safety 2018a, Accord on Fire and Building Safety In Bangladesh 2020d, 2018e, 2020a).

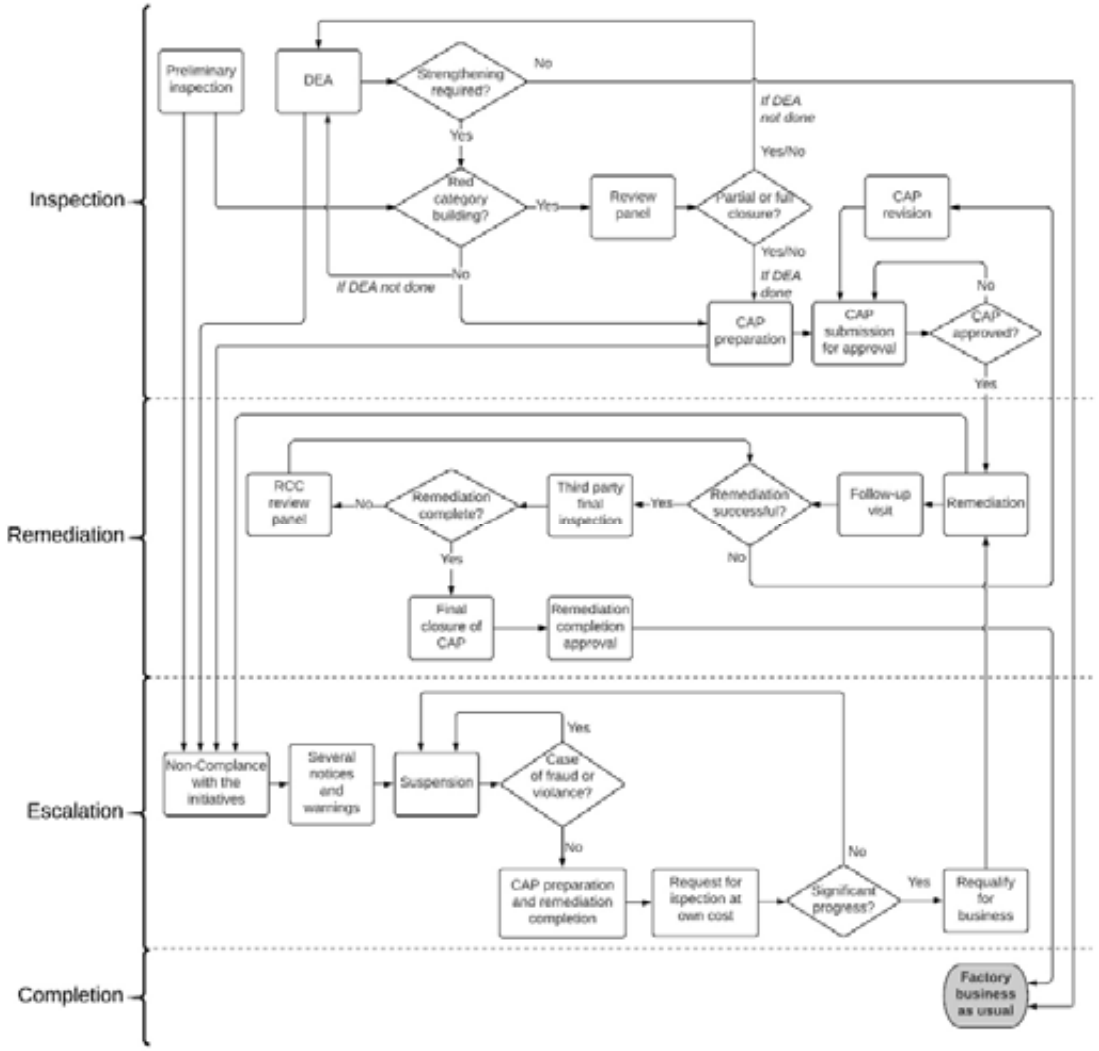

Figure 2: Overall process flow to ensure structural safety in the Bangladesh RMG sector

5. Progress of achieving structural safety of RMG factory buildings

To achieve the goal for structural safety by ensuring appropriate assessment and remediation, all three initiatives emphasized capacity building. The DIFE appointed 60 engineers under a government-funded project to strengthen RCC, where the ILO is supporting RCC for capacity building with a team of 54 members including 47 Engineers (RCC 2018b, f). Additionally, DIFE is issuing certificates to firms and enlisting them who are eligible to carry out the activities accordingly to ensure correctness in the process. Till 2018, 26 structural auditing firms have been listed for remediation works (RCC 2018e). The Accord invested in efforts to increase the Accord engineers' capacity and experience with support from international structural engineering company (Accord on Fire and Building Safety In Bangladesh 2020b).

Table 1 shows the status of structural safety initiatives for RMG factory buildings in Bangladesh including the status of inspection, suspension, and remediation. Except for new, unlisted and extended factories, initial inspection of all the RMG factories has been completed under all the initiatives (Accord on Fire and Building Safety In Bangladesh 2020b, Alliance for Bangladesh Worker Safety 2018f, RCC 2020). Many non-compliances with standards were found in the factories under different initiatives through structural assessment (RCC 2018b). Among them, the main structural safety issues found include the highly overstressed columns; cracks in beams and floor slabs; discrepancies between design information and building structure; inadequate additional construction onto cantilevers; absence of load plan or poor management of the existing load plan; undocumented constructions and inconsistencies with the structural plan and design drawings; lack of design check against lateral load; etc. (Accord on Fire and Building Safety In Bangladesh 2018f, 2020b, c). After completion of the inspection phase, the emphasis was switched to remediation (ILO 2018).

From Table 1 it can be observed that, under the National Initiative, the progress of remediation is not at the expected level due to inactiveness and deferral by factory owners (RCC 2018b). On the contrary, the Accord and the Alliance have completed remediation in the vast majority of its affiliated factories, marking an enormous step forward in creating a safer industry for millions of workers indicating the real change in the sector (Accord on Fire and Building Safety In Bangladesh 2020b, Alliance for Bangladesh Worker Safety 2018f). With time, the pace of remediation has been accelerated dramatically, and the rate of suspensions has slowed drastically indicating a strengthened foundation of safety across the industry (Alliance for Bangladesh Worker Safety 2018f). Thus, both the Accord and the Alliance made a timely review of remediation activities and based on the progress put necessary pressure for timely completion of remaining works.

Table 1: Status of structural safety initiatives for RMG factory buildings in Bangladesh

Status	Accord	Alliance	National Initiative
Total inspected	1631	714	689
Suspended/Ineligible	183	180	-
Remediation completed	92%	94%	39%

Source: Adapted from (Accord on Fire and Building Safety In Bangladesh 2020b, Alliance for Bangladesh Worker Safety 2018f, RCC 2020)

Another important component of the structural safety initiatives is the public release of all inspection reports as well as periodic updates to each CAP of all factories throughout Bangladesh in a single platform. The assessment reports and CAPs for the factories under Accord and the Alliance have been made public through their websites (Accord on Fire and Building Safety In Bangladesh 2018b, Alliance for Bangladesh Worker Safety 2018g). Moreover, data sharing in a single platform has been done through RCC, though the reports are not updated regularly (RCC 2018k, i, j).

6. Way forward

The assessment initiative has reached its target and the status of remediation is showing significant progress in structural safety. But, due to limited capacity in terms of human resources, technical issues, and database management, the process of remediation under the National Initiative is getting hampered which is reflected by the lack of remediation progress. Such lack of remediation completion may lead to continued risk of (partial) collapse of the factory buildings. Therefore, the capacity of the National Initiative should be further strengthened.

Many factories have not been included in the process due to the unwillingness of the factory owners. Therefore, the co-operation of rented or shared building owners housing RMG factories is necessary to make the structural safety initiative successful. Again, the list of factories provided by BGMEA and BKMEA is incomplete. There also remain many factories which are not a member of any organizations such as BGMEA and BKMEA. Due to exclusion from membership, these factories fall out of the programs and can no longer export their products. Despite this fact, these factories are still operating for the local market and often work as subcontractors for export-oriented factories. So, the list of factories needs to be updated and verified including the remaining factories to ensure quick completion of the assessment. The safety concerns of backward linkage activities of RMG enterprises (e.g. textiles, accessories, etc.) have also been excluded from monitoring and inspection which also need to be taken into consideration.

Whatever the progress is, if accuracy in the whole process is not ensured then the target of achieving structural safety in the Bangladesh RMG sector may remain unachievable leading to more accidents like Rana Plaza. The RCC listed the common mistakes in the inspection process for structural safety which includes general mistakes, mistakes in architectural and structural drawings, common mistakes of structural DEA firms, and mistakes in the DEA

report (RCC 2018d). These mistakes may lead to inaccurate structural assessment and thereby misguide the remediation process. This in turn may fail to achieve the goal of structural safety in the RMG sector.

Another challenge is that CAP completion requires a great deal of time and investment, where some remediation items are costly and burdensome to factory owners (Alliance for Bangladesh Worker Safety 2018d, f). Despite this fact, such investments can mean the difference between life and death for the workers (Alliance for Bangladesh Worker Safety 2018f). Thus, these measures are necessary to create a safer workplace and thereby build a more positive image of the Bangladesh RMG sector to ensure business continuity complying with all relevant safety standards (Alliance for Bangladesh Worker Safety 2018d, ILO 2018). On average, $250,000 to $350,000 per factory is required for remediation, and for this, many factories will require external financing which is difficult for the factory owners in Bangladesh due to high-interest rates (Alliance for Bangladesh Worker Safety 2018h, ILO 2018).

To financially help the factory owners for remediation, special credit facilities at a low-interest rate (4-7%) were established by several development partners including Japan International Cooperation Agency (JICA), French Development Agency (AFD), German Development Agency (GIZ), International Finance Corporation (IFC), KFW Development Bank and United State Agency for International Development (USAID) (ILO 2019, 2018). To facilitate these schemes, some workshops between and among factory owners, employers' organizations, commercial banks, and financing institutes have been organized by the ILO (ILO 2019). Moreover, several outreach activities have been organized jointly by the ILO and Bangladesh Bank, and the DIFE targeting factory owners to orient them about the available schemes and the remediation application process (ILO 2019). Furthermore, to improve the remediation finance application process taking feedback from the factory owners and business associations, the "Support to Safety Retrofits and Environmental Upgrades in Bangladesh RMG sector (SREUP)" programme has been launched with support from ILO and jointly financed by AFD, EU, KFW and GIZ (ILO 2017a, b).

In addition to these facilities, the Alliance has created several opportunities for financial support. A combined total of $100 million has been committed to being provided by the individual Alliance members in this regard. To provide low-cost loans to factory owners with lower interest rates and longer payback periods, the Alliance partnered with the International Finance Corporation (IFC) to provide financing to five local banks providing a total of $50

million and the Alliance has directly contributed $250,000 to fund its operation. To finance the smaller factories ineligible for the IFC program (already undergone an inspection and have a CAP in place), the Alliance worked with the USAID Development Credit Authority (DCA) with $18 million workings with two local banks where the Alliance contributes $1.5 million to the risk-sharing facility (Alliance for Bangladesh Worker Safety 2018h). To support the Accord factories a Factory Remediation Fund was established in 2017, which is available to all Accord-covered factories since July 2019, meeting certain criteria; e.g. must have completed at least 75% of the initial remediation (Accord on Fire and Building Safety In Bangladesh 2018a). The fund would contribute to cover 75% remediation costs, which would be distributed in four instalments considering factory cooperation and Accord verified completion of the remediation commensurate with each preceding instalment (Accord on Fire and Building Safety In Bangladesh 2020b). Appropriate disbursement of the fund is necessary to ensure that the fund is allocated at the right place as required.

After completing the five-year term in Bangladesh the Alliance has ceased operations in December 2018 (Alliance for Bangladesh Worker Safety 2018b). In 2018, the Bangladesh High Court issued a restraining order against the Accord prohibiting Accord activities in Bangladesh beyond November 2018. In May 2019, a labour-brands-industry organization named RMG Sustainability Council (RSC) was planned to be established to resolve the court case which was accepted by the High Court's Appellate Court. As a result, the functions of the Accord in Bangladesh were intended to be transitioned to the RSC after June 2020. The purpose of this council is to ensure the sustainability of the process, which was intended to be governed by a Board of Directors consisting of an equal number of representatives from industry, brands, and trade unions; and closely co-operating with and supporting the regulatory functions of the Government of Bangladesh. It was intended to inherit all operations, staff, infrastructure, and functions of the Accord and to continue with factory safety programs until May 2020 (Accord on Fire and Building Safety In Bangladesh 2020b).

However, completion of the remediation does not mean an end to the initiative (RCC 2018h). These initiatives have led to important organizational learning for Bangladesh as well as for other apparel manufacturing countries. Therefore, to ensure the sustainability of the process and the system after completion of these initiatives, the remediated factories will have to maintain safety compliance and to ensure this regular inspection system of DIFE will be continued (RCC 2018h). In this vision, the RCC will transition into a government-led Industrial Safety Unit in the long run and will take over the responsibility for relevant

workplace safety issues and non-remediated factories once the Accord, Alliance, and development partner support end (RCC 2018a, c, ILO 2018). It will also identify and include unlisted, newly established, expanded, and relocated factories in the safety process (ILO 2018). In this regard, the RCC will contribute to enhance the national regulators' capacity facilitating knowledge transfer from the Accord and the Alliance as well as enhance collaboration between them in the long run (RCC 2018g, ILO 2018). It will also be tasked to monitor workplace safety of all industrial sectors in Bangladesh (RCC 2018h, g, ILO 2018). But the challenge remains in the successful transition in this regard.

7. Can RANA Plaza Happen Again in Bangladesh?

From the above discussion it can be said that even though the structural safety initiatives have largely reached its target of inspection and remediation of factories, there is still a long way forward to reach the goal of workplace safety in Bangladesh RMG factories. There are many success stories. One of the many success stories is the case of Libas Textiles Ltd. Under the Accord. After an initial inspection in 2014, the factory buildings were found to be unsafe and needed to be evacuated and production temporarily suspended. In 2016, the factory completed its remediation accordingly (Accord on Fire and Building Safety In Bangladesh 2018c). But to achieve the ultimate goal, the way forwards will have to be addressed accordingly.

There are many cases where factory owners are doing wrong deeds to get a positive report from the assessment. We have one recent experience with two factories supposedly named AL and PR, during the training of the DIFE inspectors regarding factory assessment and follow up. These factories located at Dhaka have been assessed under the National initiative in December 2013. There are two buildings under the factories: one is a 6-storied and the other is an 8-storied building having a basement. The ground floor of the two buildings are housing several shops and go-downs, the basement of the 8-storied building has been used as the fabric store for one of the factories (factory AL). This factory is occupying both buildings up to the 3rd floor (connected internally) and up to the 5th floor of the 6-storied building, while the other factory (factory PR) is occupying the 4th to 7th floor of the 8-storied building. During the inspection in 2013, the 8-storied building was found safe having larger columns and smaller spans. On the other hand, the 6-storied building was found unsafe having smaller columns and larger cantilevers for which remediation measures were suggested accordingly. In early 2015, factory AL moved under Accord. While applying for the Accord, the owner of the factory has only used the 8-storied building intentionally hiding the 6-storied building.

Thus, the 6-storied building was never assessed by the Accord. During a recent visit to the factory PR (which is still under National Initiative), the DIFE inspectors have found several cracks in the top floor beams of the 6-storied factory. But when DIFE inspectors were checking the factories, the owner of factory AL told them that the whole factory is under Accord and has been fully assessed.

This is just a case among many. If these conditions cannot be taken care of then, surely, Rana Plaza can happen again. More researches are necessary in such cases to explore and understand different dimensions of the problems in the way of achieving structural integrity in the RMG sector in Bangladesh.

BANGLADESH NETWORK
OFFICE FOR URBAN SAFETY

PART-IV

DYNAMIC RESPONSES OF REINFORCED SOIL MODEL WALL ON SOFT CLAY FOUNDATION

BANGLADESH NETWORK OFFICE FOR URBAN SAFETY (BNUS), BUET, DHAKA

Prepared By: Ripon Hore

Mehedi Ahmed Ansary

INTRODUCTION

Seismic influence on soil structures played an important role in the area of earthquake geotechnical engineering and was found considerable development in the recent past. Two aspects of model testing were given importance, namely a rigid box, and a laminar box. A laminar box is a sophisticated container than a rigid box which can enhance the accuracy in assessing the ground behavior. In this research, a wrap reinforced soil wall was fabricated on clay soil enclosed by a laminar box and subjected to sinusoidal input motions through the shake table. Moreover, the spacing between the reinforcements and relative density of the backfill were kept constant in all shaking table tests. Based on shaking table tests, this paper attempts to investigate the effect of the frequency and acceleration of the base sinusoidal motion, surcharge pressure, pore water pressure and the number of layers on the accelerations, horizontal face displacements and soil pressures in wrap-faced retaining walls under simulated seismic conditions. Wrap faced reinforced soil retaining wall on soft clay is popular in all over the world because wrap faced layer consumes less space in both sides of the wall, which is economic and less susceptible to dynamic loading.

According to worldwide experiences, the reinforced soil walls show a flexible behavior and considerable deformation under seismic loads (Edgar et al. 1989; Collin et al. 1992; Ho and Rowe 1996; White and Holtz 1997; Tatsuoka et al. 1995, 1997; Ling et al. 2001). Reinforced soil walls exhibit better performance level when compared to conventional retaining walls under seismic load (Roessing and Sitar 1998). Moreover, the cost of constructions of reinforced soil wall is less than a conventional retaining wall as stated by Latha and Krishna (2006). Many researchers (e.g., Murata et al. 1994; Matsuo et al. 1998; Bathurst et al. 2002; Nimbalkar et al. 2006) studied full scale rigid retaining walls and segmental retaining walls (Nova-Roessig and Sitar 1999; Huang et al. 2003; Ling et al. 2005; Huang and Wu 2006). The practice of wrap-faced reinforced soil increased rapidly worldwide due to its better seismic performance. In spite of its importance, very few studies (e.g., Sakaguchi et al. 1992; Koerner 1999; Perez and Holtz 2004; Benjamim et al. 2007) are available in this regard.

Richardson and Lee (1975) attempted first small-scale shaking table tests on reinforced soil walls with metallic reinforcement. Sakaguchi et al. (1992) and Sakaguchi (1996) carried out shaking table tests on 1.5m high reinforced model walls and discussed the influence of various parameters. Parameters like relative density of soil, frequency and

amplitude of the motion, reinforcement's types, and spacing between the reinforcements, tensile strength and soil interaction, friction angle between reinforcements, facing material, surcharge pressure and others have influence on deformations of the reinforced soil walls under seismic load (Roessing and Sitar 1998; Paulsen 2002). The seismic performance of reinforced soil walls using different reinforcing materials and facing systems were inspected through experimentations and numerical analyses conducted under various conditions (Richardson et al. 1977; Ling et al. 1997; Matsuo et al. 1998; Koseki et al. 2006; Shahri et al. 2010).

Several shaking table studies were carried out on wrap-faced reinforced soil retaining walls to gain insight into their behavior under dynamic loads was conducted by Latha and Krishna (2006; 2008), Krishna and Latha (2007), Sabermahani et al. (2009) and Esmaeilabadi et al. (2014). Moreover, a series of laboratory shaking table tests were performed for observing the performance of unreinforced and reinforced soil slopes by Srilatha et al. (2013; 2014) and Latha and Nandhi (2014). Two different slope angles and reinforcement were used in their tests. A reduced-scale shake table test investigating the seismic response of slurry wall and sandy soil was presented by Xiao et al. (2014). Moreover, shaking table tests were performed effectively to investigate the behavior of excess pore water pressure in different soft soil-foundations of soil-structure interaction (SSI) system (Zhang, et al. 2009). The performance of geo-cell retaining walls inside a laminar box under seismic shaking conditions was described by Latha and Manju (2016). Moreover, a series of shaking table tests on 0.9 m high reinforced-soil wall models with different steel strip lengths were performed by Yazdandoust (2017).

This study focuses on the seismic design of roadway or railway embankment on soft clay soil. A scale model testing platform was developed for a single degree of freedom shaking table tests that symbolize the dynamic free-field conditions of clayey soil where a wrapped geotextile-sand retaining wall was erected on clay soil subjected to seismic loading. A total of 90 shaking table tests were carried out on this model embankment. In order to explore the possible influence of the impact on the soil, the test implements repeated loading and unloading process. The effects of frequency, amplitude, surcharge, pore water pressure and displacement along the different elevations were observed in this study.

OBJECTIVE AND SCOPE

The objectives of this study were to (a) observe the behavior of wrap-faced reinforced soil wall under harmonic sinusoidal input motions, (b) fix a suitable scaling for constructing a dummy embankment, (c) conduct a series of shaking tests effectively, (d) observe the seismic response of the scale model embankment due to alterations in frequency, surcharge and acceleration of base shaking and (e) determine the layer by layer response of soil wall due to these shaking. The specific purpose of the study was to evaluate the seismic response of a constructed embankment model regarding the input of sinusoidal motions.

TESTING EQUIPMENTS AND TESTING MATERIALS

Equipment Used in This Study

Shaking Table

A computer-controlled servo-hydraulic single degree of freedom shaking table facility was used to simulate the horizontal shaking action, associated with seismic and other vibration conditions. The testing platform was made of a 2 m by 2 m size steel base with a 1500 kg of payload capacity as shown in Figure 1. Shaking was provided by a digitally controlled servo-hydraulic actuator with an acceleration capacity of 0.05g to 2g and a frequency range of 0.05Hz to 50 Hz having a maximum amplitude of ±200 mm. The total operating system was controlled in a dedicated room.

Laminar Box

The ideal container is one that gives a seismic response of the soil model identical to that obtained in the prototype. In this study, embankment with soft clayey soil model was constructed in a laminar box to reduce boundary effects. The fabricated laminar shear box consists of 24 hollow aluminum layers of frames. Each layer consists of an inner frame with an inside dimension of 915 mm × 1220 mm × 1220 mm. The gap between the successive layers is 2 mm, and the base layer is rigidly connected to the solid aluminum base plate (915 mm x 1220 mm x 15 mm).

The Layers

Each layer consists of a rectangular frame with an internal dimension of 1220 mm × 920 mm × 50 mm. Transfer ball bearings were used to minimize the friction between the layers. Ball

bearings consist of one main ball, with a diameter of 12 mm, placed in a hemispherical space filled with fine balls.

Base Plate and Saturation and Drainage Systems

The lowest layer is fixed on a steel base, rigidly fixed on a steel plate having the same dimension of laminar layers. The base has some space for watering and dewatering via four valves. The area of water entry into to the model is covered with porous stone. This arrangement facilitates both the saturation and drainage of the samples.

Membrane

A 2 mm thick rubber membrane, as shown in Figure 2, was placed inside the laminar box for the hydraulic cut-off system and for the protection of the ball bearings. The significance of using this fabric was that it is designed to fold or unfold as sand moves against it rather than to stretch like a conformist silicone rubber membrane.

Portable Pluviator

Many researchers (e.g., Fretti et al. 1995, Zhao et al. 2006, Choi et al. 2010) attempted in developing methods to control uniformity and to achieve desired relative density (D_r) of sand specimen (Miura and Toki 1982, Rad and Tumey 1987, Lo Presti et al. 1993, Choi et al. 2010, Dave and Dasaka 2012, Srinivasan et al. 2016, Gade et al. 2016). Among these techniques, air pluviation method is preferred because of its advantage to reconstitute uniform sand bed for laboratory testing.

In this study, a portable traveling pluviator developed by Hossain and Ansary (2018), was used to maintain the corresponding relative density of sand layer at 64%. Components of the pluviator are shown in Figure 3. The physical model was prepared with two soil layers—clayey soil as the lower layer and sandy soil as the upper layer.

Materials Used in This Study

Clayey Soil

The clayey soil sample was collected at a depth of 1.5 m below the existing ground level from a location within BUET, Dhaka city, Bangladesh. This sample was at first oven-dried;

subsequently, the dry lumps were powdered gently by using a wooden hammer; and finally sieved through #200 standard sieve to obtain clean clayey soil powder. The particle size distribution of the clean clayey soil is presented in Figure 4. The specific gravity G_s of the soil was determined, from the laboratory test, to be 2.64. X-ray diffraction tests (XRD) was performed, at a scanning speed of 8° (2θ) min^{-1} by using Ni-filtered CuKα radiation to identify the mineral composition of clayey soil. XRD test results are summarized in Table 1. A careful examination of these data reveals that the predominant mineralogical composition of the clayey soil was Kaolinite (75%), followed by Illite (25%). An Atterberg limit test was performed on five representative samples. Average liquid limit (LL) and plastic limit (PL) was established to be 41% and 16%, respectively. The soil was defined as Lean Clay (CL), as per USCS classification.

Reconstituted Clayey Soil

Burland (1990) demonstrated that the essential engineering properties of reconstituted clay—shear strength and compressibility—provides a basis to interpret the corresponding properties of the in-situ natural clay soil (regardless of it being normally consolidated or over consolidated). Consequently, in this study, clayey soil was reconstituted by thoroughly mixing the oven-dried clayey soil powder with an initial water content equal to the LL—a procedure described by Burland (1990). The thorough mixing of the slurry was attained with the aid of a 'Hobart' rotary mixer. With this slurry, a 610 mm (24 inches) thick reconstituted clayey soil layer was constructed in the laminar shear box; and then consolidated under the undrained isotropic condition at loads: 15kPa, 20kPa, 25kPa, 30kPa, 40kPa, 60kPa, 80kPa and 100kPa, respectively. The consolidation process was observed through the settlement of clayey soil versus time graph, plotted with the aid of calibrated mechanical dial gauges, instrumented on either side of the laminar shear box. The average settlement curve is shown in Figure 5. This curve shows progressive soil structure collapse, a kind of time dependent bond weakening in the soil. Moreover, pore water pressure dissipates slowly then due to quicker dissipation settlement increases.

UU triaxial test is suitable for saturated clay, silt, peat in both undisturbed and remolded or reconstituted sample for providing the actual field conditions. UU triaxial test was performed on the collected soil sample with a shear rate of 1.5 mm/min for each test. The applied confining stresses for the reconstituted clayey soil samples were 50 kPa and 100 kPa. The obtained value of undrained shear strength (S_u) is 28 kPa.

Sandy Soil

Sand was utilized in the construction of the 0.4 m (16") high reinforced soil zone and backfill soil. The representative sample was oven dried and sieved through ASTM standard sieves (Passing sieve #4 and retaining on #200) to investigate the properties. The resulting particle size distribution is shown in Figure 6. The coefficient of uniformity (C_u) and the coefficient of curvature (C_c) was 2.19 and 0.68, respectively. Tthe result indicates a poorly graded, medium to fine sand (SP). Fineness modulus of the sand was 2.7. Other physical parameters such as specific gravity (G_s) and maximum dry density (γ_d) had been determined to be 2.65 and 16.6 kN/m^3, respectively. The portable traveling pluviator was operated to maintain a target relative density of 64% for the sand layer. This was achieved by ensuring that sand falls from the pluviator at a predetermined constant height for each layer laterally and longitudinally. Strength parameters were determined using the direct shear test. The test establishes an internal angle of friction φ of 33°.

Reinforcement

The non-woven polypropylene multifilament geotextile (DF50) was used in reinforcing the sand. Table 2 summarizes the properties of the geotextile. Universal tensile testing machine was used for determining the tensile properties of geotextile. 500 mm × 200 mm sized geotextile sample was taken for this test and the gauge length was 100 mm. Three samples were collected for X and Y direction. Elongation of specimens with increasing load was measured. The load-elongation response of the geotextile was obtained from the wide-width tensile strength test in both X and Y directions. The average initial modulus (Ei) and secant modulus (Es) in both directions (X and Y) were 40 KN/m, 141 KN/m, and 47kN/m, 123 KN/m, respectively.

EXPERIMENTAL PROCEDURE

Model Geometry

Height of Clayey Soil Layer

The present study was conducted with a thickness of 610 mm (24 inches) clayey soil layer foundation above which a 50 mm (2 inches) sand blanket was provided as shown in Figure 7. This clayey soil layer reflects the height limitation of the laminar box and the total weight of

the model. Approximately 1 m^2 geotextile was placed between the clayey soil foundation and sand blanket. The toe boundary of the wall was horizontally free sliding since the wall was constructed on the surface of the foundation. The height of the clayey soil layer of 610 mm (24 inches) was made in three 200 mm (8 inches) stages. Considering the prototype to model scale being N=10 and scale factor 1/N, the height of the prototype was 6 m (20 ft).

Wall Height and Layers

Wall height is a significant factor governing scale effects and the reaction of the model in contrast with the prototype. Better results were found with the higher height of the sand wall. The average height of traditional walls usually ranges from 4.5 to 5 m (Sabermahani et al. 2009). A 400 mm (16 inches) high model with a scale factor of 10 was fabricated for the current study. Many shake table tests, on the different height of the sand wall, such as 1.5 m (Sakaguchi et al. 1992; Sakaguchi 1996), 1 m (Matsuo et al. 1998; El-Emam and Bathurst 2007), 0.6 m (Krishna and Latha 2007), and 0.33 m (Richardson and Lee 1975) were performed in the past. The schematic geometry of the experimental model for this study is shown in Figure 7. The sand wall consists of 4 layers and each layer was 100 mm (4 inches) thick. A concrete block as a surcharge load was placed at the top of the upper layer of the wall after the full construction of four layers.

Facing Type

Wrap-around type wall facing was used with flexible geotextile as shown in Figure 8. Hence, it allowed free movement of the reinforcing enclosure and had no interaction with the rigid bottom. As per Koerner (1999), each individual facing was formed by wrapping each layer with soft flexible geotextile element. The extended geotextile was anchored by partial burial at the end by backfill material.

Sensor Arrangement

The accelerations and lateral displacement were measured using accelerometers and displacement transducers (LVDT sensors), respectively at different locations within the clayey soil layer, geotextile wrapped face wall and backfill soil. Six accelerometers (A1, A2, A3, A4, A5, and A6), two pore water pressure sensors (P1 and P2), four strain gauges (Sg1,Sg2, Sg3 and Sg4), and three linear variable differential transformers (LVDT1,LVDT2

and LVDT3) were used in this model test. All the sensors were positioned at predefined locations during the layer by layer construction of the physical model. One accelerometer, A1, was fixed to the shake table to record the base acceleration. The other five accelerometers A2, A3, A4, A5, and A6 were placed at elevations 457 mm (18 inches), 710mm (28 inches), 810 mm (32 inches), 915mm (36 inches), and 1015mm (40 inches) mm, respectively, from the base as shown in Figure 7. A3, A4, A5, and A6 were positioned at a constant distance of 100 mm (4 inches) from the middle of each sand slice. Two pore water pressure sensors; P1 and P2, where P1 was set at the base of the clayey soil layer and P2 was positioned at elevation 457 mm (18 inches) from the base is shown in Figure 7. The pore water pressure sensor (P2) was placed at a height of 457 mm (18 inches) from the base. However, it was placed to maintain 254 mm (10 inches) horizontal distance from the left face of the laminar box. Strain gauges were attached with geotextile layers. Sg1 was placed at the bottom of the first layer which was just above the sand blanket. However, the other three strain gauges Sg2, Sg3 and Sg4 were placed at elevation 100 mm (4 inches), 200 mm (8 inches), 300 mm (12 inches), respectively from the top surface of the sand blanket as depicted in Figure 7. Three displacement transducers (LVDT1, LVDT2, and LVDT3) were placed at elevations 150 mm (6 inches), 250 mm (10 inches) and 350 mm (14 inches), respectively from the top of the sand blanket to measure horizontal displacement of the geotextile facings of the top three layers. LVDTs were positioned in place using a hanging T-shaped bracket rigidly connected to the laminar box frame.

Surcharge Load and Relative Density

A portable pluviator was used in this study to achieve a uniform density of the backfill material as described by Hossain and Ansary (2018). 64% relative density of the backfill soil was achieved by maintaining 200 mm height of fall. The sand which was used for backfill material had been passed ASTM standard sieve number 4 (4.75 mm) and was retained at 200 number sieve (0.075 mm).

Three different surcharge loads 0.7 kPa, 1.12 kPa and 1.72 kPa were employed in this study. The surcharge load was made in the form of a concrete slab. 0.1g, 0.2g, 0.3g, 0.4g and 0.5g acceleration based sinusoidal waves were applied to the model for each surcharge load and corresponding measurements were made using the different sensors described before.

Prototype-Model Similitude

The reliability of model tests depends on whether the model can represent the real behavior of the prototype system. Model size in this study was fixed according to the facilities available for this test. Precise scaling of soil walls and reinforcement properties is needed for considering the stress-dependent behavior of the soil and boundary conditions.

The model is scaled to achieve similitude with the prototype wall. It is not possible to predict the accurate behavior of the prototype with compared to the reinforced model wall using 1g shaking table test (Krishna and Latha 2007, Latha and Krishna 2008 and Sabermahani et al. 2009). The exponent of confining pressure (α) was assumed to be 0.5 for sand (Kokusho 1980, Yu and Richart, 1984). Considering limitations due to the dimensions of the model container and the capacity of shaking table, the prototype to model scale ratio (N) usedwas 10 as presented in Table 3.

Fundamental Frequency

As physical models are shorter versions of prototype walls, the frequency of induced input motions is recommended to scale accurately to produce similar effects to those of earthquakes on prototype walls. It is an essential phase in the seismic design to determine the natural frequencies of the structure.

Reinforced-soil retaining walls of typical heights (i.e., H > 10 m) and backfill material are generally considered as short-period structures as addressed by Sabermahani et al. (2009). The response of the wall to ground motion is dominated by the fundamental frequency of the structure (Hatami and Bathurst, 2000). The resonant frequen cy of the walls also changes significantly with the height of the wall (Latha and Krishna, 2008).The fundamental frequency of wall model was calculated based on impact test performed before the first shaking of actual tests. The fundamental frequency of the soil embankment model was around 16 Hz. Wall response is critically dependent on the base frequency of the structure, the range of the applied frequencies were kept in a range distant from the fundamental frequency of the walls to avoid resonance which was addressed by Kramer (1996) and Bathurst and Hatami (1998).

Input Motions

Harmonic sinusoidal type of base acceleration was designated for this current parametric study. This harmonic sinusoidal base acceleration is more aggressive than an archetypal earthquake with the same predominant frequency and amplitude which was observed by different researchers in the past (Bathurst and Hatami 1998; Matsuo et al. 1998; El-Emam and Bathurst 2007).

Keeping in mind the fundamental frequency of the embankment modelwere subjected to 1Hz, 3Hz, 5Hz, 10Hz, 12Hz, and 15 Hz frequencies as input motions. The frequency range used in the present study was less than the natural frequency of the system and hence the models were not subjected to resonance. Since frequencies of 2–3 Hz are representative of typical predominant frequencies of medium to high frequency earthquakes (Bathurst and Hatami, 1998), the rest of the frequency ranges were used to evaluate the seismic behavior patterns of the existing embankment models. Based on the scale factor of frequency presented in Table 3, these values are respectively corresponding 0.18Hz, 0.54Hz, 0.90Hz, 1.8Hz, 2.16Hz and 2.7 Hz frequencies for the prototype. Moreover, the statement is relevant only if the exponent of confining pressure for soil stiffness α is kept equal to 0.5.

A few researchers experimented with base accelerations of low amplitude, such as 0.1g to 0.2g (Krishna and Latha 2007; Latha and Manju 2016; Helwany et al. 2017) and some were with high amplitude, such as 0.3g to 0.5g (Sabermahani et al., 2009; Edinçliler and Toksoy, 2017). In this current research embankment model was subjected to several different excitations from 0.1g (low amplitude) to 0.5g (high amplitude) peak base accelerations, each being employed after completion of the previous motion. The duration of each shaking was decided to be kept for at least 5 seconds. Exactly 90 numbers of harmonic sinusoidal shaking were used for this research as presented in Table 4. All the shaking tests were applied to the newly constructed individual embankment models. A specific base acceleration was achieved through changes in input amplitude for each frequency (1Hz, 3Hz, 5Hz, 10Hz, 12Hz, and 15 Hz) and surcharge pressures (0.70 kPa, 1.12 kPa, and 1.72kPa).

RESULTS AND DISCUSSION

Results were obtained from several shaking table tests on the embankment model as discussed earlier. The parameters varied in tests were base acceleration, frequency, and surcharge pressure. The base acceleration was kept as 0.1g, 0.2g, 0.3g, 0.4g, and 0.5g in different tests as shown in Figure 9. The range of frequency was varied from 1 Hz to 15 Hz.

The surcharge pressure was kept as 0.70 kPa, 1.12 kPa and 1.72 kPa. The thickness of the soft clayey soil layer was 610 mm. Reinforced-soil wall was constructed using sand upon the clayey soil layer in equal lifts (S_v) of 100 mm to achieve a total wall height (H) of 400 mm. The height of clayey soil and reinforced sand wall together including the sand blanket (50 mm thick) had been taken as the full model height (M) which was 1060 mm. The length (L) of the geotextile reinforcement at the interface of the sand layers was kept the same in all tests as 510 mm. The model wall was subjected to 5 to 75 cycles of sinusoidal shaking for obtaining 5 seconds of data.

Acceleration Response

Typical time-acceleration histories of the shake table tests ST1, ST7, ST13, ST19 and ST25 with 0.7 kPa surcharge and 0.1g, 0.2g, 0.3g, 0.4g, and 0.5g base acceleration and 1 Hz frequency of base sinusoidal motion at same elevation are shown in Figure**s** 9a to 9e. Acceleration amplification is the proportion of maximum peak to peak acceleration value in the soil to that of the corresponding value of the base motion. The acceleration amplification profile along the height of the wall for various inputs of base motion after each test of 5 to 75 cycles of sinusoidal motion is presented in Figures 10a to 10f. However, to compare the acceleration amplification within the reinforced sand wall, the elevation (z) was represented in non-dimensional shape subsequent to normalizing by the full reinforced sand wall height (H=400 mm) as can be seen from Figures 10a to 10c. On the other hand, to compare the acceleration amplification between clayey soil layer and reinforced sand wall, the elevation (z) was represented in non-dimensional shape subsequent to normalizing by the height of clayey soil and reinforced sand wall together (M=1060 mm) as can be seen from Figures 10d to 10f. Maximum acceleration amplification was observed almost at the top of the wall in all the tests. This observation was in consensus with the results of physical tests reported by Telekeset al. (1994), Murata et al. (1994) and El-Emam and Bathurst (2005).

Effect of Base Acceleration on Acceleration Amplification in Reinforced Sand Wall

The acceleration amplifications along the height of the wall for different base accelerations of 0.1g, 0.2g, 0.3g, 0.4g and 0.5g from ST2, ST8, ST14, ST20, and ST26 tests, respectively, which was conducted at 3 Hz frequency and 0.7 kPa surcharge pressure is presented in Figure 10a. Acceleration amplifications were found to be higher with increased base accelerations. After analyzing all the test results, it was observed that acceleration amplifications at the top

of the wall for 0.1g and 0.2g base accelerations were close to 1.11, whereas it was 1.19, 1.29 and 2.01 for 0.3g, 0.4g, and 0.5g base acceleration, respectively. The present study was also compared with the study of Krishna and Latha (2007) as shown in Figure 10a. The acceleration amplification along the height of the wall for different base accelerations of 0.1g, 0.15g and 0.2g from T4, T6 and T7 model tests (Krishna and Latha, 2007) was compared with the present study. In that study, tests were conducted at 2 Hz frequency, 0.5 kPa surcharge, and four layers of reinforcement (total reinforced wall height of 600 mm, each layer thickness was 150 mm). Acceleration amplifications were increased with increased base accelerations for all the curves. However, acceleration amplifications at the top of the wall, for 0.15g and 0.2g base accelerations, were very close to 1.70. At the top of the wall, the value of acceleration amplifications was 1.42 for 0.1g base acceleration. The pattern of amplification for the current study and the study of Krishna and Latha (2007) are almost same. The only difference are observed at the lower part of the curves, where for the current study, amplification values are relatively high since there is a soft clay layer at the bottom of the reinforced sand wall.

Effect of Surcharge on Acceleration Amplification in Reinforced Sand Wall

Acceleration response against different surcharge pressures was presented from tests ST1, ST31 and ST61 as depicted in Figure 10b. These tests were conducted with 0.7 kPa, 1.12 kPa and 1.72 kPa surcharge pressures at 1 Hz frequency and 0.1g base acceleration. Accelerations at the top of the wall were inversely proportional to the surcharge pressures for all the tests. It is observed from the figure that the acceleration amplification values were 1.85, 1.64 and 1.42 for 0.7 kPa, 1.12 kPa and, 1.72 kPa surcharge pressures, respectively. Comparison of the present study with the study of Krishna and Latha (2007) is also shown in Figure 10b. The acceleration amplifications for 1 Hz frequency and 0.1g base acceleration along the height of the wall for surcharge pressures of 0.5 kPa, 1.0 kPa and 2.0 kPa from T1, T2, and T3 model tests of Krishna and Latha (2007) was compared with the present study. Accelerations at the top of the wall were inversely proportional to the surcharge pressures, with amplification values of 1.63, 1.47 and 1.37 for 0.5 kPa, 1.0 kPa, and 2.0 kPa surcharge pressures, respectively. The pattern of amplification for the current study and the study of Krishna and Latha (2007) are almost same.

Effect of Frequency on Acceleration Amplification in Reinforced Sand Wall

The effect of frequency on the acceleration response along the height of the wall for tests ST1, ST2, ST3, ST4, ST5 and ST6 with frequencies of 1Hz, 3Hz, 5Hz, 10Hz, 12Hz and 15 Hz which were conducted at 0.1g base acceleration and 0.7 kPa surcharge pressure is shown in Figure 10c. From the figure, it is observed that the acceleration response against frequency variation is not directly proportional. In fact, within the range of tests conducted accelerations were amplified less for 1Hz, 3Hz and 5 Hz and more for 10Hz and 12Hz frequencies compared with that of 15 Hz frequency at all elevations. Moreover, accelerations at normalized elevations of 0.125, 0.375, 0.625 and 0.875 were amplified closer or slightly more than 1 for the frequency 1 Hz. The differences in acceleration amplifications for various frequencies were increased with increase in wall height. At a normalized height of 0.875, for 1Hz, 3Hz, 5Hz, 10Hz, 12Hz, and 15 Hz frequency, the values of acceleration amplification were 1.04, 1.24, 1.46, 3.26, 2.47, and 1.80, respectively. Moreover, the acceleration amplification values were 0.94, 0.99, 1.05, 1.51, 1.38 and 1.24 for 1Hz, 3Hz, 5Hz, 10Hz, 12Hz, and 15 Hz, respectively at a normalized height of 0.125. These observations highlight the role of the fundamental (resonance) frequency of the system and the proximity of the base excitation frequency (Kramer, 1996). Figure 10c also compares the present study with the study of Krishna and Latha (2007). The acceleration amplifications along the height of the wall for different frequency of 1Hz, 2Hz and 3 Hz from T1, T4, and T5 model tests of Krishna and Latha (2007) was compared with the present study. These three tests were conducted with the base acceleration of 0.1g and 0.5 kPa surcharge on the test wall with four layers of reinforcement. The pattern of amplification for the current study and the study of Krishna and Latha (2007) for 1 Hz to 3 Hz frequency are almost same.

Comparison of Acceleration Response between Reinforced Sand Wall and Clayey Soil Layer

To compare the acceleration amplification between clayey soil layer and geotextile wrap faced sand wall, the height of clayey soil and reinforced sand wall together (M) had been taken as the full model height, which is 1060 mm. The acceleration amplifications along the height of the wall for different base accelerations of 0.1g, 0.2g, 0.3g, 0.4g and 0.5g from ST2, ST8, ST14, ST20 and ST26 tests, respectively, which were conducted at 3 Hz frequency and 0.7 kPa surcharge is shown in Figure 10d. From this figure, it is observed that in the clayey soil layer at a normalized elevation of z/M=0.43, the acceleration amplifications were increased with increased base accelerations. It is also observed that in clayey soil layer at

z/M=0.43, acceleration amplifies less with compared to the top of the wall (z/M=0.95). At the top of the wall acceleration amplification ranged from 1.11 to 2.01 which were greater than amplification of 1.05 to 1.23 at z/M=0.43.

It is observed that in clayey soil layer at z/M=0.43, for 0.7 kPa, 1.12kPa and 1.72 kPa surcharge pressures at 1 Hz frequency and 0.1g base acceleration (from ST1, ST31, and ST61 tests), the acceleration amplitude was 0.99, 0.92, and 0.84, respectively. Moreover, at the top of the wall, for 0.7kPa, 1.12kPa and 1.72 kPa surcharge pressures, the acceleration amplitude values were 1.68, 1.49, and 1.29, respectively as presented in Figure 10e. Accelerations at the top of the wall were inversely proportional to the surcharge pressures for all the tests, which is logical.

In clayey soil layer at the normalized elevation of 0.43, the acceleration amplitude values were 0.89, 1.07, 0.96, 1.42, 1.21 and 1.18 for 1, 3, 5, 10, 12, and 15 Hz frequencies (from ST1, ST2, ST3, ST4, ST5, and ST6 tests), respectively. However, at the top of the wall (z/M=0.95), for 1 Hz, 3 Hz, 5 Hz, 10 Hz, 12 Hz, and 15 Hz frequencies, the acceleration amplitude values were 0.95, 1.11, 1.17, 3.26, 2.27, and 1.74, respectively as shown in Figure 10f. The highest acceleration amplitude at top of the wall is for a base input frequency of 10 Hz as can be seen from Figure 10f. From the figure, it is observed that the acceleration response against frequency variation is not directly proportional.

Displacement Response

Horizontal face displacement along the height of the wall was monitored using three LVDTs positioned as shown in Figure 7. The displaced face profiles from various tests after 5 to 75 cycles of sinusoidal motion are presented in Figures 11a to 11c. Here elevation (z) and horizontal displacements (δh) are presented in non-dimensional from after normalizing them by the height of the wall (H=400 mm).

Figure 11a depicts the normalized displacement profile for different base accelerations of 0.1g, 0.2g, 0.3g, 0.4g and 0.5g from tests ST66, ST72, ST78, ST84, and ST90 (as shown in Table 4), respectively. From the figure, it is observed that the normalized displacements were relatively high at higher base accelerations at the normalized elevation of z/H= 0.875. This phenomenon had similarity to the test results of Sakaguchi et al. (1992) and Krishna and Latha (2007). A maximum horizontal displacement of 2.11% of the total wall

height (H), for 0.5g, was observed compared with 1.96% for 0.1g base accelerations. No significant change of displacements had occurred at z/H= 0.375 and z/H= 0.625 compared to at z/H= 0.875.

The normalized displacement profile for tests ST2, ST32, and ST62 after 5 to 75 cycles of base motion, which were conducted at 0.1g base acceleration and 3Hz frequency, were providing an insight into the effect of different surcharge loadings of 0.7kPa, 1.12kPa and 1.72 kPa as shown in Figure 11b. It was observed that the displacement response against surcharge variation was inversely proportional at all elevations. Moreover, this observation was concurrent with the test performed by Krishna and Latha (2007). The maximum displacement of the wall was (δh/H=2.00%) at a surcharge pressure of 0.7 kPa, whereas it was decreased to (δh/H=1.92%) at a surcharge pressure of 1.72 kPa.

According to the Figure 11c, it can be said that, the displacement response against frequency variation was not directly proportional. The normalized displacement profile observed for tests ST1, ST2, ST3, ST4, ST5, and ST6 with frequencies 1 Hz, 3 Hz, 5 Hz, 10 Hz, 12 Hz, and 15 Hz, respectively, which were conducted at 0.1g base acceleration and 0.7 kPa surcharge pressure as presented in Figure 11c. The displacement had occurred more at z/H=0.875 from the range of tests were conducted. The maximum displacement of 2.04% was observed for 12 Hz frequency at z/H=0.875.

Pore Pressure Response

Typical pore water pressure variations obtained from the tests are presented in Figures 12a, 12b and 12c. The height of clayey soil layer (S) was taken as 610 mm in the case of pore water pressure. The variations of the pore water pressure from model tests ST65, ST71, ST77, ST83, and ST89 with base accelerations 0.1g, 0.2g, 0.3g, 0.4g, and 0.5g, respectively for 15Hz frequency and surcharge load of 1.72 kPa is shown in Figure 12a. The pore water pressure response against base acceleration variation was directly proportional as can be seen from the figure. The maximum pore water pressure was 0.38 kPa at a base acceleration of 0.5g. The maximum pore water pressure for model tests ST66, ST72, ST78, ST84, and ST90 was0.06kPa, 0.09 kPa, 0.17 kPa, 0.26 kPa, and 0.38 kPa, respectively.

Variations of the pore pressure from model tests ST24, ST54 and ST84 with of surcharge 0.7 kPa, 1.12 kPa and 1.72, kPa, respectively for 15Hz frequency and base

acceleration of 0.4g is presented in Figure 12b. From the figure, it is observed that pore water pressure response against surcharge variation was inversely proportional at all elevations. The maximum pore water pressure was 0.37 kPa at a surcharge load of 0.7 kPa. The maximum pore water pressure for model tests ST24, ST54 and ST84 were 0.37 kPa, 0.33 kPa, and 0.26 kPa, respectively.

The effect of frequency for a given base acceleration and surcharge load on pore water pressure for tests ST1, ST2, ST3, ST4, ST5, and ST6 with the frequency of 1 Hz, 3 Hz, 5Hz, 10Hz, 12Hz and 15Hz for 0.1g base accelerations and 0.7 kPa surcharge is shown in Figure 12c. From the figure, it is observed that pore water pressures response against frequency variation is not directly proportional. In fact, pore water pressures increased less for 1 Hz, 3 Hz and 5 Hz and more for 10 Hz, 12 Hz frequencies compared with that of 15 Hz frequencies at all elevations. The highest pore water pressure was 0.105 kPa at 10 Hz frequency.

SUMMARY AND CONCLUSIONS

A series of shaking table studies were carried out on a 1/10 scale model wrap-faced reinforced soil wall to obtain apparent insight into their behavior under harmonic sinusoidal input motions. It was observed that the seismic response of the scale model embankment was significantly affected by changing frequency, and acceleration of base shaking and surcharge loads.. Accelerations were amplified both for sand and clayey soil layers, at higher elevations and with high base acceleration. Aaccelerations were also amplified with low surcharge pressures. It was observed that the acceleration amplification response against frequency variation was not directly proportional. However, the face deformations were high for high base acceleration at the top of the reinforcing layer and impact was relatively low at the other layers. In general, the face deformations were high for low surcharge pressures. It was also observed that the frequency had an inverse impact on face deformations. Pore water pressure gets intensified with increased base acceleration. Increase in surcharge pressure shaking results in a decrease in pore water pressure and the difference being more at higher elevations. These results are helpful to observe the dynamic behavior of the wrap faced soil retaining wall resting on the soft clay layer which is helpful for the design process of this type of retaining walls considering the seismic environment of Bangladesh.

Figure 1: Testing platform

Figure 2: Membrane is being attached inside the laminar box

Figure 3: Portable pluviator for construction of the model wall

Figure 4: Grain size distribution of clayey soil

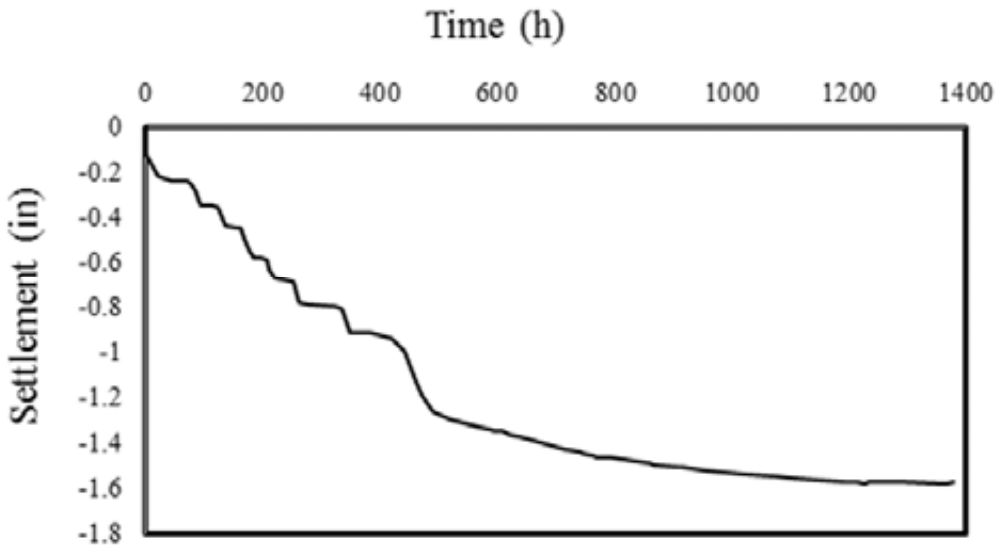

Figure 5: Average settlement curve

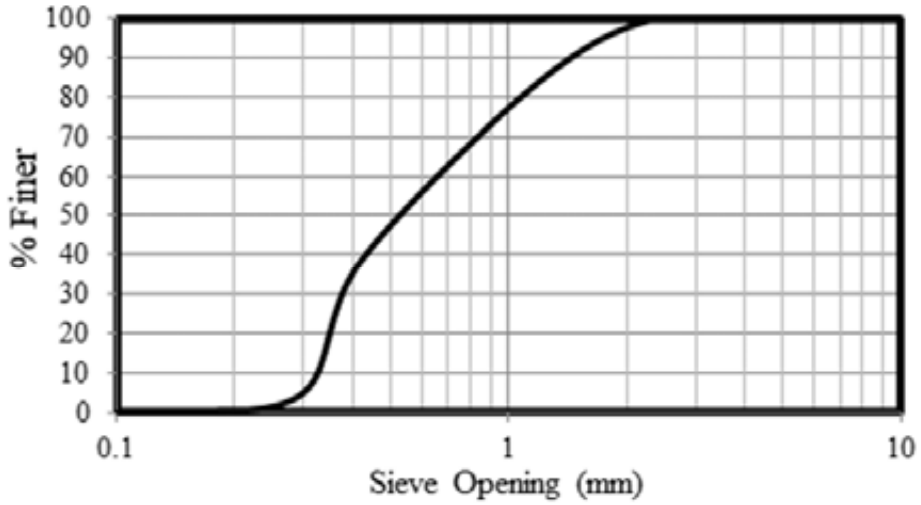

Figure 6: Grain size distribution of sand

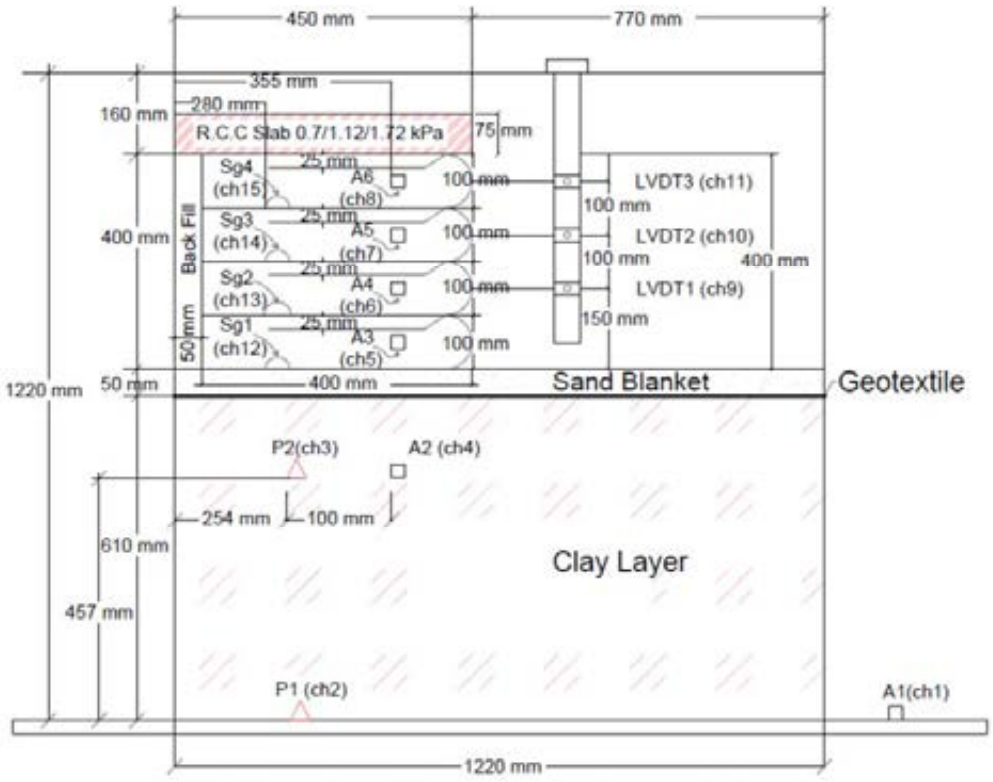

Figure 7: Schematic illustration of physical model with configuration and instrumentation

Figure 8: Finished wrap-faced wall

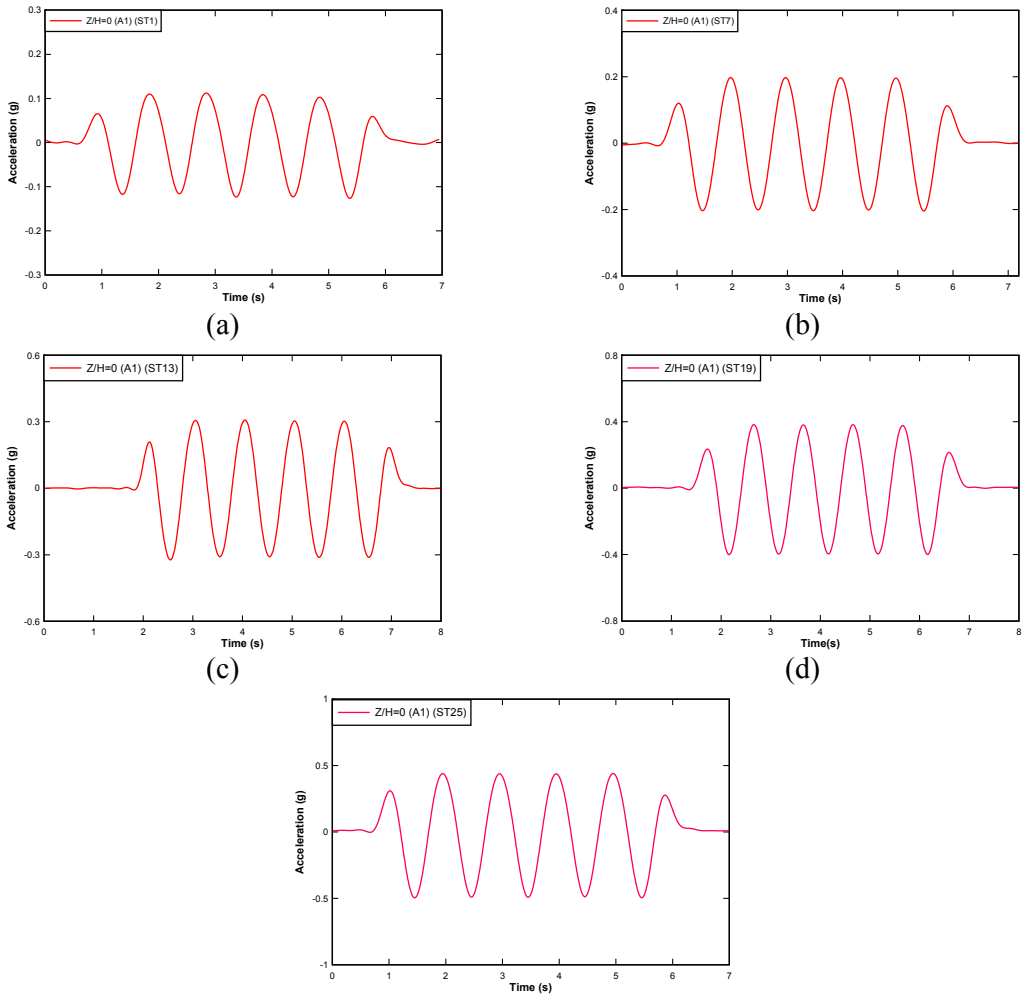

Figure 9: Input time-acceleration curves (0.1g to 0.5g) at frequency 1 Hz

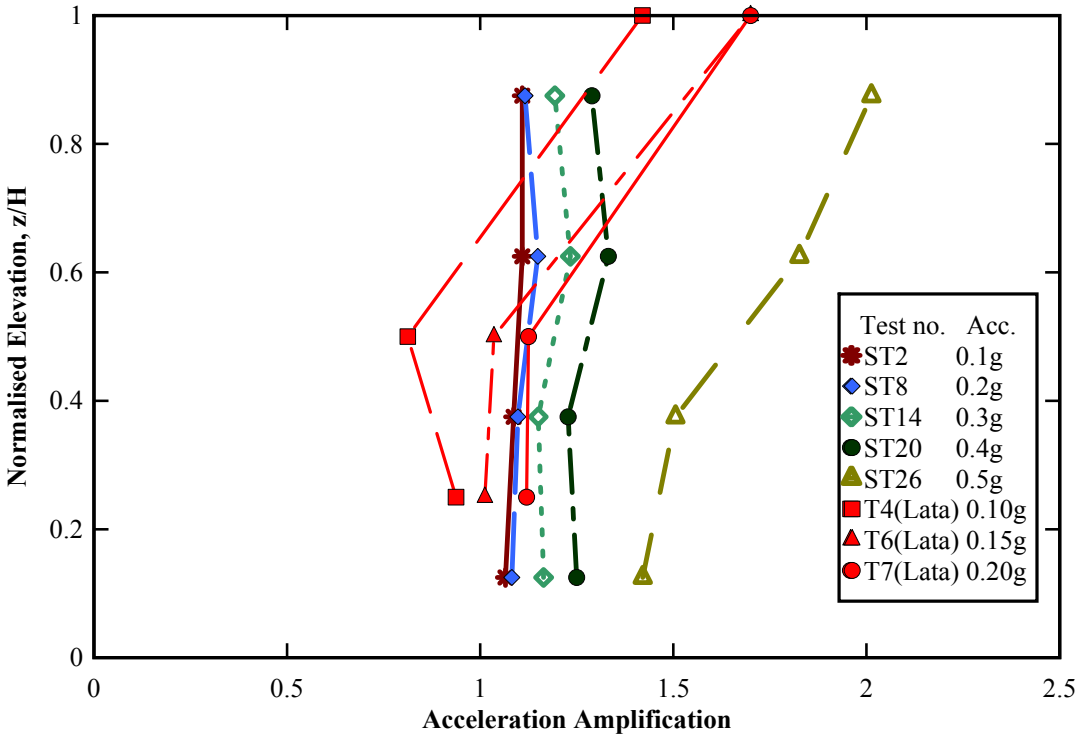

Figure 10a: Effect of base acceleration on acceleration amplification

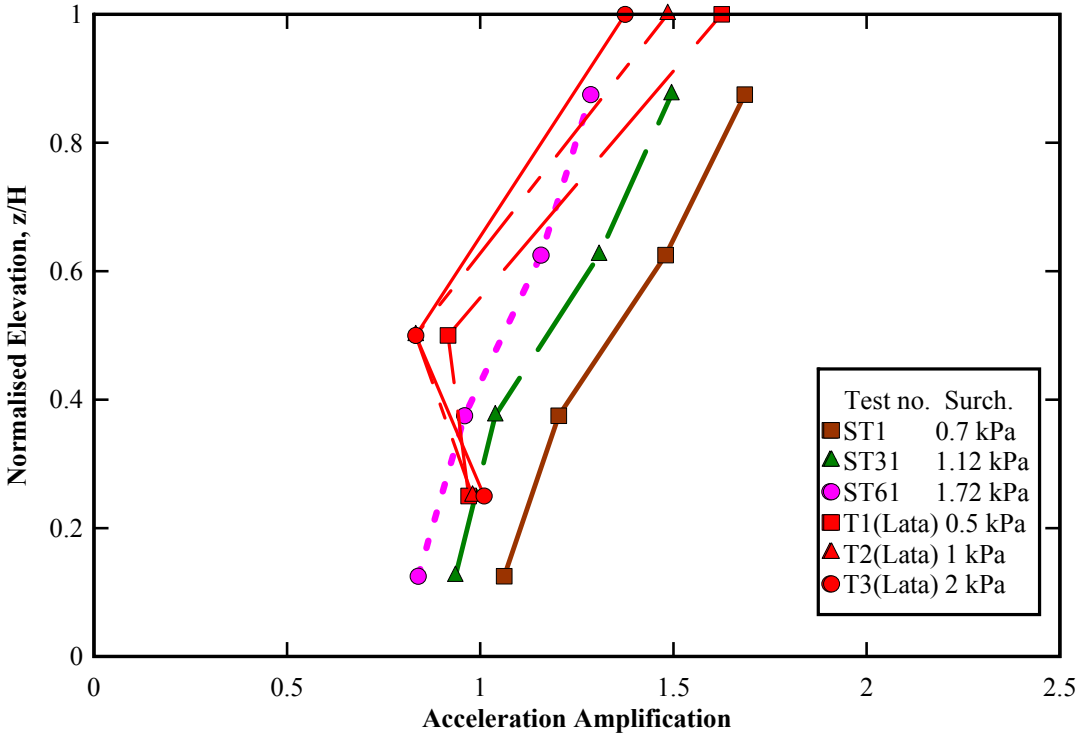

Figure 10b: Effect of surcharge on acceleration amplification

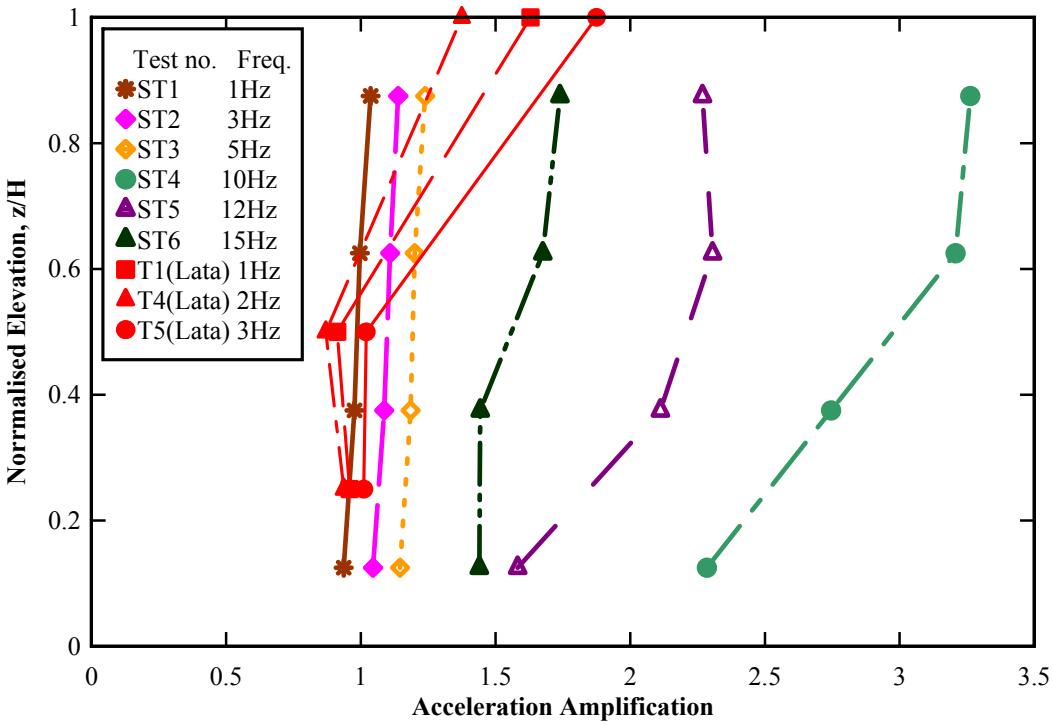

Figure 10c: Effect of frequency on acceleration amplification

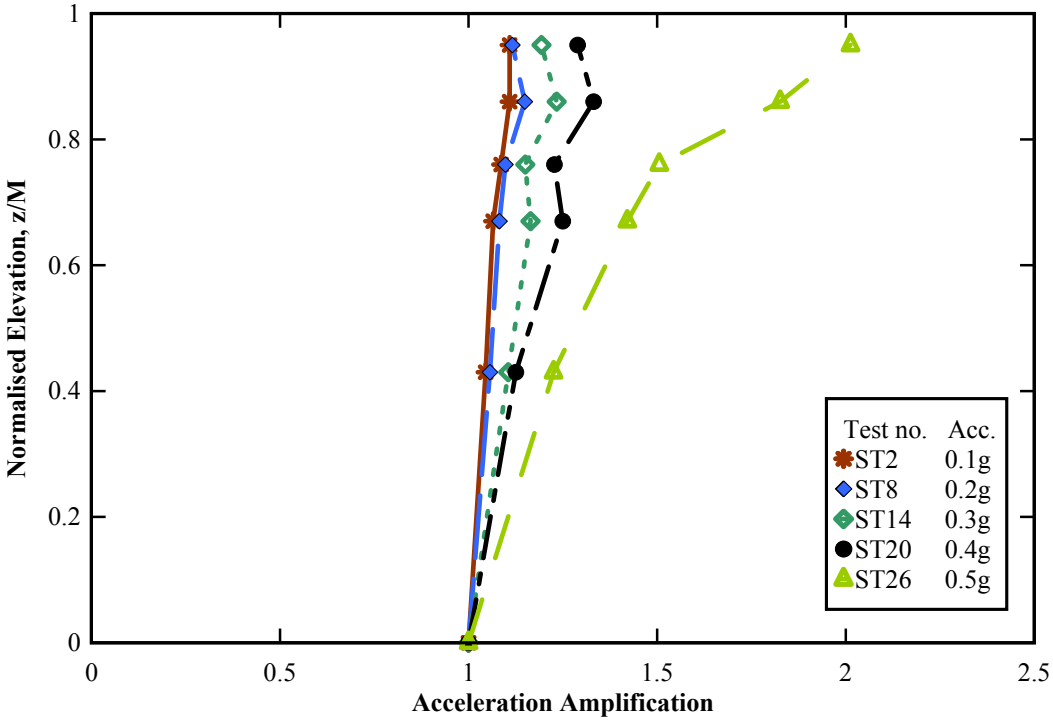

Figure 10d: Effect of base acceleration on acceleration amplification (considering total height of the model including the clay layer for normalization, M=1060 mm)

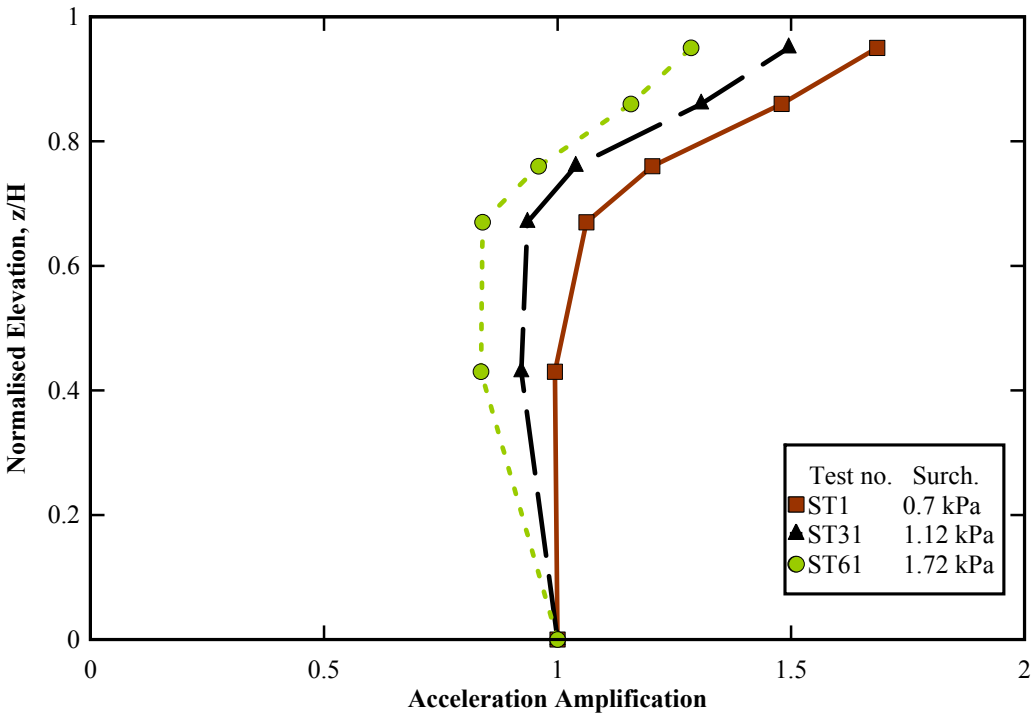

Figure 10e: Effect of surcharge on acceleration amplification (considering total height of the model including the clay layer for normalization, M=1060 mm)

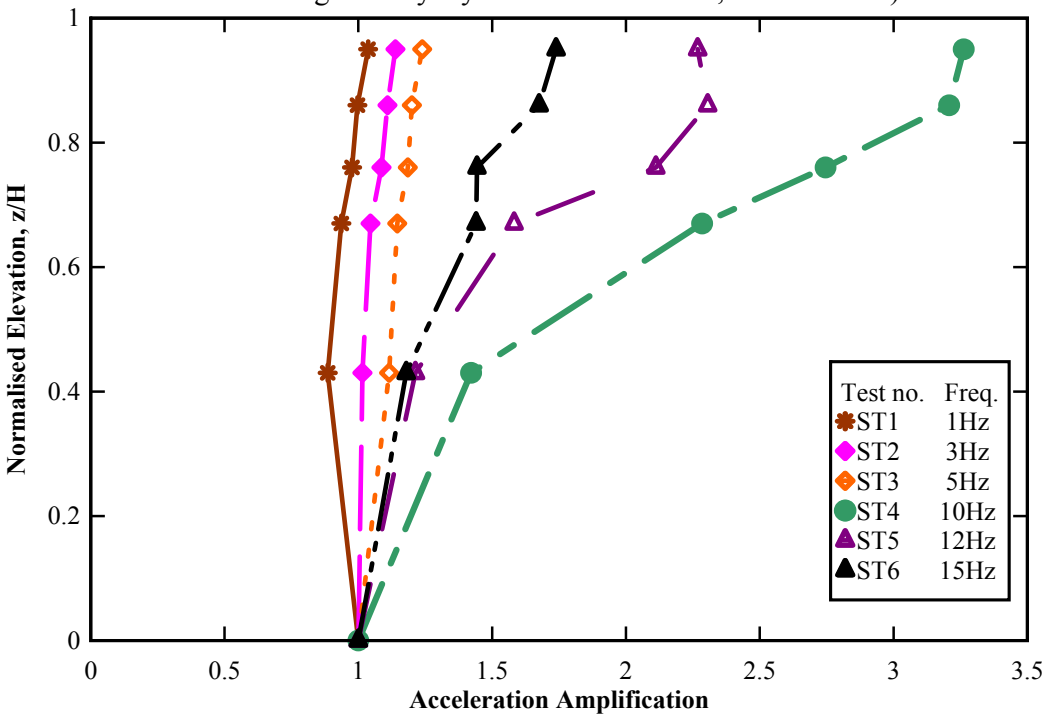

Figure 10f: Effect of frequency on acceleration amplification (considering total height of the model including the clay layer for normalization, M=1060 mm)

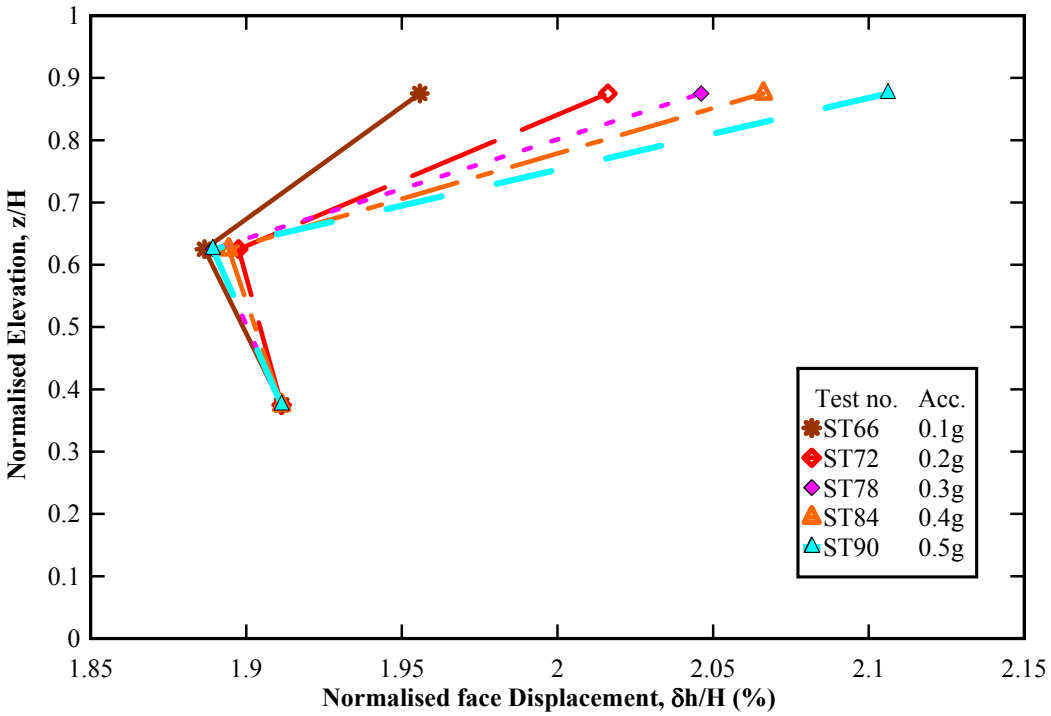

Figure 11a: Effect of base acceleration on displacement profile

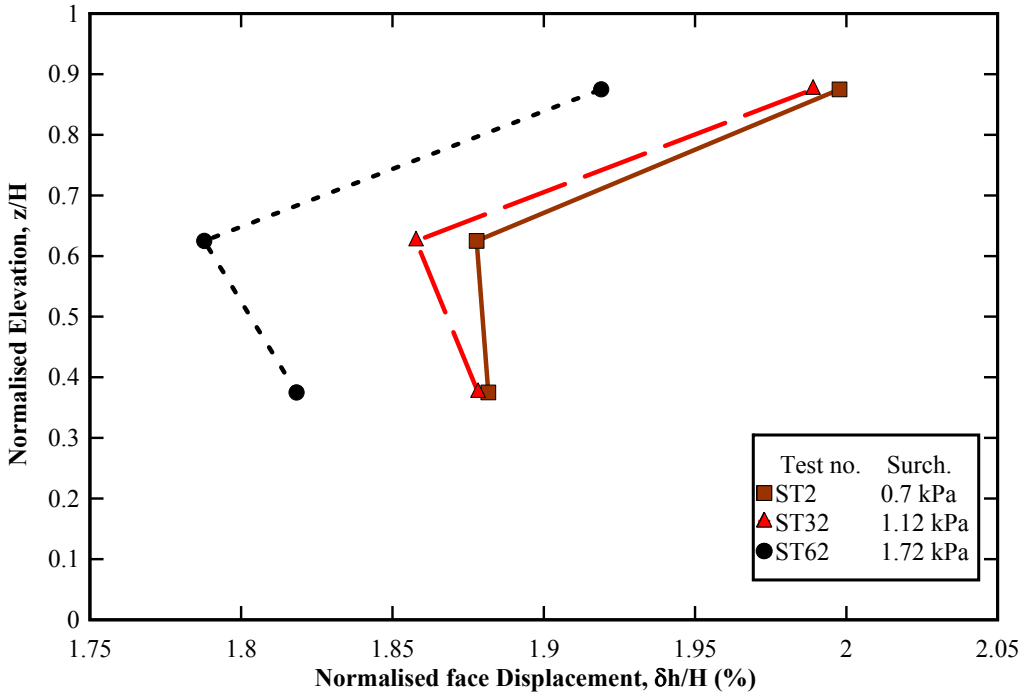

Figure 11b: Effect of surcharge on displacement profile

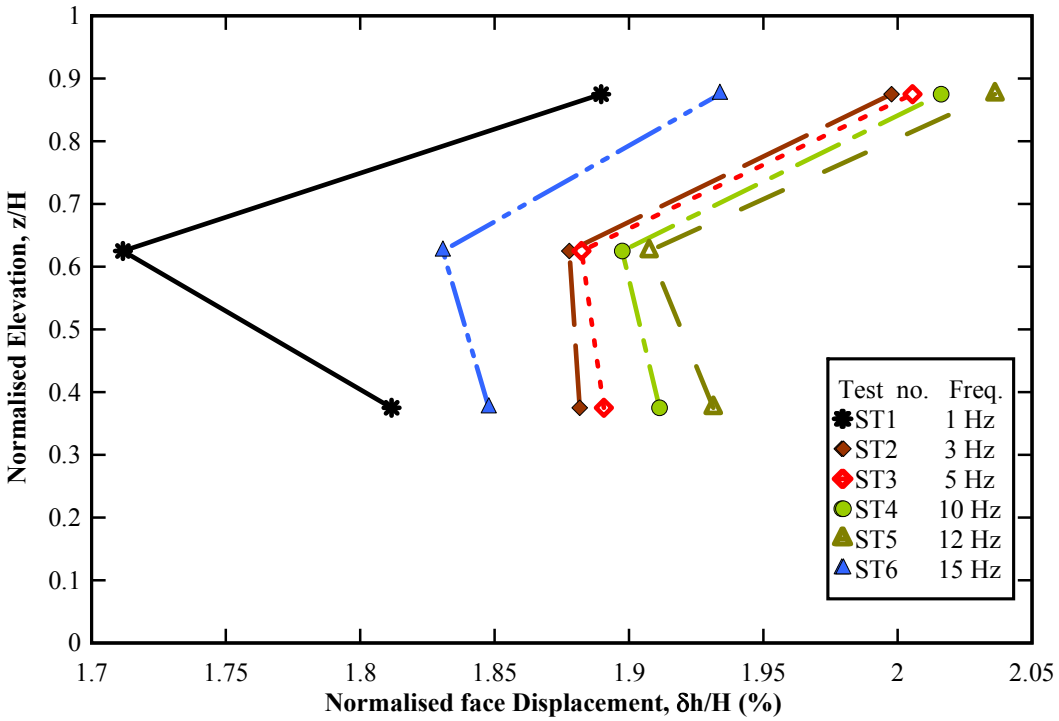

Figure 11c: Effect of frequency on displacement profile

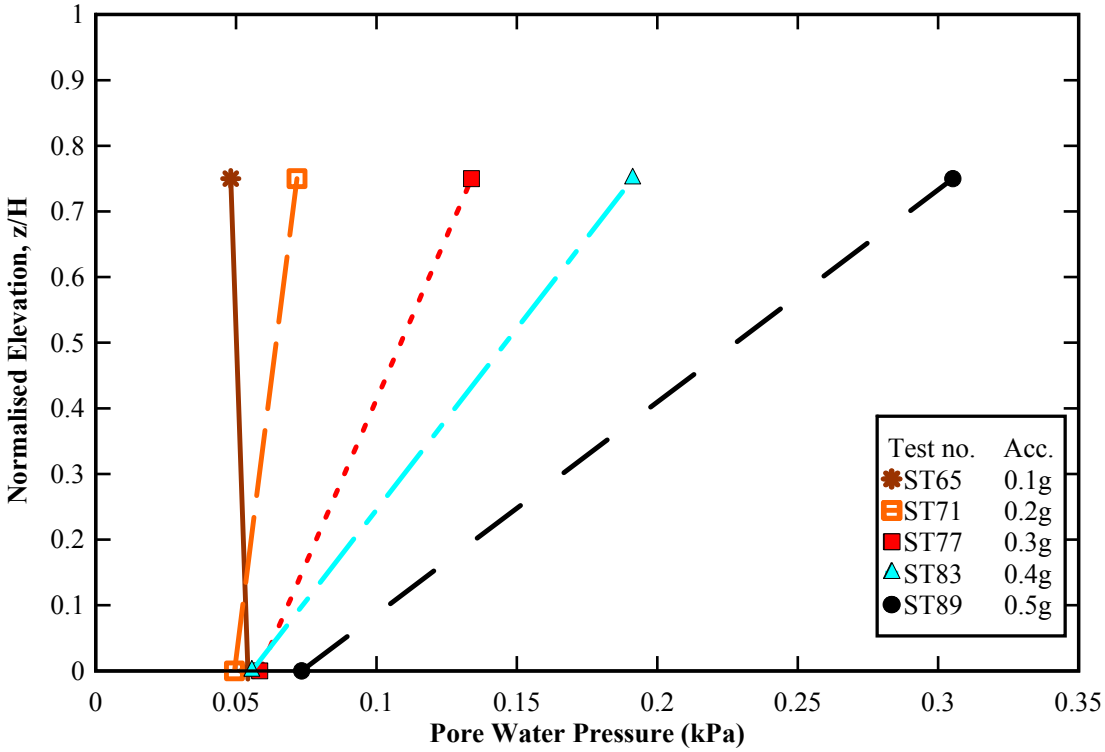

Figure 12a: Effect of base acceleration on pore water pressure

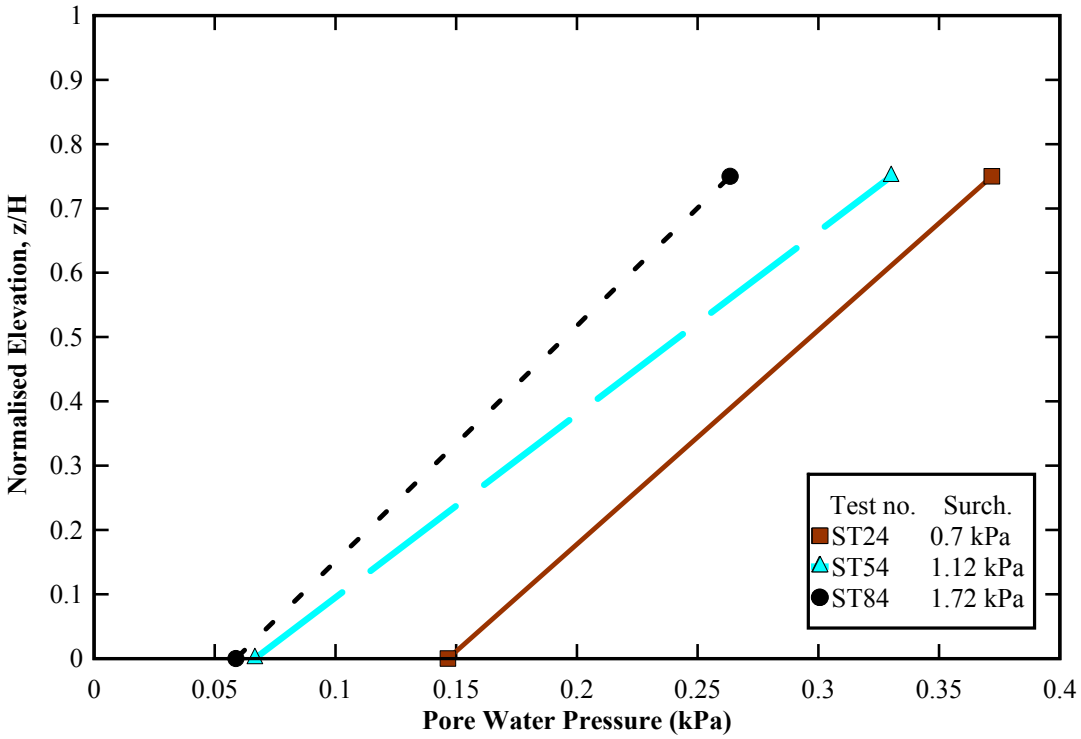

Figure 12b: Effect of surcharge on pore water pressure

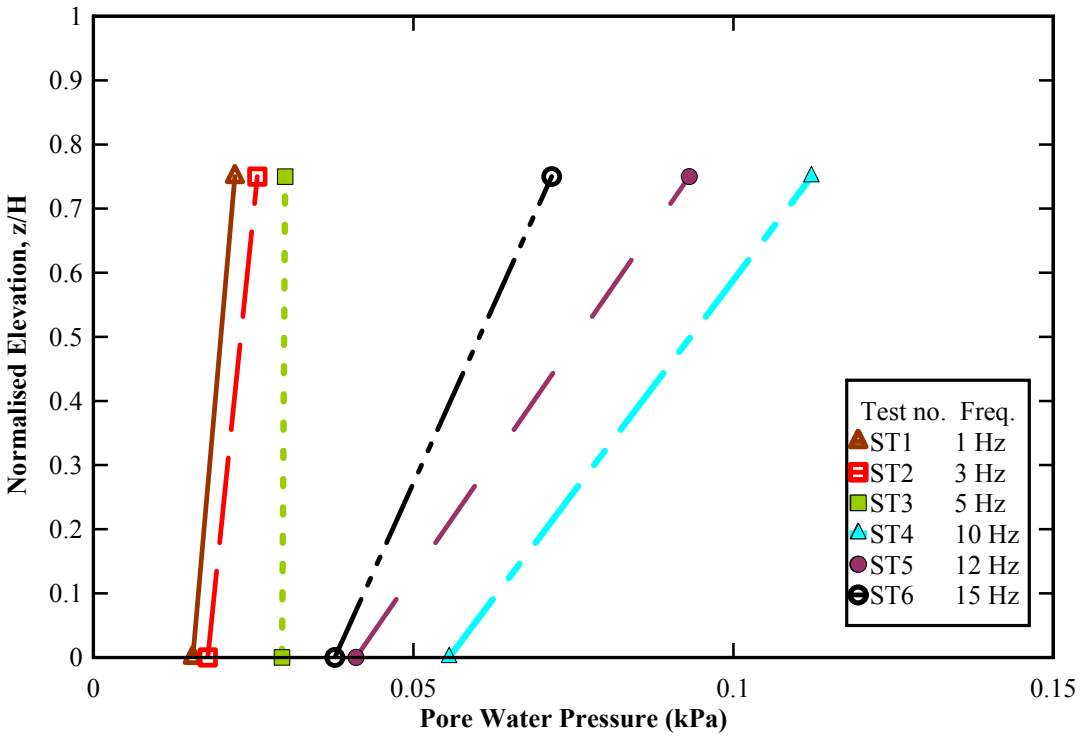

Figure 12c: Effect of frequency on pore water pressure

Table 1: Brief description of XRD test

Compound Name	Percent (%) by atomic weight
SiO_2	67.1747
Al_2O_3	15.8718
Fe_2O_3	7.7982
K_2O	3.8247
MgO	1.9221
TiO_2	1.4624
CaO	0.7423
Na_2O	0.6149
P_2O_5	0.1960
SO_3	0.1568
MnO	0.0960
ZrO_2	0.0439
Cr_2O_3	0.0339
Rb_2O	0.0246
ZnO	0.0205
SrO	0.0171

Table 2: Geotextile specification

No.	Details	DF 50
1.	Reinforcement type	Mechanically bonded needle punched
2.	Yarn material (staple Fibre)	Polypropylene
3.	Mass/unit area (gsm)	322
4.	Aperture Size , O_{95} (μm)	130
5.	Thickness (mm)	2.54
6.	Ultimate Tensile Strength (kN/m)	15.5
7.	Ultimate Tensile Strength at 2% strain (kN/m)	15.97
8.	Ultimate Tensile Strength at 5% strain (kN/m)	16.57

Table 3: Scale factors of selected engineering variables (Prototype-Model Similitude)

Description	Parameter	Scale factor	Scale factor M/P	Scale factor P/M
Acceleration	a	1	1	1
Density	ρ	1	1	1
Length	L	1/N	0.10	10
Stress	Σ	1/N	0.10	10
Strain	g	$1/N^{1-\alpha}$	0.32	3.125
Stiffness	G	$1/N^{\alpha}$	0.32	3.125
Displacement	d	$1/N^{2-\alpha}$	0.031	32.25
Frequency	f	$N^{1-\alpha/2}$	5.62	0.18
Force	F	$1/N^3$	0.001	1000
Force/L	F/L	$1/N^2$	0.01	100
Shear Wave velocity	V_s	$1/N^{\alpha/2}$	0.56	1.785
Time	t	$1/N^{1-\alpha/2}$	0.178	5.62

***P-Prototype; M-Model**

BANGLADESH NETWORK
OFFICE FOR URBAN SAFETY

PART-V

A STUDY ON RECENT EARTHQUAKES IN AND AROUND BANGLADESH

BANGLADESH NETWORK OFFICE FOR URBAN SAFETY (BNUS), BUET, DHAKA

Prepared By: ASM Fahad Hossain

Mehedi Ahmed Ansary

INTRODUCTION:

An earthquake is a sudden shaking movement of the surface of the earth that is known as a quake, trembler or tremor. Earthquakes can range in size from those that are so weak that they cannot be felt to those violent enough to toss people around and destroy whole cities. The seismicity or seismic activity of an area refers to the frequency, type and size of earthquakes experienced over a period of time. Bangladesh is consistently ranked one of the most vulnerable countries to natural disasters, but this is primarily because of the frequent occurrence of tropical cyclones, floods, heat waves and other weather-related disasters, combined with the massive population living in vulnerable conditions. Bangladesh is situated in a modestly dangerous domain and the density of population here and the infrastructural condition are been constantly a matter of worry here. As there is no technology developed to predict the time of occurring, makes earthquake a far devastating one. Recent earthquake in several parts of the world and the destruction occurred, clearly showing that Bangladesh has to take necessary steps to face the earthquake at any time in future.

Bangladesh is surrounded mostly by India and a few by Myanmar and she lies where three tectonic plates- Eurasia, India, and Burma meet making her one of the most tectonically active regions in the world. In the past 200 years, Bangladesh has experienced many devastating as well as mild earthquakes. After the independence in 1971, Bangladesh has been shaken up by more than 250 earthquakes and some of those were greater than 6.0 magnitude. But the risks cannot be ignored. The 1897 Great Indian Earthquake with a magnitude of 8.7, which is one of the strongest earthquake in the world killed 1542 and affected almost the whole of Bangladesh (Oldham, 1899). Recently, Bilham et al. (2001) pointed out that, there is a very high possibility that a huge earthquake will occur around the Himalayan region based on the difference between energy accumulation in this region and historical earthquake occurrence. The population increase around this region is the last 50 times than the population of 1897 and city like Dhaka has population exceeding several millions. It is a cause for great concern that the next great earthquake may occur in this region at any time. So that detailed seismic response analysis of his area is necessary. Also observation of recent earthquake record is needed. If we observe the rate of noticeable earthquake is increasing year wise. In April 2015 Nepal earthquake (also known as the Gorkha earthquake) killed nearly 9,000 people and injured nearly 22,000. It occurred at 11:56 Nepal Standard Time on 25 April 2015, with a magnitude of 7.8M_w or 8.1M_s and a maximum Mercalli Intensity of VIII (Severe). The 2009 Bhutan earthquake occurred on 21 September at 14:53 BTT (08:53 UTC) in the eastern region of Bhutan with moment magnitude of 6.1. The tremors were felt as far as Tibet. At least eleven people are reported to have been killed and seven in Bhutan.

SEISMOLOGY OF BANGLADESH:

Bangladesh is located close to the boundary of two active plates (Indian plate in the west and Eurasian plate in the east and north) the country has always been under threat of an earthquake that might be so catastrophic it will kill people in less than a minute. Bangladesh is surrounded by a number of tectonic blocks responsible for many earthquakes in the past. Calcutta, Assam, Tripura are the three very earthquake prone regions that are joined to Bangladesh in the borders in the Northern, Western and North-Eastern part respectively. If we consider the tectonics and geology, five major faults are significant for the occurrences of devastating earthquakes:

1. Bogra Fault Zone
2. Tripura Fault Zone
3. Shilong Plateau
4. Dauki Fault Zone
5. Assam Fault Zone

Bogra fault is a normal or gravity fault. It is very close to the Bogra town and Jamuna River. It was active in Palaeogene andNeogene times. Movement along the Bogra fault led to the depositionof a large amount of sedimentary pile within the Bogragraben.**Tripura** is one of the states of India surrounded by Bangladesh and two other states Mizoram and Assam of India. The area is surrounded by Koplili fault; Kaladan fault etc. which have produced many earthquakes. The Tripura Naga orogenic belt is a zone of highly faulted tertiary deposits which has witnessed earthquakes of moderate magnitudes.**Shillong** plateau is characterized as a seismically active and geologically complex region located on the collision boundary betweenIndian and Eurasian plate in the Meghalaya state of India. The general altitude of the Plateau is about 1,500 m. The plateau is composed of the Precambrian Metamorphic rocks and the Tertiary and Quaternary deposits are limited on the southern foothills of the Shillong Plateau indicating the successive uplift of the Shillong Plateau and the process started from the Pliocene time. **Dauki** fault zone is a 300 km long north dipping reverse fault along the Meghalaya-Bangladesh border and inferred to go through the southern margin of Shillong plateau. It has a major role in deforming the surrounding areas. The Dauki fault is believed to be active in the past. Though it is inactive in the recenttimes still it is considered as one of the major threats for Bangladesh forthe occurrence of devastating earthquakes.Figure 1 shows stechtonic framework of Bangladesh.

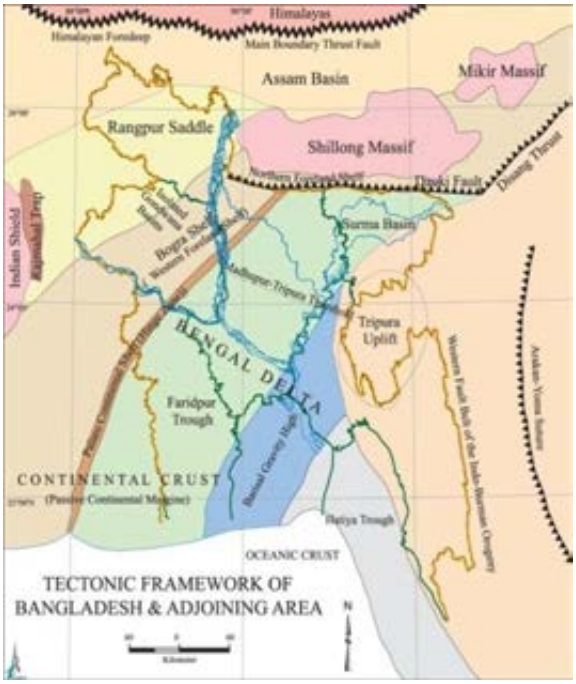

Figure 1: Tectonic Framework of Bangladesh (Banglapedia, 2015)

Dhaka city, the soul of Bangladesh is highly vulnerable to the earthquake disaster due to high density of population, unplanned infrastructure and close proximity with India and Myanmar's active seismic area, poor economic condition, poor emergency preparation and recovery capability.Bangladeshwas divided into four main earthquake zones in BNBC 2014 (Figure 2) where four zones have PGA values varied to 0.12, 0.20, 0.28 and 0.36. Figure 2 shows the seismic zoning map of Bangladesh. A seismicity map of Bangladeshis also shown in Figure 3.

Figure 2: Earthquake zones of Bangladesh (BNBC 2014)

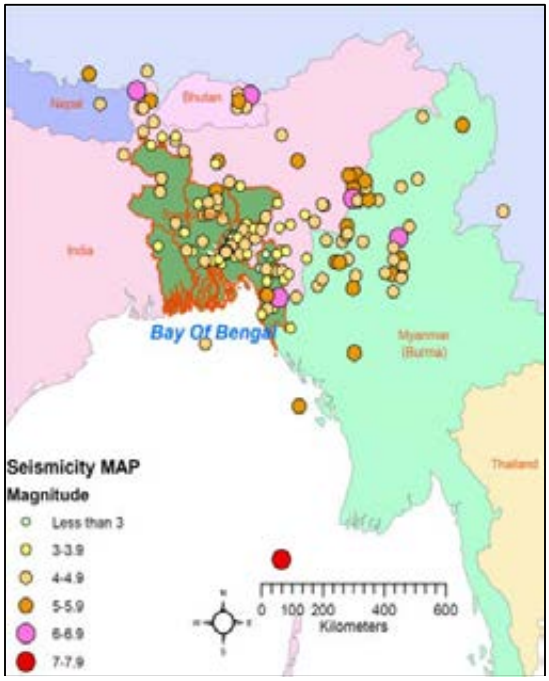

Figure 3: Seismicity Map of Bangladesh (M. A. Ansary)

RECENT EARTHQUAKE RECORD (MAGNITUDE AND FOCAL DEPTH):

The magnitude, focal depth and locations of five year's earthquake having Richter magnitude more than 3 that was felt from 2015 to 2019 (up to October) near Bangladesh are represented in the table 1 to table 5 below.

GRAPHICAL REPRESENTATION OF EARTHQUAKE RECORD ACCORDING TO MAGNITUDE AND YEAR:

From the earthquake records of five years shown above, two maps were prepared according to magnitude and earthquake occurrence year. They are shown in figure 4 and figure 5. From the magnitude graph it was seen that, earthquake with magnitude of 5 to 7.9 occurred at Nepal, magnitude of 3 to 4.9 were happened at the northern outside of Bangladesh that means at the area between Bangladesh and Bhutan. At the eastern outside of Bangladesh that means the portion between Bangladesh and Myanmar, the values were within 4 to 5.9. From the year wise graph it was seen that, considerable earthquake records were at the northern outside of Bangladesh at last year 2019 that indicates a major earthquake may happen here from the stored energy and can make a devastating effect.

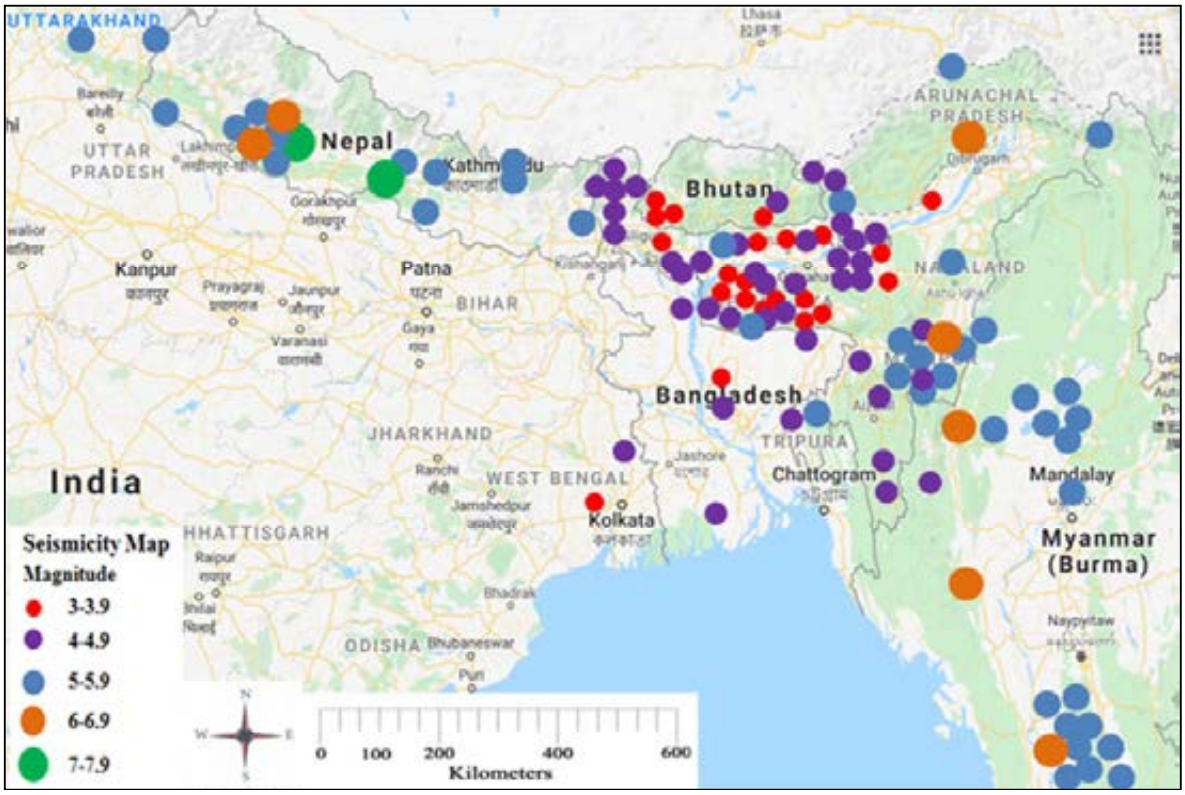

Figure 4: Earthquake Magnitude in and around Bangladesh from 2015 to 2019

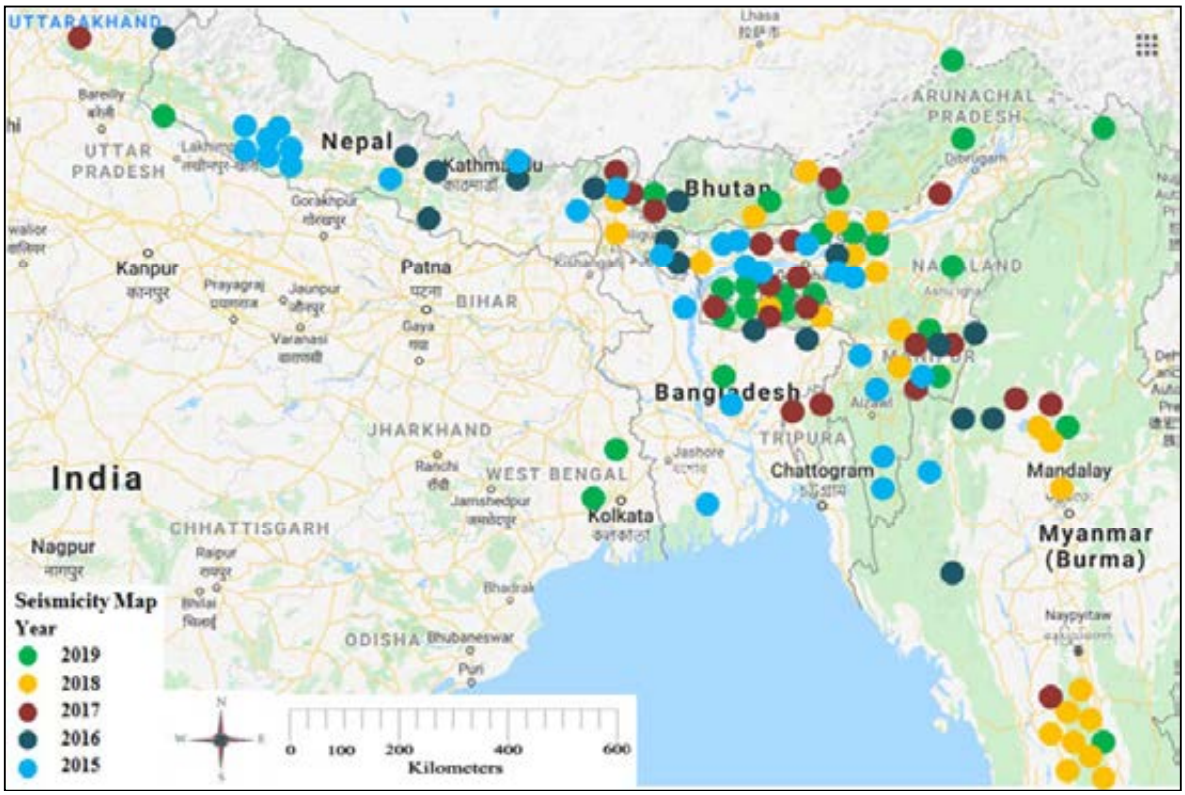

Figure 5: Earthquake occurrence in and around Bangladesh from 2015 to 2019

COMPARISON BETWEEN MAGNITUDE AND FOCAL DEPTH OF DIFFERENT EARTHQUAKE IN VARIOUS DATES:

Some comparisons between magnitude and focal depth of different earthquake in 2019 (up to October), 2018, 2017, 2016 and 2015 are shown in figure 6 and figure 7. It was seen that Earthquake with more than 3 Ricter magnitudes was occurred in all five years in February, April, August and September. January and December have comparatively less earthquake record. Focal depth was higher in 2016 related to others in April August.

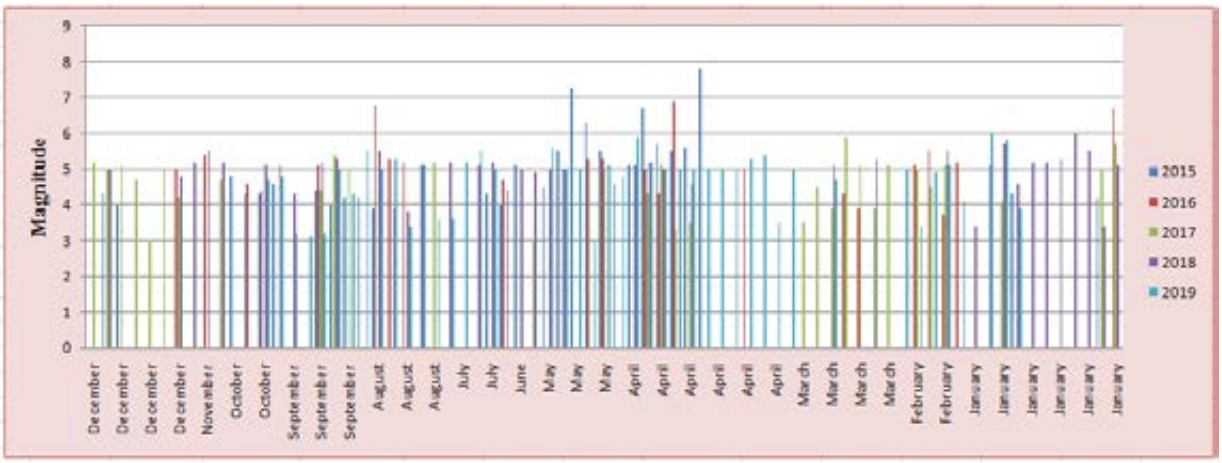

Figure 6: Comparison between magnitudes of different earthquake from 2015 to 2019

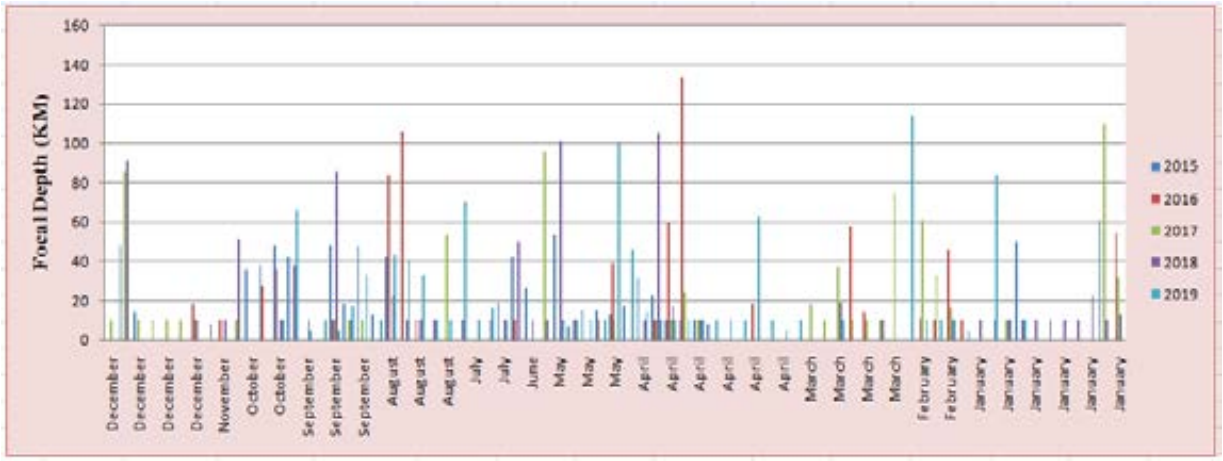

Figure 7: Comparison between focal depths of different earthquake from 2015 to 2019

All data of magnitude vs focal depth of earthquake record shown in this article of five years were plotted in a graph and an equation was developed from the straight line graph. The straight line graph is shown in figure 8 and the equation is given below.

$$\mathbf{(Y = 2.416X + 14.54)}\ (R^2 = 0.005)$$

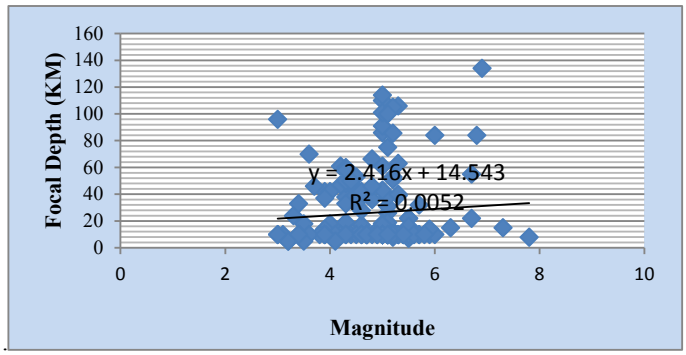

Figure 8: Focal Depth vs Magnitude of different earthquakes from 2015 to 2019

EFFECT OF SOME MAJOR RECENT EARTHQUAKE:

The primary effects of earthquakes are ground shaking, ground rupture, landslides, tsunamis, and liquefaction. Fires are probably the single most important secondary effect of earthquakes. Some major effects occurred from recent earthquake around Bangladesh are described below:

►Nepal experienced a major earthquake on 25 April 2015, which has a magnitude of Mw 7.8 earthquake with an epicenter 77 km (48 miles) northwest of Kathmandu, which devastated large parts of the country. The quake hit at 11:56 am local time (06:11 GMT) according to US Geological Survey (USGS).The main shock of 25 April and several other aftershocks including that of 12 May caused the death of about 9,000 people, injury to 22,000, and loss and damage equivalent to USD 7 billion. Figure 9 shows the devastating effect of Nepal Earthquake.

Figure 9: Nepal Earthquake 2015 (todayonline.com and theguardian.com)

►The 2016 Imphal earthquake struck northeast India in the state of Manipur on January 4 with a moment magnitude of 6.7 and a maximum Mercalli intensity of VII (Very strong). Its epicenter was located in the Tamenglong district; about 30 km west of Imphal. At least eleven people were killed, 200 others were injured and numerous buildings were damaged, as shown in figure 10. The quake was also strongly felt in Bangladesh. It was also extensively felt in eastern and north-eastern India.The earthquake, which hit at 4:35 a.m. on 4 January local time (23:05 UTC, 3 January), was centered in an isolated area. Imphal has a population of more than 250,000.

Figure 10: Imphal Earthquake 2016(indianexpress.com)

►A magnitude 6.8 earthquake struck Myanmar 25 km (16 mi) west of Chauk on 24 August 2016 with a maximum Mercalli intensity of VI (Strong). It struck at 5:04 pm local time (10:34 UTC), and was centered in an isolated area. The estimated depth was 84.1 km. Tremors from the earthquake were felt in Yangon, in the eastern cities of Patna, Guwahati, and Kolkata in India, in Bangkok in Thailand and in Dhaka, the capital of Bangladesh.According to reports, several temples in the nearby ancient city of Bagan were damaged and four people were reported dead, as shown in figure 11.

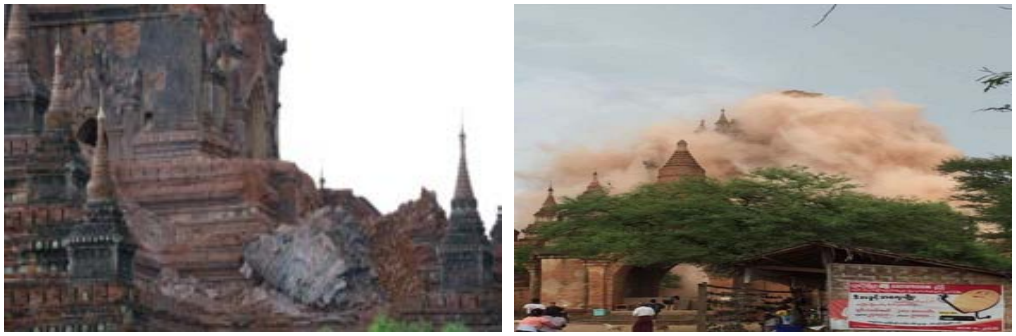

Figure 11: Mawlaik, Myanmar Earthquake 2016 (asiasociety.org and bangkokpost.com)

►A magnitude 5.7 earthquake struck India 20 km (12 mi) east north-east of Ambassa in the state of Tripura on 3 January 2017 with a maximum observed intensity of 6-7 EMS. It struck at 2:39 pm local time (09:09 UTC), and was centered in an isolated area. The estimated depth was 32.0 km. One person died and five others were injured in India. At least 50 houses were damaged due to landslides that occurred in Dhalai district, while roads were blocked after trees were uprooted. According to the Tripura State Disaster Management Authority, at least 6,727 buildings were damaged in Tripura in the districts of Dhalai and Unakoti, as shown in figure 12. Shaking was felt in many parts of north-eastern India including as far as Kolkata. The tremor was also felt in neighboring Bangladesh, where two people died and three others were injured.

Figure 12:Ambassa, India Earthquake 2017 (financialexpress.comand livemint.com)

►A strong 6.1-magnitude earthquake struck Arunachal Pradesh the US Geological Survey said.The epicenter of the shallow earthquake was about 40 kilometers (25 miles) southeast of Along, and 180 kilometers southwest of the state capital Itanagar.The devastating effect is shown in figure 13.

Figure 13: Along, Arunachal Pradesh, India Earthquake 2019(hindustantimes.com and cnbctv18.com)

EFFECTS AND DAMAGES IN BANGLADESH DUE TO NEPAL EARTHQUAKE 2015:

On April 25 the earthquake jolted the Dhaka, Chittagong, Barisal, Rajshahi, Dinajpur, Rangpur, Kushtia and different parts of the Bangladesh. According to disaster management and relief ministry eighteen districts of Bangladesh have been affected in this earthquake, which were felt in almost all corners of the country. Department of Disaster Management (DDM) has received further feedback from local level officials in total 19 Districts [5] .In Dhaka, residents of high-rise buildings were seen running down in panic as apartments started shaking. According to the ministry's disaster Response Centre, four people died in as many districts. It said at least 200 people were injured during evacuation and 17 buildings had either tilted or cracked (bdnews24.com).

Figure 14 shows people frightened and come out of their offices when the strong motion was felt. Figure 15 shows one building has tilted over another one. Seismograph recording of earthquake in Bogra, Jamuna Bridge and Ruppur are shown in Figure 16.

Figure 14: Many people come out of their offices when a strong earthquake was felt in Dhaka and elsewhere (The Daily Star)

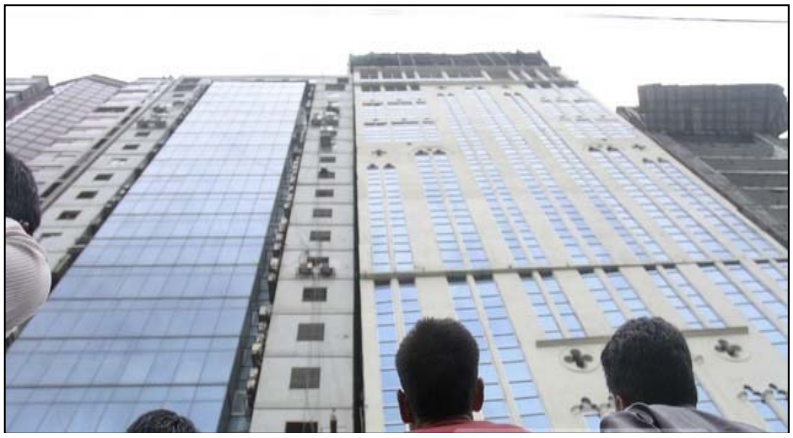

Figure 15: One building has tilted over another one (bdnews24)

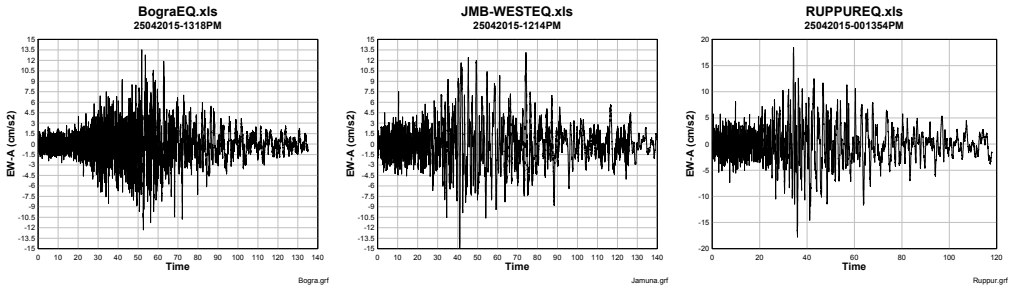

Figure 16: Seismograph Recording in Bogra, Jamuna Bridge and Ruppur (M. A. Ansary)

CONCLUSION:

Bangladesh is consistently ranked one of the most vulnerable countries to natural disasters, but this is primarily because of the frequent occurrence of tropical cyclones, earthquake, floods, heat waves and other weather-related disasters, combined with the massive population living in vulnerable conditions. From the above data indicate that the earthquake occurred in Bangladesh was not so devastating. But it actually does not show the real picture of the risk of Bangladesh about the earthquakes. In this article, only the magnitude and focal depth

of five years of earthquakes in and around Bangladesh were represented. From the findings from the research, it can be easily noticed that the northern and eastern side of Bangladesh is very much vulnerable that may cause major earthquakes anytime with a great loss of life and property and also the recent earthquake occurrence rate is increasing. The topographical position and the historical quakes obviously demonstrate that the administration of Bangladesh should put much stress on seismic tremors and how to limit its harm. Dhaka is situated at high hazard zone for seismic tremor and a phenomenal human fiasco may happen in the city whenever for even a moderate to substantial tremor. The disaster management system of Bangladesh should be more developed to minimize the loss during earthquake. The building codes should be followed by the citizens and the government should try to increase the awareness about the safety rules of earthquakes among the mass people.

BANGLADESH NETWORK
OFFICE FOR URBAN SAFETY

PART-VI

SITE RESPONSE AND LIQUEFACTION SUSCEPTIBILITY ESTIMATION OF A SITE IN NORTHERN PART OF BANGLADESH

BANGLADESH NETWORK OFFICE FOR URBAN SAFETY (BNUS), BUET, DHAKA

Prepared By: Nusrat Jahan

Mehedi Ahmed Ansary

INTRODUCTION

For important sites like ports, power plants, etc, estimation of liquefaction potential is important owing to the existence of some important infrastructures. Resistance of soil to liquefaction has turned into an essential condition to be estimated before any major construction during recent times. Liquefaction is the alteration of the previously secure coarse aggregate of soils becoming a liquid mass owing to the enhancement of pore water pressure. According to Marcuson (1978), liquefaction is mainly observed in areas where the soil mainly consists of the sandy type and the water table is situated near the ground level. The cyclic random loading of a seismic event is the source for water pressure inside the soil pores to enhance, which causes the soil mass to perform as a fluid. The 1964 Alaska, USA, and Niigata, Japan earthquakes are the major examples where liquefaction played the main role in increasing the damage level of those two events (Kramer, 1996; Youd, 2014). After these two events, liquefaction becomes an important factor to be assessed before any new important construction takes place. Also, a wide-ranging investigation has been done recently in this field to avoid any such catastrophic damages in the future (He et al, 2020; Jamali and Tolooiyan, 2020; Karanjekar and Pachpor, 2020; Thokchom et al, 2018; Zhang et al., 2015; Zhang and Goh, 2016; Zhang et al., 2021). In addition, there are numerous studies for site response analysis (Chandran and Anbazhagan, 2020; Groholski et al., 2016; Kaklamanos et al., 2015; Rahman et al., 2021) being carried out recently. The findings of many researchers (Ansary, 2003; Ansary and Sharfuddin, 2002; Ansary and Arefin, 2020; Rahman et al., 2021) advocate that important cities of Bangladesh have been struck by numerous historical large earthquakes, that is why the current study is important.

In this research, the solar power plant site in a neighborhood in Gaibandha town, Bangladesh has been considered. The site is located beside the Brahmaputra River in the North-Western part of Bangladesh. The soil of the site is mainly composed of loose to medium dense silty fine sand up to a depth of 25m.

In this study, through 1D site response analysis, PGA values at the surface have been estimated and later used for determining liquefaction potential index at the site. Although, many reseaches have been carried out to estimate liquefaction potential of different sites as mentioned above, there are almost no research where 1D site response analysis (using equivalent nonlinear, nonlinear and average shear-wave velocity based on top 30m) has been

specifically carried out to obtain the PGA value at the site for liquefaction potential estimation.

EXISTING FAULTS AROUND BANGLADESH

Raoof et al. (2017) has developed 3-D seismic velocity structures for the adjoining areas of Bangladesh to gain knowledge about the geodynamic processes of this region. This study gives useful information about the site condition. The Indian plate is under-thrusting the Himalayas at low angles at the Main Boundary Thrust (MBT) along the entire ~2500 km long Himalayan belt (Molnar et al., 1973; Baranowski et al., 1984). It is subducting at dip angles ~30°–50° at the Indo-Burmese arc with the Benioff zone down to depths ~150–200 km, as observed from the intermediate-depth seismicity (Satyabala, 1998, 2003; Li et al., 2008). Several researchers suggested that subduction along the Indo-Burmese arc has slowed down or may have stopped, and the Indian plate is dragged to the north, which is partly accommodated by the long Sagaing fault in central Burma (Le Dain et al., 1984; Chen and Molnar, 1990). The Sagaing is a fault in the plate boundary. Its sinistral movement shows a part of the junction of Burma and India plates.

The major faults that have an impact on the study area are: The Indus-Tsangpo Suture (ITS), the Main Boundary Thrust (MBT), the Main Central Thrust (MCT), and the Main Frontal Thrust (MFT) (see Figure 1). These are the major Himalayan crustal discontinuities spanning the length of the northern border of the northeast Indian region (Yin and Harrison, 2000; Yin, 2006).

SEISMIC HAZARD ASSESSMENT

Seismic Data Processing

A homogeneous seismic database is a vital instrument in any assessment of earthquake hazards. An earthquake database that involves pre-1900 (all historical), and post-1900 (that occurred after 1900) events need to be compiled. Organizing lists of seismic events in a database that covers the studied region; requires collecting data from the various published catalogs, literature, and those provided by national and international agencies.

The earthquake catalog has been assembled from the International Seismological Centre (ISC) UK and the United States Geological Survey (USGS) event data. The maximum

seismic magnitude for this study has been estimated from this catalog. The developed catalog has been homogenized to obtain a unified magnitude value M_W. This has been carried out applying conversion relations for magnitude provided by Scordilis (2006) and Kolathayar and Thallak (2012). The past earthquakes from the period 1760 to 2020 have been selected using the cut-off value of magnitude $M_W \geq 3$, the events are presented in Figure 2.

In probabilistic seismic hazard analysis, it is generally considered that the seismic occurrences follow a Poisson distribution (Kadirioğlu et al., 2018). For this purpose, a declustering algorithm to remove aftershock and foreshock from the original catalog is used. Numerous declustering processes have been suggested over the years such as Gardner and Knopoff (1974), and Reasenberg (1985) algorithms with different space-time windows. These methods are implemented in the software ZMAP (Wiemer, 2001). In the present study, the Gardener and Knopoff (1974) algorithm has been applied for declustering. After declustering, 1038 seismic events have been compiled for the above-mentioned period. This study assumed equal weightage to all faults considered. Linear, as well as smoothed point source models, have been considered to estimate the PGA values (Kolathayar et al., 2012). Figure 3 presents the study location together with the in-situ test locations.

Ground Motion Prediction Equations

Ground motion prediction equation (GMPE) is a relation among ground motion, magnitude, distance, and other relevant parameters. Through these equations, ground motion at any location can be estimated if magnitude, distance, and other parameters are known. GMPEs pertinent to the current tectonic region with shallow earthquakes such as Abrahamson and Silva (1997), Iyengar and Raghukanth (2004), Amiri et al. (2007), and Tabassum and Ansary, (2020) have been used in this study to determine PGA at the bedrock. Equation (1) presents the GMPE developed by Tabassum and Ansary, (2020) for rock type soil based on 273 earthquake data from 2005 to 2017 for Bangladesh and North-East Indian region, where PGA_h is the horizontal acceleration which depends on magnitude (M) and hypocentral distance (r). σ is the standard error.

$$log\ PGA_h = 0.80532 + 0.00029*r + 0.36134*M - 0.92616*log\ r \pm 0.3705\ \sigma \quad (1)$$

Finally, for the assessment of liquefaction at the study site, PGA value needs to be determined at the surface. For this purpose, DEEPSOIL software has been used here to obtain the PGA value.

METHODOLOGY FOR SITE RESPONSE AND LIQUEFACTION ASSESSMENT

Figure 4 shows the flow chart of the total methodology employed in this study. The properties for dynamic analysis of soils, such as accelerogram of earthquakes, shear wave velocity (Vs), material damping, and shear modulus reduction curves are necessary to estimate site amplification parameters through site response analysis. Other soil parameters, for example, internal friction angle, over-consolidation ratio, plasticity index, and unit weight are also required for this purpose. This information is gathered from 66 borehole locations and one PS-Log location (near BH-23) of the study site as shown in Figure 3 to carry out the site response analysis.

SPT and Shear-wave Velocity Profile

Figure 5 presents a typical cross-sectional profile of the study site. Generally, the top 10m is composed of very loose to loose silty fine sand, from 10m to 30m, the soil consists of medium dense silty fine sand, from 30m to 80m, the soil consists of dense silty fine sand and beyond 80m, the soil consists of dense silty fine sand with gravel. Appendix-A presents the SPT contours at various depths of the study site.

The shear wave velocity (Vs) information from the study location has been compiled from the ground level up to a depth of 120 m (Figure 6). The data has been determined utilizing a suspension PS-log system. In nearby Jamuna Railway Bridge and Rooppur Nuclear Power Plant sites, the bedrock (when the shear-wave velocity is larger than 760 m/s) is located at 150 m below the ground level. So, the bedrock for this site is also assumed to be at 150m depth.

Material damping and shear modulus reduction relations

For the site response analysis, the dynamic parameters of shallow ground layers are significant. These are illustrated by the damping ratio and shear modulus reduction curves to assess the soil condition under cyclic loading. Due to the unavailability of these curves for the study site, the suggestion of many researchers (Kumar et al., 2014; Chandran and

Anbazhagan, 2020) to utilize the existing standard curves may be followed. Several damping ratios and shear modulus reduction relations can be found in different available literature (such as Seed and Idriss, 1970; Sun et al., 1988; Darendeli, 2001) to estimate the dynamic parameters of numerous soil patterns. According to different researchers (Darendeli, 2001; Bajaj and Anbazhagan, 2019), effective confining pressure, loading frequency, plasticity index, loading cycle numbers, strain, and soil type are the main essential properties that affect the damping ratio and shear modulus reduction. In the study site, the soil layer from the ground level up to 120 m deep is mostly consisting of sandy soils (Figure 6). According to Hashash et al. (2010) for sandy deposits, the damping ratio and shear modulus reduction relations recommended by Darendeli (2001) are preferred to analyze the site assessment by nonlinear means. Hence, the material damping and normalized shear modulus reduction relations suggested by Darendeli (2001) are applied to estimate the sandy deposits nonlinear characteristics of the study site (Figure 7).

Bedrock and surface hazard spectra

According to the BNBC (2020), site classes are defined as follows: type SA, when Vs30>760m/s; type SB when Vs30 varies between 360m/s and 760m/s; type SC when Vs30 varies between 180m/s and 360m/s; type SD, when Vs30<180m/s. The normalized design acceleration response spectrum proposed in BNBC (2020) for ground condition (Vs > 760 m/s) [soil type SA] has been considered in this study as shown in Figure 8a. This spectrum for soil type SA has been multiplied by PGA for a return period of 475 years (in this case, it is 0.23g) to obtain the target spectrum, which is here referred to as the hazard spectra at the bedrock (UHS). In this particular site, the mean shear-wave velocity for the initial 30m of a soil column is 183 m/s (using Figure 6), which falls in the soil type C (SC) category. The normalized design acceleration response spectrum for soil type SC as per BNBC (2020) has been multiplied by 0.23g to obtain the surface UHS. Both these UHSs are shown in Figure 8b.

Earthquake acceleration time history and spectral matching

Recently, Bangladesh has set up a seismic network all over the country (Ansary and Arefin, 2020). Although this network has recorded several weak ground motions, so far no strong ground motion has been recorded by this system. Strong ground motions having the time history data expressed in terms of acceleration are needed for site assessment. For this

purpose, freely available six worldwide data are used: the 1940 Imperial Valley USA (USGS station 5115), the 1989 Loma Prieta USA (090 CDMG station 47381), the 1994 Northridge USA (090 CDMG station 24278), the 1995 Kobe Japan (Kakogawa CUE90), the 1999 Kocaeli Turkey (Yarimca, KOERI330) and the 1999 Chi-chi Taiwan (TCU045) earthquakes. Also, four strong ground motion time histories have been generated using synthetic accelerogram following the algorithm suggested by Halldorsson and Papageorgiou, (2005).

The spectral acceleration of the earthquake and synthetic accelerograms are fitted to the target bedrock response spectra to generate time history data compatible with the target spectra (Figure 9a and 9b). The matching of spectra has been done by using the SEISMOSOFT software to adapt the time history data by fitting its spectral acceleration with the target response spectrum (Figures 9 and 10). The spectral response of 6 earthquakes and 4 synthetic acceleration time histories are fitted with the target spectra for a return period of 475 years (Figures 11 and 12). The time versus acceleration data of the fitted spectral acceleration curve has been applied for the site assessment (see Figure 10).

One-dimensional site assessment

DEEPSOIL software resulted from the research of Hashash et al. (2010) has been used to carry out one-dimensional nonlinear and equivalent-linear site assessment analysis. The Equivalent Linear (EL) model employs an iterative procedure in the selection of the shear modulus and damping ratio soil properties as pioneered in program SHAKE. These properties can be defined by discrete points or by defining the soil parameters that define the backbone curve of one of the nonlinear models. Non-linear (NL) analysis solves the equations of motions in time domain using the Newmark β method (implicit) or the Heun's Method (explicit). The available soil models are: General Quadratic/ Hyperbolic Model (GQ/H), Pressure-Dependent Modified Kondner Zelasko (MKZ), Discrete Points (Equivalent Linear) and User-Defined (UMAT). The analysis can be performed with or without porewater pressure generation.

The soil model for response analysis requires material damping and shear modulus reduction relation in normalized form. The relations suggested by Darendeli (2001) have been utilized in this research. To utilize the relationships of Darendeli (2001), the following soil parameters are needed: vertical stress under the effective condition in the initial state, initial

coefficient of lateral earth pressure, loading frequency, loading cycle numbers, OCR ratio, and plasticity index (Figure 7).

DEEPSOIL has numerous soil models to carry out the site assessment analysis as mentioned earlier. In the current study, the model suggested by Groholski et al. (2016) has been applied to match material damping and modulus reduction relations of the materials of the soil column with the benchmark relations of Darendeli (2001) for certain shear strength. This model consists of a non-Masing reloading-unloading hysteretic setup based on the general quadratic/hyperbolic model (GQ/H). The effective shear strength condition has been applied for all calculations by considering the water table at the top of the surface. According to Groholski et al. (2016), the GQ/H form can depict the relatively big shear stress-strain characteristics of the materials to precisely approximate the motion of the ground at the surface for relatively big strains. Viscous damping term which has been frequency-independent has been utilized for nonlinear response assessment in the time domain. During response analysis, the accelerogram of the matched bedrock spectral acceleration has been applied for the motion of the ground at the bottom of the soil column.

Liquefaction assessment techniques

Several methods have been built up to evaluate the liquefaction susceptibility of soils. This paper focuses on the following methods to estimate liquefaction potential: Seed-Idriss simplified procedure (Seed and Idriss, 1971), Japanese Code of Bridge Design (Tatsuoka et al., 1980), Japanese Code of Bridge Design based on the Chinese criterion (Ishihara, 1993), and Chinese Code for Seismic Design of Buildings method (GB50011-2010) (as outlined on Sun et al., 2015). These methods are Standard Penetration Test (SPT) based liquefaction assessment methods where empirically determined curves—utilizing Cyclic Stress Ratio (CSR) and Cyclic Resistance Ratio (CRR)—are employed to predict liquefaction and no-liquefaction occurrence. Appendix-B presents the description of these three methods. After the detailed assessment, liquefaction severity is evaluated based on liquefaction potential index (LPI), similar to that suggested by (Iwasaki et al., 1978; Iwasaki et al., 1981, 1984). Iwasaki et al. (1984) has classified the LPI in three levels: (a) LPI < 5, implies 'Low liquefaction potential; b) $5 \leq$ LPI ≤ 15, implies 'High' liquefaction potential and c) LPI > 15, implies 'Very High' liquefaction potential.

RESULTS AND DISCUSSIONS

Development of surface hazard spectra

The hazard spectra at the surface (UHS) of the study site have been developed utilizing the three site assessment methods: site coefficients based on Vs30, equivalent-linear, and nonlinear (Figure 13). The spectral acceleration of the hazard spectra at the surface at different periods are at all times bigger than that of the hazard spectra at the bedrock for Vs30-based site coefficients, whereas the spectral acceleration of hazard spectra at the surface are smaller at relatively low periods (from 0.06 s to 0.20 s) and bigger at large periods (0.20 s and 4 s) in comparison with the spectral accelerations of the hazard spectra at the bedrock during equivalent-linear response assessment. Similarly, the spectral acceleration of the hazard spectra at the surface is smaller at low periods (from 0.02 s to 0.35 s) and larger at large periods (0.35 s and 4 s) in comparison with the spectral accelerations of the hazard spectra at the bedrock during nonlinear response assessment. The period of the highest acceleration has moved towards the larger periods during the equivalent-linear and nonlinear models for the Vs30 dependent assessment.

The equivalent-linear model-based hazard spectrum (UHS) is in general larger than the nonlinear-based model. The period of the highest acceleration is almost equal for both cases. The Vs30 dependent UHS is not suitable to represent the characteristics of the alluvial deposits of sufficient thickness of the site well since the bedrock is located at a depth of around 150m. Kaklamanos et al. (2015) have commented that the equivalent-linear model happens to be erroneous at a shear strain of around 0.1 to 0.4%. Also, they mentioned that the nonlinear model can better predict the motion at the ground surface at large shear strain. The obtained biggest shear strain is larger than 0.1% in the majority of the layers throughout site response analysis. Hence, for thick sedimentary deposits, the nonlinear site assessment is suitable for the determination of UHS at the surface. The average obtained PGA value at the surface for a return period of 475 years is around 0.27g using the nonlinear assessment technique.

Liquefaction susceptibility estimation

In this study, the liquefaction susceptibility at each layer of 1.5m intervals where SPT-N value exists and liquefaction potential index (LPI) values have been estimated for 66 boreholes located all over the site up to a depth of 20m. The locations where borehole data are not present, LPI have been estimated by the Kriging method. LPI estimation has been

made for the three methods Seed and Idriss (1971) method (later amended by Youd and Idriss, 2001), Japanese method (Tatsuoka et al., 1980), and Chinese method (Sun et al., 2015) for two cases: (a) A lower bound value of PGA=0.19g (for 23% probability of exceedance in 50 years or a return period of 200 years) and M_w = 7.5 and (b) an upper bound value of PGA=0.27g (estimated through nonlinear site assessment for a return period of 475 years) and M_w = 8.15 which has been estimated with the help of past seismic data. Figure 14 shows the factor of safety versus depth plot at BH-01 for the three methods for PGA=0.19g and M_w=7.5 (lower bound case). Tables 1 and 2 have presented LPI values for the three methods and for lower and upper bound cases. To show LPI contours, the three levels of hazard as described by Iwasaki et al. (1984), have been utilized as shown in Figure 15 for the lower bound case. The LPI plot of the upper bound case has not been shown here since all the values exceed 15.

It is apparent from the results of the LPI values that the site is mainly composed of inferior quality soil. There is a high probability that sand boils and lateral spreading may occur at the site during a seismic event. This may become decisive for essential structures within the power plant site. From the findings of the current study, it may be concluded that structures with a shallow foundation for this site may be recommended only if the entire soil up to a depth of 20m is fully improved by suitable ground improvement techniques. Alternatively, the length of the pile greater than 20m below EGL may be recommended along with ground improvement of the top 5m of the loose sand soil zone. In this research, borehole data of 66 locations with SPT have been utilized for a relatively small area. A large number of boreholes for a relatively small area of the site would generally produce dependable results in the assessment of LPI.

CONCLUSIONS

During the whole design lifecycle, the assessment of the Liquefaction Potential Index (LPI) is important for the development of a power plant site in inferior quality soils for the proper working condition of the facility. The PGA value at the bedrock level has been evaluated utilizing past seismic data, seismo-tectonic details, and suitable GMPE relations. To approximate the time history at the surface in a site where the loose soil deposits of larger than 30 m thick are located on top of the bedrock, 1D nonlinear site assessment is needed. A nonlinear site assessment using DEEPSOIL has been performed to estimate the site amplification and consequently to obtain the surface level PGA at the site. The LPI of the

power plant site has been assessed utilizing the SPT-N value data at 66 locations of the site applying three methods and two sets of PGA values and magnitudes up to a depth of 20m. The soil of the entire power plant site is highly vulnerable to liquefaction up to a depth of about 20 m. For this reason, two alternative foundation solutions are recommended for this site. The first one is providing a shallow foundation above an improved ground up to a depth of 20m or providing 20m deep piles. Also, the LPI contours will be helpful for future development in the vicinity of the current site.

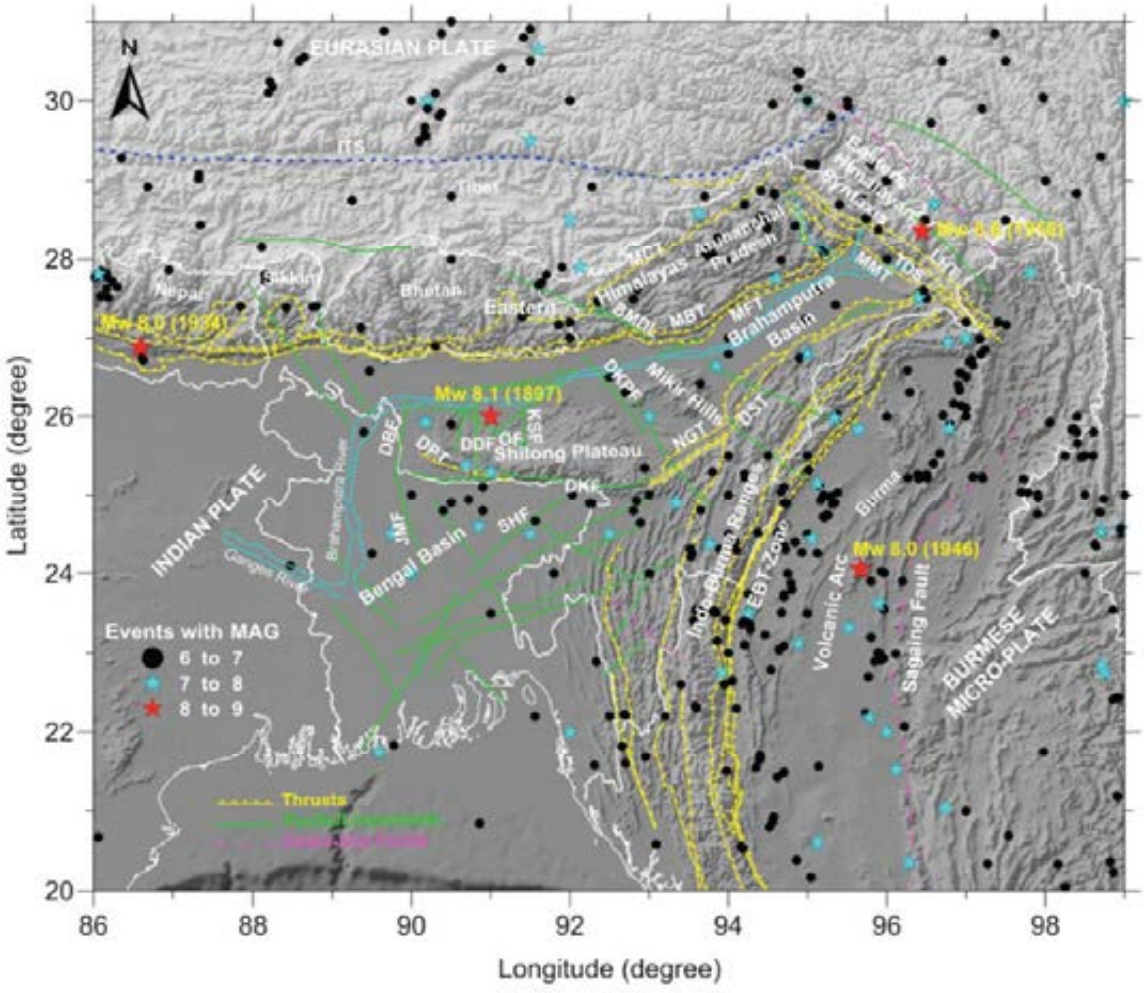

Figure 1 Tectonic map of the area. Abbreviations: ITS: Indus–Tsangpo–Suture, MCT: Main Central Thrust, MBT: Main Boundary Thrust, MFT: Main Frontal Thrust, LHT: Lohit Thrust, TDS: Tidding Suture, MMT: Mishmi Thrust, EBT: Eastern Boundary Thrust, DKPF: Dhansiri–Kopili Fault, NGT: Naga Thrust, DST: Disang Thrust, SHF: Sylhet Fault, JMF: Jamuna Fault, DPT: Dapsi Thrust, DBF: Dhubri Fault, DDF: Dudhnoi Fault, KSF: Kulsi Fault, OF Oldham Fault, DKF: Dauki Fault, BMDL: Bomdila lineament (after Raoof et al 2017)

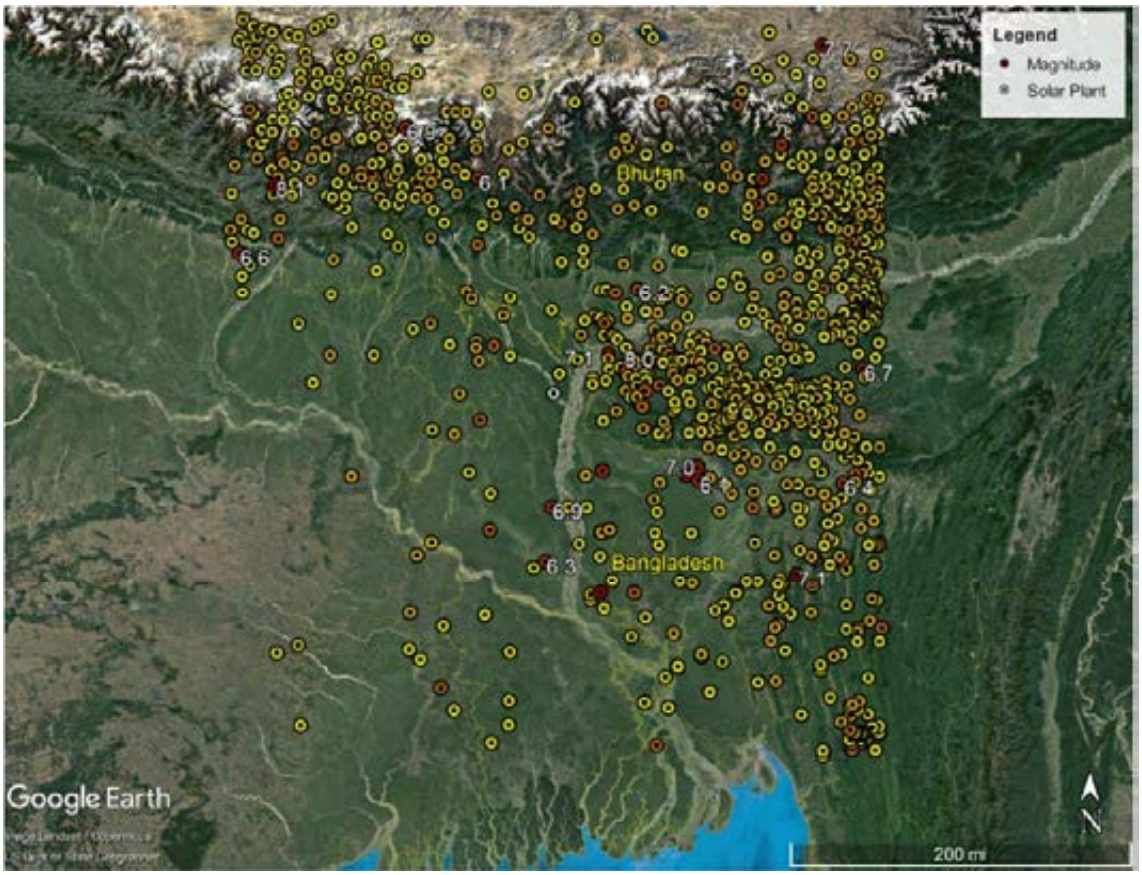

Figure 2 Earthquakes in and around 300 km radius from the solar power plant. The magnitude is low when marked by yellow color and high when marked by red color.

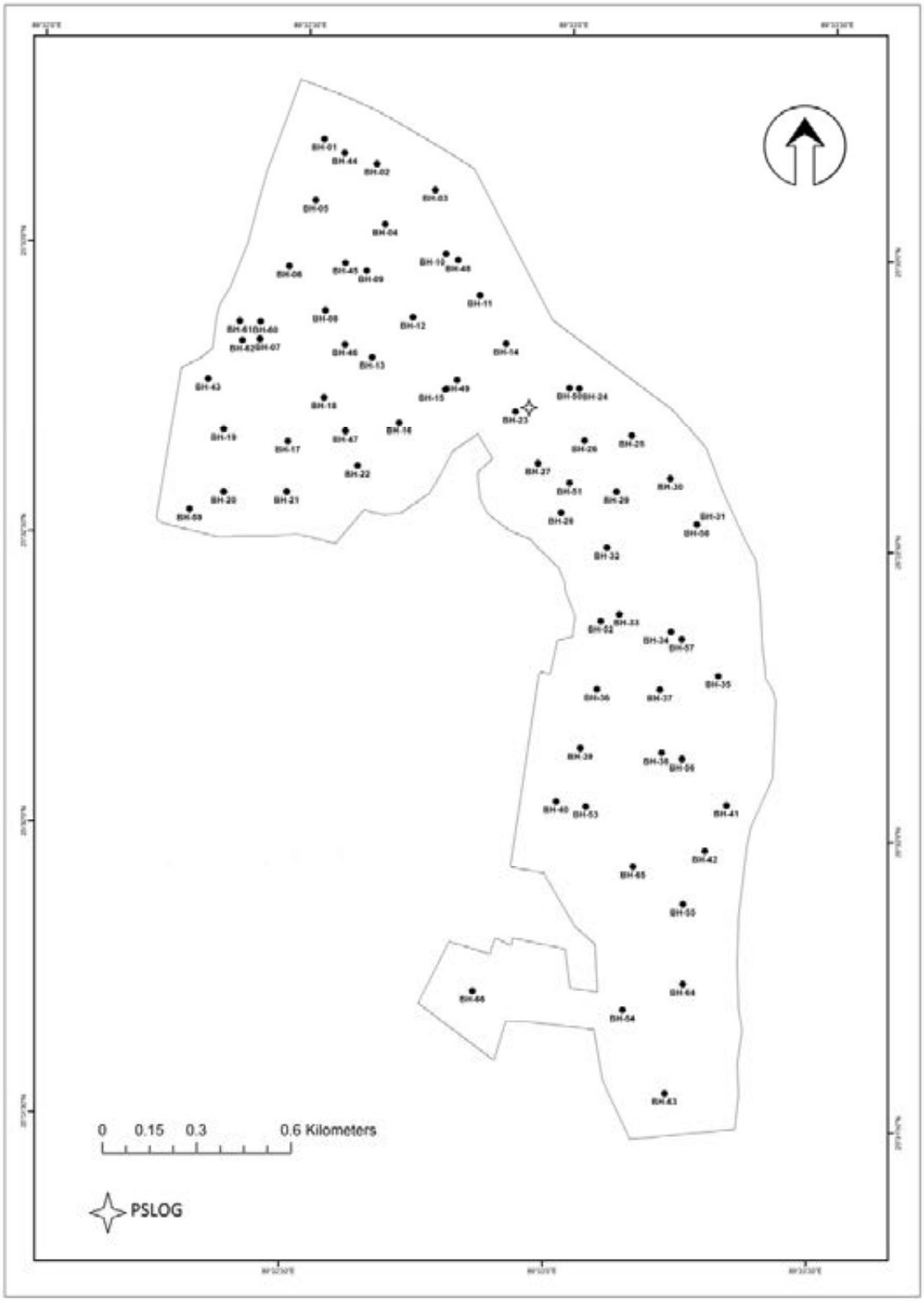

Figure 3 Plant area showing borehole locations

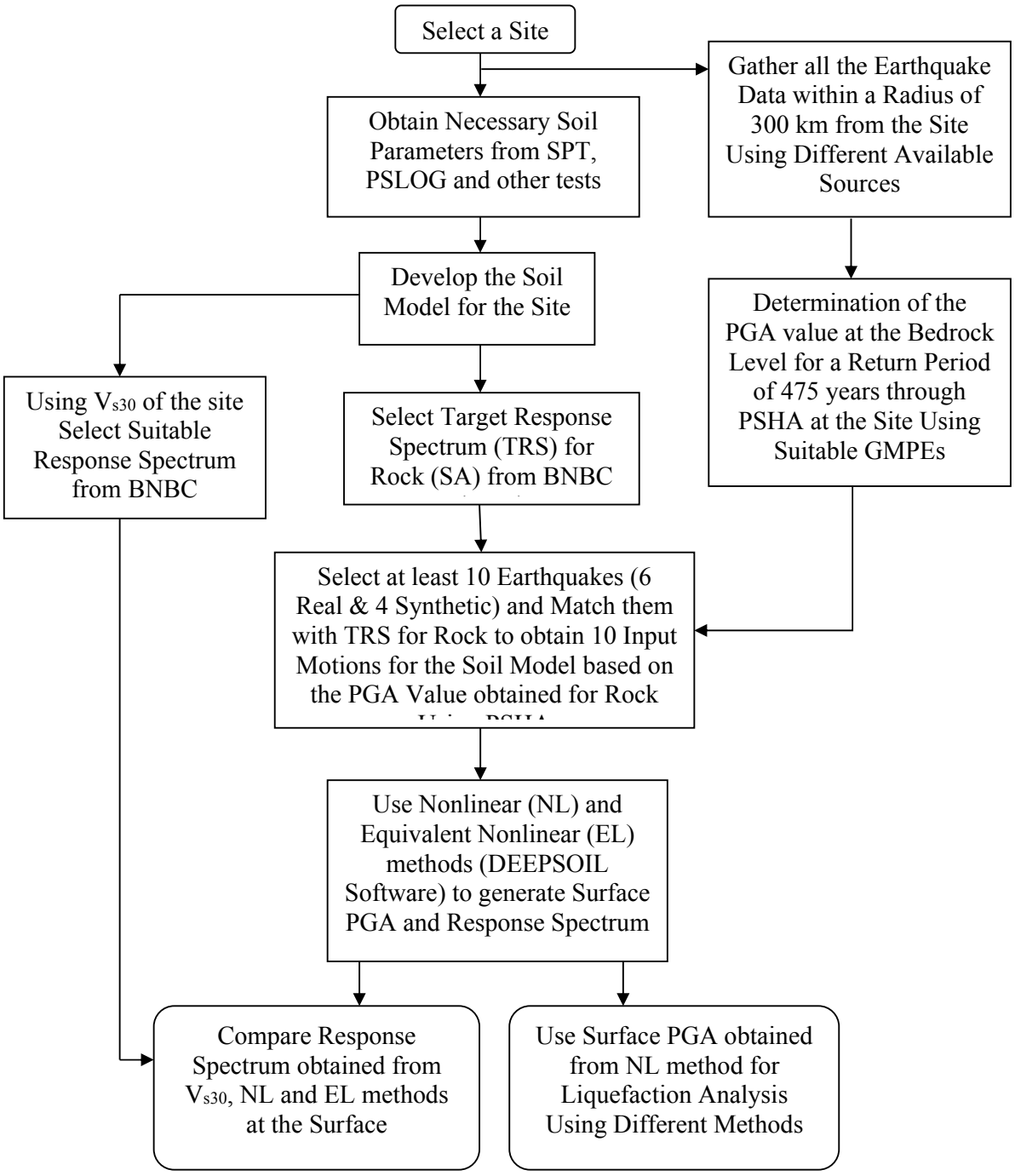

Figure 4 Flow chart of the methodology used in this study

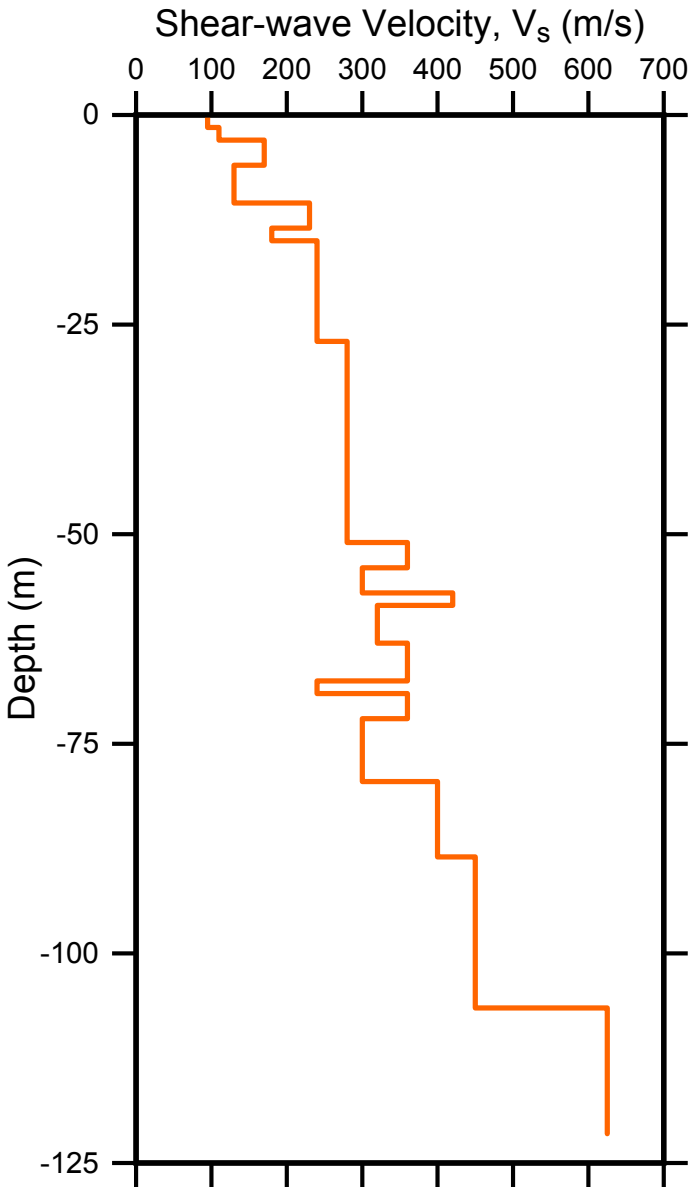

Figure 6 Shear wave velocity (Vs) profile at location BH-23 of the plant site

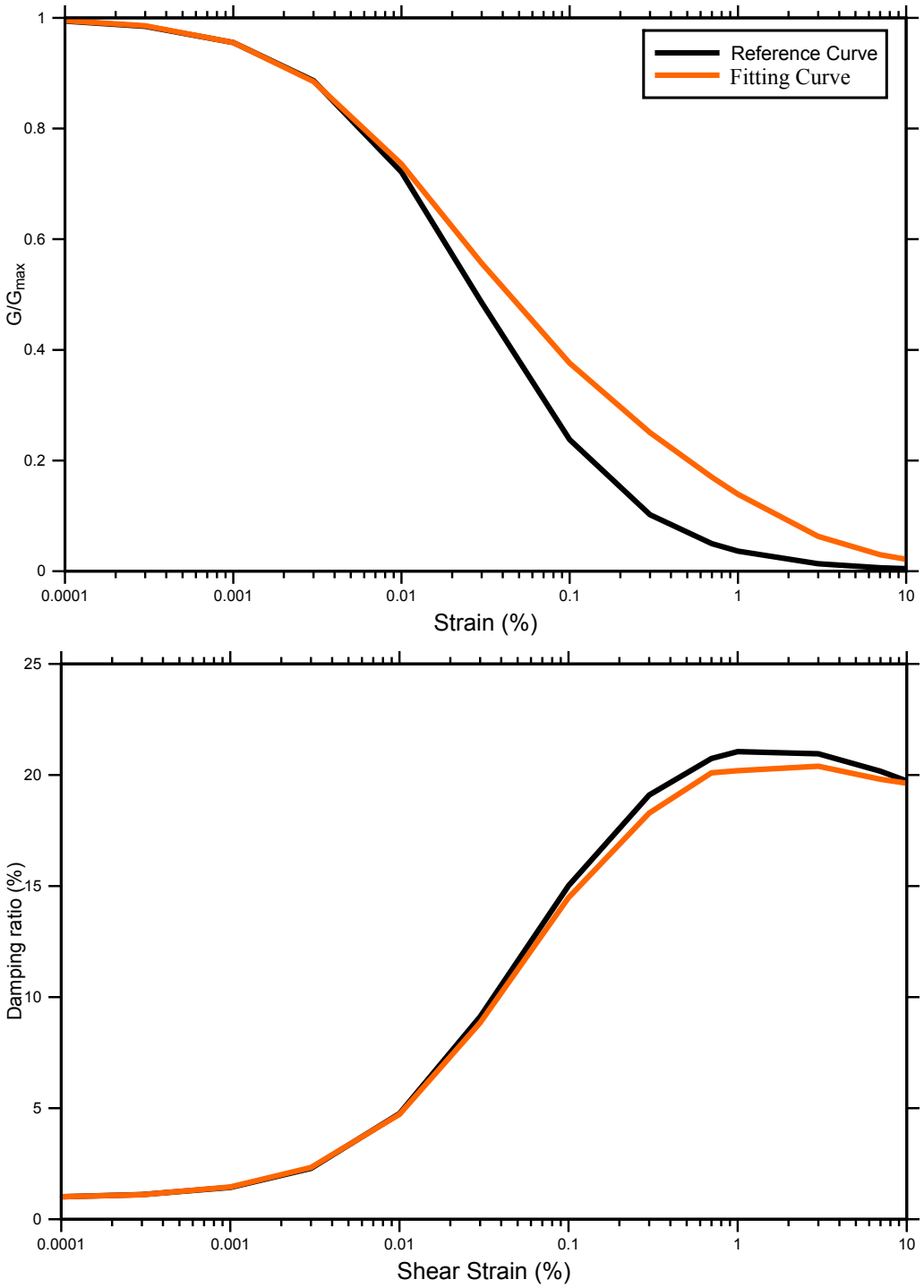

Figure 7 Sample of normalized shear modulus reduction and material damping curves where the reference curves are taken from Darendeli (2001)

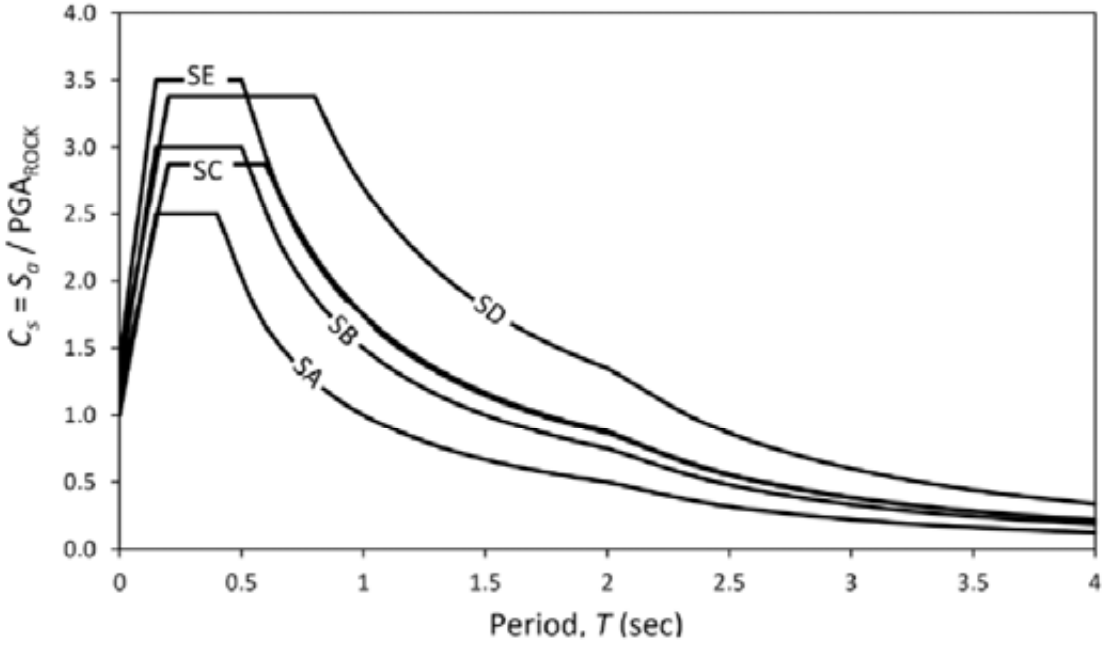

(a)

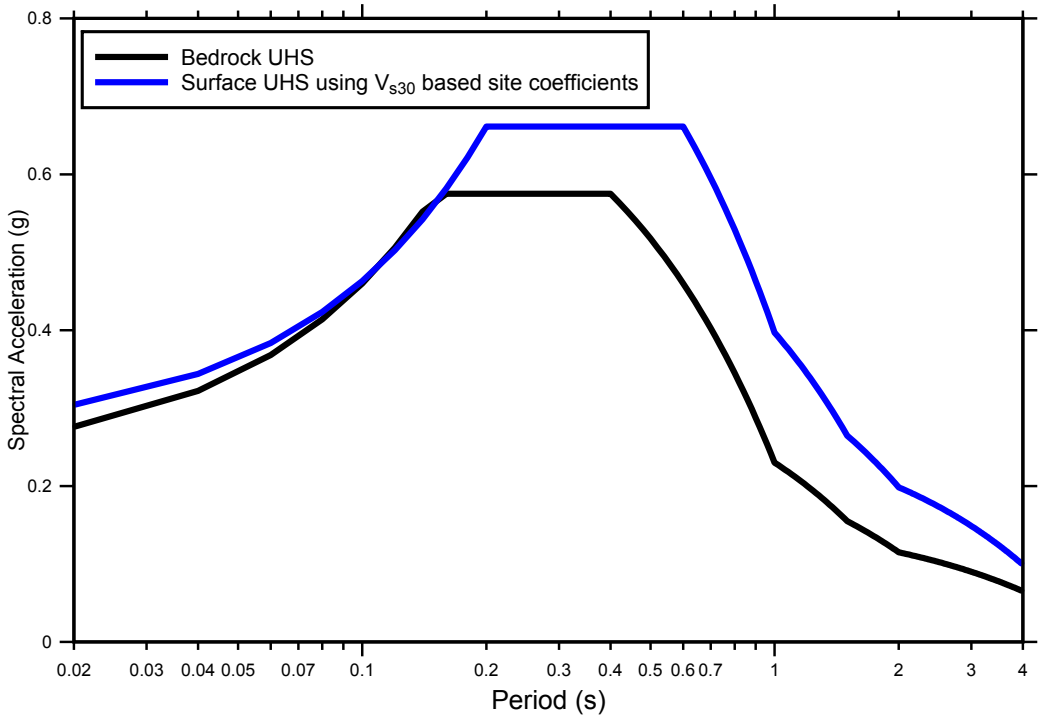

(b)

Figure 8 (a) Normalized design acceleration response spectrum for different site classes (after BNBC, 2020) and (b) UHS for a return period 475 years for soil class SA and SC

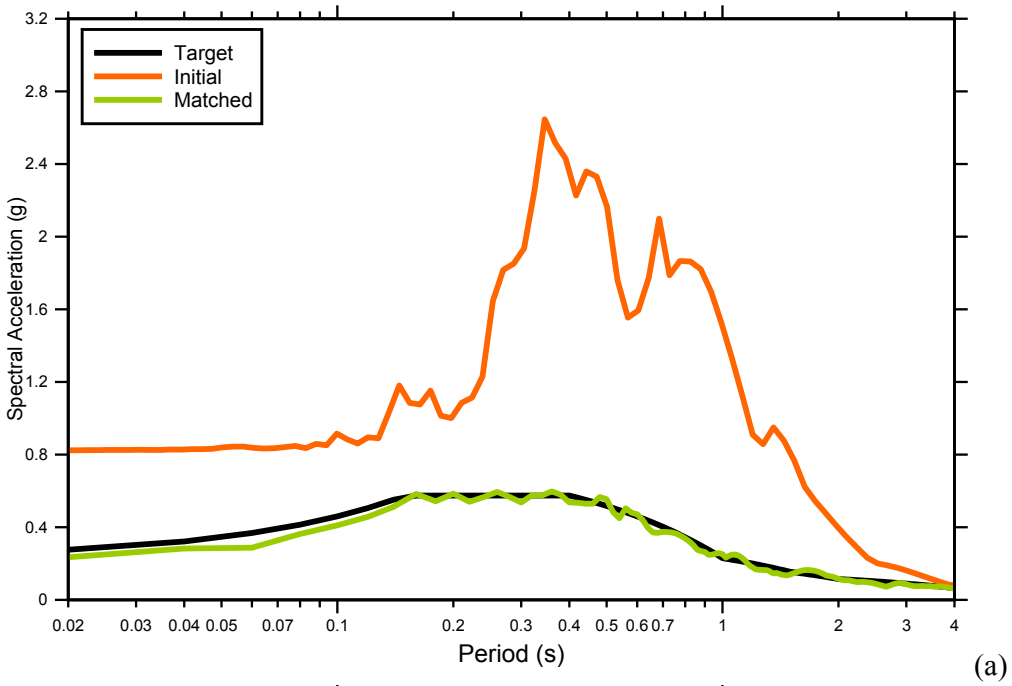

(a)

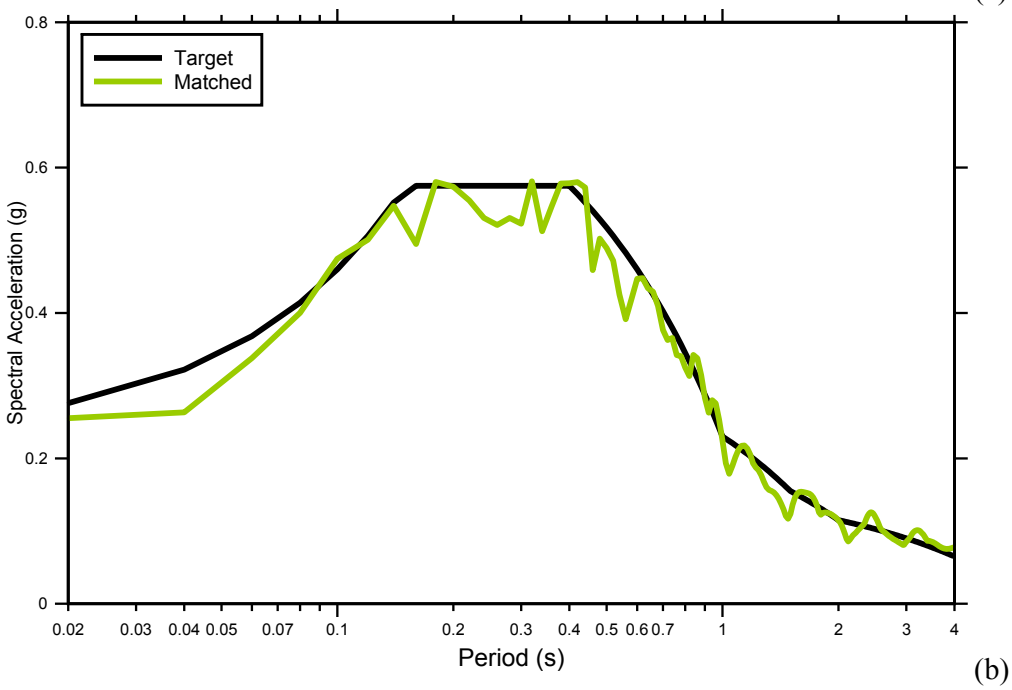

(b)

Figure 9 Spectral matching of the response spectrum of (a) the earthquake time history and (b) synthetic accelerogram with target response spectra for a return period 475 years. Initial is the response spectrum of the earthquake time history (orange), and green is the matched response spectra with target response spectra (black) of bedrock ground condition

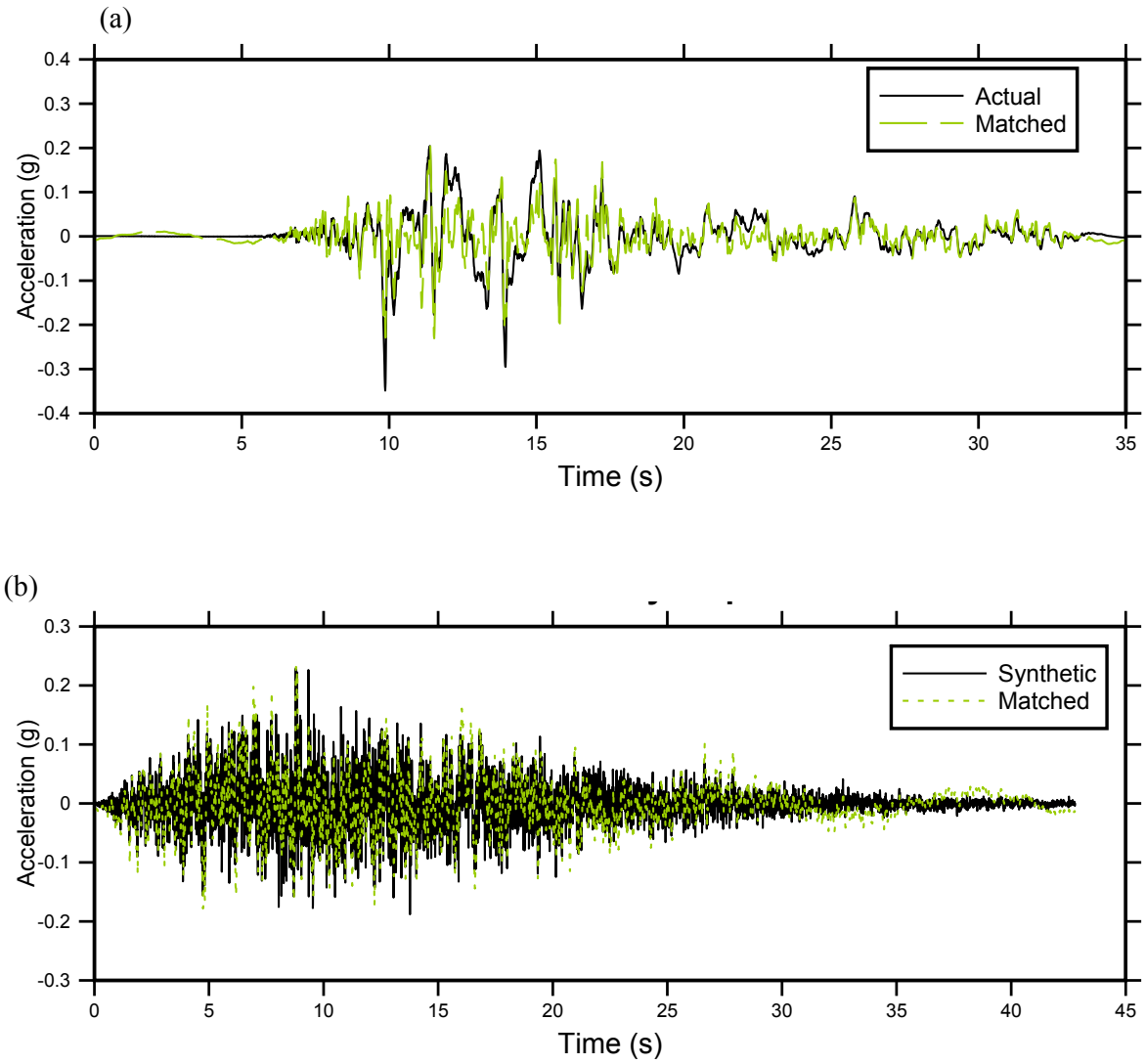

Figure 10 Initial earthquake time history (solid black line) from the database and matched time history (dashed green line) for a return period 475 years at bedrock ground condition

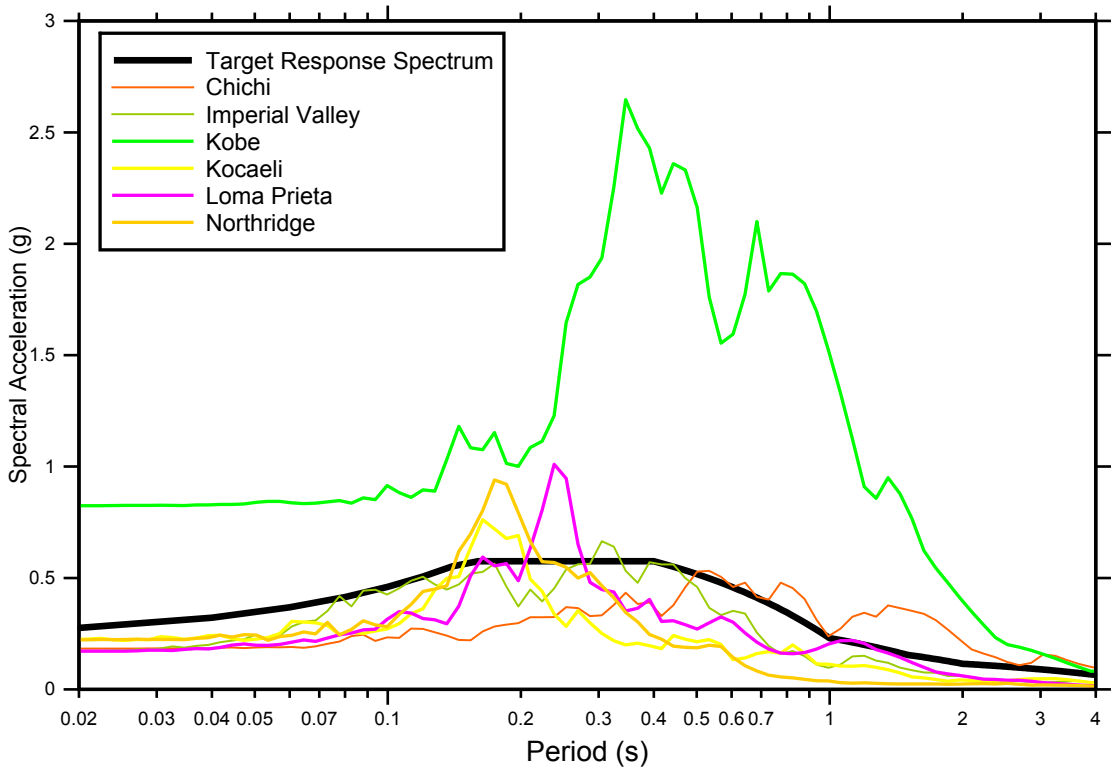

Figure 11 Response spectra of 6 time histories from real earthquakes with target response spectrum for a return period 475 years at the site

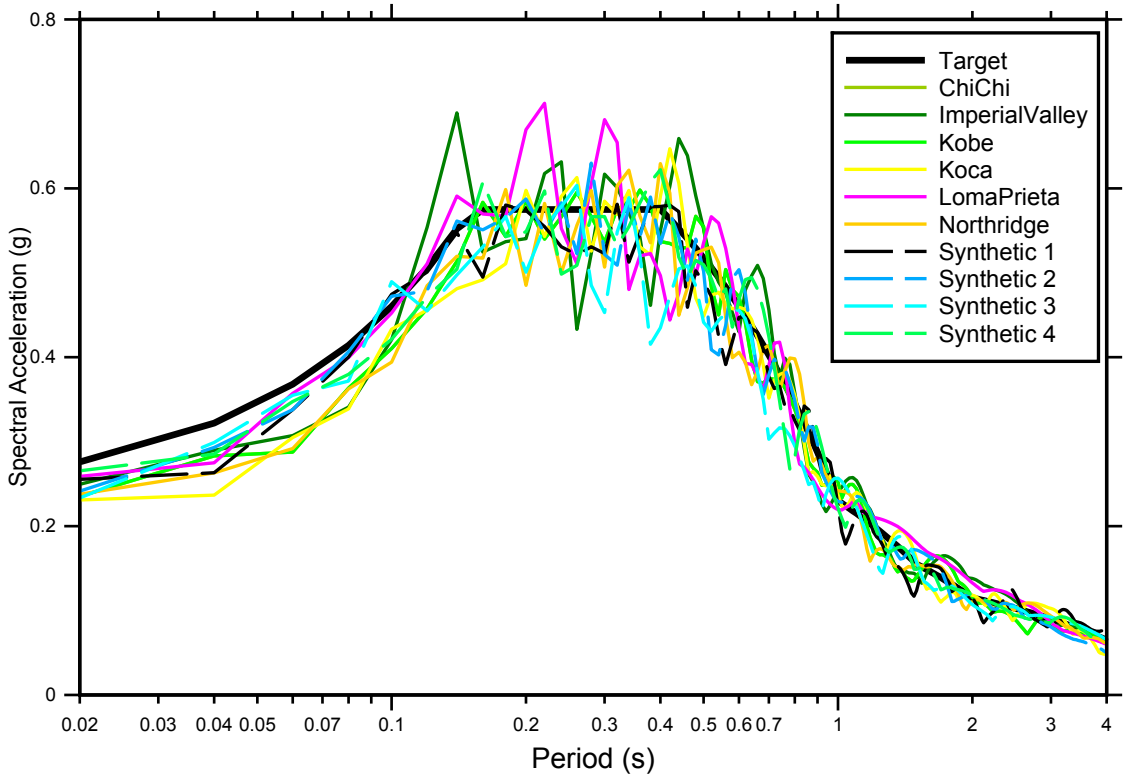

Figure 12 Matched response spectra of 10 time histories with target response spectrum for a return period 475 years at the site

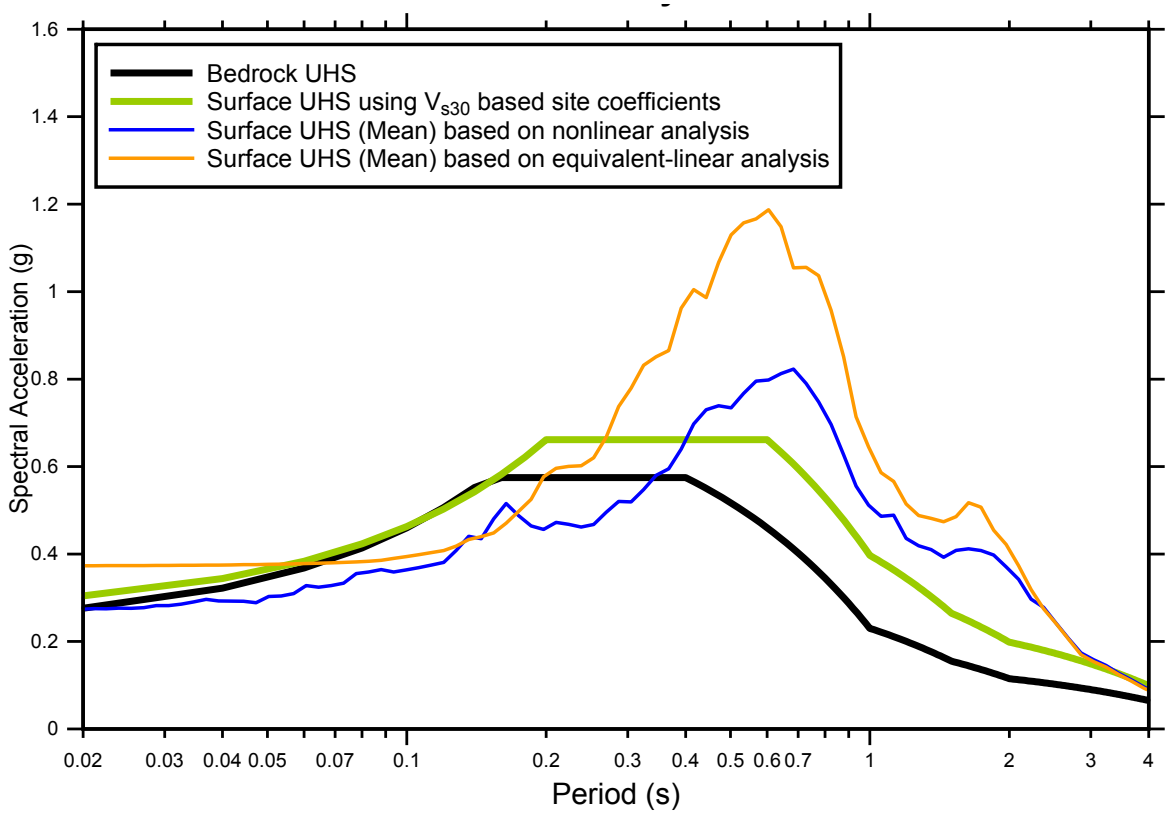

Figure 13 Uniform hazard spectra (UHS) at ground surface using Vs30-based site coefficients and UHS at ground surface using equivalent-linear, and nonlinear ground response analysis at the site for a return period 475 years

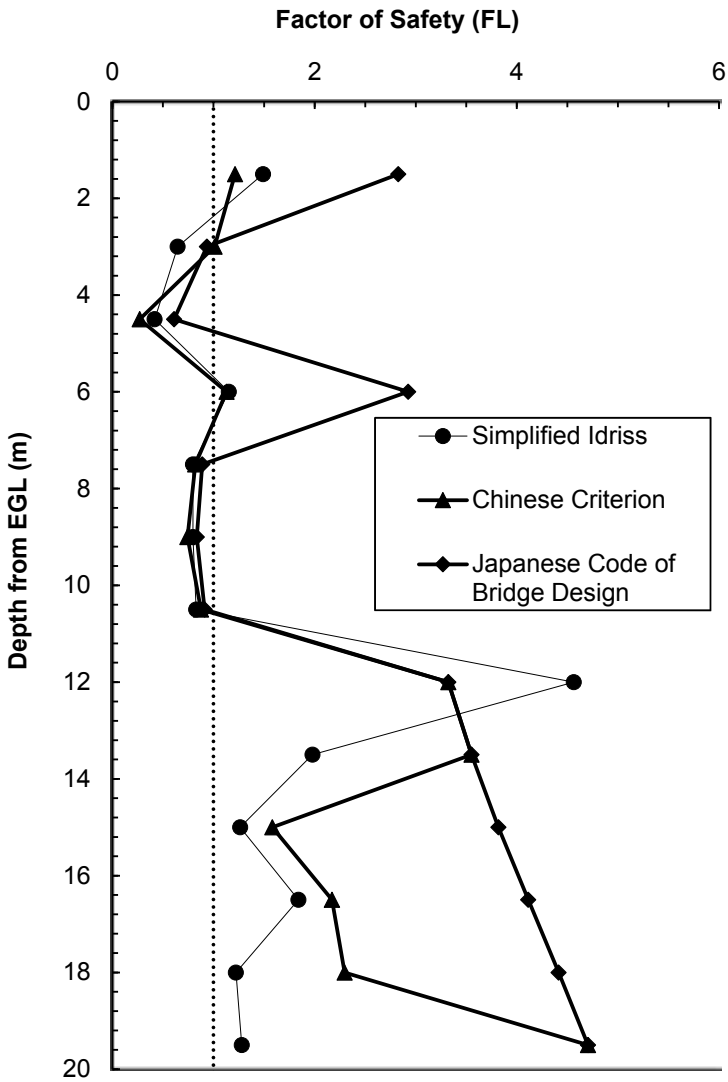

Figure 14 Factor of safety versus depth plot at BH-01 of the three methods for PGA=0.19g and M_w=7.5

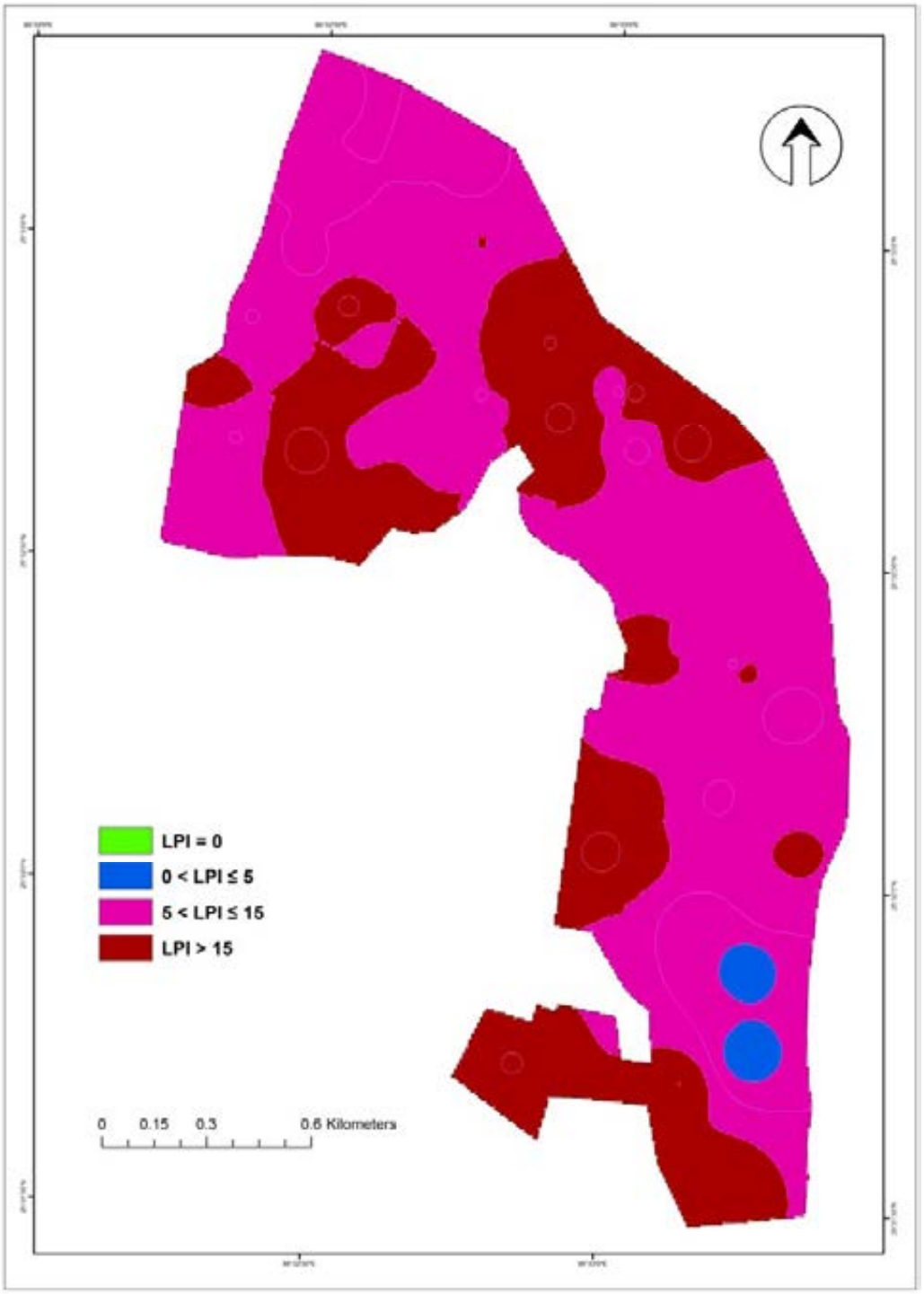

Figure 15 LPI contour of the site for PGA=0.19g and M_w=7.5

BANGLADESH NETWORK
OFFICE FOR URBAN SAFETY

PART-VII

SEISMIC SOIL-STRUCTURE-INTERACTION OF A TALL BUILDING ON PILE-RAFT FOUNDATION IN DHAKA CITY

BANGLADESH NETWORK OFFICE FOR URBAN SAFETY (BNUS), BUET, DHAKA

Prepared By: Md. Mahadi Hasan

Mehedi Ahmed Ansary

INTRODUCTION

One of the most common challenges that civil engineers face is the problem of seismic-soil-structure-interaction (SSSI) when the buildings are located in potential earthquake areas. The seismic soil–structure interaction (SSSI) plays an important role to the response of that structure. The foundation is a part of a structure system in which the gravity load and live load from the structure are applied to. However, the seismic load comes from some depths of the earth and transfers the load to the structure via foundation. This demands the survival of structure even if they occur a few times in hundred years, suddenly without prediction.

The main components of the seismic response of building include displacement, and drift of each floor, foundation rocking and also the recorded acceleration at any point in models. This can produce the response spectrums. All of these parameters need to satisfy certain requirements from design codes.

In order to determine the seismic response of structures, the assumption that the structure is fixed at its base has been made frequently in practice. In general, this assumption can be acceptable if the ground under the structure is stiff enough (similar to structure founded on solid rock). However, when the soil under the structure is soft, two modifications factors need to be considered to determine the seismic response. First of all, the imposed motion to the structure is different from free field motion due to the presence of the structure and foundation. Secondly, additional dynamic deformations are induced within the structure due to the soft soil underneath. According to Kramer (1996), soil-structure-interaction (SSI) is the process in which response of the soil influences the motion of the structure and also response of the structure influences the motion of the soil.

Bangladesh is the largest delta on the earth and its land is formed by the alluvial soils. Here, it is hardly possible to find the solid rock stratum. Soil profiles established for Dhaka Metropolitan area, in general, showed soft to very stiff cohesive layers at the top strata up to depth of 20 ft to 60 ft (Bashar, 2000). The surface deposits are usually soft clay. In seismically active regions, building structures with unfavorable geotechnical conditions are sometime inevitable. To accommodate fast growing population with rapid urbanization it has become essential to construct tall buildings or skyscraper. In Dhaka city, such

skyscrapers on pile mat foundation are in the planning. The critical nature of these structures requires a better understanding of their performance under strong seismic shaking. It has been found from investigation of some recent earthquakes (e.g., Christchurch earthquake of New Zealand in 2011 and Tohoku-Oki earthquake of Japan in 2011) that the aspect of the fixed-base assumption is often misleading (Bilotta et al. 2015; Bagheri et al. 2018; Berger et al. 2012; Sotiriadis et al. 2017). This increases the possibility of unsafe designs, especially for ignoring seismic soil-pile-structure interaction (SSPSI) impacts upon the super structures resting on soft soils. Impacts of SSPSI on super structure responses have been studied by many researchers during the last two decades and frequent analytical formulations have been conducted to solve the complex practical problems based on linear and elastic soil structure interaction (Stewart et al. 1999; Galal et al. 2008; Khalil et al. 2007; Tabatabaiefar et al. 2010). In particular, considering the effects of SSPSI on structure founded on soft soil, lateral displacements and inter-story drifts of unbraced frames may be significantly amplified, thus compromising the building integrity and safety. However, the realistic simulation of SSPSI is mostly dependent on the behavior of soil nonlinearity which is complex and time-consuming process (Bolisetti et al. 2018; Luo et al. 2016; Mucciacciaro et al. 2018; Wang, 2012; Maheshwari et al. 2011; Bourgeois et al. 2012; Hokmabadi et al. 2014; Carbonari et al. 2014). Under the light of above discussion, it becomes essential to investigate the impact of SSPSI for the structure to be built in high seismic zone considering nonlinear behavior of soil beneath the structure.

This study aims to numerically analyze a tall building resting on pile-mat foundation for studying seismic soil-pile-structure interaction (SSPSI) effects in Dhaka soil under different earthquakes. The study will throw light on the effects of considering seismic soil-pile-structure interaction (SSPSI) on the design parameters of a tall building for Dhaka soil conditions. The results are expected to give some guidelines whether SSI effects should be considered while designing tall buildings/skyscrapers on pile-mat foundations in Dhaka city.

1.2 Objectives

The main objectives of this research work are follows:

i. To develop a suitable numerical model for studying seismic soil-pile-structure

interaction (SSPSI) effects for a tall building resting on pile-mat foundation using time-history analysis.

ii. To study modal shapes and natural frequencies of the tall building resting on pile mat foundation in Dhaka soil considering SSPSI effects and ignoring SSPSI effects.

iii. To compare principal design parameters of a tall building on Dhaka soil considering SSPSI effects and ignoring SSPSI effects. The lateral displacements and inter-story drifts criteria are vital indicators of performance of tall building during an earthquake, these become more important for skyscrapers.

iv. Studying the deformation of pile under seismic loading

v. To study the settlement of the raft foundation and piled raft foundation resting on Dhaka soil by static analysis

1.3 Outline of Methodology

In this research, a numerical simulation has been carried out for a tall building resting on piled raft foundation using a geotechnical software midas GTS NX to quantitatively assess the effects of soil-pile-structure interaction subjected to seismic loads. Key steps regarding this work are stated below:

1. Experimental work performed in the University of Sydney Lab has been verified through numerical analysis using midas GTS NX software.
2. Accordingly, the performance of a tall building model consists of 42 stories with 4-basements has been evaluated by equivalent linear static analysis according to BNBC-2020.
3. After satisfying linear static analysis according to the code, the building has been analyzed for seismic soil- pile-structure interaction using finite element method.
4. The analyses has been performed for both fixed-base model and flexible base model resting on soil continuum.
5. Typical Dhaka soil stratigraphy has been used for three-dimensional continuum soil model.
6. All the structural members of the frame has been modeled using a beam element. The general shell element and eight nodded solid brick elements will be used for floor slabs and soils respectively to the numerical model.

7. Implicit unconditionally stable time integration scheme has been used considering three earthquakes as a dynamic load.
8. Finally, the lateral displacements and inter-story drifts of the numerical model has been ascertained.

Flow chart of the methodology is shown in Figure 1.1 below.

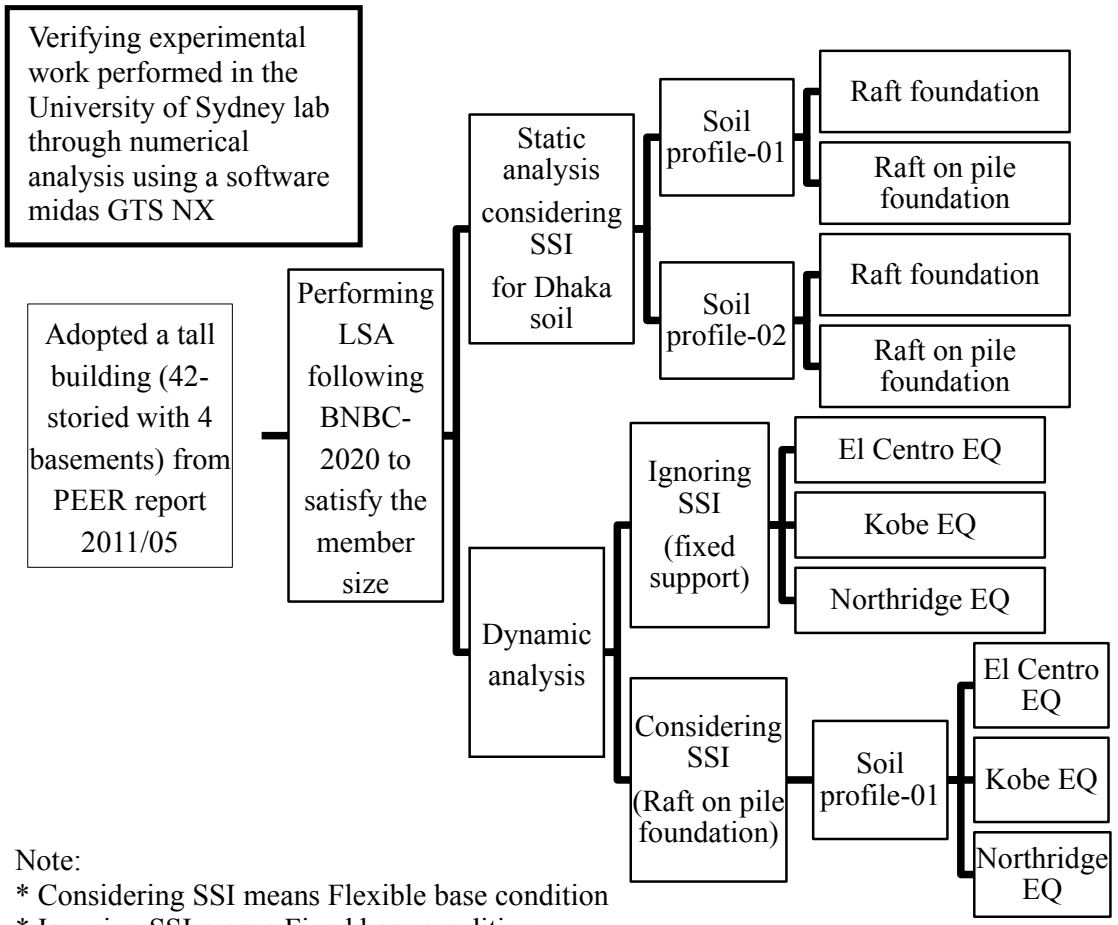

Figure 1.1: Flowchart of the study

NUMERICAL MODEL DEVELOPED IN THE CURRENT STUDY

4.1 Introduction

In order to conduct a fully coupled analysis of the entire soil-pile-structure system, a three-dimensional numerical soil-structure model has been developed in this study which treats the behaviors of the soil and the structure with equal rigor. Adopting direct method of analysis, the numerical model can perform nonlinear time-history dynamic analysis to simulate realistic dynamic behavior of the soil and the structure under seismic excitations.

In this study, a three-dimensional finite element analysis using a commercial software called midas GTS NX is performed for a tall building (42 stories with 4 basement) with soil continuum. It should be noted that there are some rigorous approaches to model soil behavior under cyclic loads such as isotropic kinematic constitutive models (Gajo and Muir Wood, 1999), incrementally nonlinear models (Darve et al., 1995), or hypoplastic models (Chambon et al., 1994). However, the modulus reduction approach is the most common approach to model the soil for dynamic analysis of soil-structure systems, and is employed in this study

All the structural members of the frame will be modeled using a beam element. The general shell element and solid elements will be used for floor slabs and soils respectively to the numerical model.

This program can simulate behavior of different types of structures and materials by elements which can be adjusted to fit the geometry of the model. Each element behaves according to a prescribed constitutive model in response to the applied forces or boundary restraints.

In this chapter, different components of the developed numerical model including soil elements, pile elements, structural elements, interface elements, boundary conditions, and dynamic loading are explained.

4.2 Parametric Study

In this study both static and dynamic SSI are studied for a tall building which is considered to be resting on Dhaka soil. Two types of soil profiles are considered which will be discussed in section 4.4. For static SSI, equivalent linear static analysis has been performed for both soil profile-01 and soil profile-02 with mat foundation and mat on pile foundation.

For dynamic SSI, nonlinear time history analysis has been performed for soil profile-01 with mat on pile foundation considering design based earthquake (DBE) for three different events

(El Centro, Kobe and Northridge). Table 4.1 summarizes the parametric study.

Table 4.1: Summarization of parametric study

Loads	Profile	Earthquake		Foundation	Model ID
Static	Soil-01	Equivalent static	Z=0.13	Mat	Flexible Base (S1)
				Mat on Pile	Flexible Base (S2)
	Soil-02			Mat	Flexible Base (S3)
				Mat on Pile	Flexible Base (S4)
Dynamic	Soil-01	El Centro	Z=0.17	Mat on Pile	Fixed Base (D1)
			Z=0.148		Flexible Base (D2)
		Kobe	Z=0.147		Fixed Base (D3)
			Z=0.123		Flexible Base (D4)
		Northridge	Z=0.134		Fixed Base (D5)
			Z=0.12		Flexible Base (D6)

4.3 Characteristic of Building Structure

In this study, a tall concrete building is selected from a case study of Tall Buildings Initiative (Moehle et al., 2011). The building consists of 4 (four) stories below ground and 42 (forty-two) stories above ground and a pent house at top of the structure. Story heights of floors below ground, ground to 2nd floor, typical floor from 2nd to 42nd, roof and pent house of the building are to be 10.5 ft, 13.67 ft, 10.5 ft, 11.5 ft, and 20 ft respectively. Slab thickness varies for different stories. Colum size, building core wall and compressive strength of concrete vary for different elements of the structure which are shown in table 4.1 and 4.2. Reinforcement, yield strength of 60 ksi, is used. Beam depth for the selected structure is considered to be 30 inch. Shear wall of 16-inch thickness is chosen. Figure 4.2 presents typical plan view of a subterranean level and figure 4.3 shows typical plan view of stories from level-2 to roof. Figure 4.4 and figure 4.5 display elevation of grid-3 and shear wall and basement wall respectively. Detail geometric data of the building is provided below.

4.3.1 General Building Properties

General building properties of the adopted building are shown below:

Number of Stories 42 above ground plus Pent-house

	4 below ground
Story Height	10.5′ (3.20 m) at levels below Ground 13.67′ (4.17 m) from Ground to 2nd floor 10.5′ (3.20 m) Typical from 2nd floor to 42nd floor 11.5′ (3.50 m) Roof 20′ (6.10 m) Pent-house
Slab Construction	10″ (254 mm) thick reinforced concrete at Basement levels 12″ (304 mm) thick reinforced concrete at Ground floor 8″ (203 mm) thick concrete typical above Ground 10″ thick reinforced concrete at Roof
Beam Depth	30″ (typical) (762 mm)
Basement Walls	16″ thick (406 mm)

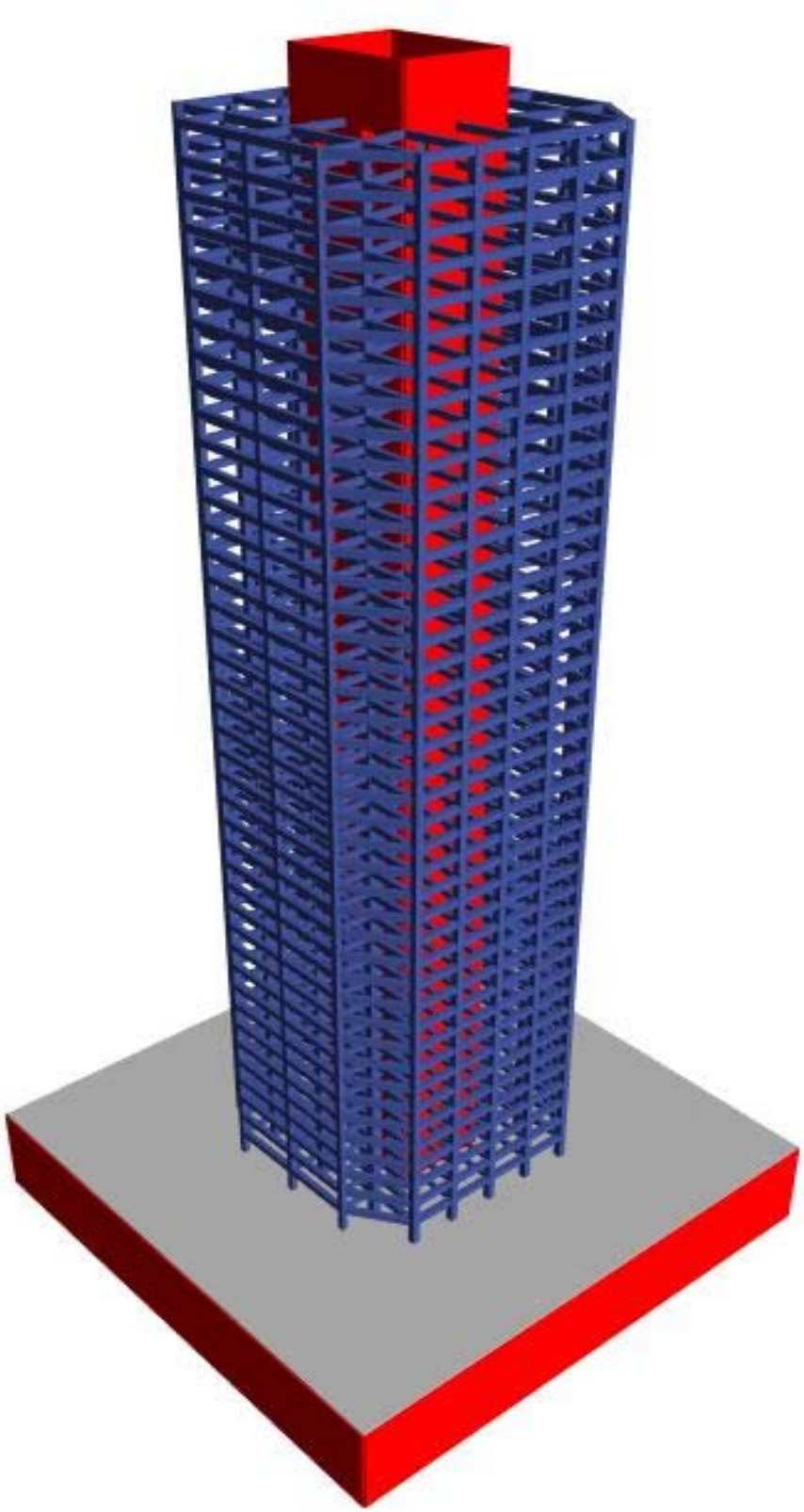

Figure 4.1: 3D View of the structure

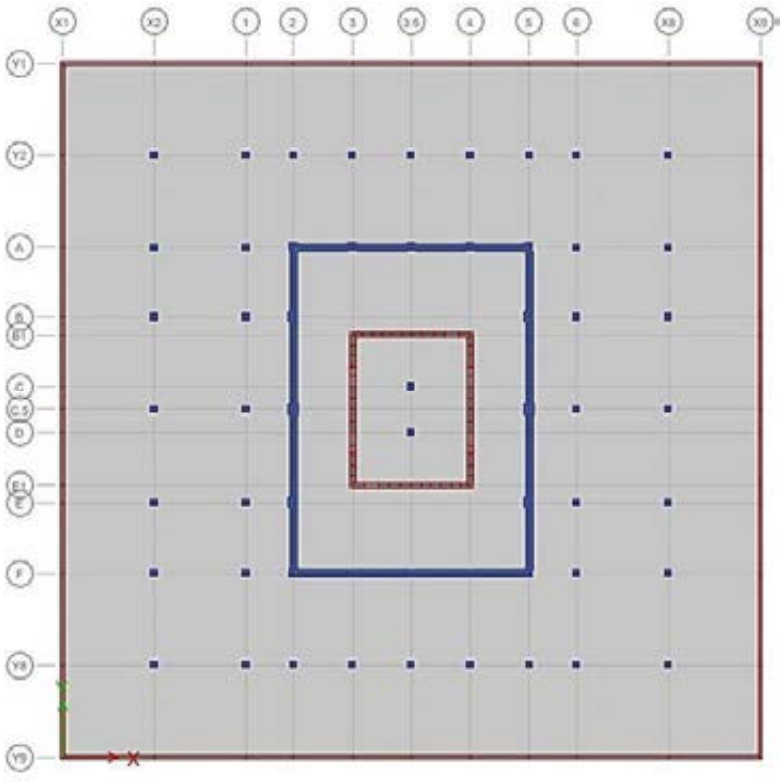

Figure 4.2: Typical plan view (bottom ~ ground floor)

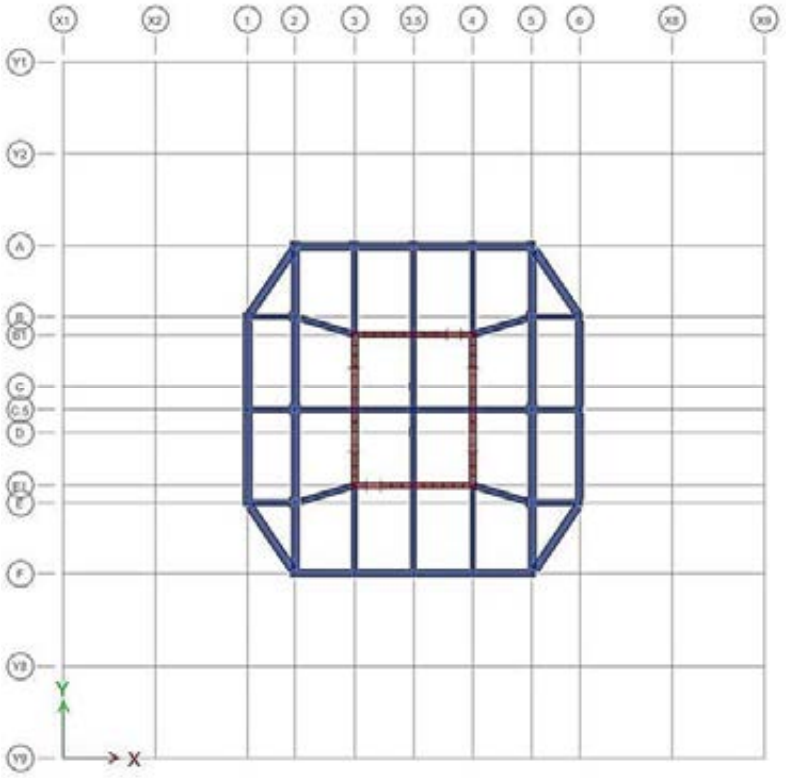

Figure 4.3: Typical plan view (Level 2 ~ Roof)

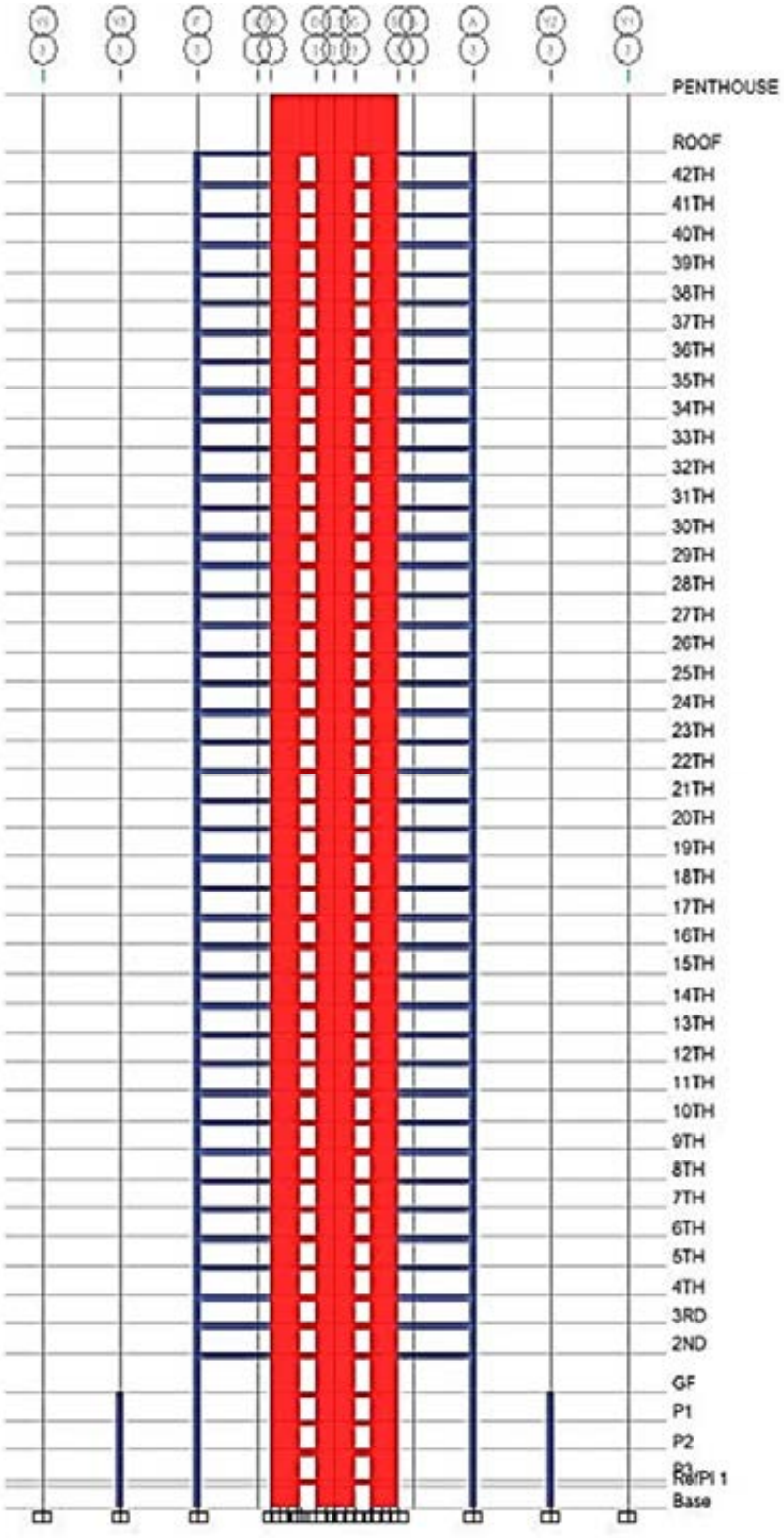

Figure 4.4**:** Elevation of grid -3

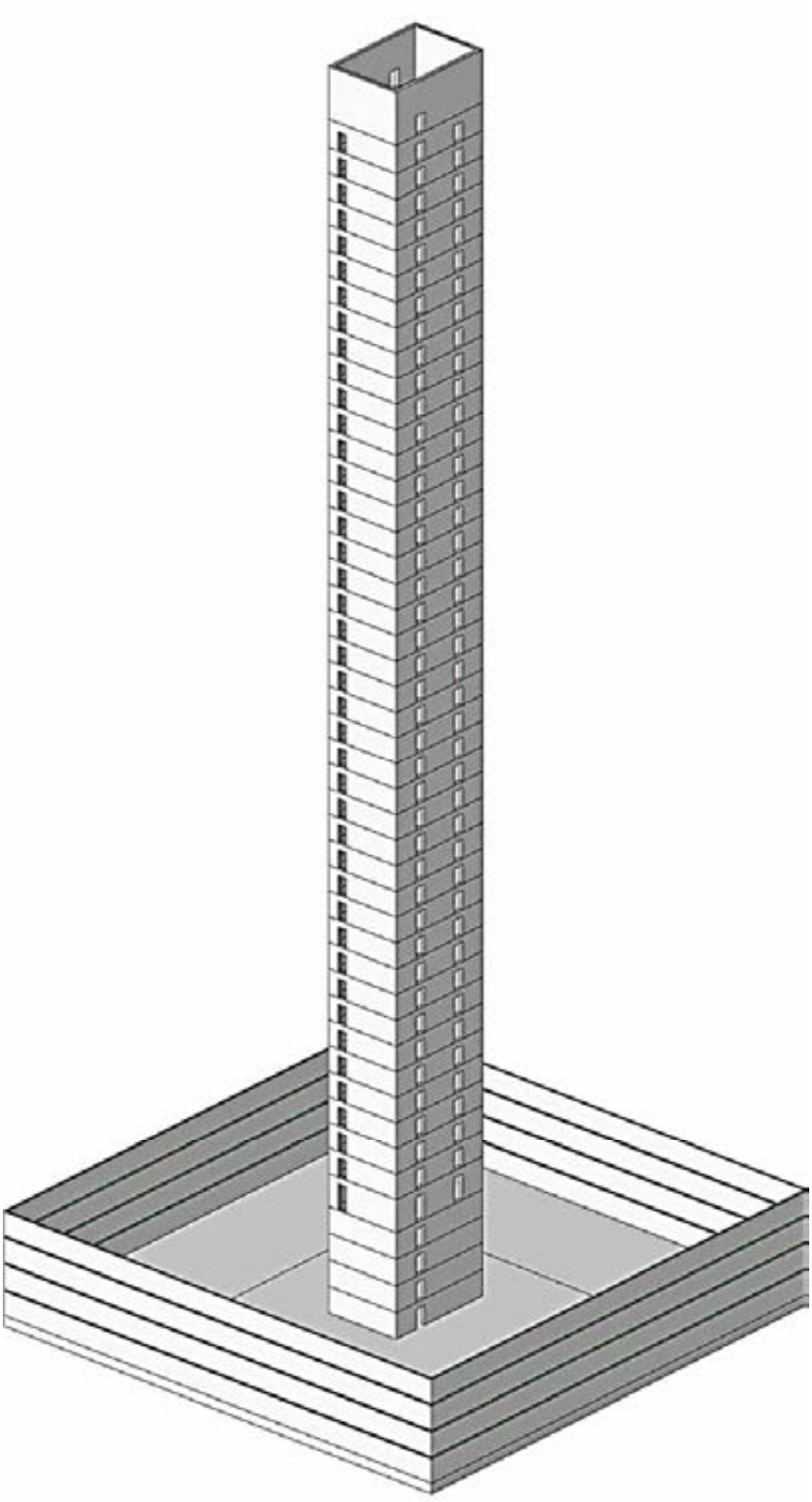

Figure 4.5**:** Core wall and Basement Wall

Table 4.2: Column properties and section

Story	Frame A and F		Frame 2 and 5		Frame C5	
	Column Dimension	f'c (ksi)	Column Dimension	f'c (ksi)	Column Dimension	f'c (ksi)
Base to GF	36" × 36"	10	42" × 42"	10	46" × 46"	10
GF to 10F	36" × 36"	8	42" × 42"	8	46" × 46"	8
10 to 15F	36" × 36"	6	42" × 42"	6	46" × 46"	6
15F to 25F	36" × 36"	5	36" × 36"	5	46" × 46"	5
25F to 42F	36" × 36"	5	36" × 36"	5	46" × 46"	5

Table 4.3: Building core wall thickness and material strength

Story	Thickness (inch)	f'_c (ksi)	f_y (ksi)
Base to 20 th	24	6	60
20 th Floor to Roof	18	5	

4.3.2 Effective Stiffness of the Structural Members

The stiffness assumptions are listed in Table 4.3 When non-linear behavior of elements is modeled, stiffness modifiers are applied to the assumed "*elastic"* portion of the force-displacement relationship.

Table 4.4: Effective stiffness of crack section

Structural Elements	**Effective stiffness**	
	Flexural (EI_g)	Shear (GA_g)
Core Walls	0.6	1.0
Basement Walls	0.8	0.8
Coupling Beams	0.2	1.0
Ground Level and Basement slabs	0.25	0.5
Moment Frame Beams	0.35	1.0
Moment Frame Columns	0.7	1.0

Note:

Modulus of elasticity is based on the following equations:

$E_C = 57000 \sqrt{f_C'}$ for $f'_c \leq 6000$ psi

$E_C = 40000 \sqrt{f_C'} + 1\times10^6$ for $f'_c > 6000$ psi (per ACI 363R-92)

4.3.3 Gravity Load Consideration

In addition to the self-weight of the structure, the loads listed in Table 4.5 are used for the

calculation of superimposed dead load and live loads.

Table 4.5: Load criteria of the building

Use	Location	Superimposed dead load (psf)	Live Load (psf)
Parking	4 stories below ground	30	50
Retail Area	Ground Level inside area	110	100
Residential	2nd floor to 42nd floor	28	40
Mechanical	At roof floor only	100 kip	25
Roof	Roof floor	28	20

4.4 Characteristics of the Adopted Dhaka Soil

This section provided a detail overview on characteristics of soil profiles.

4.4.1 Subsoil Stratigraphy

A case study has been performed to investigate the variation of the soil properties with depth and to establish approximate correlation among different geotechnical properties of the subsoil of the Dhaka Metropolitan Area (Bashar, M.A., 2000). About 300 sub-soil investigation reports consisting of 674 boreholes data were collected from the different drilling companies, consulting firms and other organizations in order to develop the generalized soil profiles of Dhaka Metropolitan area. In order to verify the existing soil data, a number of test bore holes were drilled up to a depth of 100 ft. From the investigation, four longitudinal soil profiles and five cross soil profiles have been established for Dhaka Metropolitan area. Soil profiles established for Dhaka Metropolitan area, in general, showed soft to very stiff cohesive layers at the top strata up to a depth of 20 ft to 60 ft. At large depths, the soil layers have been found to consist of medium dense to very dense sandy soils. In some areas of the eastern region of Dhaka Metropolitan, however, cohesive layers up to a depth of 100 ft have been encountered. These areas include Uttarhan, Dakkhinkhan, Saterkul and Daina. Based on the case study, two soil profiles, namely soil profile-01 and soil profile-02, have been adopted and soil properties except modulus of elasticity have been taken from the case study. The value of modulus of elasticity is calculated using an equation developed by Bowel (El-kasaby, 1991).

For Clay, $Es = 500\ C_u$, $C_u = 166\ N$ (psf)

For Sand, $Es = 1200\ (N+6)$ (kpa)

The SPT values (N), cohesion (c), and friction angle (φ) of different layers of Dhaka soil were

obtained from the Geotechnical Subsoil Investigation Report of the well-known drilling company Engineering and Research Associates (ERA). Soil profiles are described below.

Soil Profile-01: Combination of Cohesive and Non-Cohesive Soil.

According to the case study performed by Bashar (2000), profile-01 represents soil strata of most of the Dhaka metropolitan area. In profile-01, cohesive soil up to a depth of around 12 m from top level is found with stiffness variation from very soft clay to stiff clay. Non cohesive soil is usually found after stiff clay layer and usually is seen to have variation of relative stiffness from medium dense to dense. Figure 4.6 shows a simplified subsoil stratigraphy of soil profile-01 of Dhaka city.

Soil Profile 02: Cohesive Soil

According to the case study performed by Bashar (2000), profile-02 symbolizes soil strata found rarely in Dhaka metropolitan area where this profile consists of cohesive soil.
In profile-02, cohesive soil is found from top level to bottom. The stiffness variation of soil profile-02 from very soft clay to stiff clay. Non cohesive soil is not found in profile-02 after a stiff clay layer as like profile-01. Figure 4.7 presents a simplified subsoil stratigraphy of soil profile-02 consisting of cohesive soil only.

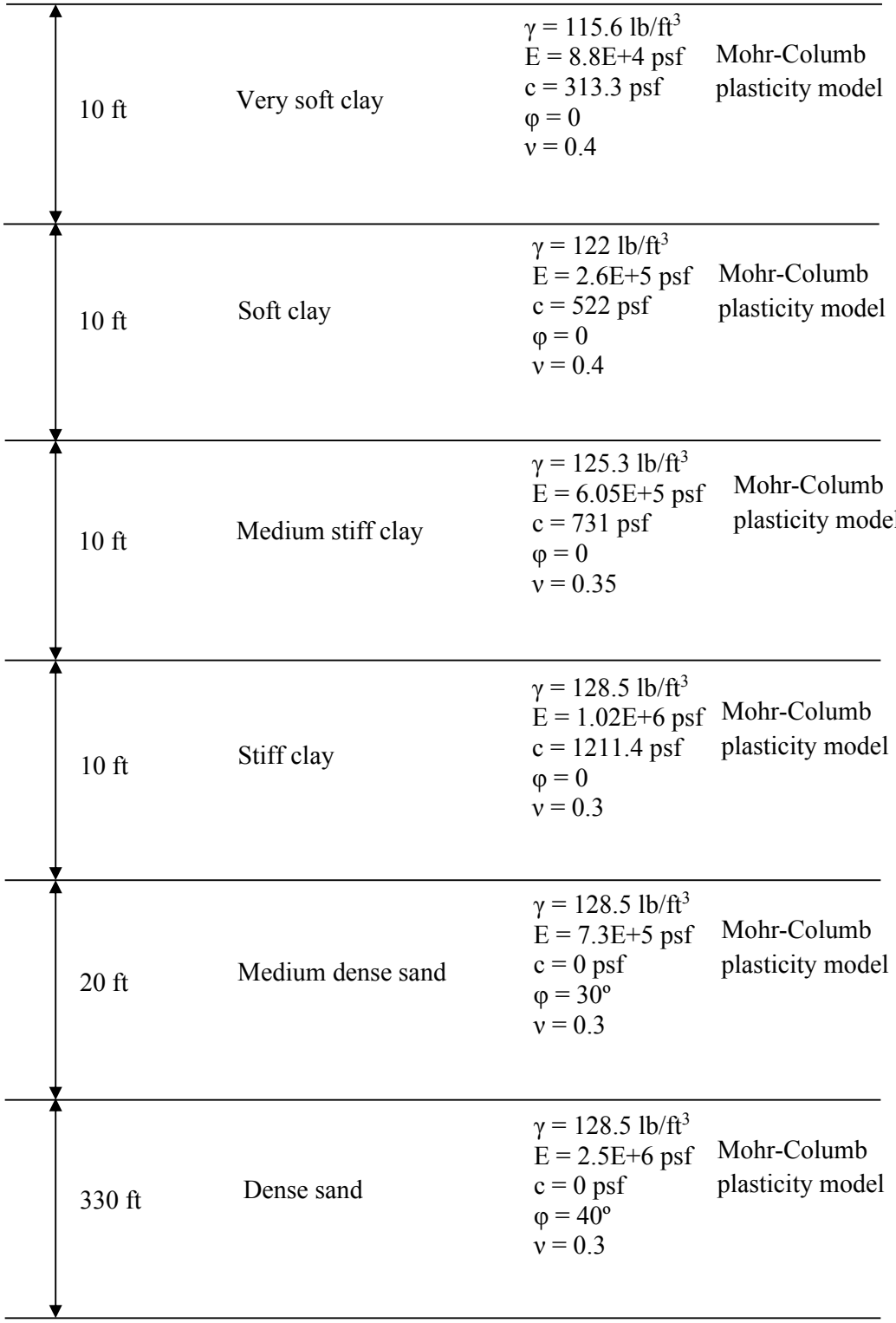

Figure 4.6: Simplified Subsoil Stratigraphy-01

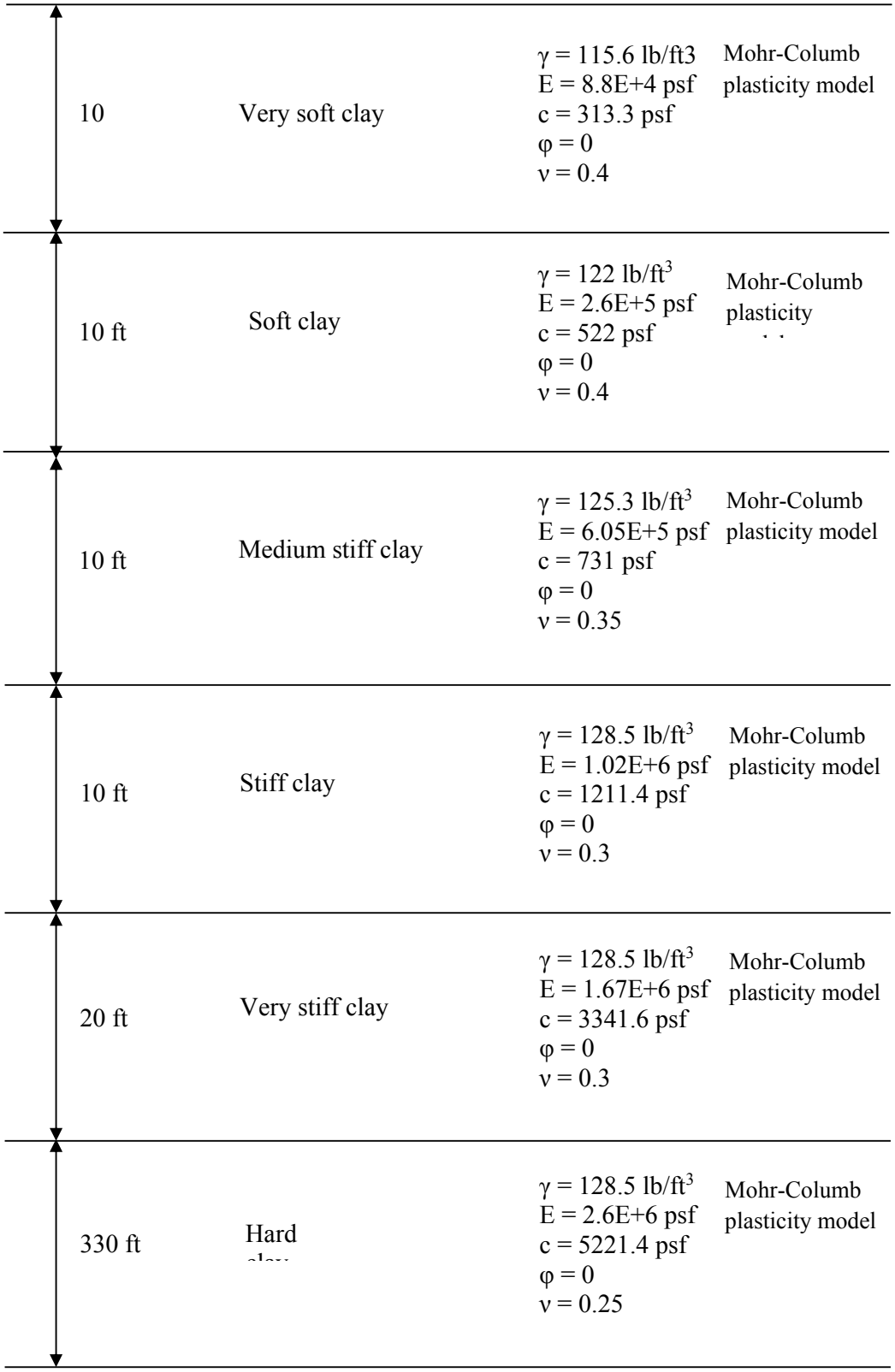

Figure 4.7: Simplified Subsoil Stratigraphy-02

4.4.2 Dynamic Soil Properties

The non-linearity of soil during an earthquake plays an important role in the dynamic response of soil-structure systems. The equivalent linear method has been used for many years to calculate wave propagation (and response spectra) in soil and rock at sites subjected to seismic excitations. In the equivalent linear method adopted in this study, a linear analysis is carried out with some assumed initial values for the damping ratio and shear modulus in various regions of the model was performed by midas GTS NX software. Then the maximum cyclic shear strain is recorded for each element and used to determine the new values for damping and modulus by referring to the backbone curves relating the damping ratio and secant modulus to the amplitude of shear strain. Some empirical scaling factors are usually utilized when relating these strains to the model strains, and then these new values for the damping ratio and shear modulus are used in the next stage of the numerical analysis. The whole process is repeated several times, until there is no further change in the properties and the structural response.

At this stage, "strain compatible" values of damping and modulus are recorded, and the simulation using these values is deemed to be the best possible prediction of the real behavior. As described by Seed and Idriss (1969), the equivalent linear method uses linear properties for each element because they remain constant under the influence of seismic excitations; those values are estimated from the mean level of dynamic motion, as explained before, but since trial and error utilizing nonlinear backbone curves to find the "strain compatible" values of damping and modulus is used, soil non-linearity was captured by this method. Dynamic soil properties are obtained only for soil profile 01 because this profile represents most of the Dhaka Metropolitan area. Figure 4.8 to Figure 4.10 shows dynamic soil properties of the soil profile 01. Soils exhibit nonlinear behavior in shear. The secant shear modulus decreases with increasing strain amplitude as shown in Figure 4.9 and Figure 4.10. Shear modulus at small strains, at which soil behavior is linear, is referred to as small-strain shear modulus, G_o. The relationship between shear modulus and strain amplitude is typically characterized by a normalized modulus reduction curve as shown in Figure 4.9 and Figure 4.10. The nonlinearity in the stress-strain relationship results in an increase in energy dissipation and, therefore, an increase in material damping ratio with increasing strain amplitude as presented in Figure 4.9 and Figure 4.10.

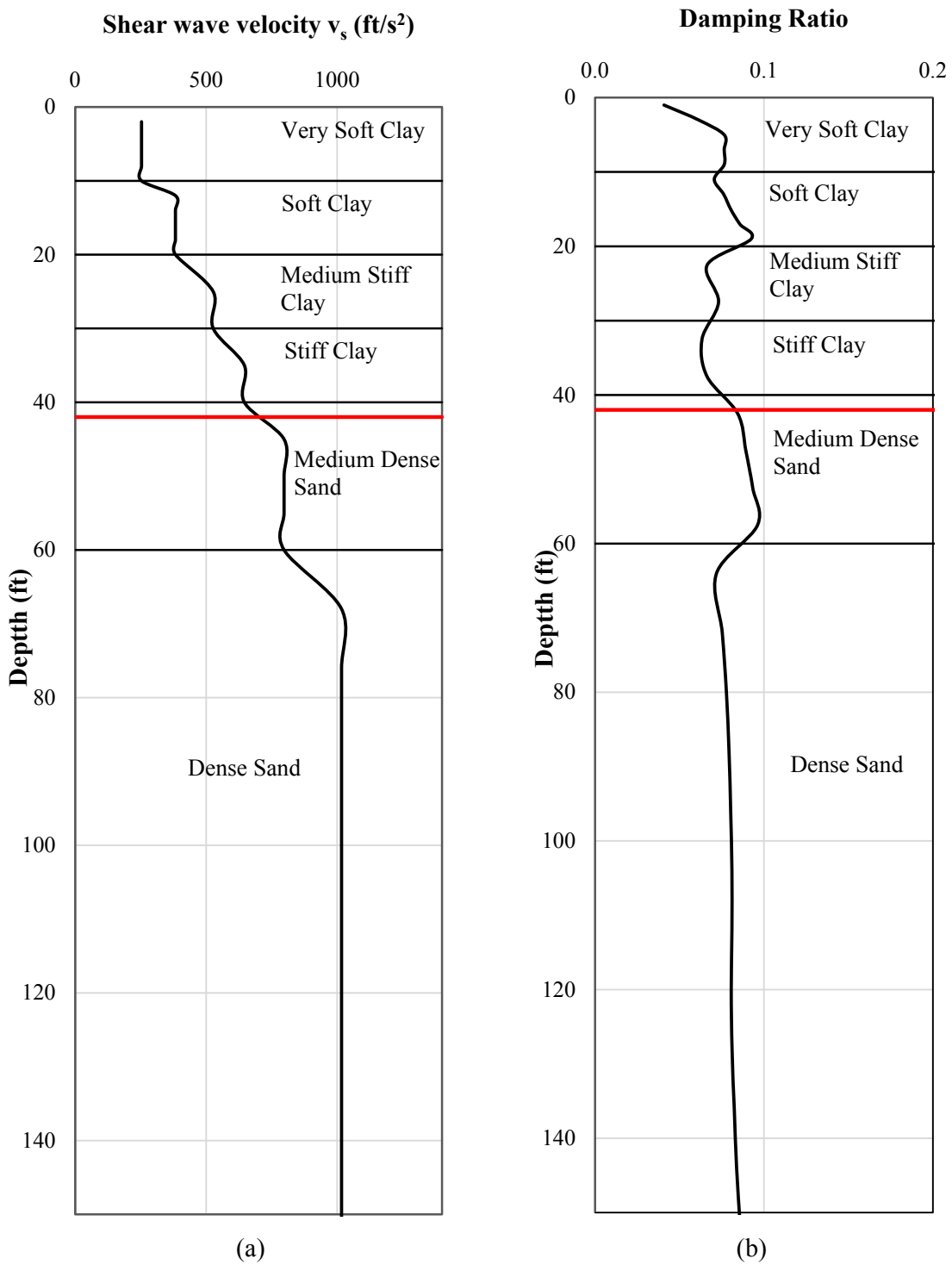

Figure 4.8: Dynamic soil properties (a) shear wave velocity, (b) damping ratio

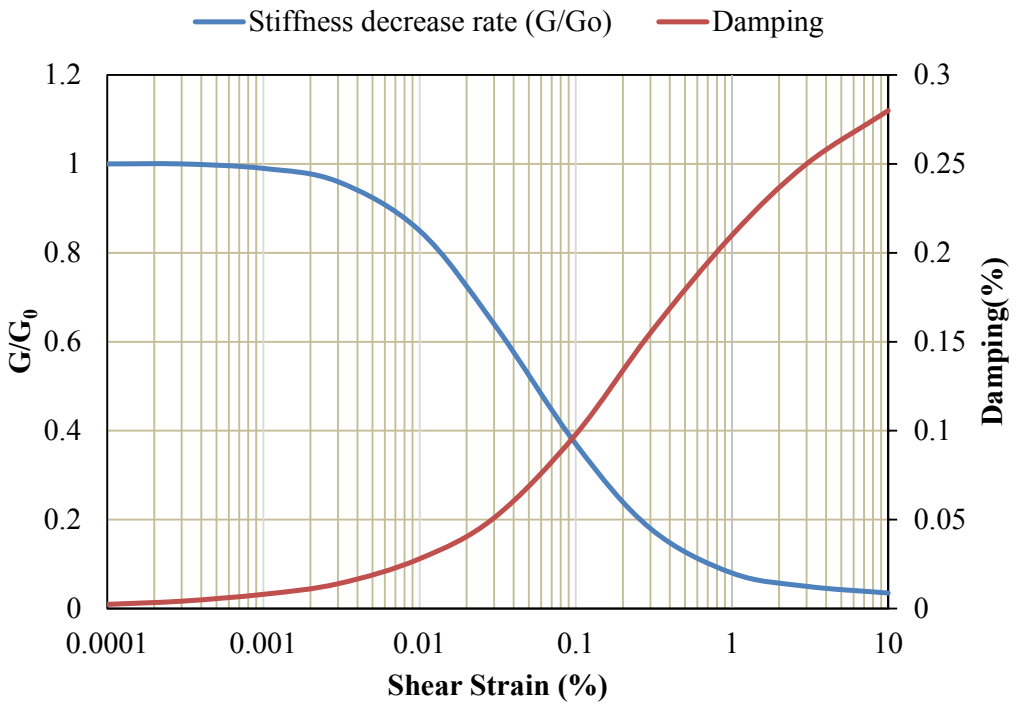

Figure 4.9: Backbone curve of stiffness decrease rate and damping to shear strain for sand

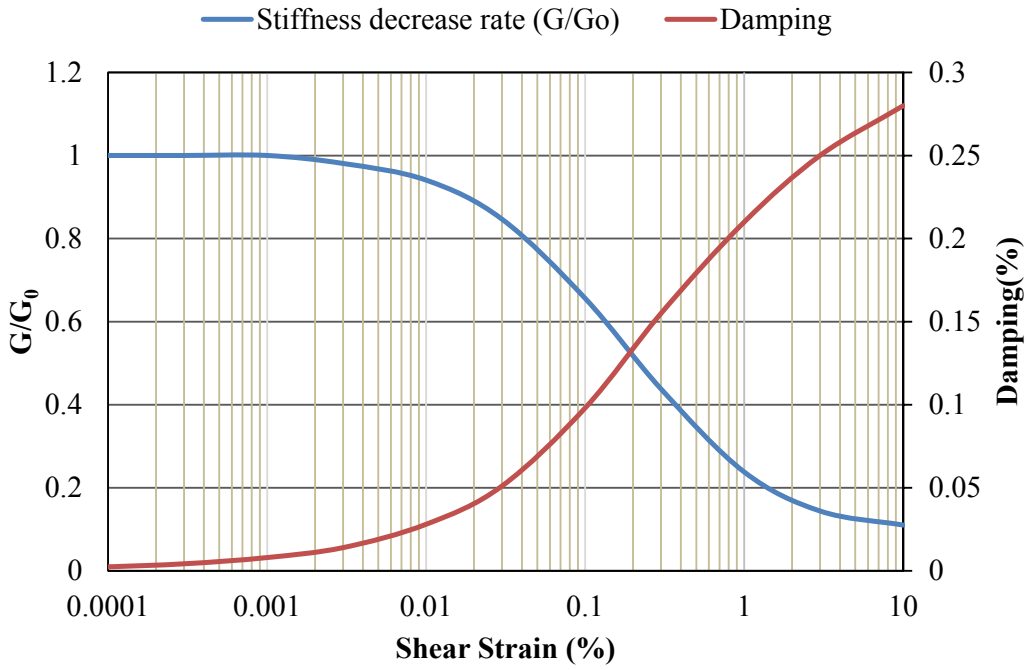

Figure 4.10: Backbone curve of stiffness decrease rate and damping to shear strain for clay

4.5 Characteristics of the Foundation

Loads from super structure to the foundation for this study are obtained considering three elements of the super-structure, namely shear wall, columns within super structure and columns within sub structure. Load intensity below core structure, covering loads from shear wall and columns within super structure, is greater than the podium structure. To meet the demand of load distribution from structure two types of piles are selected. Piles of 36-inch diameter and of 150 ft in length are considered below core structure, whereas piles of 24-inch diameter and of 60 ft in length are considered below podium structure. Load capacity of 36-inch diameter pile is found to be 2000 kip for soil profile- 01, where for 24-inch diameter pile load capacity is found to be 330 kips for the same soil profile. Number of piles of 36-inch and 24-inch dimeters are considered to be 81 and 72 respectively. Table 4.6 summarizes loads on foundation from super structure and pile capacity, diameter and number of piles.

Table 4.6: Summarization of loads from super structure and pile capacity, diameter and number of pile

Elements	Loads Kips (kN)	Pile Capacity kips (kN)	Pile (Dia) inch (mm)	Pile Length ft (mm)	No of Pile (Considered)
Shear wall	100528 (447171)	2000 (8896)	36 (914)	150 (45720)	81
Columns within Super Structure	93433 (415610)				
Columns within Sub Structure	22213 (98808)	330 (1468)	24 (609)	60 (18288)	72

Figure 4.11 represents arrangement of piles under mat. 36-inch diameter piles are provided in middle part of the structure where load intensity is greater and where the load intensity is smaller than the central structure, 24-inch diameter piles are used. Figure 4.12 shows the 3D view of pile arrangements under mat and Figure 4.13 shows the 3-D view of mat above the pile.

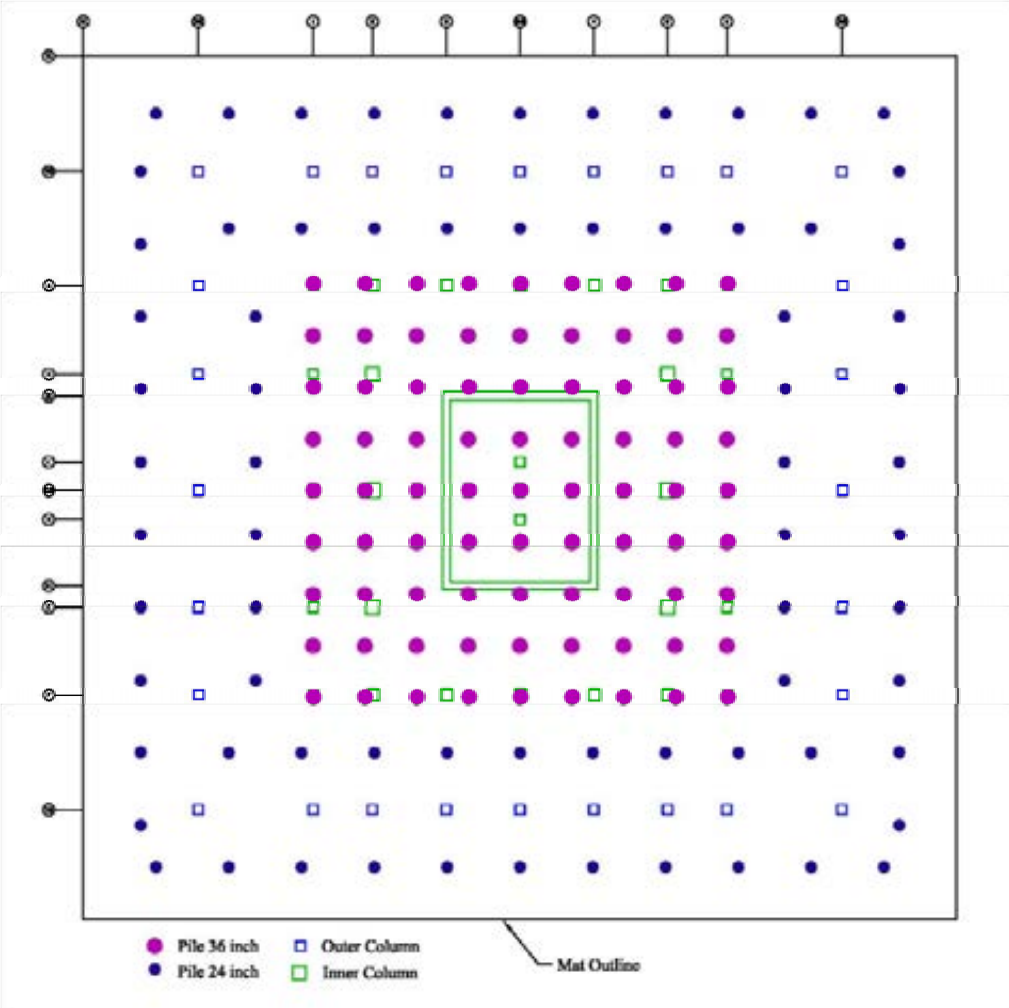

Figure 4.11: Arrangements of piles

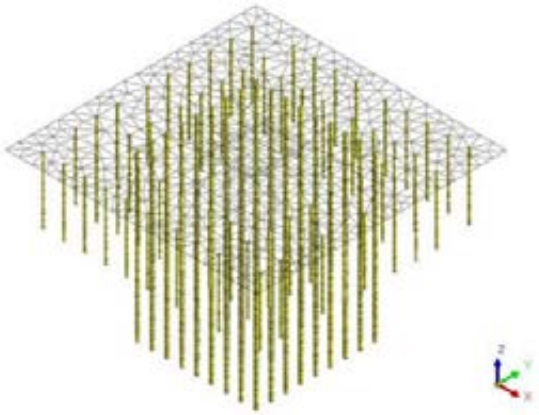

Figure 4.12: 3-D view of piles under mat

Figure 4.13: 3-D view of mat

Structural model adopted for this study is shown in figure 4.14 with mat on pile foundation.

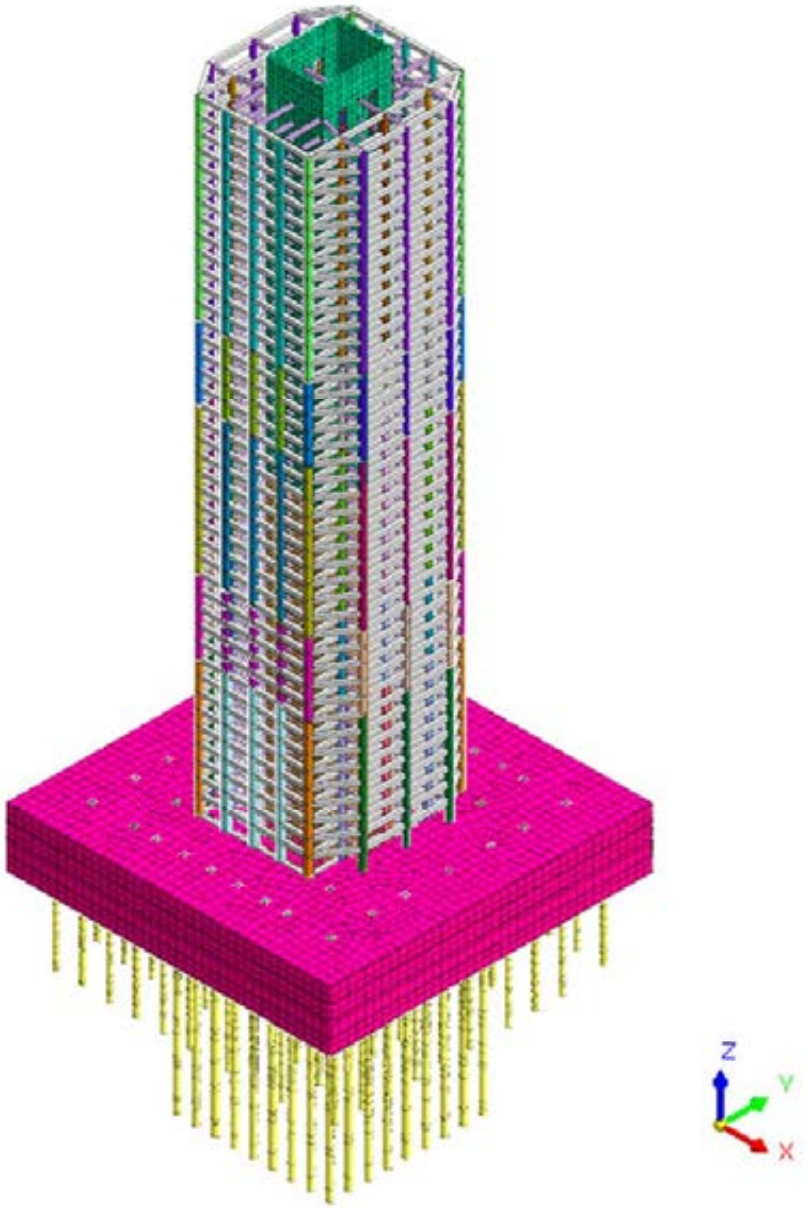

Figure 4.14: 3-D view of the super structure and sub structure

4.6 Earthquake Parameters

Three major earthquakes, namely El Centro, Kobe and Northridge, chosen to stimulate the numerical model for this study. Lists of earthquake motion, actual magnitude and peak ground accelerations are seen in Table 4.7. Earthquake induced ground motions have different characteristics regarding site conditions, intensity and frequency content. It is realistic to scale down specifications of actual ground motion for dynamic analysis. Actual records of peak

ground acceleration of three different earthquakes are scaled down by spectral matching in this study.

Table 4.7: Lists of earthquakes motion used for numerical analysis

Earthquake	Record Description	Magnitude (Richter)	Actual Peak Ground Acceleration
El Centro	Imperial Valley, May 1940	7.2	0.35g
Kobe	Kobe, January 1995	6.9	0.80g
Northridge	Sylmar County Hospital, January 1994	6.6	0.89g

Based on the average shear wave velocity and SPT value, the site class of soil profile-01 is determined to be "SC" as per BNBC 2020. (Table 4.8)

Table 4.8: Site classification based on soil properties for profile-01

Depth from GL(ft)		Thickness (ft)	N	h/N
From	To	(h)		
0	10	10	2	5.00
10	20	10	3	3.33
20	30	10	7	1.43
30	40	10	12	0.83
40	50	10	21	0.48
50	60	10	21	0.48
60	85	25	40	0.63
85	110	25	40	0.63
110	135	25	40	0.63
135	160	25	50	0.50
160	185	25	50	0.50
185	210	25	50	0.50
210	235	25	50	0.50
235	260	25	50	0.50
260	285	25	50	0.50
285	310	25	50	0.50
310	335	25	50	0.50
335	360	25	50	0.50
Sum		360.00		17.92
			Average N=	20.09
			Site Class	SC

4.7 Response Spectrum for Soil Profile -01 as per BNBC 2020

The design basis earthquake (DBE) ground motion is selected at a ground shaking level that is 2/3 of the maximum considered earthquake (MCE) ground motion. The spectral acceleration of soil profile -01 for DBE are shown in Figure 4.15.

Parameters for determining the spectral acceleration are illustrated below.

Long Period, T_L=	4 sec		
Site Coefficient , F_a =	1.15		
Site Coefficient , F_v =	1.725		
Spectral Response Acceleration, S_s =	0.5		
Spectral Response Acceleration, S_1 =	0.2	To =	0.12 sec
Spectral Response Acceleration, S_{DS} =	0.383	Ts =	0.6 sec
Spectral Response Acceleration, S_{D1} =	0.23	T_L =	4 sec

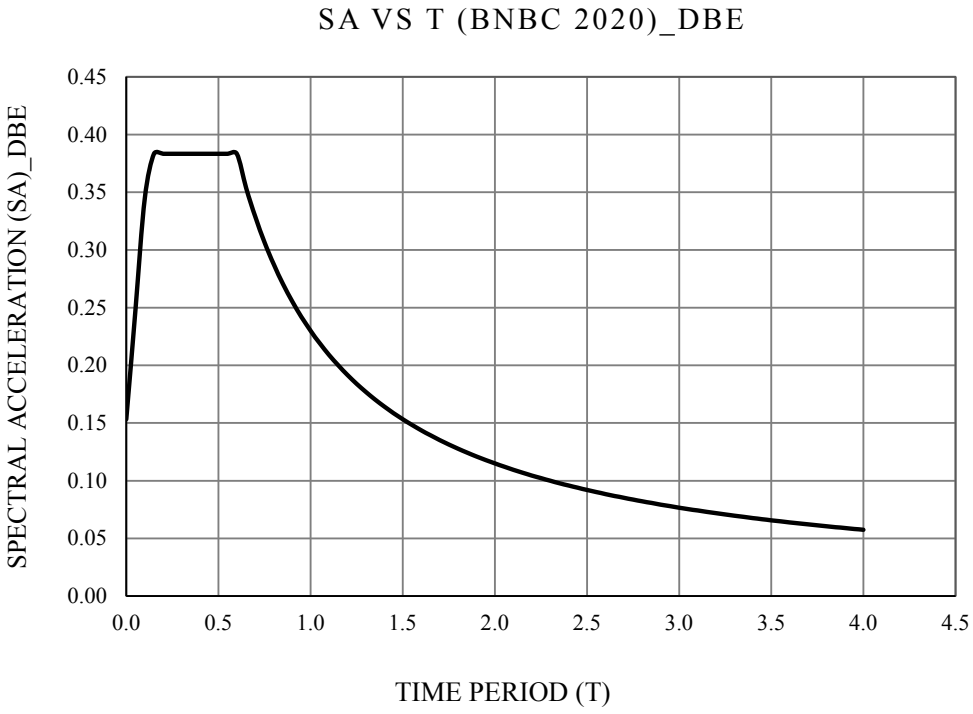

Figure 4.15: Spectral acceleration for soil profile-01 as per BNBC 2020

Fig. 4.16 shows the simulation output of three acceleration records in the form of response spectrum curve and the target response spectrum for the site class SC of Dhaka soil. The average of these three spectrums is scaled by a factor, which is the ratio of the area under

spectrum curve between the matched and target spectrum along 0.2T to 1.5T.

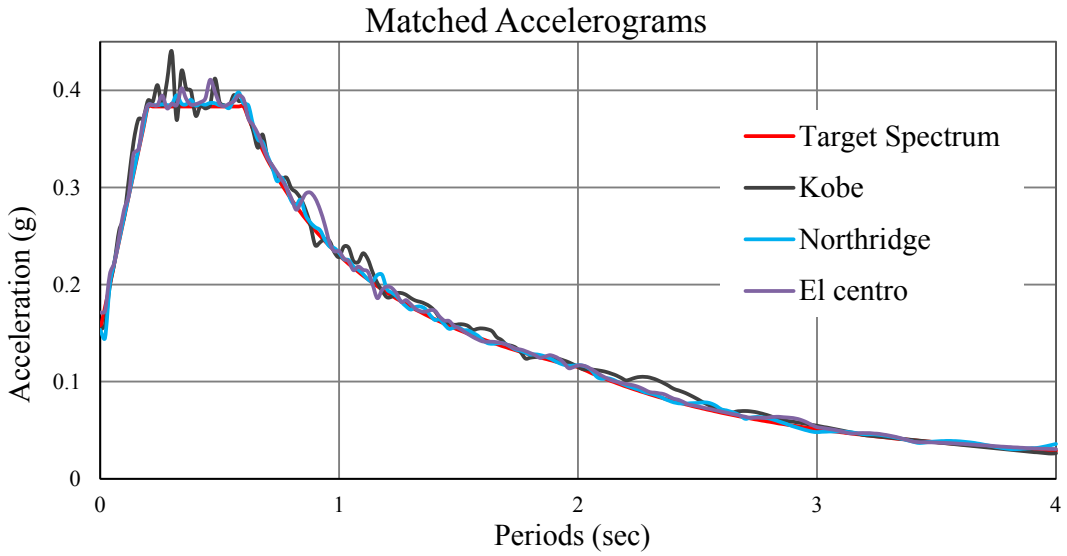

Figure 4.16: Matched accelerograms of three earthquake with code based target spectrum

The matched spectrums are then used to generate new time history accelerograms. These newly generated accelerograms are then utilized to analyze for fixed base model.

However the accelerograms for flexible base model are not same as the fixed base model. In the case of generating accelerograms for flexible base model, the effects of soil factor must be nullified. As the matching spectrums have met the requirement, the adopted acceleration records can be used in dynamic time history analysis for fixed base model and flexible base model.

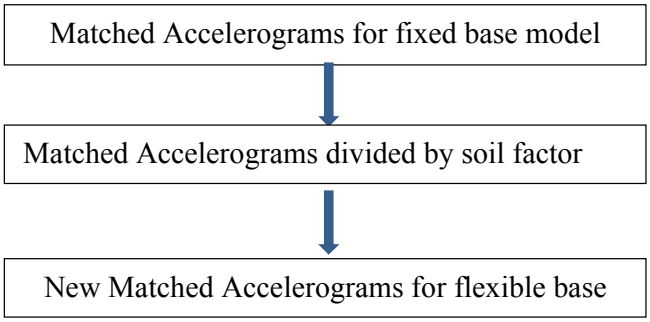

Figure 4.17: Flow chart of conversion of accelerograms from fixed base model to flexible base model

Matched Acceleration, velocity and displacement of three earthquake for fixed base model and flexible base model are illustrated in Figure 4.17 to Figure 4.34

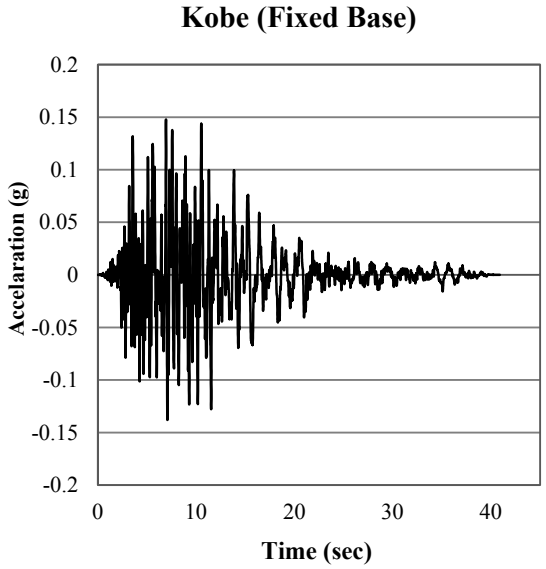

Figure 4.18: Acceleration vs Time of Kobe EQ for fixed base model

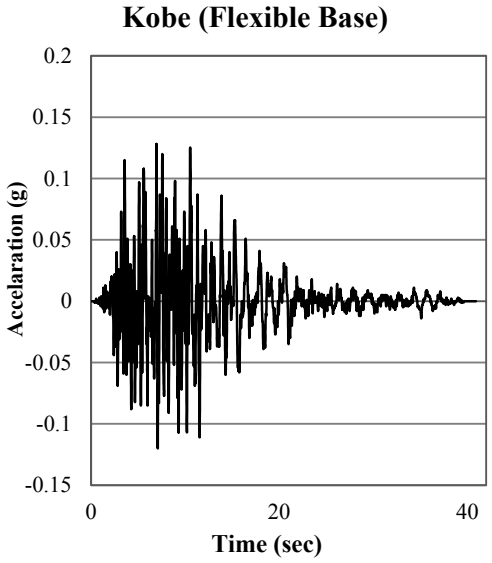

Figure 4.19: Acceleration vs Time of Kobe EQ for flexible base model

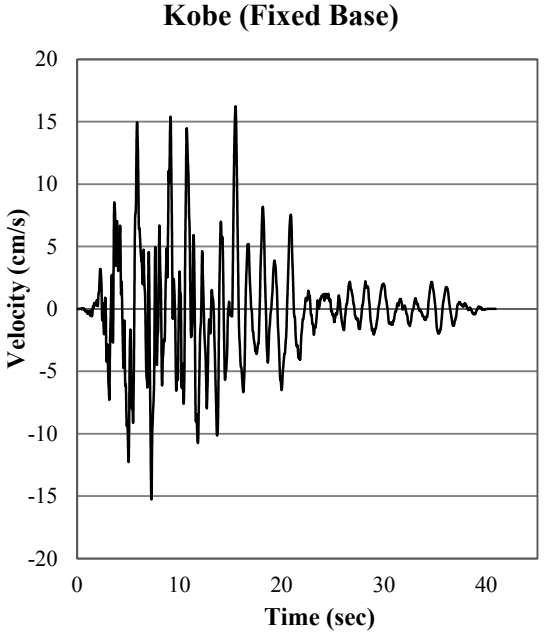

Figure 4.20: Velocity vs Time of Kobe EQ for fixed base model

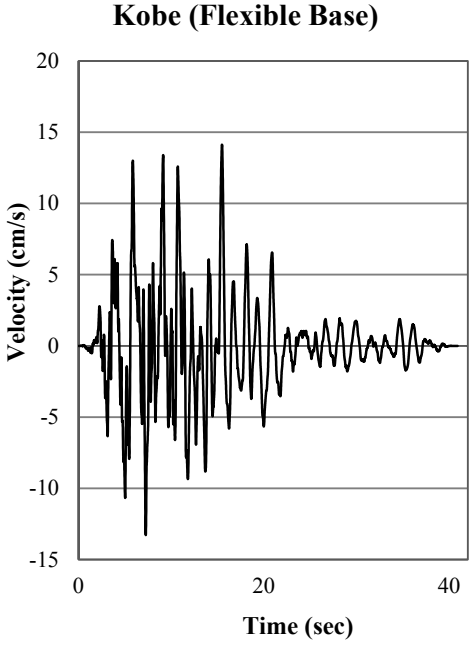

Figure 4.21: Velocity vs Time of Kobe EQ for flexible base model

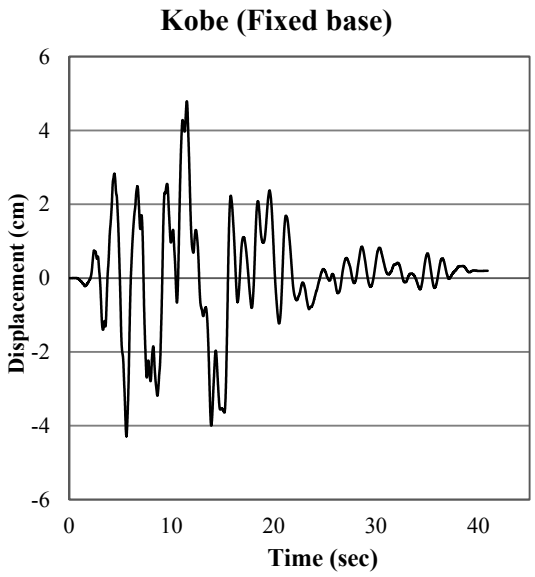

Figure 4.22: Displacement vs Time of Kobe EQ for fixed base model

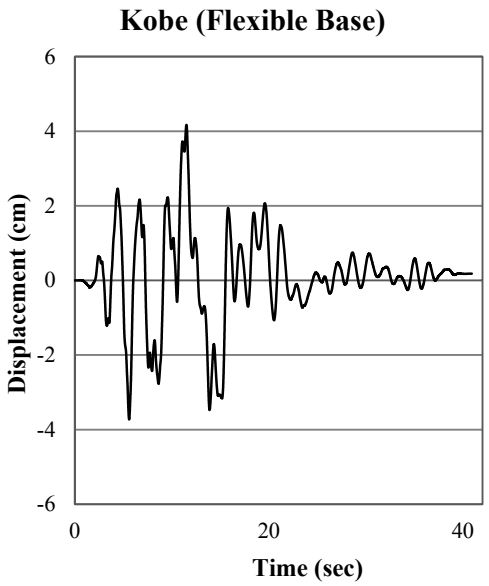

Figure 4.23: Displacement vs Time of Kobe EQ for flexible base model

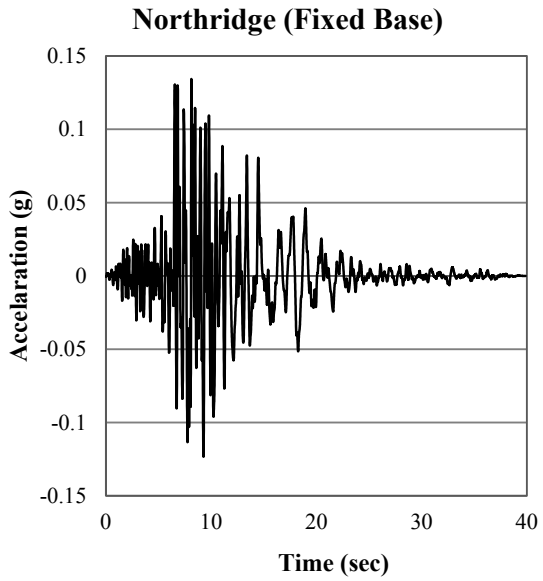

Figure 4.24: Acceleration vs Time of Northridge EQ for fixed base model

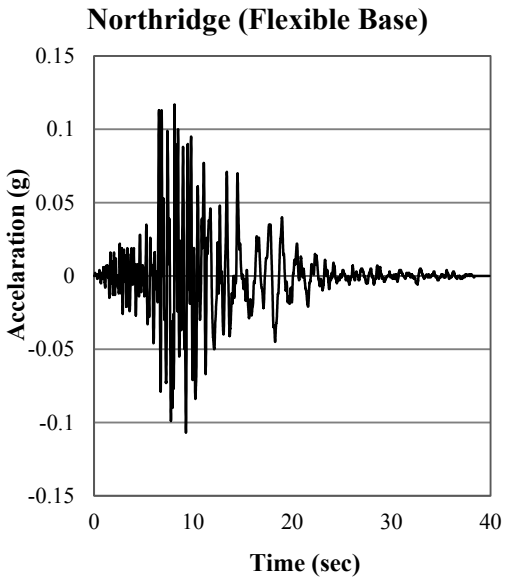

Figure 4.25: Acceleration vs Time of Northridge EQ for flexible base model

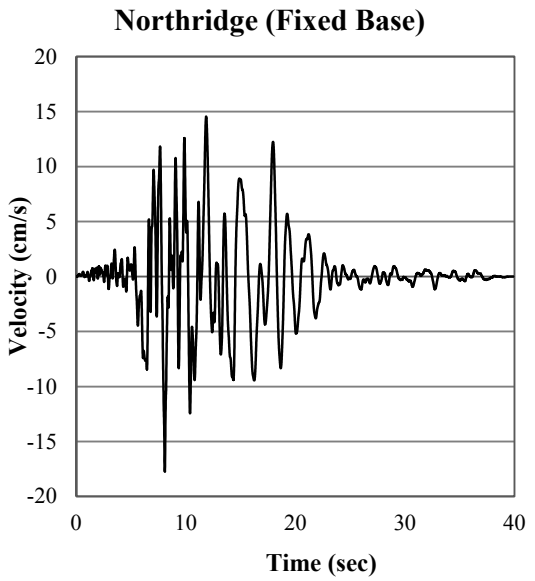

Figure 4.26: Velocity vs Time of Northridge EQ for fixed base model

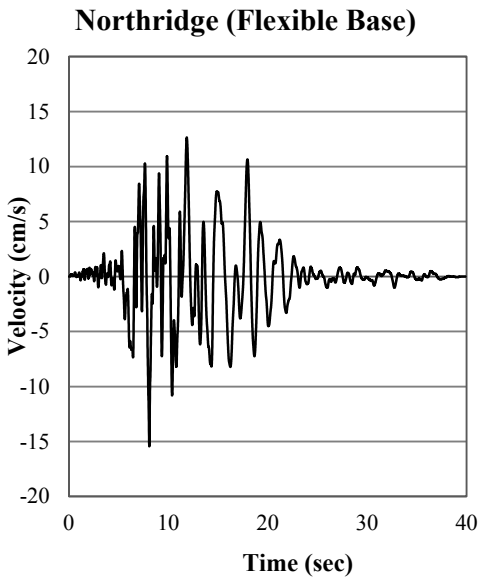

Figure 4.27: Velocity vs Time of Northridge EQ for flexible base model

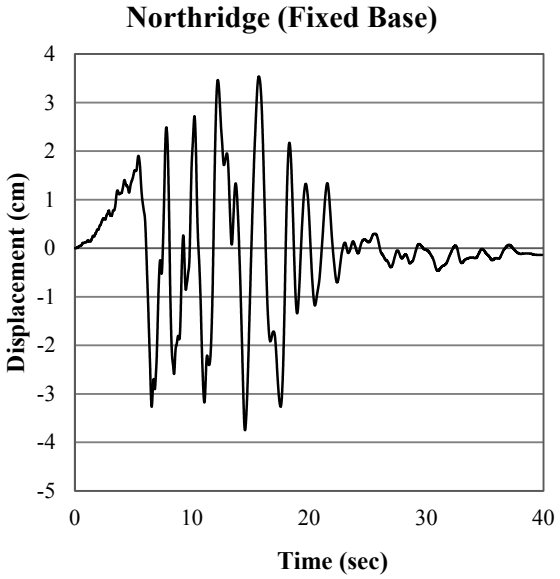

Figure 4.28: Displacement vs Time of Northridge EQ for fixed base model

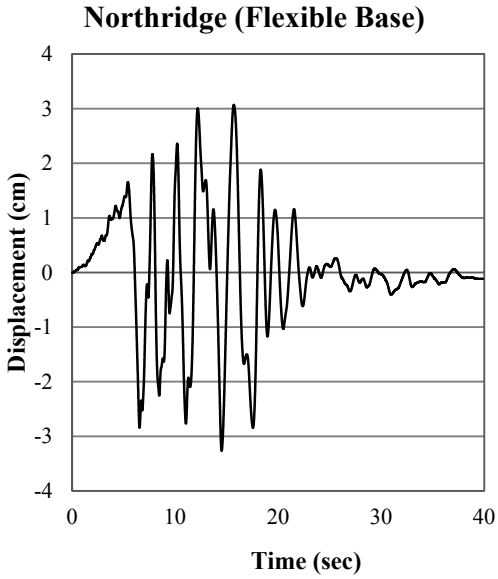

Figure 4.29: Displacement vs Time of Northridge EQ for flexible base model

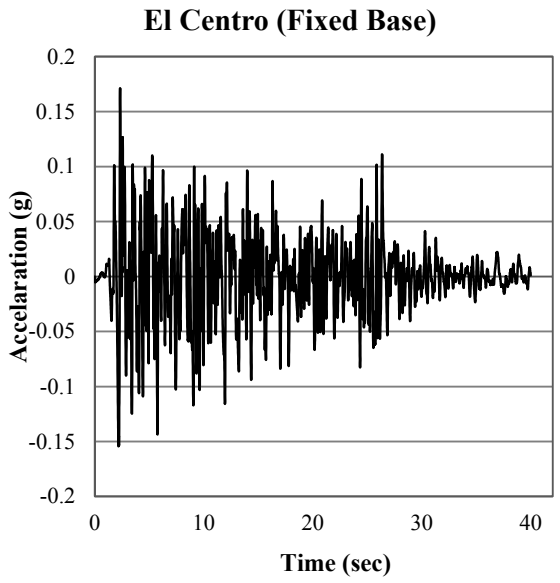

Figure 4.30: Acceleration vs Time of El Centro EQ for fixed base model

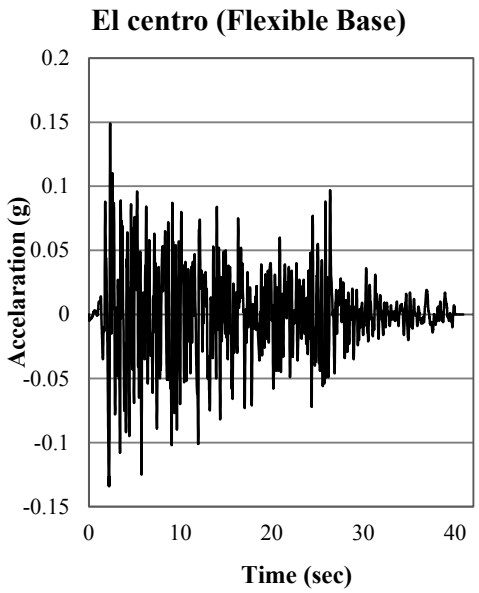

Figure 4.31: Acceleration vs Time of El Centro EQ for flexible base model

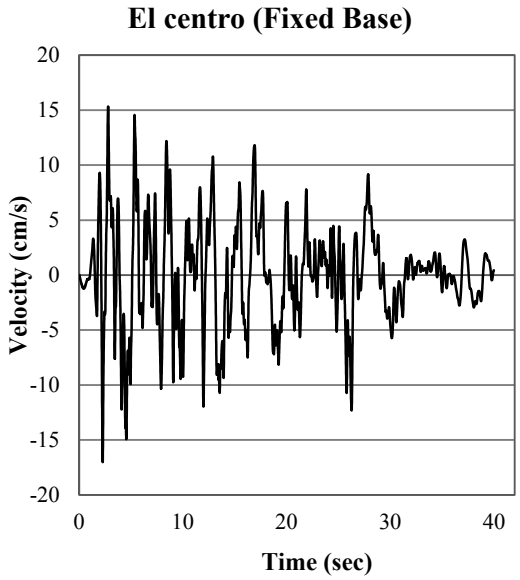

Figure 4.32: Velocity vs Time of El Centro EQ for fixed base model

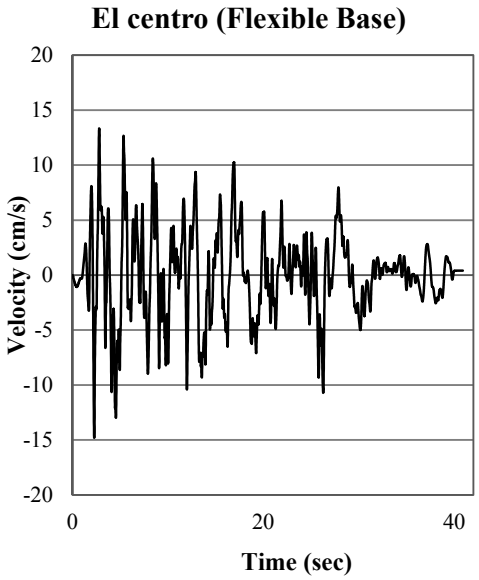

Figure 4.33: Velocity vs Time of El Centro EQ for flexible base model

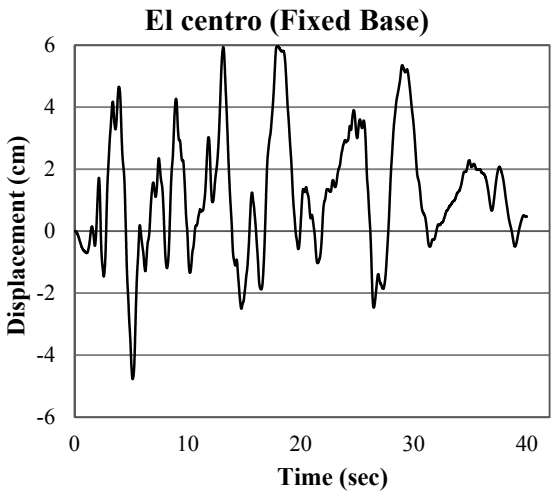

Figure 4.34: Displacement vs Time of El Centro EQ for fixed base model

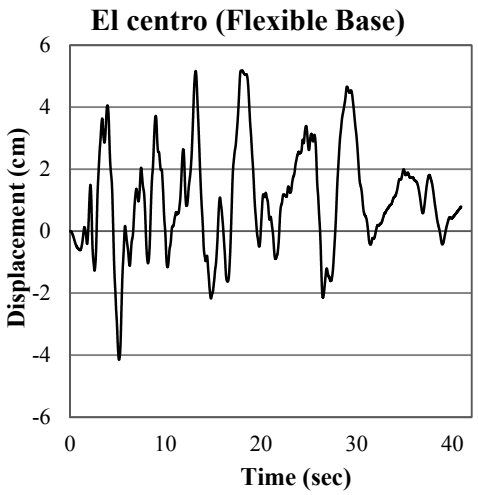

Figure 4.35: Displacement vs Time of El Centro EQ for flexible base model

After matching the accelerograms with code base spectrum the maximum acceleration of three earthquakes.(1) Kobe, (2) Northridge, (3) El Centro are illustrate in figure 4.35. For three earthquakes, the maximum acceleration value of the flexible base model was found to be lower than that of the fixed base model. Since the soil factor (S) is not taken into account, the maximum acceleration of the flexible base model is lower.

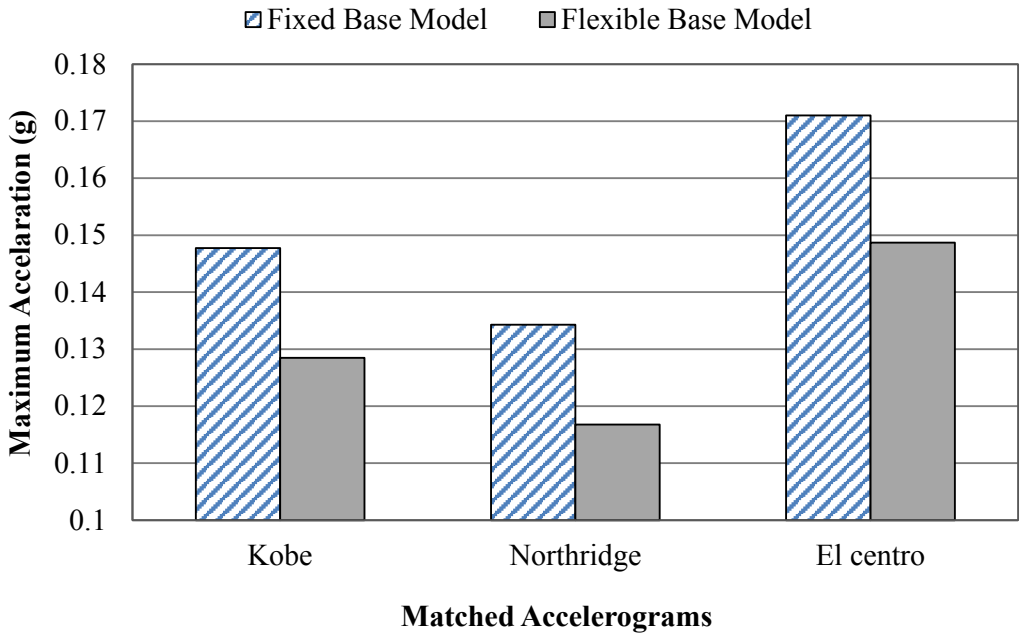

Figure 4.36: Maximum acceleration of three earthquakes.

4.8 Boundary Conditions

Two different sets of boundary conditions are employed for static and dynamic analyses. Detail descriptions of boundary conditions are written below.

4.9.1 Boundary Conditions for Static Analysis

Gravity loading was applied in the static analysis; thus, the bottom boundary was fixed in all directions, while all the four side boundaries were fixed in the horizontal direction only. In this study, rigid boundary condition is adopted to simulate the bedrock at the bottom of the soil medium for static analysis. Support condition of soil medium along two side of x-direction are constrained for Ux and soil medium along two side of y-direction are constrained for Uy.

4.9.2 Boundary Conditions for Dynamic Analysis

In the dynamic analysis, however, as mentioned by Semblat (2011), the boundaries at the sides of the model must account for free-field motion. As shown in Figure 4.36, the free-field elements, consisting of dashpots in the normal and shear directions, transfer the free-field motion from the free-field grids to the main grid of the 3D numerical model. Moreover, the viscous boundaries consisting of independent viscous dampers were coupled to the free-field grids to eliminate the reflection from outgoing waves by applying resistant tractions in the normal and tangential directions. The applied resistant tractions in the viscous boundaries, governed by the equations proposed by Lysmer and Kuhlemeyer (1969), are expressed as follows:

$t_n = - \rho C_p V_n$

$t_s = - \rho C_s V_s$

Where tn and ts = tractions in the normal and shear directions, respectively;

ρ = density of the medium;

Cp and Cs = velocities of the p-wave and s-wave, separately; and

Vn and Vs = normal and shear components of the velocity in the near-boundary material.

The viscous boundary may not perfectly absorb the outgoing waves when ±30° (Han et al.

2016). Therefore, to minimize the adverse effect of the waves reflected from the artificial boundaries, according to Syed and Maheshwari (2014), horizontal distance between the side boundaries along the earthquake shaking direction was set to be consid- erably larger than the foundation width as presented in Figure 4.37, Furthermore, a rigid boundary condition, utilized to simulate the strong bedrock and the significant impedance difference between the soil deposit and the strong bedrock, was applied to the bottom of the model during the seismic analysis, following the suggestion made by Maheshwari and Sarkar (2011).

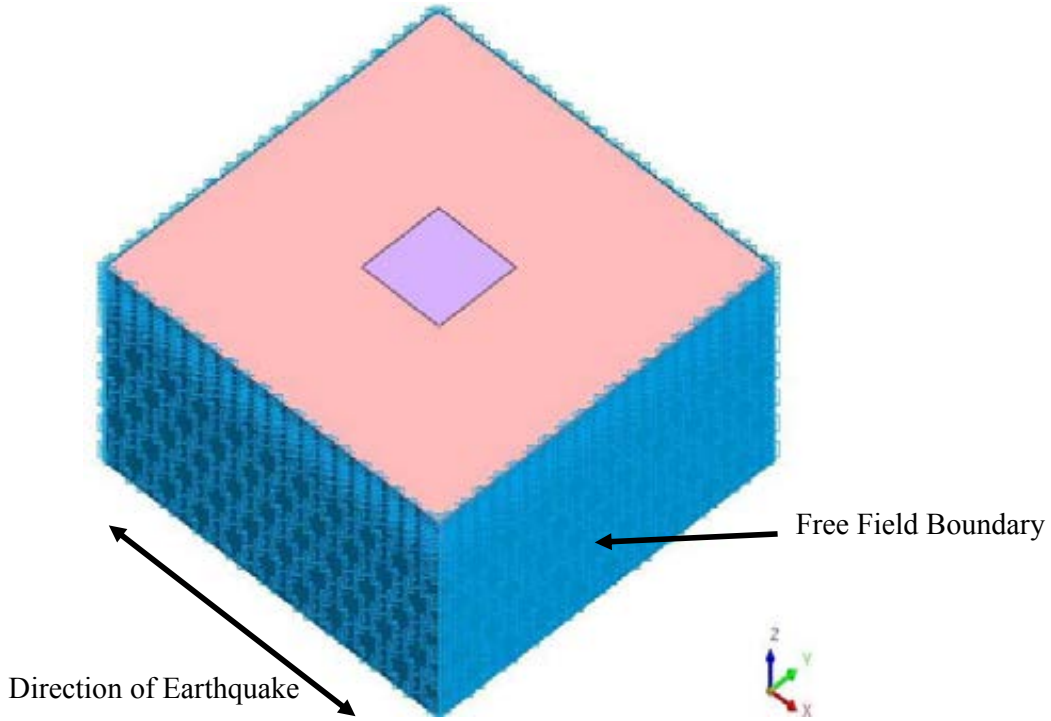

Figure 4.37: Boundary condition of the soil model

4.10 Size of the Numerical Model

Rayhani and El Naggar (2008), after undertaking comprehensive numerical modelling and centrifuge model tests, concluded that the horizontal distance of the soil lateral boundaries should be at least five times the width of the structure in order to avoid reflection of outward propagating waves back into the model. The boundary condition of the soil model is shown in Figure 4.37. In this study, the bedrock depth of 377 ft is adopted. The horizontal distance of the soil lateral boundaries is assumed to be 984 ft.

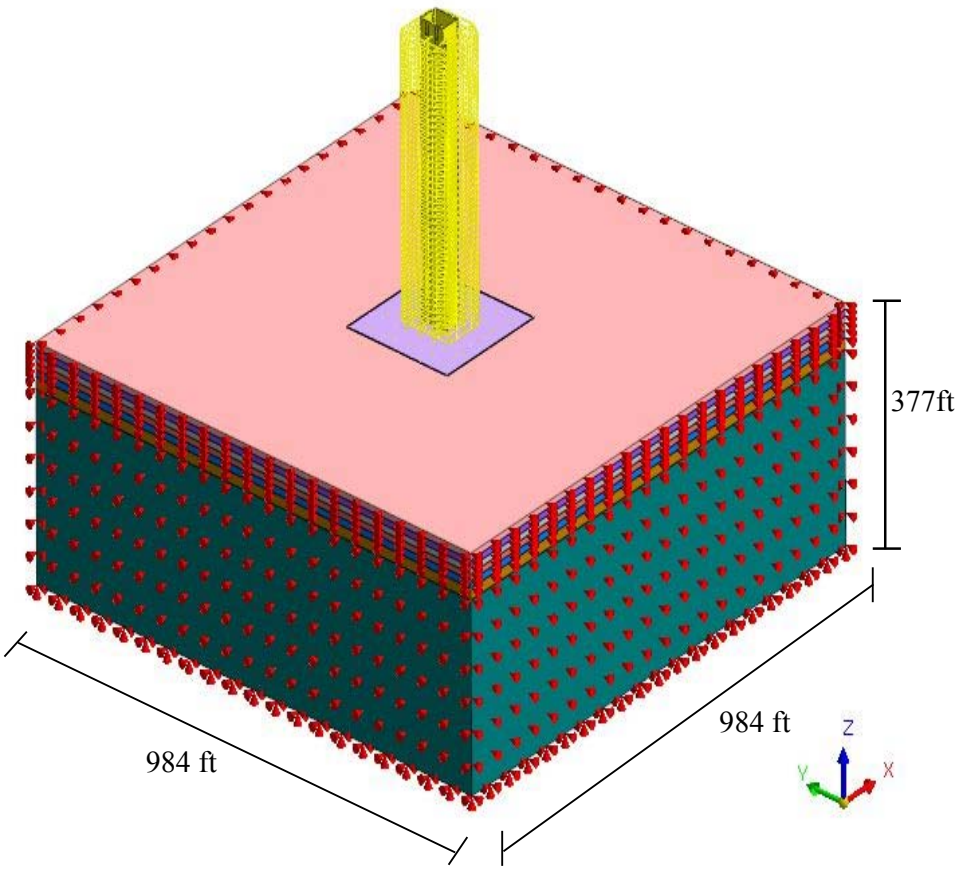

Figure 4.38: Boundary condition of the soil model

4.11 Summary

In this chapter, the 3D numerical model using midas GTS NX have been used to investigate the influence of SSPSI on the behavior of superstructures under seismic loads. The developed numerical model performs SSPSI analysis in a fully coupled manner, without resorting to independent calculations of site or superstructure response, or application of pile group interaction factors. The main feature of the developed numerical model is incorporating the nonlinear behavior of soil together with linear behavior of structural elements simultaneously throughout the three-dimensional numerical analysis.

In this study, a three-dimensional finite element analysis using midas GTS NX is performed for a tall building (42 stories with 4 basement) with soil continuum.

Two types of typical Dhaka soil profiles are considered. For static SSI, equivalent linear static analysis has been performed for both soil profile-01 and soil profile-02 with mat foundation and mat on pile foundation.

For dynamic SSI, nonlinear time history analysis has been performed for soil profile-01 with mat on pile foundation considering design based earthquake (DBE) for three different events Nonlinear Mohr-Coulomb model has been adopted in this study to simulate the nonlinear soil behavior and possible shear failure in the soil elements during the excitation. Moreover, hysteretic damping of the soil is implemented to represent the variation of the shear modulus reduction factor and the damping ratio of the soil with the cyclic shear strain.
Solid nonlinear elements were adopted to simulate soil elements, while linear solid elements were used for wall elements. Columns and pile were modelled as beam elements. Slabs and Raft were simulated as shell elements.
Adjusting the boundary conditions for the static analysis, in which the system is under the gravity loads only, the bottom face of the model is fixed in all directions, while the side boundaries are fixed in the horizontal direction. During the dynamic time-history analysis, in order to avoid reflection of outward propagating waves back into the model, quiet boundaries consisting of independent dash-pots in the normal and shear directions are placed at the lateral boundaries of the soil medium

Sliding can occur at the raft-soil interface. A gap or separation can form at the pile-soil interface. Due to the different characteristics of the soil and the superstructure/piles, two sets of interface elements are modelled in this study. For the raft foundation case, the interface elements are placed between the foundation and the soil surface. However, for the pile foundation case, the interface elements were attached to the outer perimeter of the piles. The adopted interfaces were modelled as spring–slider systems, while the shear strength of the interfaces was defined by Mohr–Coulomb failure criterion.

BANGLADESH NETWORK
OFFICE FOR URBAN SAFETY

PART-VIII

RECENT MAJOR FIRE OCCURRENCES IN BANGLADESH

BANGLADESH NETWORK OFFICE FOR URBAN SAFETY (BNUS), BUET, DHAKA

Prepared By: Sayma Ahmed

Mehedi Ahmed Ansary

UKHIYA ROHINGYA CAMP: MASSIVE FIRE RAZES HOMES

Eleven Rohingyas, including two children and a woman, were reportedly killed and around five hundreds of others were injured in deadly fires that burned several thousand shanties at Balukhali refugee camp in Ukhiya, Cox's Bazar on 22nd March 2021. The fire started around 4:00pm and firefighters almost doused it an hour later. But another wave of fire broke out shortly after 11:00pm and was burning down shanties at the densely populated camp as of 12:30am, locals said. Refugees gather at the Balukhai Rohingya camp in Cox's Bazar's Ukhiya to see for themselves the damage caused by a fire on 22nd March. Around 10,000 shanties were gutted and about 45,000 refugees became homeless.

NARAYANGANJ FOOD FACTORY FIRE

The massive fire in a food processing factory in Narayanganj has left at least 52 people killed with dozens of workers still missing on July 08, 2021. Firefighters recovered 49 charred bodies from the burning factory building of Hashem Food Ltd, a concern of Sajeeb Group, taking the death toll to 52. Three deaths were reported in the immediate aftermath of the fire at the six-storey factory building at the Kornogop area of Bhulta in the district's Rupganj upazila. Over 50 other workers were also injured after jumping off the building immediately after the fire broke out.

MOGBAZAR GAS EXPLOSION IN DHAKA

The Moghbazar explosion took place on 27 June 2021 at the wireless gate of Moghbazar in Dhaka, the capital of Bangladesh. At least 7 people were killed and more than 100 injured, out of which 66 were admitted to various hospitals. Police suspect the incident was caused by frozen gas. The force of the explosion caused significant damage to at least seven nearby buildings, as well as three buses and other cars. Many of the injured came from the passenger buses and other cars which were stuck in traffic in front of the building when the explosion took place.

BANGLADESH NETWORK
OFFICE FOR URBAN SAFETY

PART-IX

RECENT EARTHQUAKES AROUND BANGLADESH

BANGLADESH NETWORK OFFICE FOR URBAN SAFETY (BNUS), BUET, DHAKA

Prepared By:

Mehedi Ahmed Ansary

APRIL 28, 2021: TEZPUR, ASSAM, INDIA

Assam earthquake: The primary earthquake had its epicentre at latitude 26.690 N and longitude 92.360 E, about 80 km northeast of Guwahati, and a focal depth of 17 km. Several houses and buildings were damaged after an earthquake of magnitude 6.4 on the Richter scale hit Assam around 8 am on Wednesday. Six aftershocks of magnitude ranging from 3.2 to 4.7, occurred in the two-and-a-half hours following the main tremor.

HFT, also known as the Main Frontal Thrust (MFT), is a geological fault along the boundary of the Indian and Eurasian tectonic plates. The Kopili Fault is a 300-km northwest-southeast trending fault from the Bhutan Himalaya to the Burmese arc. People look on at debris after a portion of few shops were damaged due to earthquake at Bhetapara in Guwahati, Wednesday, April 28, 2021. (PTI Photo)

The United States Geological Survey (USGS), a scientific agency of the US federal government, defines a fault as “a fracture along which the blocks of crust on either side have moved relative to one another parallel to the fracture”.

Prof Chandan Mahanta of the Department of Civil Engineering at the Indian Institute of Technology, Guwahati, said: “The Northeast is located in the highest seismological zone, so we must have constant earthquake preparedness at all levels. Continuous tectonic stress keeps building up particularly along the faultlines. Today’s earthquake was an instance of accumulated stress release — probably, stress was constrained for a fairly long time at this epicentre, and hence the release was of relatively higher intensity.”

Prof Mahanta said the timing of the earthquake and its duration ensured the damage was restricted. “The earthquake occurred early in the day when people were mostly home. Had it happened during working hours, say when there were workers at under-construction high-rise buildings, the earthquake might have taken lives,” he said.

“The duration is also important,” Prof Mahanta said. “Had the main tremor continued for more than 30 seconds with the same intensity, the resultant acceleration and resonance could have cause greater damage to structures.”

1. 

1 / 9

People watch an earthquake-damaged building at Bhetapara in Guwahati. (PTI Photo)

1. 

2 / 9

A man searches for his belongings amidst the debris after a boundary wall of his house collapsed following an earthquake in Nagaon district in Assam. (Reuters photo)

1. 

3 / 9

A woman points towards the crack in a building caused due to an earthquake, in Guwahati. (PTI Photo)

1. 

4 / 9

Impact of earthquake caused damage to houses and building. Also, the CM Sarbananda Sonowal tweeted, “PM Shri Narendra Modiji has taken stock of the damage due to the earthquake over the phone with me and has assured all support to Assam.” (Express Photo)

1. 

5 / 9

Epicenter of earthquake was near Dhekiajuli town, north of Guwahati, Assam. (Express Photo)

1. 

6 / 9

Many buildings in Tezpur, the district headquarters of Sonitpur, Guwahati and other places developed cracks. (Express Photo)

1. 

7 / 9

Most parts of the region felt the impact of the massive earthquake as people ran out of their homes and other places in panic.

1. 

8 / 9

Union Home Minister Amit Shah on Wednesday spoke to Assam Chief Minister Sarbananda Sonowal after the state was hit by an earthquake. (Express Photo)

1. 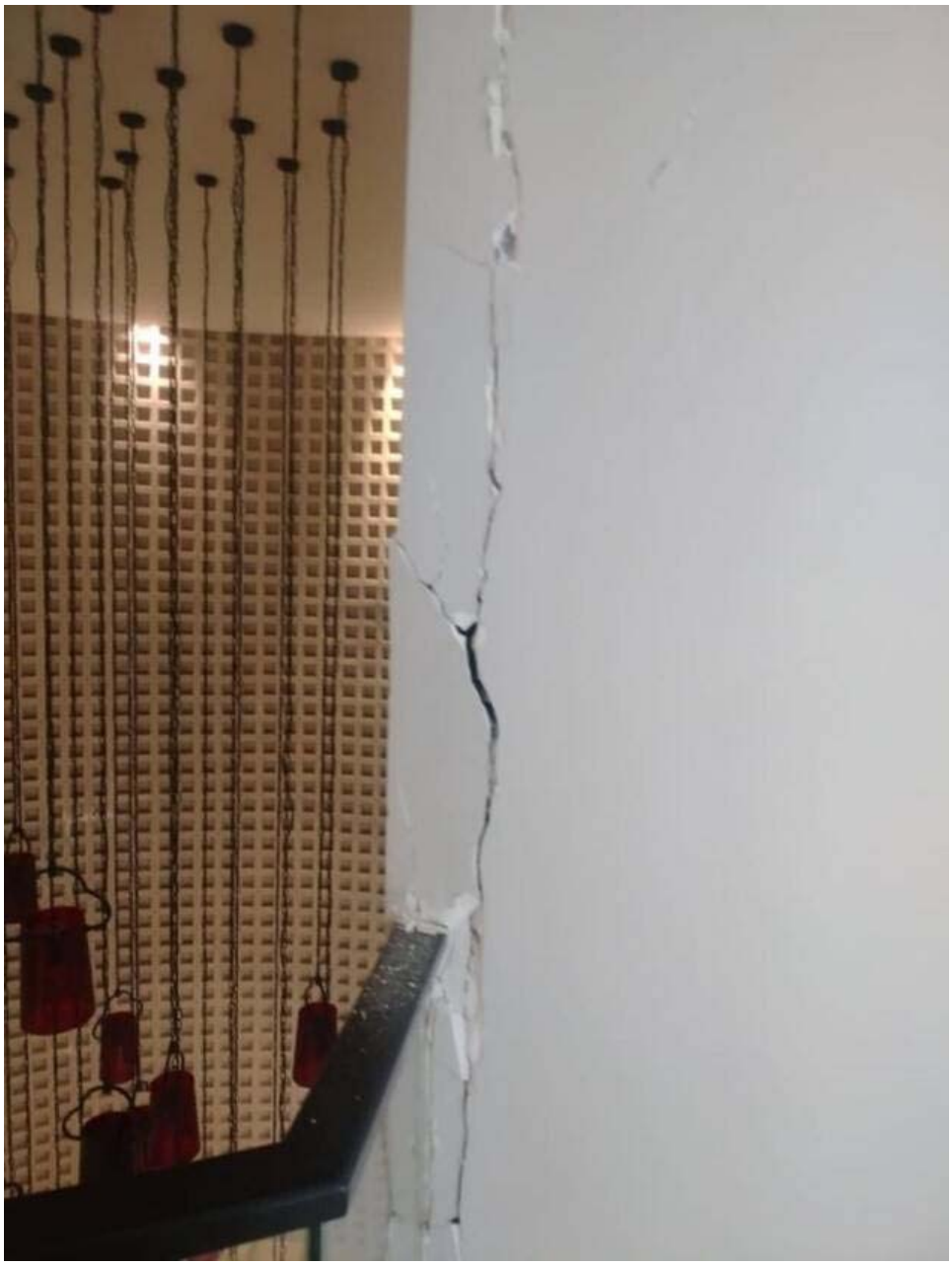

9 / 9

According to the Seismology department, the tremors were felt for at least 30 seconds.

MAY 29, 2021: SYLHET, BANGLADESH

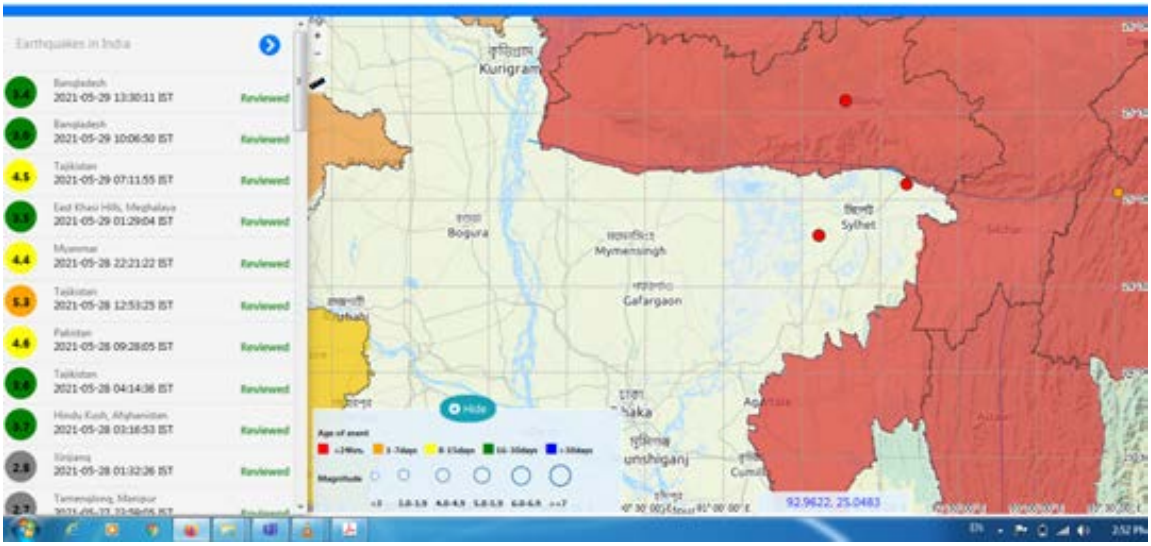

Tilted School

Although the owners want to demolish Raja Mansion, as the structure was deemed vulnerable to earthquakes, tenants are opposing the move. This photo was taken yesterday. PHOTO: SHEIKH NASIR

RAJA Mansion and Modhubon Market